Forming of UD fibre reinforced thermoplastics

a critical evaluation of intra-ply shear

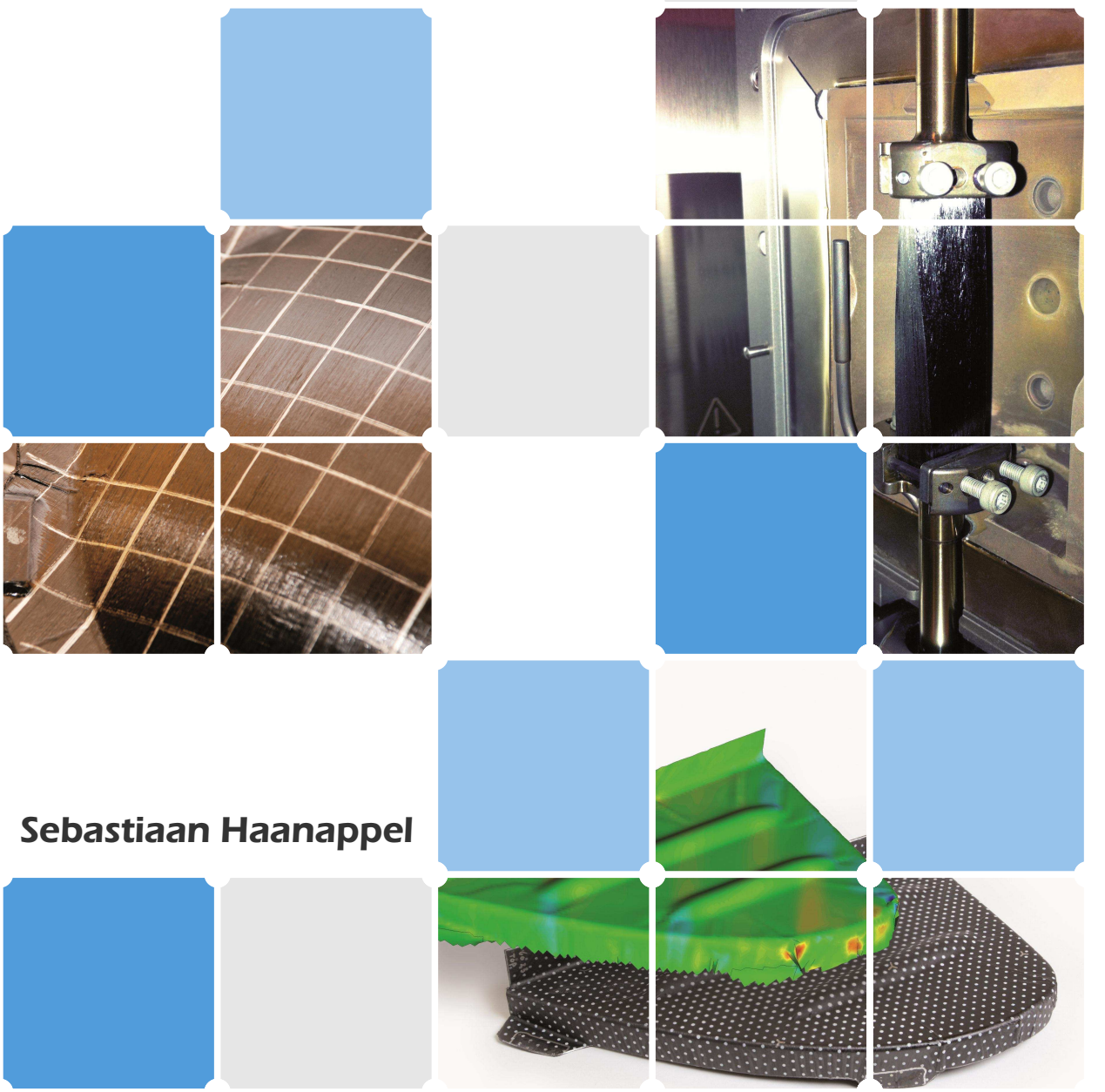

Sebastiaan Haanappel

FORMING OF UD FIBRE REINFORCED THERMOPLASTICS

A CRITICAL EVALUATION OF INTRA-PLY SHEAR

Sebastiaan Haanappel

De promotiecommissie is als volgt samengesteld:

Voorzitter en secretaris:
prof.dr. F. Eising — Universiteit Twente

Promotor:
prof.dr.ir. R. Akkerman — Universiteit Twente

Leden (in alfabetische volgorde):
prof.dr.ir. A.H. van den Boogaard — Universiteit Twente
em.prof.dr.ir. L.J. Ernst — Technische Universiteit Delft
prof.dr.-ing.dipl.-wirt.ing. T. Gries — RWTH Aachen University
prof.dr.ir. F.J.A.M. van Houten — Universiteit Twente
prof.dr.ir. J.W.M. Noordermeer — Universiteit Twente

This research project was financially supported by the ThermoPlastic composite Research Center (TPRC).

Forming of UD fibre reinforced thermoplastics: a critical evaluation of intra-ply shear,
Haanappel, Sebastiaan Pieter
PhD Thesis, University of Twente, Enschede, the Netherlands
April 2013

ISBN 978-90-365-3501-4
DOI 10.3990/1.9789036535014

Printed by Ipskamp Drukkers B.V., Enschede, the Netherlands

Front cover design is inspired by a Studio MAD design for TPRC.

FORMING OF UD FIBRE REINFORCED THERMOPLASTICS

PROEFSCHRIFT

ter verkrijging van
de graad van doctor aan de Universiteit Twente,
op gezag van de rector magnificus,
prof.dr. H. Brinksma,
volgens besluit van het College voor Promoties
in het openbaar te verdedigen
op vrijdag 12 april 2013 om 14:45 uur

door

Sebastiaan Pieter Haanappel

geboren op 28 maart 1983

te Berkel en Rodenrijs

Dit proefschrift is goedgekeurd door de promotor:

prof.dr.ir. R. Akkerman

Summary

Composite materials are a serious competitor for lightweight metals used in the aerospace and automotive industry. Uni-directional (UD) carbon fibre reinforced thermoplastics are favoured due to their high specific strength and stiffness, but also their good toughness, impact and chemical resistance properties. By heating UD reinforced thermoplastic laminates sufficiently above the melting point of the polymer, these can be stamp-formed to relatively complex geometries. The product is released after a relatively short cooling time. Hence, high production rates can be achieved, which makes this process very appropriate for the large volume production of high performance thin-walled products of complex shapes.

Nevertheless, process-induced defects such as wrinkling are frequently encountered, which disqualify the final product. A thorough understanding of the deformation behaviour of UD laminates is required to anticipate those defects, which is therefore one of the objectives in this research. Forming simulation tools can be employed in the product design phases to anticipate the defects observed, ultimately leading to a reduction in product development costs. The predictive capability of forming simulations was therefore carefully analysed.

Forming an initially flat laminate to a doubly curved surface invokes in-plane and out-of-plane deformations, such as intra-ply shear, inter-ply slippage, and bending. These are described with constitutive models, which require material data input. The sensitivity of composite forming predictions to this input was firstly investigated for a dome-shaped geometry. The resulting product shape was found to be determined by a delicate balance between the mechanisms considered, which highlights the importance of a thorough material characterisation.

Wrinkle-free forming of UD laminates to doubly curved surfaces requires in-plane deformations of the plies, in particular by shear. The work therefore focuses on the intra-ply shearing mechanism, where fibres slide parallel to each other. A new shear characterisation test for UD fibre reinforced thermoplastics was proposed. Torsion bar specimens from polyetheretherketone (PEEK) with a UD carbon fibre reinforcement (UD-C/PEEK) were subjected to oscillating loads in order to determine the dynamic shear moduli from the linear visco-elasticity theory. The composite system shows a predominantly elastic behaviour for small strains, which is attributed to multiple fibre-fibre interactions. A low temperature and frequency dependency was found as well. The latter indicates the presence of yield behaviour at larger strains.

Forming experiments were conducted with quasi-isotropic UD-C/PEEK laminates on a representative product geometry used in the aerospace industry: a wing stiffening rib. These laminates are sensitive to wrinkling near areas with double curvature. Limited intra-ply shear strains develop in the final stage of forming, where further bending and wrinkling are prohibited by the tooling. The formability issues of the UD-C/PEEK material are explained by the relatively high resistance to intra-ply shear.

The wing stiffening rib was used to study the predictive capabilities of finite element based forming simulations. The laminate was modelled by incorporating the characterised behaviour of intra-ply shear and inter-ply friction. The predicted intra-ply shear strain fields and the large wrinkles match well with those observed in the experiments. However, the results were dependent on the unknown bending parameters, for which an extensive characterisation programme is necessary. The small wrinkles observed in practice cannot be predicted with the element size used, however, predicted waviness at the corresponding locations may indicate potential critical spots. The simulations conducted have proven to be instrumental in obtaining a better understanding of the laminate deformations during the stamp forming process. They can be employed for design optimisation, as well as to derive design guidelines in a more general sense.

Samenvatting

Composietmaterialen zijn een veelbelovend alternatief voor lichtgewicht metalen die in de vliegtuig- en automobielindustrie worden toegepast. Thermoplasten met een unidirectionele (UD) koolstof vezelversterking zijn populair vanwege hun hoge specifieke stijfheid en sterkte, maar ook vanwege de uitstekende taaiheid, slagvastheid, en chemische resistentie. Door vezelversterkte thermoplastische laminaten op te warmen tot boven het smeltpunt, kunnen deze gevormd worden tot complexe geometrieën met behulp van het persvormproces. Het gevormde product koelt vervolgens relatief snel af waardoor de warme thermoplast weer stolt. Hierdoor kunnen hoge productiesnelheden gehaald worden die dit proces zeer geschikt maakt voor serieproductie van hoogwaardige dunwandige producten met complexe vormen.

Desalniettemin loopt men relatief snel aan tegen productiefouten, zoals plooien in het gevormde laminaat. Eén van de doelstellingen van dit onderzoek is het verkrijgen van een goed begrip van het deformatiegedrag in UD vezelversterkte thermoplastische laminaten, zodat de ontwerper kan anticiperen op dergelijke productiefouten. De ontwerpfase van een product kan ondersteund worden door simulatiegereedschappen die het persvormproces voorspellen, hetgeen kan leiden tot een kostenbesparing tijdens het productontwikkelingstraject. De voorspellende capaciteit van persvormsimulaties is daarom kritisch geëvalueerd.

Tijdens het vormen van een initieel vlak laminaat naar een dubbelgekromd oppervlak ontstaan laminaatdeformaties 'in het vlak' en 'uit het vlak'. De deformatiemechanismen bestaan uit intralaminaire afschuiving, interlaminaire slip en buiging. Deze worden beschreven met materiaalmodellen die op hun beurt weer materiaalparameters nodig hebben. Voor het vormen van een vlak laminaat naar een dubbelgekromd boloppervlak was de gevoeligheid van de persvormvoorspelling op de materiaalparameters bestudeerd. Het blijkt dat de uiteindelijke vorm wordt bepaald door een delicate balans tussen de beschouwde mechanismen, waarmee de noodzaak voor grondige materiaalkarakterisatie is aangetoond.

Het plooivrij vormen van UD laminaten naar dubbelgekromde oppervlakken is mogelijk als de individuele lagen van het laminaat 'in het vlak' afschuiven. Daarom is in dit werk vervolgens naar longitudinale intralaminaire afschuiving gekeken. Dit is het mechanisme waarbij de vezels parallel langs elkaar glijden. Een nieuwe karakterisatiemethode voor dit afschuivingsmechanisme is geïntroduceerd. De

dynamische afschuivingsmoduli volgens de lineaire viscoelastische theorie kunnen worden bepaald aan de hand van een oscillerend torsie-experiment op staafvormige thermoplastische proefstukken met een UD vezelversterking. Torsieproefstukken van polyetheretherketone (PEEK) met een UD koolstof vezelversterking (UD-C/PEEK) zijn getest. Dit composietmateriaal laat een voornamelijk elastisch gedrag zien bij kleine rekken, hetgeen kan worden toegeschreven aan de vele vezel-vezel interacties. Een lage temperatuur- en frequentieafhankelijkheid zijn gemeten, waarvan dat laatste een aanwijzing is voor vloeigedrag bij grotere vervormingen.

Persvormexperimenten met quasi-isotrope UD-C/PEEK laminaten zijn uitgevoerd op een representatieve productgeometrie uit de vliegtuigindustrie: een vleugelverstijvingsrib. Deze laminaten zijn gevoelig voor plooivorming in en rondom gebieden met dubbelgekromde oppervlakken. Wanneer de ontwikkeling van plooivorming wordt tegengehouden in de eindfase van het proces door de sluitende maldelen, zal beperkte intralaminaire afschuiving optreden. Deze beperkingen in vervormbaarheid van de laminaten zijn het gevolg van de relatief hoge weerstand tegen intralaminaire afschuiving.

Deze vleugelverstijvingsrib is tevens gebruikt om de voorspellingsmogelijkheden van de eindige-elementensimulaties te bestuderen voor het persproces. De gekarakteriseerde intralaminaire afschuiving en interlaminaire wrijving zijn verwerkt in het gemodelleerde laminaat. De voorspellingen van intralaminaire rekvelden en grote kreukels komen overeen met de experimentele bevindingen in het product. De resultaten zijn wel afhankelijk van de onbekende buigingseigenschappen van het materiaal, waarvoor een toekomstig uitgebreid karakterisatieprogramma nodig zal zijn. De gebruikte elementgrootte kunnen de kleinere kreukels in het product niet representeren, al kunnen de voorspelde golfjes in het elementenrooster wel dienen als een indicatie voor potentiële probleemgebieden. De uitgevoerde simulaties hebben hun meerwaarde bewezen voor het verkrijgen van een beter begrip van laminaatdeformaties tijdens het persvormproces. Ook kunnen dergelijke simulaties gebruikt worden voor productoptimalisatie en het ontwikkelen van algemene ontwerpregels.

Contents

Chapter 1

Introduction

Composite materials are a good alternative for lightweight metals used in load-bearing structures. The aerospace and automotive industry increasingly apply composite materials in their structural designs, since weight reduction in combination with excellent structural properties can be achieved. Till the year 2000, up to 15% [1] of the total volume in commercial aircraft was represented by continuous fibre reinforced polymers (CFRPs). These materials have been increasingly applied ever since. Whereas CFRPs accounted for 12% of the total weight of the Boeing 777 commercial airplane, the recently introduced Boeing 787 Dreamliner [2] in figure 1.1 already contains a 50% fraction of composite materials.

The high strength-to-weight ratio of composite materials is realised by combining stiff and strong fibrous reinforcements with a more compliant matrix material. Figure 1.2 shows a small selection of the many types of reinforcements available. Dry fabrics are, for example, available as braids, textiles or woven fabrics, and non-

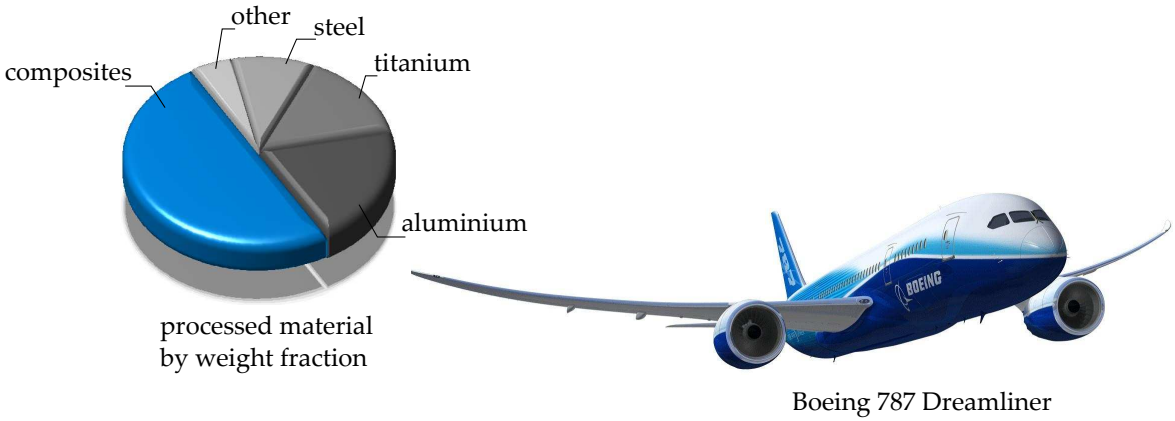

Figure 1.1 *Weight fractions of materials processed in the Boeing 787 Dreamliner, source: [2]. Photo courtesy of Boeing.*

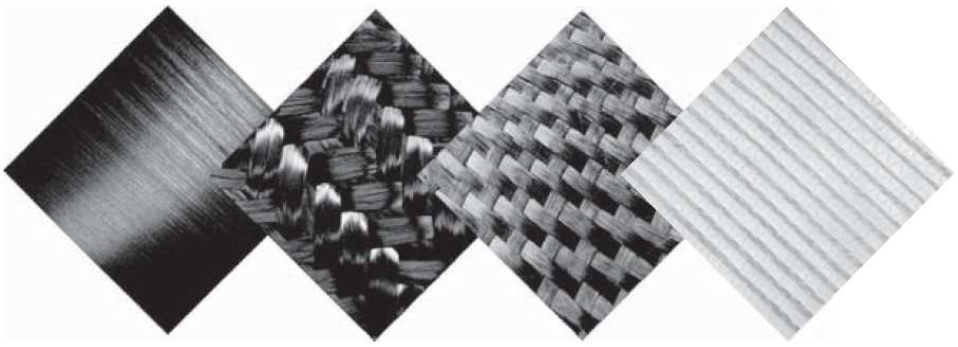

Figure 1.2 *Several types of continuous fibre reinforcements.*

crimp fabrics. After a draping process, liquid composite moulding techniques can be applied to impregnate matrix material such as uncured epoxies. Solidification is realised by a cross-linking process, which is activated or accelerated at elevated temperatures. Using epoxy pre-impregnated (pre-pregs) sheets [3] involves a less complex impregnation process. After draping the pre-preg sheets to the aimed geometry, a curing cycle at a high pressure is usually performed in an autoclave.

Fast production rates can be achieved by using thermoplastic matrix materials. These exhibit fluidic properties sufficiently above the melting temperature and solidify during cooling. High cooling rates are possible, to be tailored to the required degree of crystallisation in the polymer. Excellent properties result from the combination of high performance polymers such as polyphenylenesulfide (PPS), polyetherketoneketone (PEKK), or polyetheretherketone (PEEK), together with a carbon or glass fibre reinforcement. These composites are attractive for application in the civil and military aerospace industry due to the high stiffness, fracture toughness, compressive strength, and good impact, fatigue and chemical resistivity properties. Another advantage is the ability to re-melt, which widens the possibilities in product and production process design. Joining or reshaping can be realised by re-melting the semi-finished product locally or globally. For example, the stamp forming technique can be utilised to form a hot laminate into a complex geometry. Another promising technique is over-moulding, where pre-shaped sheets are stiffened in a second stage by over-moulding resin-rich ribs [4].

The current production techniques, but also the design strategies, need to reach a higher level of maturity to achieve a broader implementation of thermoplastic composite structures [5]. This must be accompanied by the development of new innovative technologies. An example is the development of integrally stiffened thermoplastic panels [6] as these fully exploit the design flexibility offered by thermoplastic composites, which makes them a cost-effective replacement to conventional

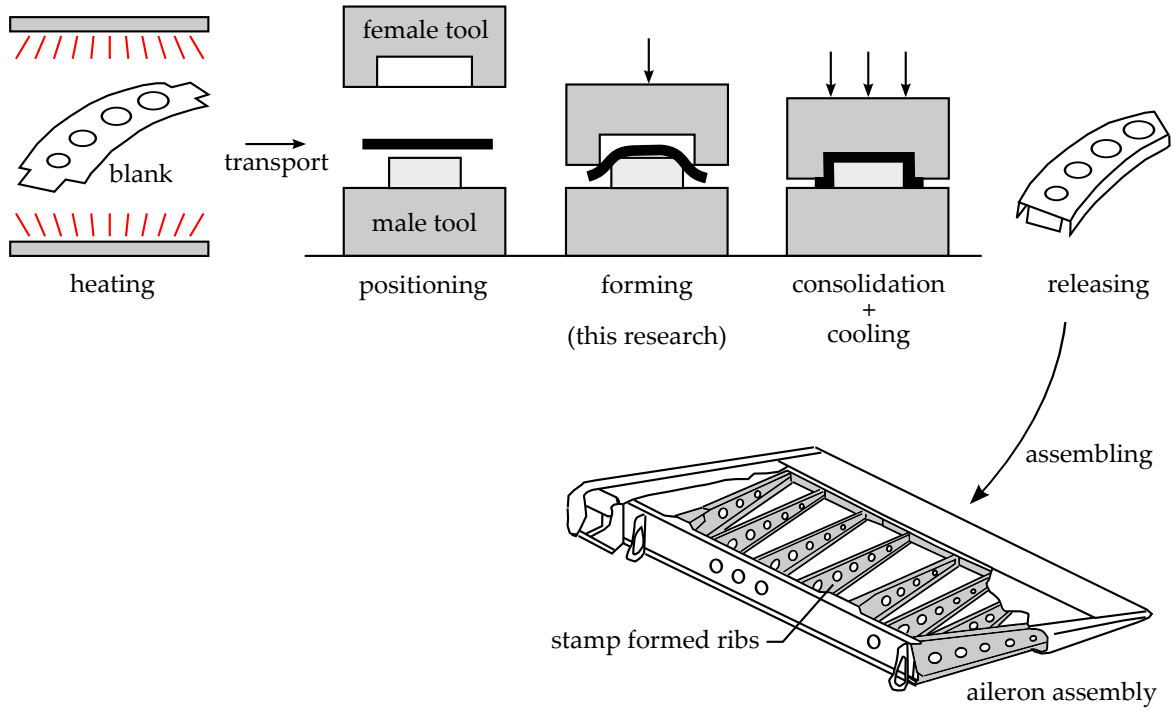

Figure 1.3 *The stamp forming process [8] and the integration of products into structural assemblies.*

structures. Achieving a higher technology readiness level is a major objective of the recently initiated ThermoPlastic composite Research Center (TPRC) [7]. The Complex Stamp Forming project is one of the road map projects of TPRC, of which part of the work is described in this thesis.

1.1 Stamp forming

The stamp forming process is ideally suited to the large volume production of thin-walled thermoplastic composite products with complex shapes. The process involves a small number of steps, as shown in figure 1.3. Usually, a blank is cut from a pre-consolidated laminate that consists of a stack of differently oriented uni-directional (UD) or textile fibre reinforced plies. The blank is positioned within a gripping frame and transported to a heating device, such as an infra-red oven. The blank is transported towards the tooling, after a sufficiently high temperature above the polymer melting point has been reached. The tooling consists of a positive male and a negative female part. Both matched-metal and rubber-metal configurations are used in practice, for which at least one of the tools is usually pre-heated to control the cooling process of the formed laminate. The blank is formed by closing the tooling, after which a high consolidation pressure is applied. The formed blank is released

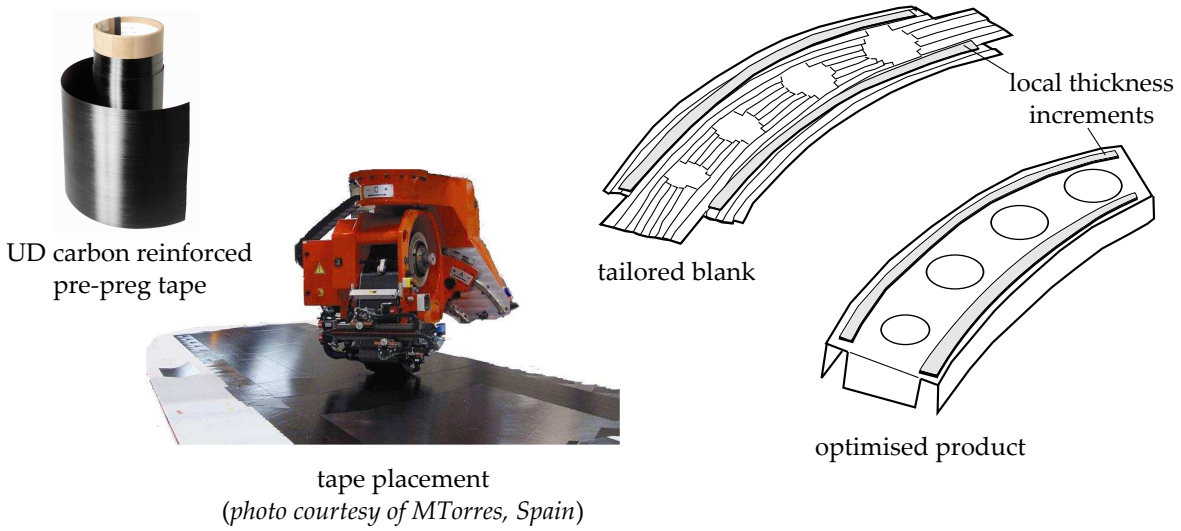

Figure 1.4 *Tailored blank manufacturing by tape-placing the UD reinforced pre-preg tapes.*

after 1 to 2 minutes of cooling. Subsequently, a trimming operation is applied to remove the excess material.

Relatively simple geometric parts with single curvature are manufactured with this process, such as clips and brackets [9]. Stamp forming is also applied to produce complex-shaped parts with double curvature, such as stringers and ribs [10]. These components are subsequently assembled in a larger structural assembly, as for example shown in figure 1.3 as well. Another example is the wing-fixed leading edge of the Airbus A380, where press-formed ribs are welded to a thermoplastic skin [11].

1.2 Motivation and objective

In order to increase the percentage of thermoplastic composites in primary load-bearing structures, it is necessary to optimise the component designs. UD fibre reinforcements are favoured due to their high mechanical properties (see table 1.1 in the appendix of this chapter). Moreover, their availability in pre-preg tape form increases the possibilities for design optimisation. For example, tape-placement techniques can be utilised to produce tailored lay-ups [12] in terms of orientation and thickness. As a result, the optimum fibre paths in a stamp-formed product can be controlled at the blank level already by locally tailoring the lay-up and thickness of the laminate preform, as shown by an example in figure 1.4.

The aerospace industry mainly applies UD reinforced laminates having at least four unique fibre orientations. An example of an eight-layered quasi-isotropic lay-up is

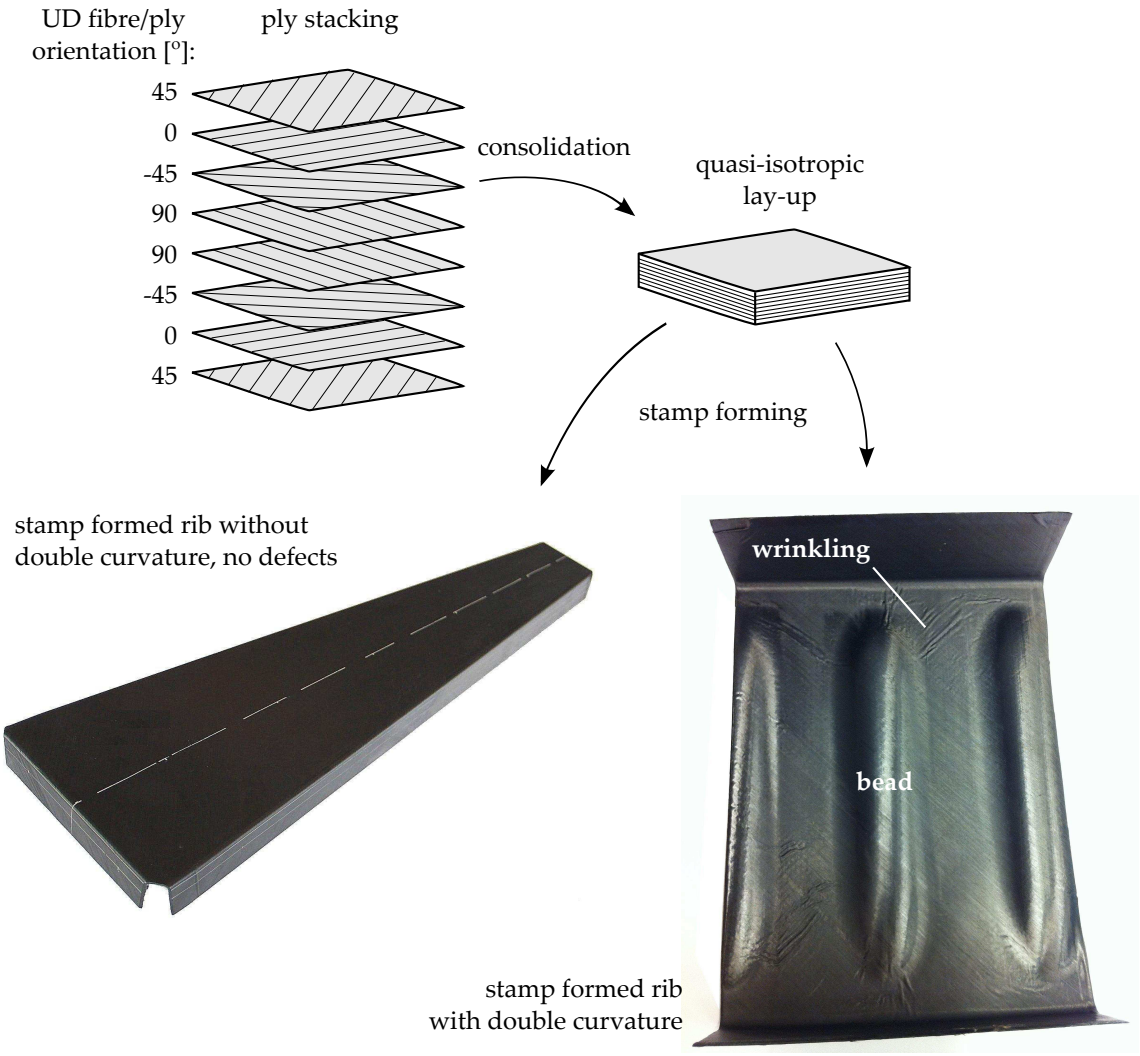

Figure 1.5 *Quasi-isotropic UD reinforced laminates formed into: stiffening rib with single curvature (left) and a part of a stiffening rib with beads, which adds double curvature (right).*

shown in figure 1.5, which is notated as $[45,0,-45,90]_S$. The number of plies is usually tailored to the product design requirements. These lay-ups are favoured due to the reasonable in-plane and out-of-plane stiffness properties in all loading directions, which also makes stress engineering relatively straightforward. These materials, however, become a serious competitor for the conventional lightweight metals when the product involves tailored fibre paths, as was illustrated in figure 1.4.

Quasi-isotropic UD reinforced laminates successfully form to geometries with singly curved areas, as shown for the rib on the left-hand side in figure 1.5. However, optimised product designs may involve doubly curved surfaces. When a flat laminate is formed to a doubly curved surface, it must deform in-plane and/or out-of-plane

by a combination of intra-ply shear, inter-ply slippage and bending. An example of a rib with integrated beads is shown on the right-hand side of figure 1.5. Severe wrinkling (an out-of-plane mechanism) occurs near the doubly curved surfaces. Process-induced defects like these are often encountered during the forming of UD reinforced laminates. Such defects lead to a knock-down of the product's in-service performance. The local thickness increments caused by the wrinkle also result in poorly consolidated spots elsewhere in the product and possibly mould damage in case of matched-metal tooling. A thorough understanding of the deformation behaviour of UD laminates is required to anticipate on such defects. Wrinkle-free forming of UD laminates to doubly curved surfaces can be achieved when the plies deform in-plane under shear. The intra-ply shearing mechanism is therefore focussed on in this thesis.

During the development process of a product, a number of phases can be distinguished [13], as schematically shown in figure 1.6. Ideally, conceptual design, embodiment design and detailed design are sequential phases of a generic product development process, followed by prototype manufacturing and testing. In practice, the early phases are repeatedly addressed with modification requests resulting from later phases. For example, forming issues encountered in the testing phase may lead to expensive tool modifications to be conducted in the detailed design phase. To minimise the associated product development costs, forming simulation tools can be employed to predict the production problems early in the design process. These tools can also be applied to develop design guidelines to be used in the earlier design phases. Currently, the predictive capabilities and limitations of such tools are unknown, which is therefore examined in this thesis as well.

In summary, the objectives of the research reported in this thesis are:

- To obtain a profound understanding of the deformation behaviour in UD reinforced laminates as these appear during the forming process, with the focus on the intra-ply shear mechanism.
- To assess the predictive capabilities of forming simulations for continuous fibre reinforced thermoplastics.

The findings will support the product development processes in industry, which aim to optimise the design with respect to formability and structural performance.

1.3 Outline

Figure 1.7 shows the outline and the scope of the research presented in this thesis. Chapter 2 starts with a brief overview of previous work that is related to the forming of UD reinforced laminates. Relevant laminate deformation mechanisms and

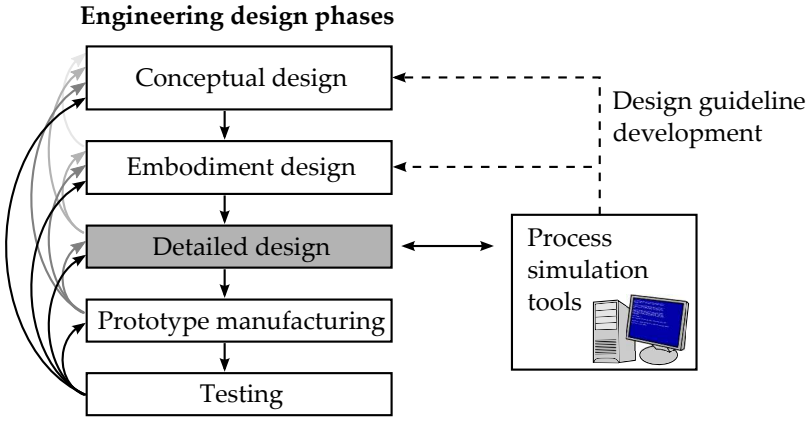

Figure 1.6 *Engineering design phases in the product development process.*

their characterisation are discussed. A sensitivity study is conducted to investigate the effect of material parameter input on the forming predictions. Forming experiments are performed for validation purposes and to highlight the forming issues encountered.

Forming simulation models need to be supplied with accurate material characterisation data. Constitutive models are employed to describe the intra-ply shear, bending, and friction mechanisms of the laminate to be formed. Chapters 3 and 4 deal with the intra-ply shear characterisation. The reader is referred to the publications of Sachs *et al.* [14] and Ten Hove [15] for information regarding the characterisation of the friction and bending mechanisms, respectively.

Chapter 3 reviews the available shear characterisation methods, after which a new test method is introduced for use in a standard rheometer. Rheological properties can be determined by subjecting a specimen to torsional loads. The implementation of this test is presented in chapter 4. UD carbon fibre reinforced PEEK (UD-C/PEEK) is characterised with torsion bar specimens. Measurements in the frequency domain are critically evaluated, after which a translation of the results to the transient domain is derived.

Chapter 5 investigates the forming behaviour of UD reinforced thermoplastic laminates experimentally for a representative product geometry used in the aerospace industry. The predictive capabilities of forming simulations in combination with material characterisation data are subsequently evaluated.

Chapters 2 to 5 are reproduced from research papers, which implies that some introductory and theoretical parts are multiple times addressed. The chapters are, however, self-contained and can be read as such. The results of these chapters are combined and discussed in chapter 6 with respect to the objectives of this research, after which the conclusions and recommendations are presented in chapter 7.

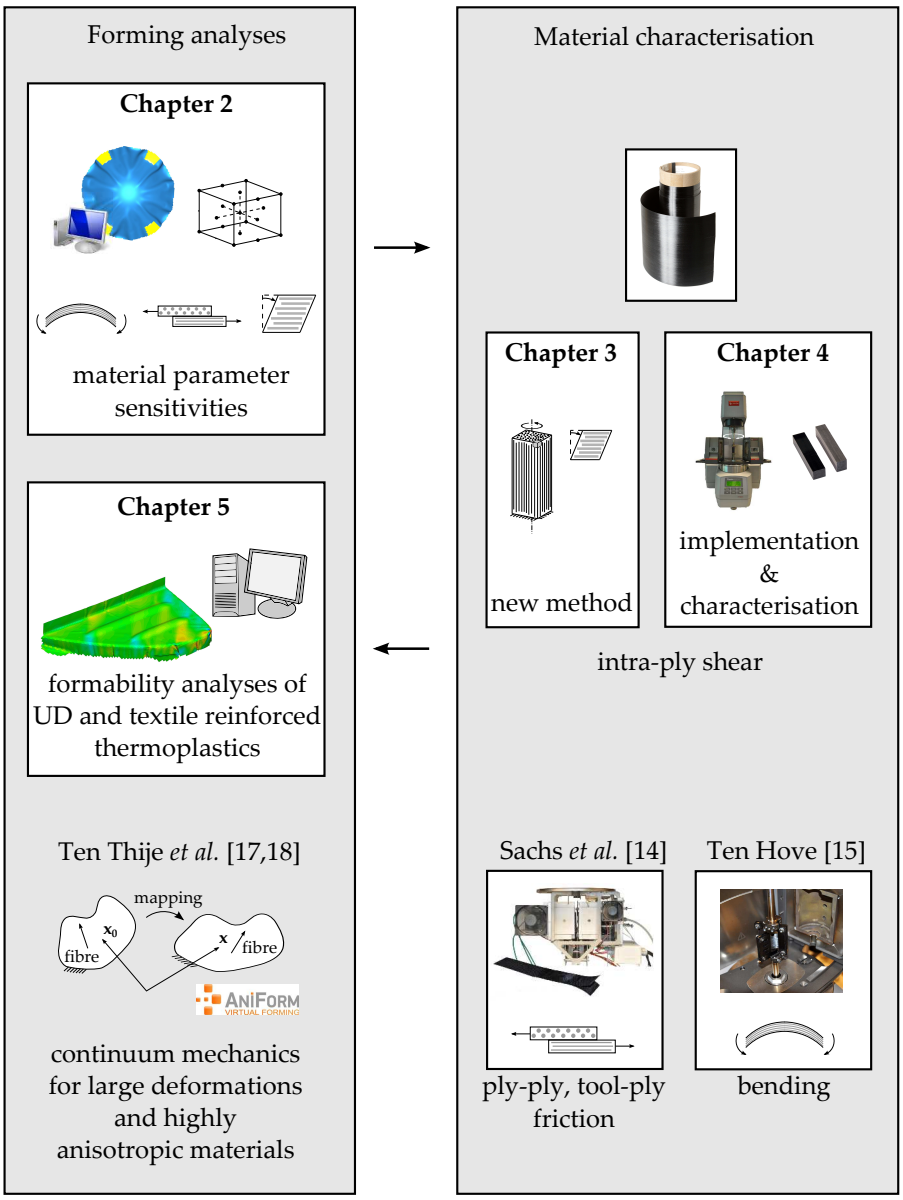

Figure 1.7 *Scope and chapter outline.*

The AniForm [16] software was utilised to perform the iso-thermal forming simulations in chapters 2 and 5. The reader is referred to the publications of Ten Thije *et al.* [17, 18] for the underlying continuum mechanics, which were especially developed to correctly describe large deformations of highly anisotropic materials.

References

[1] G. Reinhart and C. Ehinger. Novel robot-based end-effector design for an automated preforming of limb carbon fiber textiles. In G. Schuh, R. Neugebauer, and E. Uhlmann, editors, Future Trends in Production Engineering, Proceedings of the First Conference of the German Academic Society for Production Engineering (WGP), 131–142, 2013.

[2] Boeing website. *http://www.boeing.com/commercial/787family/programfacts.html*. *Visited: January 2013*.

[3] Y.R. Larberg. Forming of Stacked Unidirectional Prepreg Materials. Ph.D. thesis, KTH Engineering Sciences, 2012.

[4] L.M. Sherman. The new lightweights: Injection molded 'hybrid' composites spur automotive innovation. *Plastics Technology*, **58**(11):27–31, 2012.

[5] A. Rubin. Thermoplastic composites for aerospace structures. In H. Borgmann, editor, Internation Conference & Exhibition on Thermoplastic Composites, 45–47. ITHEC, WFB Wirtschaftsförderung Bremen GmbH, 2012.

[6] A. Offringa. Integrally stiffened thermoplastic skin panels. In H. Borgmann, editor, Internation Conference & Exhibition on Thermoplastic Composites, 56–59. ITHEC, WFB Wirtschaftsförderung Bremen GmbH, 2012.

[7] TPRC website. *http://www.tprc.nl*.

[8] A.R. Offringa. Thermoplastic composites - rapid processing applications. *Composites Part A: Applied Science and Manufacturing*, **27**:329–336, 1996.

[9] A. Deterts, A. Miaris, and G. Soehner. Serial production of thermoplastic CFRP parts for the Airbus A350 XWB. In H. Borgmann, editor, Internation Conference & Exhibition on Thermoplastic Composites, 60–63. ITHEC, WFB Wirtschaftsförderung Bremen GmbH, 2012.

[10] Dutch Thermoplastic Components (DTC) website. *http://www.composites.nl/products/aerospace-structures/*. *Visited: January 2013*.

[11] A. Offringa. Thermoplastics in aerospace, a stepping stone approach. In H. Bersee and G. Niño, editors, Proceedings of the first CETEX conference, 1–13, 2006.

[12] A. Burkhart and D. Cramer. Continuous-fibre reinforced thermoplastic tailored blanks. *JEC Composites Magazine*, **43**(22):41–43, 2006.

[13] R. Akkerman, B. Rietman, S. Haanappel, and U. Sachs. Towards design for thermoplastic composites manufacturing using process simulation. In H. Borgmann, editor, International Conference & Exhibition on Thermoplastic Composites, 78–82. ITHEC, WFB Wirtschaftsförderung Bremen GmbH, 2012.

[14] U. Sachs, R. Akkerman, S.P. Haanappel, R.H.W ten Thije, and M.B. de Rooij. Friction in forming of UD composites. In G. Menary, editor, the 14th International ESAFORM Conference on Material Forming, volume 1353 of *AIP Conference Proceedings*, 984–989. American Institute of Physics, 2011.

[15] C.H. ten Hove. Bending of CF/PEEK prepregs. Master's thesis, University of Twente, 2012.

[16] AniForm Virtual Forming. *http://www.aniform.com*.

[17] R.H.W. ten Thije. Finite element simulations of laminated composite forming processes. Ph.D. thesis, University of Twente, 2007.

[18] R.H.W. ten Thije, R. Akkerman, and J. Huétink. Large deformation simulation of anisotropic material using an updated Lagrangian finite element method. *Computer Methods in Applied Mechanics and Engineering*, **196**(33-34):3141–3150, 2007.

[19] TenCate material datasheets. *http://www.tencate.com/emea/aerospace-composites/default.aspx*, 2013.

1.A Mechanical properties of thermoplastic composites

Table 1.1 *Indicative mechanical properties (in fibre or weft direction) of continuous fibre reinforced thermoplastics: UD versus textile reinforcements, source: TenCate Advanced Composites [19]. C = Carbon, G = Glass.*

	UD reinforced		textile reinforced		
Material	Cetex® Thermo-Lite® 1467I carbon AS4-PEEK	Cetex® Thermo-Lite® 1466P carbon AS4-PPS	Cetex® 5HS T300J carbon fabric-PEEK	Cetex® 5HS T300J carbon fabric-PPS	Cetex® fiberglass 8HS US7781-PPS
Reinforcement architecture	UD-C	UD-C	5HS-C	5HS-C	8HS-G
Matrix	PEEK	PPS	PEEK	PPS	PPS
Tensile strength [MPa]	1930	2045	840	759	348
Tensile modulus [GPa]	132	127	57	54	22
Compression strength [MPa]	1253	1117	595	642	335
Compression modulus [GPa]	116	118	50	52	25
Shear strength [MPa]	83	77	162	119	93
Max. in-service temperature [°C] for aerospace applications	130	80	130	80	80

Chapter 2

Material parameter sensitivities in composite forming simulations*

Abstract

Forming thin-walled products with composite materials is often accompanied by process-induced defects such as wrinkling. Simulations can be utilised to minimise these defects, but require material property data for the intra-ply shear, bending, and inter-ply friction mechanisms. It is not straightforward to make a proper selection for the material data with the large variety in characterisation methods, constitutive models, and the data available. A sensitivity study was conducted to show the effects of material parameter combinations on the forming predictions. The forming process of a quasi-isotropic laminate into a doubly curved dome geometry was considered. The predicted shape distortions of the laminate were quantified with a tool-blank mismatch number. An analysis of variance showed that this number is significantly affected by the parameters for bending, shear, and the combination of bending with friction. Forming experiments were conducted for validation purposes. A number of wrinkles were observed in practice, which run from the edge of the product towards its centre. Agreement was found with the simulations, depending on the parameter input used. It is concluded that the predicted wrinkle patterns are determined by a delicate balance between the mechanisms considered, which highlights the importance of obtaining reliable material parameter input.

*Reproduced from: S.P. Haanappel, R.H.W. ten Thije, R. Akkerman. Material parameter sensitivities in composite forming simulations. Submitted to: *Composites Part A: Applied Science and Manufacturing*, **2013**.

2.1 Introduction

Hot stamp forming of fibre reinforced thermoplastic laminates is ideally suited to the production of thin-walled products with complex shapes. Nevertheless, process-induced defects such as local buckling and subsequent wrinkling appear frequently and disqualify the final product. Better anticipation of these defects results in lead-time reductions and can be achieved by predicting such defects in the early product design stages. Numerous forming prediction tools can be utilised to facilitate this.

Forming a flat laminate into a product geometry is accompanied by several deformation mechanisms. These mechanisms are modelled with constitutive models, which include material parameters. Simulations require input data for these parameters, which can be obtained from material characterisation experiments. It is not straightforward to make a proper selection for the material data with the large variety in characterisation methods, constitutive models, and the data obtained. In this chapter, we show to what extent forming predictions are affected by varying the material parameter input. Uni-directional (UD) fibre reinforced thermoplastic laminates with a quasi-isotropic lay-up are considered in this research, however, the analyses can straightforwardly be applied to other materials such as fabrics with or without a polymer constituent.

Firstly, a brief overview of previous work in the area of forming of UD reinforced composites is given. Relevant deformation mechanisms and their characterisation for this UD material are discussed. The forming process of a doubly curved dome is modelled. Simple constitutive models are selected, which are supplied with an educated guess for the material parameter input. Forming experiments were conducted and the results are compared with the initial forming predictions. A sensitivity study is presented in order to analyse the effect of the material parameter input on the predicted product shapes. The results are qualitatively evaluated, followed by a systematic quantitative analysis.

2.2 Forming of UD reinforced thermoplastic laminates

Several production processes can be used to form fibre reinforced thermoplastics into complex shapes. Most of these processes use blanks, which are cut from pre-consolidated laminates. These laminates are manufactured by consolidating a stack of pre-impregnated plies or pre-pregs. The pre-preg contains the uni-directional fibres, which are embedded in a thermoplastic matrix material, as shown in figure 2.1. A forming operation is initiated after the laminate or blank has been heated up sufficiently above the melting temperature of the thermoplastic resin. Diaphragm forming deforms the molten laminate by means of an applied pressure difference in the laminate thickness direction, which could, for example, be applied with the aid

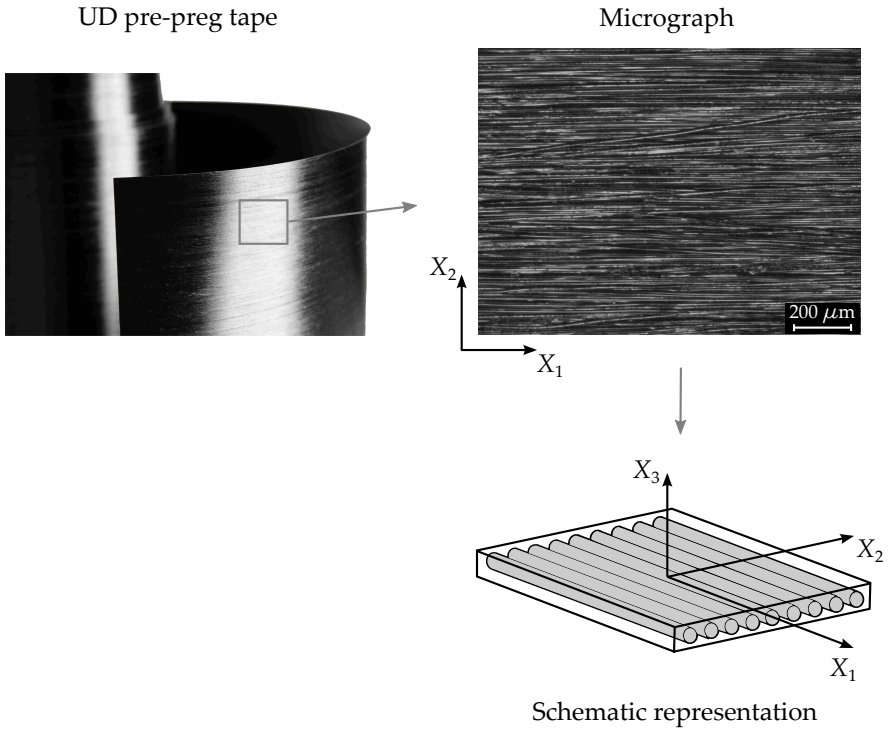

Figure 2.1 *UD carbon pre-preg tape and a micrograph giving an impression of the micro structure. The schematic representation of the fibres is shown as well.*

of an autoclave [1]. Other techniques deal with a stamping device such as a hydraulic press, equipped with matched-metal or rubber-metal die tooling [2, 3].

Gripping systems are necessary to transport the hot blank between the heating area and the tooling. Simple metal grippers can be used that adhere locally to the blank. More sophisticated systems consist, for example, of blank holders that apply a normal pressure to the circumference of a blank, allowing for some control of laminate deformation as was shown by De Luca *et al.* [4] and Rietman *et al.* [5]. An alternative gripping system makes use of polyamide (PA) diaphragms, which are applied to both sides of the blank [2, 6]. Both the laminate and the diaphragms are formed during the process.

Forming prediction tools can be utilised in order to assess the formability of a laminate with respect to a certain tooling geometry. Several approaches can be followed to model the forming process, as briefly outlined in a review by Lim and Ramakrishna [7]. For example, discrete approaches that are based on analytical mapping expressions were used by Tam and Gutowski [8] and Golden *et al.* [9]. The mapping of an initially flat geometry onto a prescribed curved mould surface was in both cases obtained by assuming inextensible fibres and incompressibility. Although it is hard to obtain a unique expression for complex mould surfaces, mapping can still be useful via numerical techniques as demonstrated by Hancock [10] for

hand lay-up. An indication of the fibre direction, inter-ply slippage and thickness distribution can be obtained. Other kinematic draping codes are available such as Pam-QuickForm, with which Vanclooster *et al.* [11] demonstrated the differences between the kinematic and finite element based predictions for a geometry with double and single curvature. The absence of constitutive models in the kinematic approach was shown to yield large deviations between the predicted shear angles and those observed in the experiments. Finite element predictions of the shear angles showed better agreement. Moreover, defects such as wrinkling cannot be modelled with the kinematic approach [12]. In summary, a constitutive model of the material is necessary in order to obtain realistic forming predictions.

The finite element method makes use of discretized domains and is generically applicable to the modelling of complex geometries. It allows for the implementation of constitutive material properties. Much research on especially UD reinforced thermoplastics was conducted in the 80s and 90s of the previous century. Ó Brádaigh and Pipes [13] used an implicit 2D code called FEFORM, which was based on PCFEAP. They used a plane stress element formulation together with a mixed penalty finite element system in order to avoid element locking problems, which develop when element edges are not aligned with the stiff fibre directions. This locking over-predicts the stresses when highly anisotropic materials are modelled. This problem was identified by Yu *et al.* [14] and Simacek *et al.* [15]. Solutions were proposed by Ten Thije and Akkerman [16].

Ó Brádaigh *et al.* [17] demonstrated how the numerical 2D code can be used to understand the observed deformation behaviour of a punched 8 ply UD carbon/PEEK (APC2) laminate. The experimental set-up comprised a punch deformation apparatus in order to punch a laminate with PA diaphragms applied to each side. Grid deformations were predicted and compared with their experimental findings. The wrinkling in practice was compared with the predicted in-plane shear and stress distributions, which show concentrations in the corresponding product areas. From such analyses, it is not known whether these stresses really invoke buckling and subsequent wrinkling. Analyses in 3D involving the bending behaviour of the laminate can be utilised to predict such mechanisms more accurately.

Pickett and De Luca [18] used an explicit 3D code that was based on an extension of PAM-STAMP^{TM4}. De Luca *et al.* [4] applied this software to analyse the formability of a stiffener with doubly curved areas. Two materials were considered: laminates that comprise UD carbon/PEEK (APC2) plies and carbon/PEI (CETEX) fabrics. A matched metal tooling process was considered. Each ply or layer was separately modelled with constitutive material laws to describe the intra-ply and inter-ply deformations. It must be noted that the meshes used were unstructured. This suggests the presence of the intra-ply shear locking problem mentioned earlier. Among others, the effect of blank holders on the wrinkling was investigated. Similar trends were found numerically and experimentally for both materials. However,

the material parameter input used was not specified and its effect on the predicted wrinkling is unknown.

Sensitivity studies can be invoked in order to analyse the sensitivity of forming predictions to the material parameter input. To the author's knowledge, such analyses are not published in the area of composite forming yet. This chapter addresses this topic, using the AniForm 3D forming simulation software. Important deformation mechanisms and their characterisation are briefly reviewed in the next section, prior to the modelling of the forming process itself.

2.3 Deformation mechanisms and characterisation

Several deformation mechanisms are invoked during the forming of UD reinforced laminates. These have been categorised by several authors, for example by Cogswell [19]. Figure 2.2 summarises the mechanisms at the interface and intra-ply levels.

Inter-ply slippage is a mechanism that appears at the interfaces between the distinctly oriented plies. Tool-ply slippage appears at the interfaces between the laminate and the tooling. Several constitutive models have been applied in the literature to describe the measured characteristics [20]. These vary in the assumption of Coulomb or hydrodynamic type of friction. The Newtonian fluid model assumes a viscous film at the interface. The in-plane surface traction τ_{tr} is then simply related to the shear rate $\dot{\gamma}$ in the fluid film and a constant viscosity η:

$$\tau_{\mathrm{tr}} = \eta\dot{\gamma} \qquad \text{with} \qquad \dot{\gamma} = \frac{v_{\mathrm{s}}}{h} \tag{2.1}$$

The shear rate is related to the film thickness h and the slip velocity v_{s} at the interface. An overview of characterisation methods has been given by Sachs *et al.* [21] and Gorczyca-Cole *et al.* [20]. The majority of test set-ups deal with a pull-through mechanism, which allows for both ply-ply and tool-ply characterisation. Variables such as pull-through velocity, normal pressure, and temperature can be controlled. Measured friction parameters are generally set-up dependent. Various benchmark activities [22] have been and are still being conducted in order to understand the variations.

Delamination appears when adjacent plies separate during the forming process. The consolidated plies initially tack to each other due to an adhesive force. A widely accepted test method for its characterisation has not been defined yet. The majority of tack characterisation work is applied to uncured epoxy pre-pregs. This characterisation can be performed according to the standardised ASTM D3167 floating roller peel test as applied by Banks *et al.* [23]. An alternative peel test was developed by Crossley *et al.* [24]. Stiffness and tack properties can be determined as a function of feed rate, compaction force and adherent material. Tack is typically

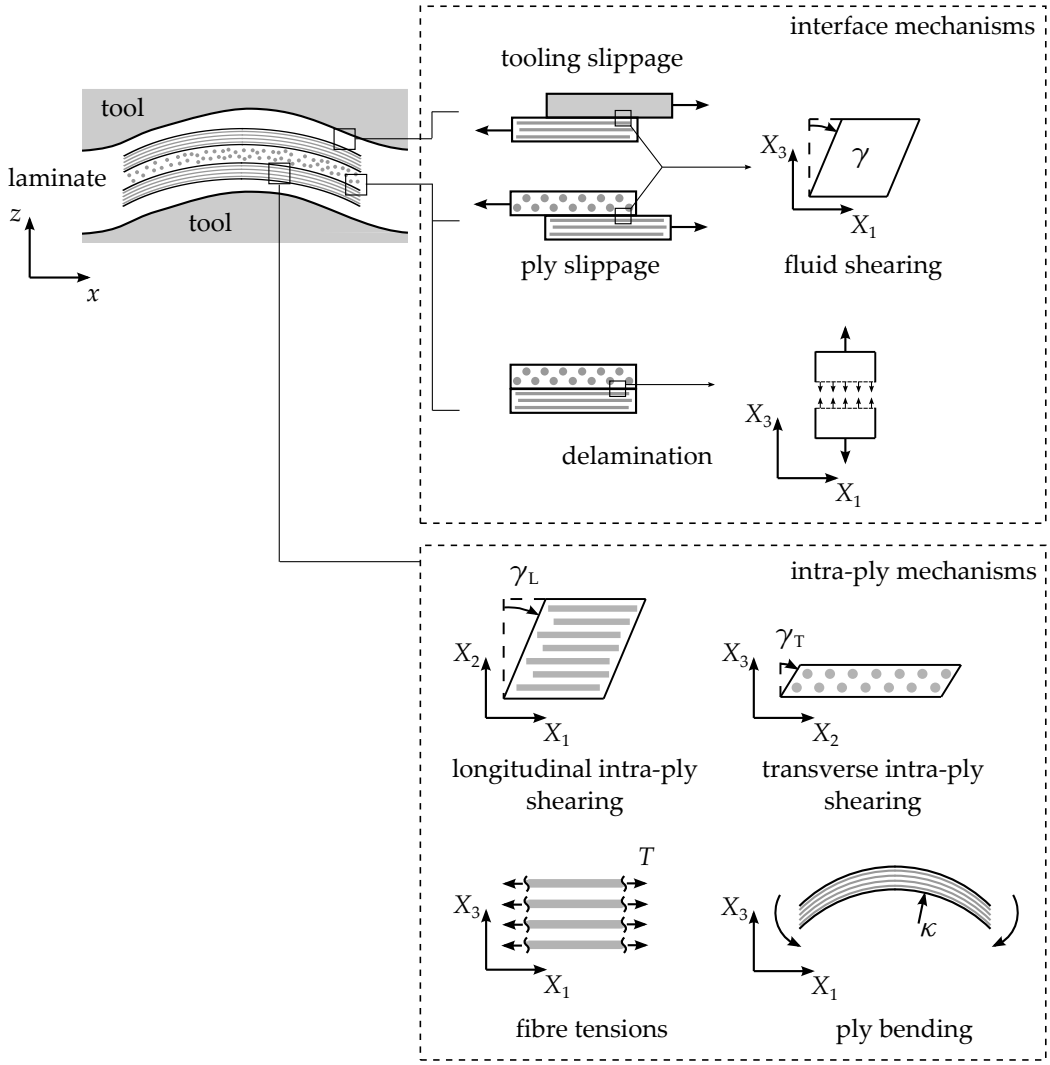

Figure 2.2 *Local forming mechanisms in a laminate comprising UD reinforced plies.*

expressed in terms of peel fracture energy release rates. No tack characterisation data is available yet for UD carbon fibre reinforced polymers at high temperatures.

Longitudinal and transverse shearing mechanisms are considered at the intra-ply level. They are related to the parallel and transverse sliding of the fibres, respectively. Overviews of its characterisation have been given by Advani *et al.* [25], Harrison and Clifford [26], and Haanappel and Akkerman [27]. Many set-ups are able to characterise both the longitudinal and transverse shearing modes. Both responses are generally closely related in terms of trends and magnitudes. Results have been presented by using the linear visco-elasticity theory, but also with models that neglect elastic contributions and consider the viscous part of the response only. For example, Goshawk and Jones [28] used the Newtonian fluid model, and Stanley and Mallon [29] used a shear rate dependent viscosity for their constitutive modelling. Other

authors considered the large deformations and fibre inextensibility of the media by using the Ideal Fibre Reinforced Newtonian fluid Model (IFRM). This model was introduced by Rogers [30]. It involves transverse shearing, longitudinal shearing, and fibre tensioning mechanisms. The simplified form assumes Newtonian viscous behaviour for both shearing mechanisms. The stress $\boldsymbol{\sigma}$ is expressed as:

$$\boldsymbol{\sigma} = -p\boldsymbol{I} + T\hat{\boldsymbol{a}}\hat{\boldsymbol{a}} + 2\eta_{\mathrm{T}}\boldsymbol{D} + 2(\eta_{\mathrm{L}} - \eta_{\mathrm{T}})(\hat{\boldsymbol{a}}\hat{\boldsymbol{a}} \cdot \boldsymbol{D} + \boldsymbol{D} \cdot \hat{\boldsymbol{a}}\hat{\boldsymbol{a}}) \tag{2.2}$$

where p is the hydrostatic pressure, and $\hat{\boldsymbol{a}}$ is a unit vector representing the current direction of the fibre. Transverse and longitudinal shearing are represented by their viscosities η_{T} and η_{L}, respectively. Any loading in the direction of the stiff fibres invokes a fibre tension T. The second order identity tensor and the rate of deformation tensor are represented by $\boldsymbol{I}$ and $\boldsymbol{D}$, respectively. Differences in characterisation set-ups and constitutive modelling resulted in material parameters that vary for 2 till 3 orders of magnitude, as was shown by Harrison and Clifford [26].

Ply bending is the last mechanism considered here. Bending characterisation of UD reinforced melts has been carried out by only a few researchers. A three-point-bending type of mechanism was introduced in hot UD glass fibre reinforced polypropylene (PP) laminates by Martin *et al.* [31]. Large deformations were introduced such that V-bent shapes developed. Their analysis assumed purely viscous intra-ply shearing in the thickness direction for uni-directionally stacked laminates. Bending is modelled often with the assumption of Kirchhof bending in many forming prediction codes. This assumption does not match with the through-the-thickness transverse shearing as observed. Transferring the measured characteristics into forming prediction models is therefore not straightforward. Wang *et al.* [32] developed a test based on large-displacement buckling, which was applied to a UD carbon/epoxy pre-preg. Also here, it is not a trivial exercise to translate the characterisation of the unstable buckling mechanism into constitutive models available in forming prediction codes.

More advances have been made so far in the field of bending characterisation of dry fabrics. A couple of methods characterise a fabric by introducing a bending action that is caused by its own weight [33, 34]. Another example is the Kawabata Evaluation System for fabric bending (KES-FB) [35], which applies a pure bending mechanism to the specimens. As a result of the limited available bending data and the difficulties mentioned above, the linear elasticity theory is often applied to model the bending behaviour. Hooke's law [36] can be used to describe the orthotropic bending properties.

2.4 Forming process of a doubly curved dome

After discussing all mechanisms that play an important role during the forming process of a laminate, it is clear that there is a large variety in characterisation methods, constitutive models applied, and material property data. It is unknown to what extent the material parameters affect the forming predictions. This is analysed here by considering the forming process of a doubly curved dome geometry. Quasi-isotropic $[0, 90, 45, -45]_S$ laminates are considered, which consist of unidirectional AS4 carbon fibres and a polyetherketoneketone (PEKK) matrix material. The forming set-up is shown in figure 2.3, which comprises a male and a female tool with the hot blank or laminate in between. The female tool moves downwards such that the laminate forming process is initiated.

Simple constitutive models were selected in order to model the deformation mechanisms, which have been discussed in the previous section. Initial forming simulations were conducted, based on an educated guess for the material parameter input. Forming experiments were conducted as well, in order to validate the initial simulation qualitatively. In the subsequent section, a sensitivity study is performed to see how deviating material input data affects the overall forming prediction.

2.4.1 Simulation set-up

Simulations were conducted with the AniForm finite element forming simulation software developed by Ten Thije *et al.* [37, 38]. This 3D code makes use of an implicit solution scheme. Together with an appropriate decomposition of the deformation gradient and a proper material update scheme, this software is most suitable for modelling large deformations of highly anisotropic materials.

Figure 2.4 shows the forming simulation set-up schematically. Normal pressures and tractions at the tool-ply interfaces are expected to be low while the laminate is being formed, prior to the application of the consolidation pressure. Minimal tooling deformations are therefore expected. For this reason, both the male and female tool are modelled as rigid surfaces, each discretized with $13 \cdot 10^3$ triangular elements. Quasi-isotropic laminates comprising eight plies were used for the experiments, however, four plies were modelled to reduce calculation times. All four fibre orientations are represented in the model.

Figure 2.4 also shows that each ply is modelled by an assembly of three different element types. Contact detection on both faces of the ply is modelled by two groups of contact elements. Ply deformations are modelled in a decoupled fashion by separately describing out-of-plane and in-plane deformations in order to avoid over-prediction of the bending stiffness [39]. As shown in figure 2.5, a shell element is composed of a Discrete Kirchhof Triangle (DKT) to model ply bending and a

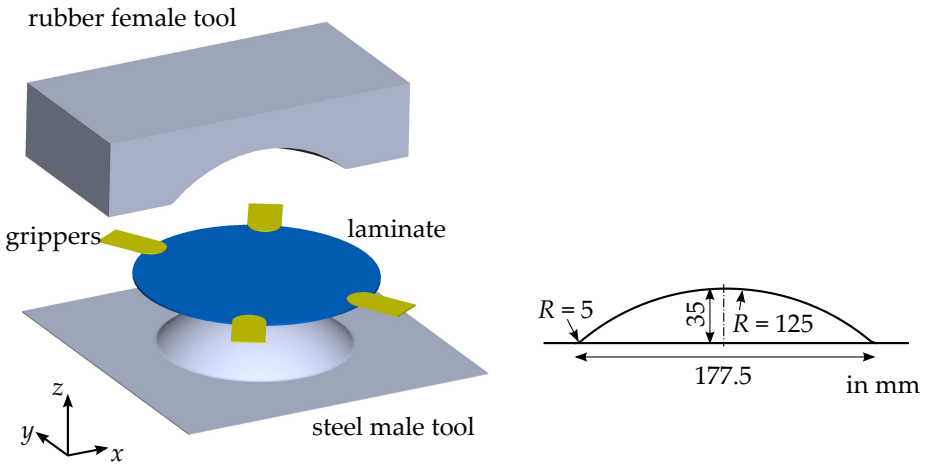

Figure 2.3 *Experimental thermoforming set-up.*

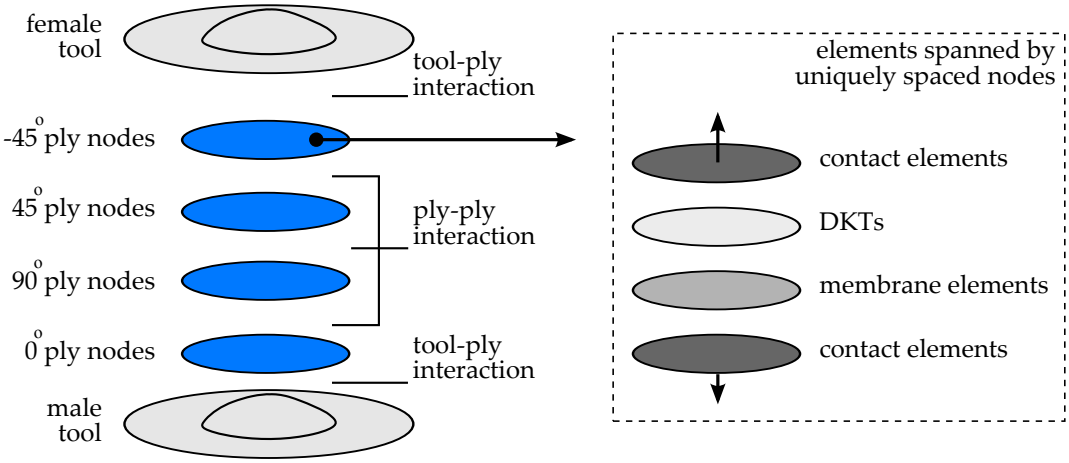

Figure 2.4 *Forming simulation set-up.*

membrane element to model the in-plane behaviour of the ply. Figure 2.5 further shows the degrees of freedom (displacements u and rotations θ) and quadrature points (triangles) used. One quadrature point is used for the membrane elements, whereas a total of six quadrature points is used for the DKT elements: three points in-plane at two positions in the thickness direction. Each element group comprised $16 \cdot 10^3$ elements approximately, such that the total amount of deformable elements summed up to $256 \cdot 10^3$, approximately.

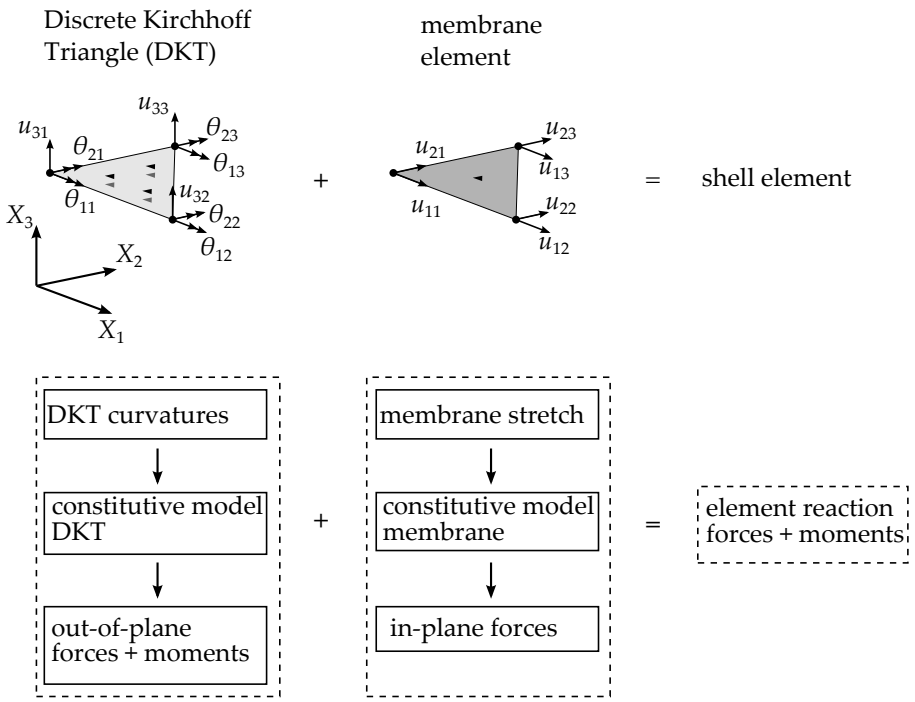

Figure 2.5 *Intra-ply deformations are described by shell elements. The shell element is decoupled by modelling the out-of plane and in-plane mechanisms separately.*

2.4.2 Constitutive modelling

In order to obtain a clear overview of the effects of material parameter input on forming predictions, simple constitutive models were selected to describe the deformation mechanisms. A summary of these models together with the parameter input is given in table 2.1. The orthotropic formulation of Hooke's law [36] was used to model the bending behaviour with the DKT elements. The principle direction of this material model was aligned with the fibre direction in the ply. A lower elasticity modulus was applied perpendicular to the fibre direction to account for its smaller bending stiffness. The material parameters were based on an educated guess, as bending characterisation data for UD carbon reinforced melts is not available. Kirchhof bending was assumed, using a ply thickness of 0.14 mm.

In-plane behaviour was modelled with the IFRM relationship in equation (2.2). Equal longitudinal and transverse viscosities were assumed. The values were based on the upper bound results given in the characterisation method overview of Harrison *et al.* [40]. These experimental results were generated by McGuinness and Ó Brádaigh [41] with the aid of a picture-frame test. The fibres were modelled elastically with an arbitrary but sufficiently large fibre stiffness E_f to yield negligible fibre extension during the simulations.

The Newtonian fluid model in equation (2.1) was selected to model the friction at

the ply-ply and tool-ply interfaces. A film thickness of 7 μm was used, as found in the literature [42]. The Newtonian viscosity was based on the measured neat resin viscosity of PEKK at forming temperatures. Adhesion was modelled as well for which an educated guess for the adhesive tension was set. It is deactivated when the plies are separated by at least 2 mm. Contact logic was modelled with the penalty method. The normal pressure at the contact surface is determined as:

$$\tau_{\mathrm{n}} = E_{\mathrm{p}}\delta \tag{2.3}$$

in which δ is the penetration depth of the surfaces in contact and E_{p} is the penalty stiffness.

In practice, lower temperatures were measured at the locations where laminate grippers adhere, which in turn leads to a more rigid material behaviour. This was modelled by assigning one order of magnitude higher viscosities and moduli at the associated locations in the ply.

2.4.3 Forming prediction

The forming process was simulated by moving the female tool 10 mm/s downwards. An automatic load step size scheme was applied in order to reach optimum

Table 2.1 *Constitutive models and parameters assigned to the virtual plies in figure 2.4.*

Element type and models assigned	Reference	Parameter(s)	Input data
DKTs (bending)			
Orthotropic Hooke	[36]	E_1 [MPa]	250
		E_2 [MPa]	125
		ν_{12} [-]	0.32
		G_{12} [MPa]	100
Membrane elements (in-plane)			
IFRM	eq. (2.2)	$\eta_{\mathrm{L}} = \eta_{\mathrm{T}}$ [Pa·s]	$3 \cdot 10^5$
		E_{f} [GPa]	1.0
Contact elements			
Newtonian fluid	eq. (2.1)	η [Pa·s]	700
		h [μm]	7
Adhesion		Tension [MPa]	0.1
		Deactivation distance [mm]	2.0
Penalty model		E_{p} [N/mm^3]	1.0

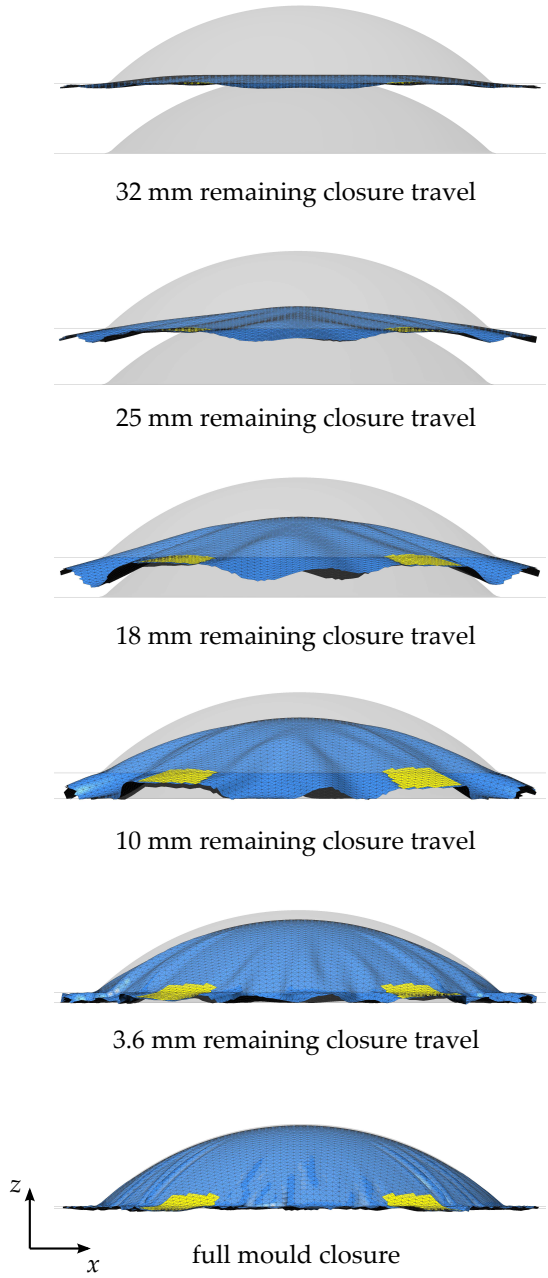

Figure 2.6 *Intermediate forming simulation steps of the doubly curved dome. Table 2.1 lists the material parameter settings used.*

simulation times, typically 4 to 12 hours per simulation with two quad-core Intel Xeon E5620 2.4 GHz processors. Intermediate forming steps are shown in figure 2.6. After first contact is made between the female tool and the outer rim of the blank, the male tool touches the centre of the blank such that deformations start. Major wrinkles develop as the simulation progresses.

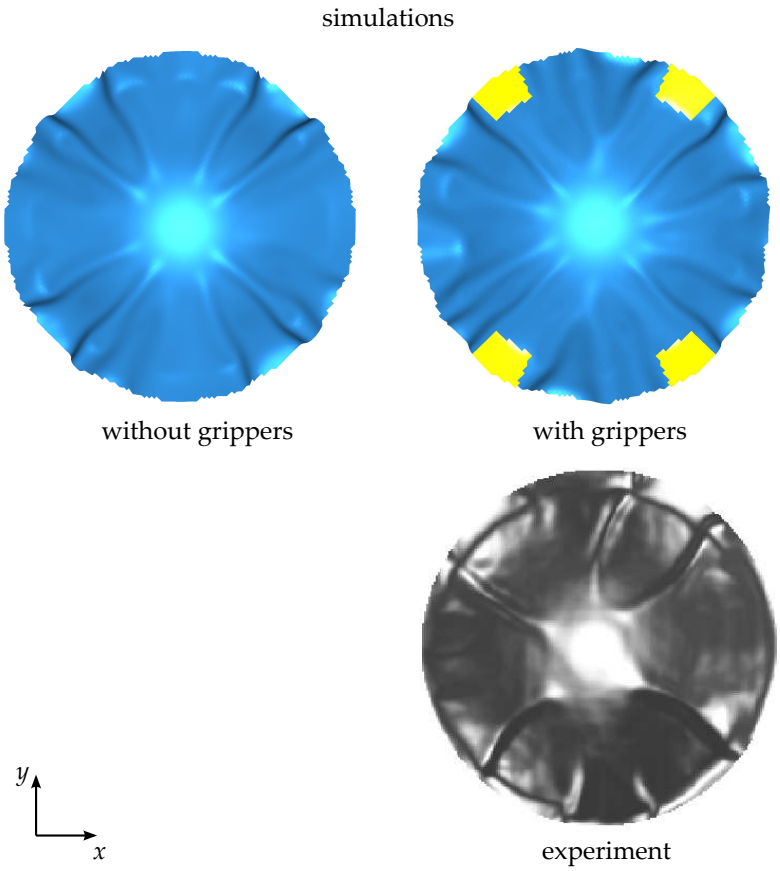

Figure 2.7 *Simulation results at a remaining closure travel of 10 mm and material parameters as shown in table 2.1.*

A good impression of the blank shape development can be obtained by analysing the forming process during the stage with a remaining closure travel of 10 mm. Figure 2.7 shows the top views of the predicted blank shapes. Only the deformations of the top -45° plies are visualised as other plies deform accordingly. Simulations with and without the grippers show that these influence the positions of the wrinkles by pushing them sideways.

2.4.4 Experiments

Forming experiments were conducted in order to validate the forming predictions. The forming set-up in figure 2.3 was used. A stamp forming machine from Pinette Emidecau Industries was made available by Fokker Aerostructures B.V. UD carbon/PEKK pre-preg material with a melting temperature of about 340°C is used. Eight plies were stacked to yield quasi-isotropic $[0, 90, 45, -45]_S$ laminates after consolidation. Averaged ply thicknesses measured 0.14 mm, corresponding to a fibre volume fraction of approximately 60%. Circular blanks with a diameter of 217.5 mm were cut. Line marks were applied in order to obtain an indication of the deformations in the formed parts. Pre-heating is achieved by means of infra-red panels to obtain a blank temperature of 380°C. The blanks were transported to the tooling, which consists of a pre-heated steel male tool and a cold rubber female tool. The hot blanks were formed by the downwards movement of the female tool with a speed of 10 mm/s. Stopping blocks of different heights were positioned between the tooling to prevent complete mould closing in order to track the intermediate blank deformations.

Figure 2.8 shows the forming stages of the quasi-isotropic laminate. The first stage shows severe buckling around the grippers. These areas are mainly turned into wrinkles in the subsequent stage and develop through all plies in the thickness direction of the blank. A small and a large wrinkle develop next to each gripper. The wrinkles are further compressed into the laminate once the tooling is fully closed. Some minor buckled areas in the first stage do not always yield wrinkles. Instead, minimal intra-ply shearing is invoked locally. Figure 2.9 summarises the observed global laminate deformation.

2.4.5 Discussion

The shape of the formed product with a remaining closure travel of 10 mm in figure 2.8 was digitised by means of an in-house developed ultrasonic measurement device. Points were scanned with a 1 x 1 mm spatial resolution. A rendered image was constructed, as is shown in figure 2.7. Large wrinkles are present in both the forming predictions and the experimental results. The simulation without the modelled grippers shows wrinkles on both sides of these grippers, which is in reasonable agreement with the experimental result. The simulation with the modelled grippers shows additional smaller wrinkles, which are partially present in the experimental result. Another publication [43] compared these experiments with the formability of cross-ply laminates. There, small wrinkles were only observed in the outer rim of the product, whereas the interior part was wrinkle-free.

The wrinkles observed are caused by the so-called shear-buckling mechanism [1, 44]. Shear mechanisms invoke compressive forces and buckling appears when a critical

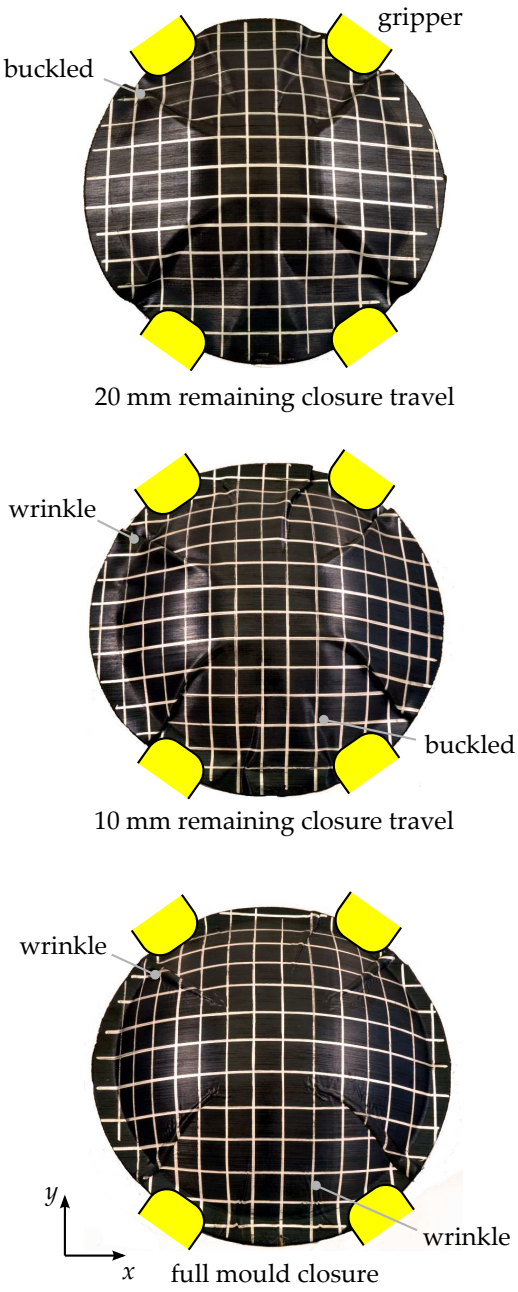

Figure 2.8 *Forming stages of the quasi-isotropic UD carbon/PEKK laminates.*

load is exceeded. This shear-buckling was also observed for cross-ply laminates in the work of Mallon *et al.* [1], who conducted experiments with UD carbon/PEEK (APC2). Hemispherical shapes were formed with the diaphragm technique. Pressures and temperatures were controlled by means of an autoclave. Hou [44] also reported this shear-buckling for uni-directional and cross-ply laminates from UD glass/PP, formed with matched die tooling. Both experimental programmes showed that

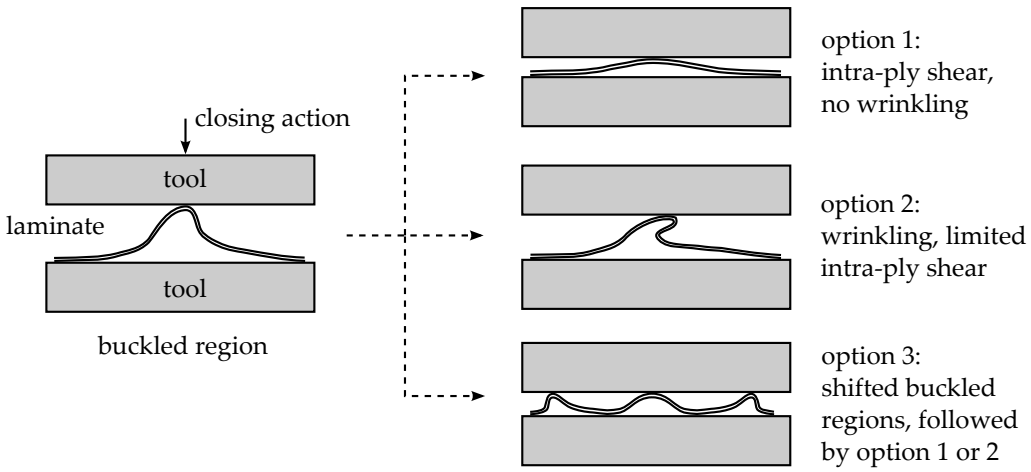

Figure 2.9 *Laminate deformations.*

excess material outside the formed area influences the shear-buckling phenomena. Temperature and blank holder pressures were also shown to have an effect on the wrinkling.

The predicted defects show reasonable agreement with the defects observed in the experiments. A design engineer who conducts the analyses without knowledge of the experimental results may conclude that this product would give formability issues. The next design step could involve modifications of the blank geometry, product geometry, or lay-up. Even another gripping configuration, blank holder system, or an alternative production process can be introduced to prevent the observed defects. However, these considerations are quite premature, as it is unknown how sensitive the forming predictions are to the material parameter input used.

2.5 Sensitivity study

A sensitivity study was performed to reveal the effects of varying material input data on the overall forming prediction. The Design of Experiments (DoE) methodology was applied. Simulations were conducted with different material parameter input combinations, followed by a qualitative and a quantitative analysis.

2.5.1 Design of Experiments (Simulations)

The parameters considered as design variables are the longitudinal shear viscosity, elastic bending parameters, and the Newtonian viscosity for friction. These parameters were varied for several orders of magnitude, as listed in table 2.2. Note

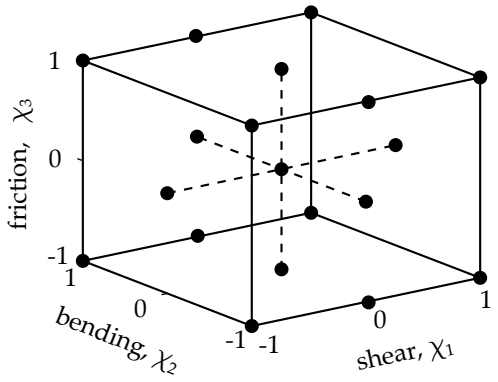

Figure 2.10 *Design space for the sensitivity study. Each point represents a simulation with a certain combination of material parameters.*

that the values are equally distributed in the logarithmic space. The levels are indicated as small, medium, and large, which corresponds with the -1, 0, and 1 codes, respectively. Simulations were carried out for several combinations of these levels. Figure 2.10 shows the considered face-centred cube design (FCD), augmented with four additional design points [45]. This results in a total of N=19 design points or simulations.

The DoE methodology is often applied to experiments where the observations are assumed to be a sample from a statistically distributed population. Consequently, replicate runs allow for an estimation of a mean and a standard deviation. For the simulation results considered here, two observations for the same design point are similar. Replicate runs were therefore not applied.

Table 2.2 *Material parameters for the selected constitutive models. These are categorised as small (-1), medium (0), and large (1) for convenience.*

			Levels		
Mechanism	Reference	Parameter(s)	small (-1)	medium (0)	large (1)
shear (χ_1)	eq. (2.2)	$\eta_L = \eta_T$ [Pa·s]	$3 \cdot 10^4$	$3 \cdot 10^5$	$3 \cdot 10^6$
bending (χ_2)	[36]	E_1 [MPa]	25	250	$2.5 \cdot 10^3$
		E_2 [MPa]	12.5	125	$1.25 \cdot 10^3$
		G_{12} [MPa]	10	100	$1 \cdot 10^3$
friction (χ_3)	eq. (2.1)	η [Pa·s]	70	700	$7 \cdot 10^3$

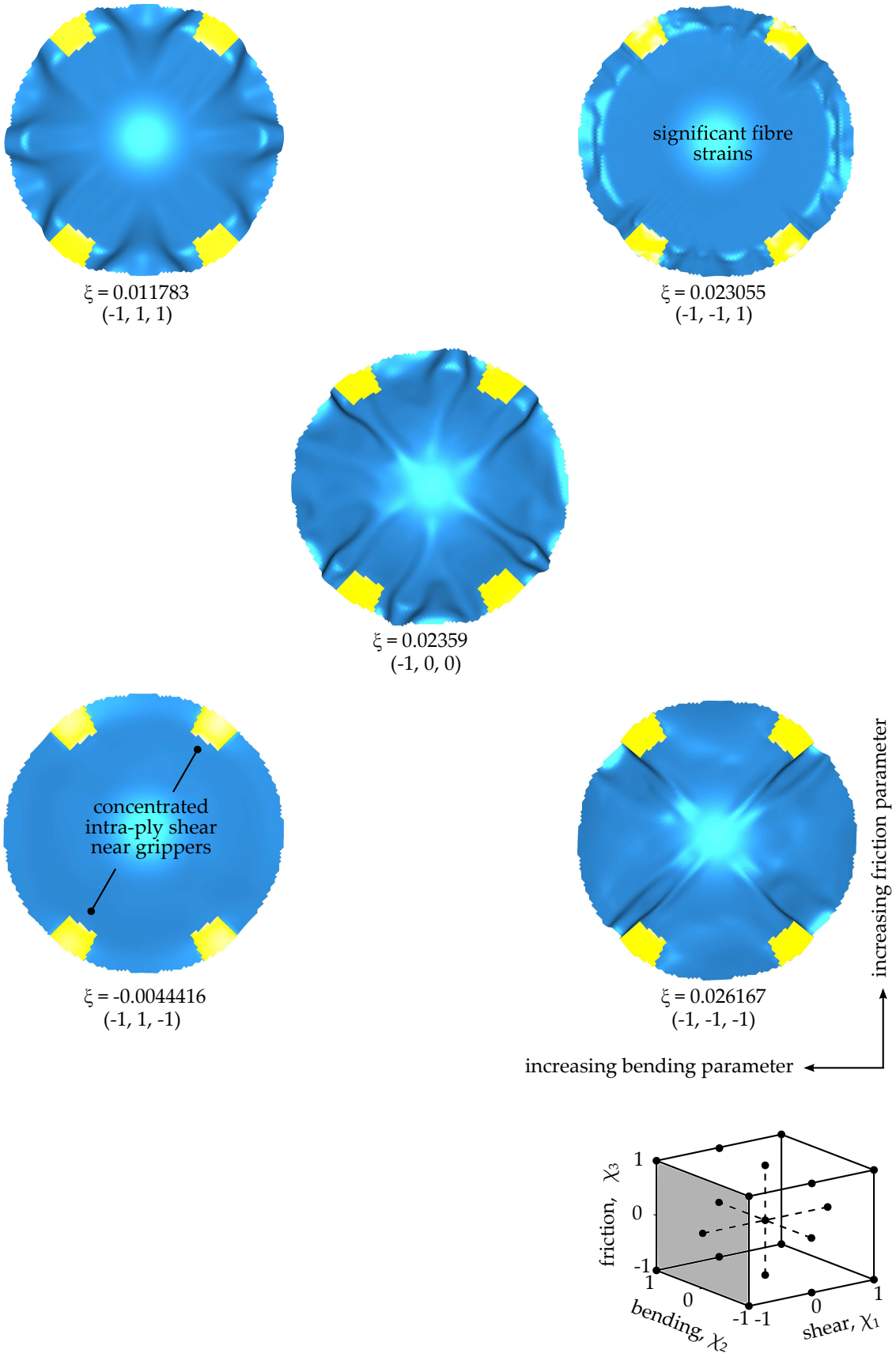

Figure 2.11 *Simulation results at a remaining closure travel of 10 mm and material parameter combinations as indicated by the points that intersect the grey plane (small shear) in the parameter sensitivity space.*

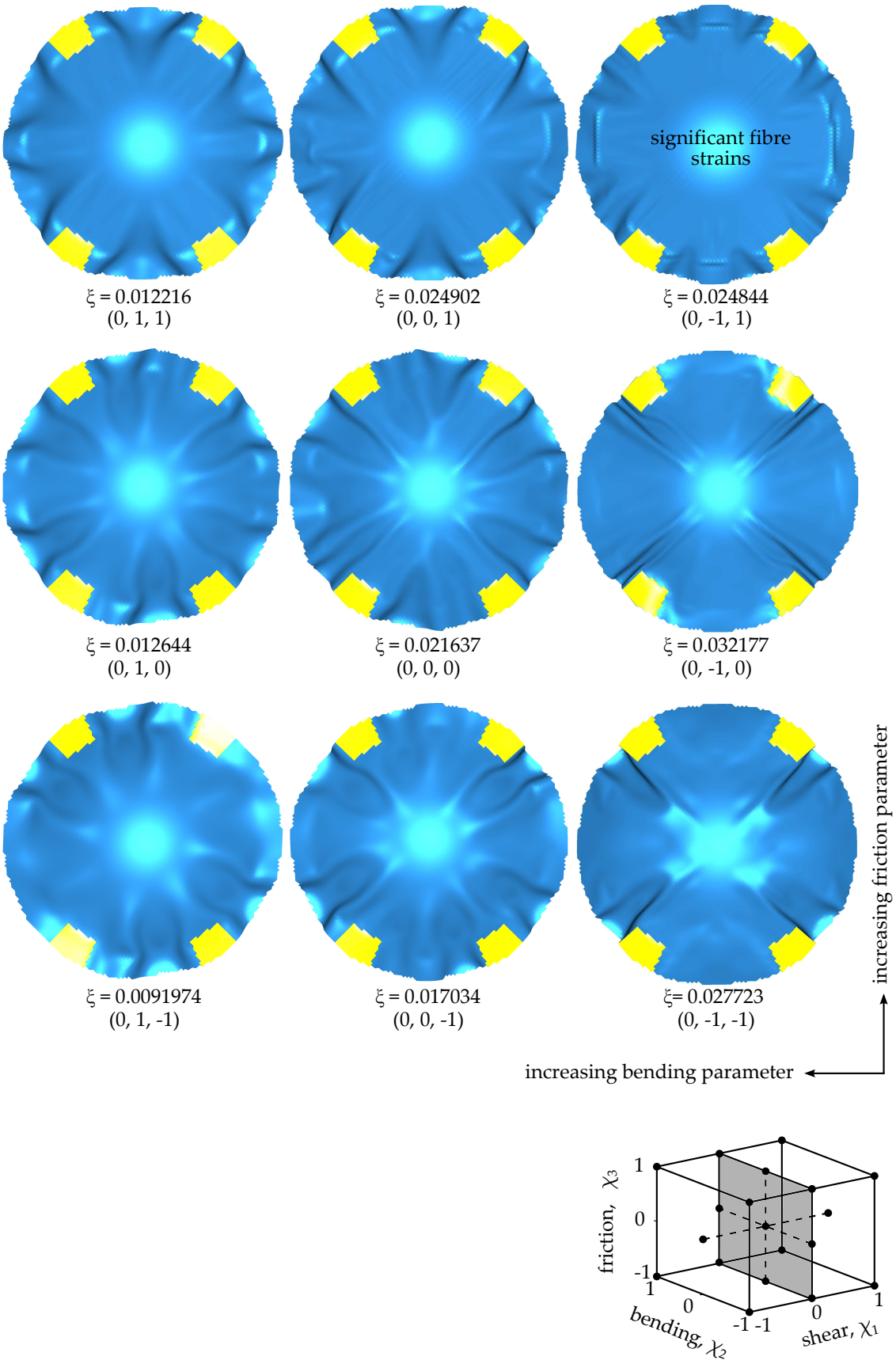

Figure 2.12 *Simulation results at a remaining closure travel of 10 mm and material parameter combinations as indicated by the points that intersect the grey plane (medium shear) in the parameter sensitivity space.*

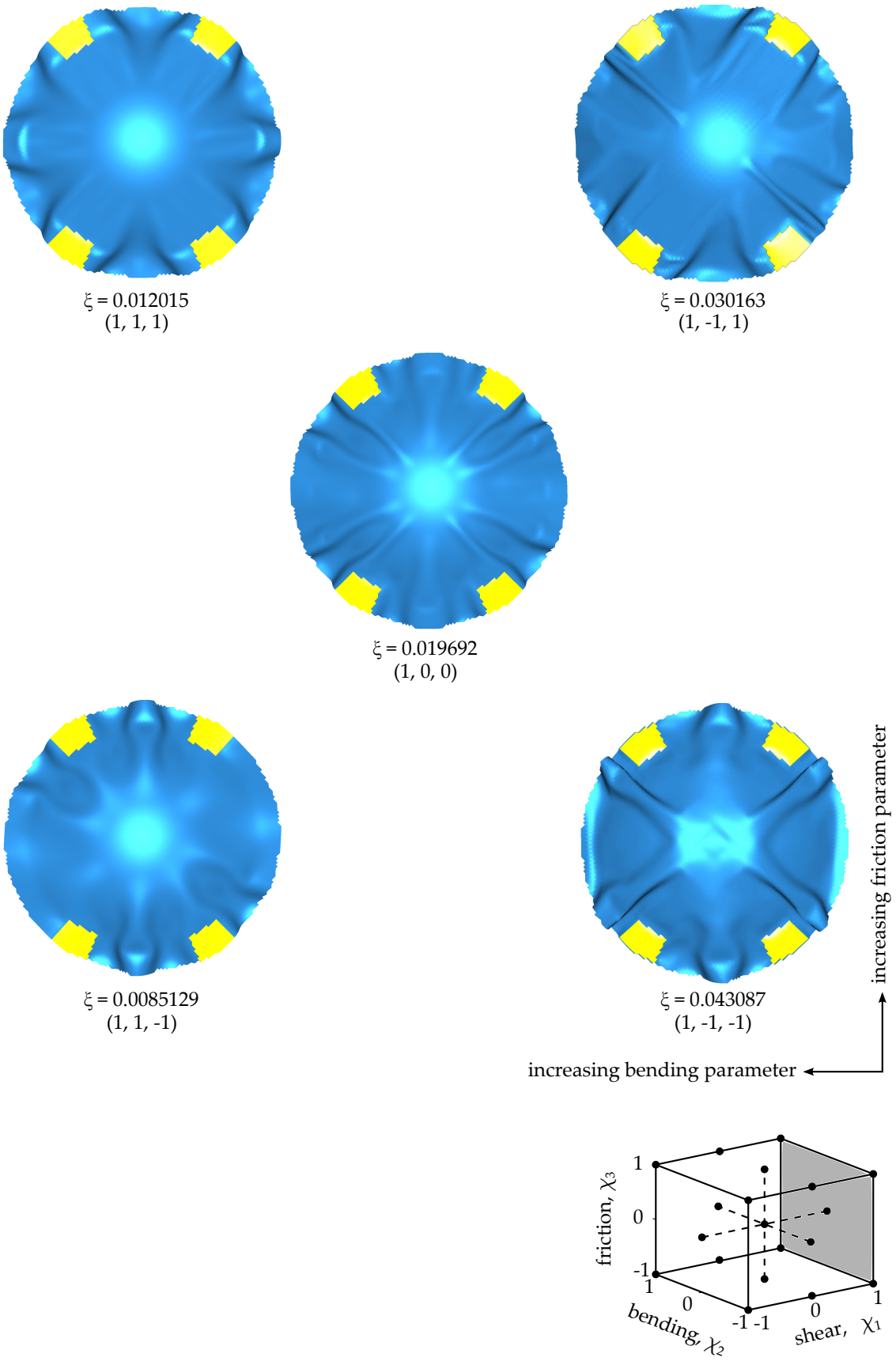

Figure 2.13 *Simulation results at a remaining closure travel of 10 mm and material parameter combinations as indicated by the points that intersect the grey plane (large shear) in the parameter sensitivity space.*

2.5.2 Qualitative results

Figures 2.11, 2.12, and 2.13 show the forming predictions according to the material parameter input defined in table 2.2, with the combinations indicated as design points in figure 2.10. The deformations of the -45° plies are visualised only, as other plies deform accordingly. The majority of the wrinkles run from the outer rim of the blank towards the centre of the product. A rough classification of the shapes can be performed visually:

- Long straight wrinkles that originate from one side of each gripper only are observed for simulations (χ_1, χ_2, χ_3) = (-1,-1,-1), (0,-1,0), and (0,-1,-1).

- Uniformly distributed wrinkles that run straight are observed for almost all the simulations in the top rows of figures 2.11, 2.12, and 2.13. The material parameter combinations read (-1,1,1), (0,1,1), (0,0,1), (1,1,1), and (1,-1,1).

- No wrinkling is visible for (-1,1,-1), whereas wrinkling is concentrated near the rim of the dome for (-1,-1,1), and (0,-1,1). These predictions are accompanied by obscure in-plane deformations. Concentrated intra-ply shearing was observed near the grippers for (-1,1,-1). Fibre stretching was observed for simulations (-1,-1,1), and (0,-1,1).

- Uniformly distributed, but more curved wrinkles are observed for (0,1,0), (0,0,0), (0,1,-1), (0,0,-1), (1,0,0), and (1,1,-1).

This last category matches best with the experimental result shown in figure 2.7, in which curved wrinkles are present as well, however, the number of wrinkles was less in practice. The sensitivity study shows that alternative material parameter combinations can result in quite similar predictions as the initial simulation (0,0,0). However, other material parameter combinations result in very different wrinkle distributions. These effects highlight the importance of obtaining a reliable material parameter input as determined from characterisation experiments.

To quantify the effects observed, one could for example assign wrinkling grades as defined in the AATCC test method [46]. It is generally applied in order to classify fabric specimens that are subjected to laundry cycles. An expert assigns a grade to the fabric, however, more objective methods were developed by using imaging techniques [47, 48]. Classifying the simulation results obtained here with such a method is difficult, because the predicted wrinkles in this work are roughly all of the same scale. The next section shows an example of another quantification by using the statistical analysis of variance (ANOVA) procedure.

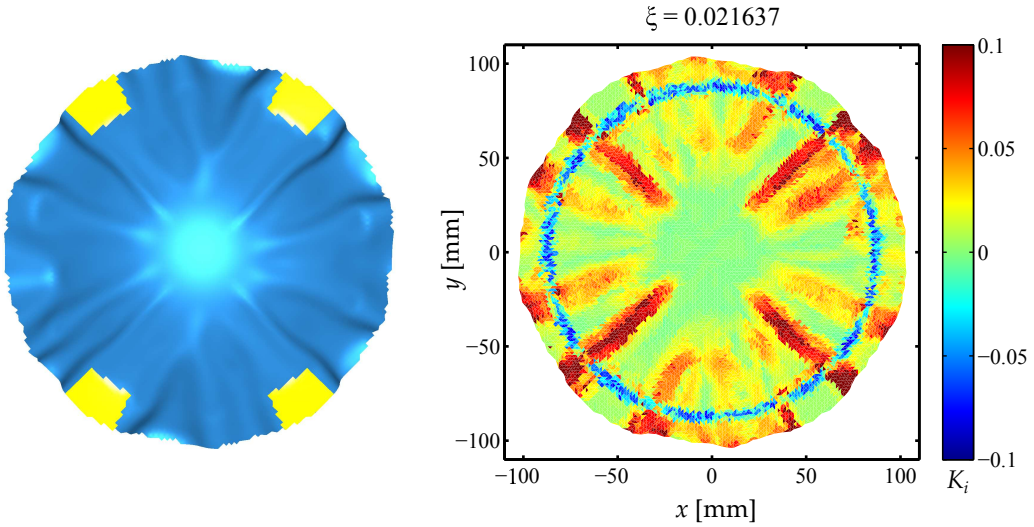

Figure 2.14 *Local tool-blank mismatch for the simulation with* $(\chi_1, \chi_2, \chi_3) = (0,0,0)$.

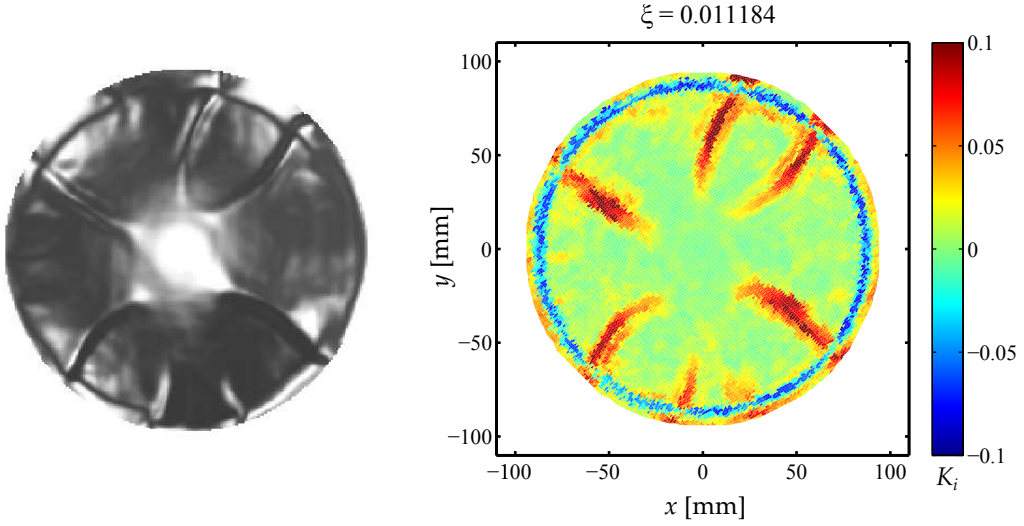

Figure 2.15 *The shape of the experimental forming trial in figure 2.8 with a 10 mm remaining closure travel (left). The local tool-blank mismatch* K_i *is shown for this digitised product (right).*

2.5.3 Quantitative results

A local formability measure is introduced to quantify the match between the deformed blank and the aimed tooling surface. Local curvatures are compared, which results in a local tool-blank mismatch:

$$K_i = \kappa^i_{\mathrm{MM,B}} - \kappa^j_{\mathrm{MM,T}} \tag{2.4}$$

where $\kappa_{\mathrm{MM,B}}$ and $\kappa_{\mathrm{MM,T}}$ are the modified mean curvatures at the blank and the tool, respectively. The modified mean curvature at a certain node i in the blank is compared with the curvature at the corresponding location in tool. The nearest tool node j is selected from this location. The modified mean curvature is defined as:

$$\kappa_{\mathrm{MM}} = \tfrac{1}{2}\left(|\kappa_{\mathrm{I}}| + |\kappa_{\mathrm{II}}|\right) \tag{2.5}$$

which takes the absolute values of the principle curvatures κ_{I} and κ_{II}. This is in contrast with the ordinary mean curvature, which is not considered here because it yields zero mean curvature in the case of a saddle point with equal but opposite principle curvatures. Several algorithms [49–51] are available to determine the curvature of a triangulation. The algorithm from Dong and Wang [51] was applied, which yields curvature information at each node.

If the local tool-blank mismatch yields $K_i > 0$, the local modified mean curvature in the blank is larger than the corresponding tool curvature, which tells us that this region is susceptible to wrinkling. For $K_i \leq 0$, the modified mean curvature in the blank is equal or smaller than the curvature at the corresponding tool node, such that no wrinkling is expected. Figures 2.14 and 2.15 show the local tool-blank mismatch for the initial simulation and the experiment, respectively. Large mismatch values indicate clearly the position of wrinkles.

The statistical ANOVA procedure [45] can be applied to quantify the effects caused by the material parameter input. For this purpose, a single response variable needs to be selected, which discriminates the predicted shapes in figures 2.11, 2.12, and 2.13. The global tool-blank mismatch ξ is used in this work, defined as:

$$\xi = \frac{1}{A_{\mathrm{B}}} \sum_{m=1}^{M} A_m K^{\mathrm{E}}_m \tag{2.6}$$

in which A_{B} is the total blank area, which consists of M elements. The surface area of element m is indicated by A_m. The element tool-blank mismatch K^{E}_m is obtained by averaging K_i over the three nodes of element m:

$$K^{\mathrm{E}}_m = \tfrac{1}{3} \sum_{i=1}^{3} K_i \tag{2.7}$$

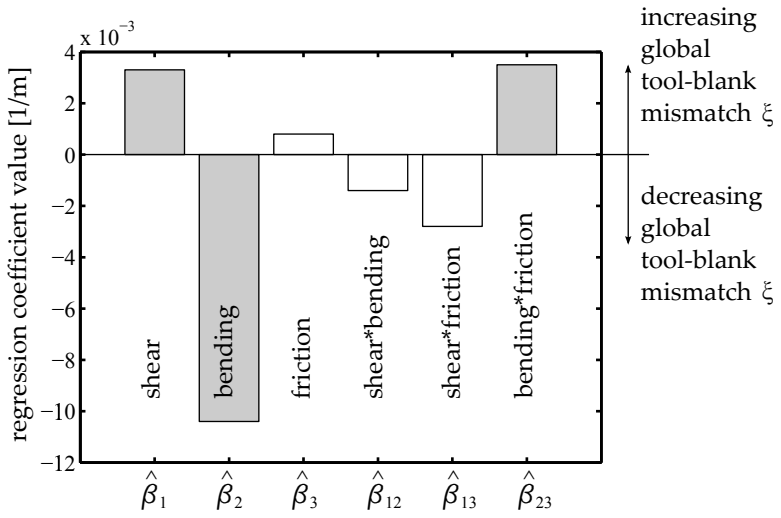

Figure 2.16 *Approximated regression coefficients. The grey bars indicate the statistically significant factors, for a significance level α of 0.05.*

The global tool-blank mismatch ξ is shown for each simulation in figures 2.11, 2.12, and 2.13. Relatively large numbers result when the predicted shapes involve sharp wrinkles, which is accompanied by large localised curvatures. Smaller numbers are found for smoother patterns. The numbers are fitted on the following response surface model:

$$\xi = \beta_0 + \beta_1\chi_1 + \beta_2\chi_2 + \beta_3\chi_3 + \beta_{12}\chi_1\chi_2 + \beta_{13}\chi_1\chi_3 + \beta_{23}\chi_2\chi_3 + \epsilon \tag{2.8}$$

A constant value is represented by β_0. The random error ϵ is allowed but minimised. Linear parameters β_1, β_2, and β_3 are related to the shear, bending, and friction models, respectively. Interacting terms are represented by β_{12}, β_{13}, and β_{23}. These regression coefficients are unknown and approximated by means of a least square regression [52]. Figure 2.16 shows the approximated regression coefficients $\{\hat{\beta}\}$, which were determined by using the coded variables χ_i as defined in the DoE in figure 2.10.

The ANOVA procedure [45] was applied in order to assess the significance of the regression coefficients $\{\hat{\beta}\}$. Table 2.3 in the appendix shows the ANOVA results, from which it is concluded that the modelled mechanisms for shear, bending, and the interaction of bending with friction show a significant effect on the global tool-blank mismatch ξ. The corresponding regression coefficients are marked in grey in figure 2.16. The modelled bending mechanism shows the largest effect on ξ. A negative regression coefficient implies that a larger bending stiffness results in a smaller global tool-blank mismatch. Smaller but significant effects are caused by shear and the interaction of bending with friction. An increase of the corresponding

material parameters results in a larger global tool-blank mismatch.

2.5.4 Discussion

The qualitative visual analysis of the predicted blank deformations showed that these are significantly affected by the material parameter input for all mechanisms considered, namely the shear, bending, and friction mechanisms. The quantitative analysis resulted in a more detailed interpretation of the sensitivity study. Bending, shear, and the combination of bending with friction were shown to affect the global tool-blank mismatch significantly.

The effect of the combination of bending with friction can be explained by the mismatch numbers of the simulations at the four corners in figure 2.11. For the bending setting $\chi_2 = 1$, the mismatch ξ increases for an increasing friction setting χ_3. However, for the bending setting $\chi_2 = -1$, the mismatch ξ decreases for an increasing friction setting χ_3. Similar trends were observed in figures 2.12 and 2.13, which can only be represented by the interaction coefficient β_{23} of equation (2.8). Such observations confirm that the predicted deformations are the result of a delicate balance between the shear, bending, and friction mechanisms considered.

It must be noted that the results of such a quantitative analysis must be treated with care, since these are dependent on:

- The terms considered by the response model. For example, higher order effects of the response variable can be present, however, it is possible that the response model does not have terms representing these effects.
- The choice of the response variable. The use of the global tool-blank mismatch here evaluates the deformed blank shape over its whole area. An alternative response variable can be selected, which discriminates the predicted shapes differently.

A weight function can be assigned to the response variable, such that higher priorities can be given to adverse deformations in certain areas of the product. Alternatively, a set of response variables can be used to separately describe wrinkle orientation, smoothness, energy, and density. Such measures were, for example, determined with the aid of wavelet analyses by Sun *et al.* [48]. A proper choice of the response variable(s) can ultimately be used in product optimisation routines [52]. The most suitable response variable(s) depends on each specific forming problem and the application of the final product.

As discussed earlier, a large variety of methods, results, and constitutive models are used to characterise composite materials in melt conditions. Friction was described here with the Newtonian fluid model, however, other constitutive models have been

proposed recently [53]. Very little work on the characterisation of bending has been conducted so far. In-plane shear parameters were shown to vary for orders of magnitude [26]. This study shows that these differences affect the forming predictions significantly, which addresses the importance of reaching consensus for the characterisation of the mechanisms considered.

2.6 Conclusions

The sensitivity of composite forming predictions to the material parameter input was investigated. A circular blank from UD carbon/PEKK with a quasi-isotropic lay-up was considered. Its forming behaviour into a doubly curved dome geometry was studied. Initial simulations were performed with an educated guess of the material parameter input related to the intra-ply shear, bending, and inter-ply friction mechanisms. Slightly curved wrinkles were predicted, which run from the outer rim of the blank towards the centre of the product. Forming experiments were conducted for validation purposes. The forming evolution of the blank was recorded, which showed the development of slightly curved wrinkles as well. A lower number of wrinkles was observed in practice.

A sensitivity study was conducted in order to investigate the effect of the material parameter input on the forming predictions. The material parameter input combinations were varied according to a design of experiments. The predicted blank shapes were significantly affected. Depending on the parameter input, wrinkles were shown be straight or slightly curved. Also the distribution and position of the wrinkles was shown to be affected.

A global tool-blank mismatch indicator was proposed to quantify all simulation results with a single number. A response surface model was fitted to these results, as a function of the shear, bending, and friction parameter input. An analysis of variance was applied. In descending order of importance, bending, shear, and the combination of bending with friction were shown to affect the global tool-blank mismatch significantly. Not the friction mechanism only, but its combination with the bending explains that the predicted forming behaviour is determined by a delicate balance between the mechanisms considered. This study highlights the importance of obtaining reliable material parameter input, which addresses the need for reaching consensus in the characterisation of deformation mechanisms in fibre reinforced melts.

Acknowledgements

The stamp forming experiments were conducted at the Fokker Aerostructures company and were guided by Steven Teunissen, Richard Roerink and Michael Wielandt. Preparations were done by Gijs Gijsbertse. Their help is highly appreciated. The authors would also like to thank the representatives of Fokker Aerostructures B.V., Ten Cate Advanced Composites, and the Boeing company for all the fruitful discussions within the ThermoPlastic composite Research Center (TPRC). Thanks to Thijs Donderwinkel for his support in collecting and visualising the simulation results.

References

[1] P.J. Mallon, C.M. Ó Brádaigh, and R.B. Pipes. Polymeric diaphragm forming of complex-curvature thermoplastic composite parts. *Composites*, **20**(1):48–56, 1989.

[2] M. Hou. Stamp forming of fabric-reinforced thermoplastic composites. *Polymer Composites*, **17**(4):596–603, 1996.

[3] S.P. Haanappel, U. Sachs, R. ten Thije, B. Rietman, and R. Akkerman. Forming of thermoplastic composites. In the 15th International ESAFORM Conference on Material Forming, 2012.

[4] P. De Luca, P. Lefébure, and A.K. Pickett. Numerical and experimental investigation of some press forming parameters of two fibre reinforced thermoplastics: APC2-AS4 and PEI-CETEX. *Composites Part A: Applied Science and Manufacturing*, **29**(1-2):101–110, 1998.

[5] B. Rietman, S.P. Haanappel, R.H.W. ten Thije, and R. Akkerman. Forming simulation sensitivity study of the double-dome benchmark geometry, volume 504-506 of *Key Engineering Materials*, 2012.

[6] T.A. Martin, D. Bhattacharyya, and R.B. Pipes. Deformation characteristics and formability of fibre-reinforced thermoplastic sheets. *Composites Manufacturing*, **3**(3):165–172, 1992.

[7] T.C. Lim and S. Ramakrishna. Modelling of composite sheet forming: A review. *Composites Part A: Applied Science and Manufacturing*, **33**(4):515–537, 2002.

[8] A.S. Tam and T.G. Gutowski. The kinematics for forming ideal aligned fibre composites into complex shapes. *Composites Manufacturing*, **1**(4):219–228, 1990.

[9] K. Golden, T.G. Rogers, and A.J.M. Spencer. Forming kinematics of continuous fibre reinforced laminates. *Composites Manufacturing*, **2**(3-4):267–277, 1991.

[10] S.G. Hancock and K.D. Potter. The use of kinematic drape modelling to inform the hand lay-up of complex composite components using woven reinforcements. *Composites Part A: Applied Science and Manufacturing*, **37**(3):413–422, 2006.

[11] K. Vanclooster, S. V. Lomov, and I. Verpoest. Experimental validation of forming simulations of fabric reinforced polymers using an unsymmetrical mould configuration. *Composites Part A: Applied Science and Manufacturing*, **40**(4):530–539, 2009.

[12] K. Vanclooster, S. V. Lomov, and I. Verpoest. On the formability of multi-layered fabric composites. In ICCM International Conferences on Composite Materials, 2009.

[13] C.M. Ó Brádaigh and R.B. Pipes. Finite element analysis of composite sheet-forming process. *Composites Manufacturing*, **2**(3-4):161–170, 1991.

[14] X. Yu, B. Cartwright, D. McGuckin, L. Ye, and Y. Mai. Intra-ply shear locking in finite element analyses of woven fabric forming processes. *Composites Part A: Applied Science and Manufacturing*, **37**(5):790–803, 2006.

[15] Pavel Simacek, Victor N. Kaliakin, and R. B. Pipes. Pathologies associated with the numerical analysis of hyper-anisotropic materials. *International Journal for Numerical Methods in Engineering*, **36**(20):3487–3508, 1993.

[16] R.H.W. ten Thije and R. Akkerman. Solutions to intra-ply shear locking in finite element analyses of fibre reinforced materials. *Composites Part A: Applied Science and Manufacturing*, **39**(7):1167–1176, 2008.

[17] C.M. Ó Brádaigh, G.B. McGuinness, and R.B. Pipes. Numerical analysis of stresses and deformations in composite materials sheet forming: central indentation of a circular sheet. *Composites Manufacturing*, **4**(2):67–83, 1993.

[18] A.K. Pickett, T. Queckbörner, P. De Luca, and E. Haug. An explicit finite element solution for the forming prediction of continuous fibre-reinforced thermoplastic sheets. *Composites Manufacturing*, **6**(3-4):237–243, 1995.

[19] F.N. Cogswell. The experience of thermoplastic structural composites during processing. *Composites Manufacturing*, **2**(3-4):208–216, 1991.

[20] J.L. Gorczyca-Cole, J.A. Sherwood, and J. Chen. A friction model for thermostamping commingled glass-polypropylene woven fabrics. *Composites Part A: Applied Science and Manufacturing*, **38**(2):393–406, 2007.

[21] U. Sachs, S.P. Haanappel, A.D. Rietman, and R. Akkerman. Friction testing of thermoplastic composites. In SAMPE Europe 32nd International Technical Conference & Forum, 2011.

[22] U. Sachs, K. Fetfatsidis, J. Schumacher, G. Ziegmann, S. Allaoui, E. Vidal-Salléand, and R. Akkerman. A friction-test benchmark with Twintex PP. In the 15th International ESAFORM Conference on Material Forming, 2012.

[23] R. Banks, A.P. Mouritz, S. John, F. Coman, and R. Paton. Development of a new structural prepreg: Characterisation of handling, drape and tack properties. *Composite Structures*, **66**(1-4):169–174, 2004.

[24] R.J. Crossley, P.J. Schubel, and N.A. Warrior. The experimental determination of prepreg tack and dynamic stiffness. *Composites Part A: Applied Science and Manufacturing*, **43**(3):423–434, 2012.

[25] S.G. Advani, T.S. Creasy, and S.F. Shuler. Composite Sheet Forming, volume 11 of *Composite Materials Series*. Elsevier Science B.V., 1997.

[26] P. Harrison and M.J. Clifford. Design and manufacture of textile composites, chapter Rheological Behaviour of Pre-impregnated Textile Composites. Woodhead Publishing Ltd., Cambridge, UK, 2005.

[27] S.P. Haanappel and R. Akkerman. A method for shear characterisation of fibre reinforced thermoplastics by means of torsion. Submitted to *Composites Part A: applied science and manufacturing*, 2013.

[28] J.A. Goshawk and R.S. Jones. Structure reorganization during the rheological characterization of continuous fibre-reinforced composites in plane shear. *Composites*

Part A: Applied Science and Manufacturing, **27**:279–286, 1996.

[29] W.F. Stanley and P.J. Mallon. Intraply shear characterisation of a fibre reinforced thermoplastic composite. *Composites Part A: Applied Science and Manufacturing*, **37**:939–948, 2006.

[30] T.G. Rogers. Rheological characterization of anisotropic materials. *Composites*, **20**(1):21–27, 1989.

[31] T.A. Martin, D. Bhattacharyya, and I.F. Collins. Bending of fibre-reinforced thermoplastic sheets. *Composites Manufacturing*, **6**(3-4):177–187, 1995.

[32] J. Wang, A.C. Long, and M.J. Clifford. Experimental measurement and predictive modelling of bending behaviour for viscous unidirectional composite materials. *International Journal of Material Forming*, **3**:1253–1266, 2010.

[33] CSIRO division of wool technology, Australia. Instructional Manual for Fabric Assurance by Simple Testing, 1990.

[34] ASTM. Standard test method for stiffness of fabrics. *Annual Book of ASTM Standards*, **07.01: D1388 - 96 R02**.

[35] S. Kawabata. The standardization and analysis of hand evaluation. The Textile Machinery Society of Japan, Osaka, 2nd edition, 1986.

[36] R.M. Jones. Mechanics of composite materials. Taylor & Francis, 2nd edition, 1999.

[37] R.H.W. ten Thije. Finite element simulations of laminated composite forming processes. Ph.D. thesis, University of Twente, 2007.

[38] R.H.W. ten Thije, R. Akkerman, and J. Huétink. Large deformation simulation of anisotropic material using an updated Lagrangian finite element method. *Computer Methods in Applied Mechanics and Engineering*, **196**(33-34):3141–3150, 2007.

[39] D. Soulat, A. Cheruet, and P. Boisse. Simulation of continuous fibre reinforced thermoplastic forming using a shell finite element with transverse stress. *Computers and Structures*, **84**(13-14):888–903, 2006.

[40] P. Harrison, T. Haylock, and A.C. Long. Measurement of the transverse and longitudinal viscosities of continuous fibre reinforced composites. In The 8th International ESAFORM Conference on Material Forming, 2005.

[41] G.B. McGuinness and C.M. Ó Brádaigh. Characterisation of thermoplastic composite melts in rhombus-shear: The picture-frame experiment. *Composites Part A: Applied Science and Manufacturing*, **29**(1-2):115–132, 1998.

[42] R. S. Jones and D. Oakley. An interpretation of rheological data in terms of model systems. *Composites*, **21**(5):415–418, 1990.

[43] S.P. Haanappel, R. ten Thije, and R. Akkerman. Forming predictions of UD reinforced thermoplastic laminates. In 14th European Conference on Composite Materials, ECCM 2010, 2010.

[44] M. Hou. Stamp forming of continuous glass fibre reinforced polypropylene. *Composites Part A: Applied Science and Manufacturing*, **28**(8):695–702, 1997.

[45] R.H. Myers and D.C. Montgomery. Response Surface Methodology: Process and Product Optimization Using Designed Experiments. John Wiley & Sons, Inc., 2nd edition, 2002.

[46] American Association of Textile Chemists and Colorists. Technical manual of standard testing methods, 1991.

[47] J. Hu, B. Xin, and H. Yan. Measuring and modeling 3D wrinkles in fabrics. *Textile Research Journal*, **72**(10):863–869, 2002.

[48] J. Sun, M. Yao, B. Xu, and P. Bel. Fabric wrinkle characterization and classification using modified wavelet coefficients and support-vector-machine classifiers. *Textile Research Journal*, **81**(9):902–913, 2011.

[49] H. Theisel, C. Rössl, R. Zayer, and H. Seidel. Normal based estimation of the curvature tensor for triangular meshes. In Proceedings - Pacific Conference on Computer Graphics and Applications, 288–297, 2004.

[50] E. Magid, O. Soldea, and E. Rivlin. A comparison of Gaussian and mean curvature estimation methods on triangular meshes of range image data. *Computer Vision and Image Understanding*, **107**(3):139–159, 2007.

[51] C. Dong and G. Wang. Curvatures estimation on triangular mesh. *Journal of Zhejiang University: Science*, **6 A**:128–136, 2005.

[52] M.H.A. Bonte. Optimisation Strategies for Metal Forming Processes. Ph.D. thesis, University of Twente, 2007.

[53] U. Sachs, R. Akkerman, S.P. Haanappel, R.H.W ten Thije, and M.B. de Rooij. Friction in forming of UD composites. In G. Menary, editor, the 14th International ESAFORM Conference on Material Forming, volume 1353 of *AIP Conference Proceedings*, 984–989. American Institute of Physics, 2011.

2.A Appendix: ANOVA results

Table 2.3 *Results from the ANOVA, which was applied to the regression of the formability ξ. $R^2 = 90.10\%$, $R^2_{adj} = 85.15\%$.*

Source of variation	Sum of squares	Degrees of freedom	Mean square	F_0	p-value
Regression	0.001851	6	0.000309	18.21	0.000
Linear	0.001629	3	0.000543	32.03	0.000
shear (β_1)	0.000111	1	0.000111	**6.55**	**0.025**
bending (β_2)	0.001508	1	0.001508	**88.97**	**0.000**
friction (β_3)	0.000010	1	0.000010	0.58	0.462
Interaction	0.000223	3	0.000074	4.38	0.027
shear*bending (β_{12})	0.000015	1	0.000015	0.87	0.370
shear*friction (β_{13})	0.000063	1	0.000063	3.75	0.077
bending*friction (β_{23})	0.000145	1	0.000145	**8.54**	**0.013**
Residual error	0.000203	12	0.000017		
Total	0.002055	18			

Chapter 3

A method for shear characterisation of fibre reinforced thermoplastics by means of torsion*

Abstract

Intra-ply shear is one of the main mechanisms that appears during the forming process of hot thermoplastic laminates with a uni-directional fibre reinforcement. A torsion bar test is proposed in this chapter to characterise the longitudinal shear mechanism. The tests are aimed to be performed with the aid of widely available standard rheometers. These allow for a thorough rheological characterisation by applying oscillatory loads to the specimen. The kinematics that occur and the relations to determine the shear property of a dynamically loaded rectangular bar in torsion have been outlined. The presence of stiff fibres in combination with fixtures that grip the specimen potentially influence the measured shear response. The sensitivity to these effects was investigated by means of a model, which resulted in guidelines for specimen geometry. Torsion bar specimens with a close to square cross section are advised, since these are less sensitive to clamping effects, compared to bars with a narrow cross section. The specimen dimensions must further be tailored to the available space in the fixtures and the measurement device considered.

*Reproduced from: S.P. Haanappel, R. Akkerman. A method for shear characterisation of fibre reinforced thermoplastics by means of torsion. Submitted to: *Composites Part A: Applied Science and Manufacturing*, **2013**.

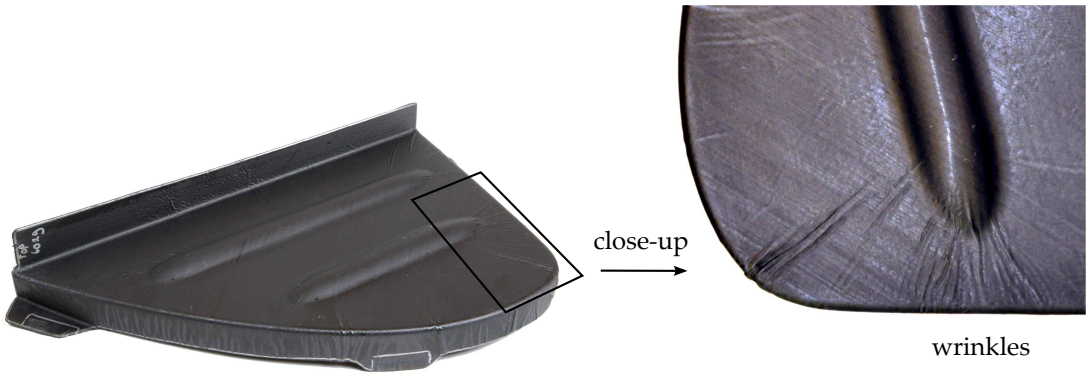

Figure 3.1 *Process-induced defects.*

3.1 Introduction

Thermoforming of fibre reinforced thermoplastic laminates is ideally suited to the production of thin-walled products with complex shapes. Nevertheless, process-induced defects appear frequently, such as the wrinkling shown in figure 3.1. Better anticipation of such defects facilitates the tooling design process by which significant lead-time reductions can be achieved. Analyses of uni-directional (UD) carbon fibre reinforced thermoplastics have been reported for decades already [1]. Nevertheless, textile reinforced thermoplastics or fabrics were favoured due to their ease of forming onto complex-shaped moulds. However, it is believed that the high directional strength and stiffness properties of UD material can be fully exploited with the aid of sophisticated deposition tooling, such as tape-placement robots [2]. A subsequent forming operation of so-called tailored blanks can be carried out. These possibilities have awakened the interest in UD material for forming applications again.

The forming process of UD reinforced thermoplastic laminates involves several deformation processes, which were previously categorised by Cogswell [3, 4]. Inter-ply slip is identified as the mechanism where individual plies slide relatively to each other, implying a discontinuous displacement field over the laminate thickness. Laminates with good consolidation quality and equally oriented plies show a more continuous intra-ply shearing deformation [5]. Intra-ply shear refers to the shearing process within a UD reinforced ply. Two intra-ply shearing processes are distinguished [6]. The first considers parallel sliding of individual fibre filaments, which is indicated as axial or longitudinal intra-ply shearing. The second is transverse sliding of individual fibres and is referred to as transverse intra-ply shearing. These mechanisms are schematically shown in figure 3.2, which appear simultaneously when forming a doubly curved part. Together with the out-of-plane bending behaviour of the laminate, the final product shape will be determined by the complex interaction of these inter- and intra-ply mechanisms.

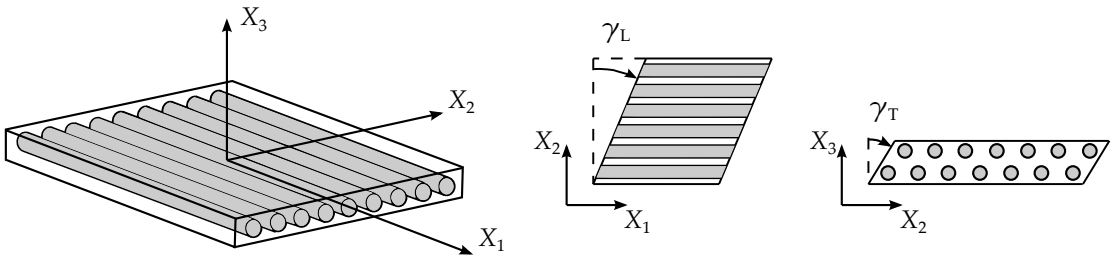

Figure 3.2 *Left: definition of the coordinate system with respect to the fibre direction. Centre: axial or longitudinal intra-ply shearing. Right: transverse intra-ply shearing.*

The wrinkles in figure 3.1 can be avoided by ensuring that the longitudinal shearing mechanism is more pronounced. The transverse shear mechanism is of less importance when solving such forming issues. In order to predict the defects in the early product design phase, it is important to have a proper description of the longitudinal shearing mechanism. Industry calls for a practicable standard test to be conducted with easily accessible devices, such as standard rheometers. The torsion bar method is introduced here, which is intended for longitudinal shear characterisation of transversely isotropic melts. The longitudinal shearing mechanism is invoked when the bar is subjected to torsion, as shown in figure 3.3.

The next section firstly addresses several constitutive models, which can be used to describe the behaviour of anisotropic media. Visco-elastic material properties can be measured by conducting small strain oscillatory tests. The Linear Visco-Elasticity (LVE) theory [7] is used for this purpose, which will be given some attention as well. Subsequently, an overview of available shear characterisation tests is given, after which the torsion bar method is introduced. The kinematics of the torsionally loaded rectangular bar are outlined. The load introduction via fixtures and the presence of axially aligned stiff fibres potentially influence the measured responses. These effects are investigated in detail. Finally, the analyses lead to guidelines for the specimen geometry.

3.2 Modelling of anisotropic media

Two approaches to describe transversely isotropic viscous fluids have been recognised in the literature. They differ in the assumption of the material form, which consists of continuously or discontinuously collimated fibres [8].

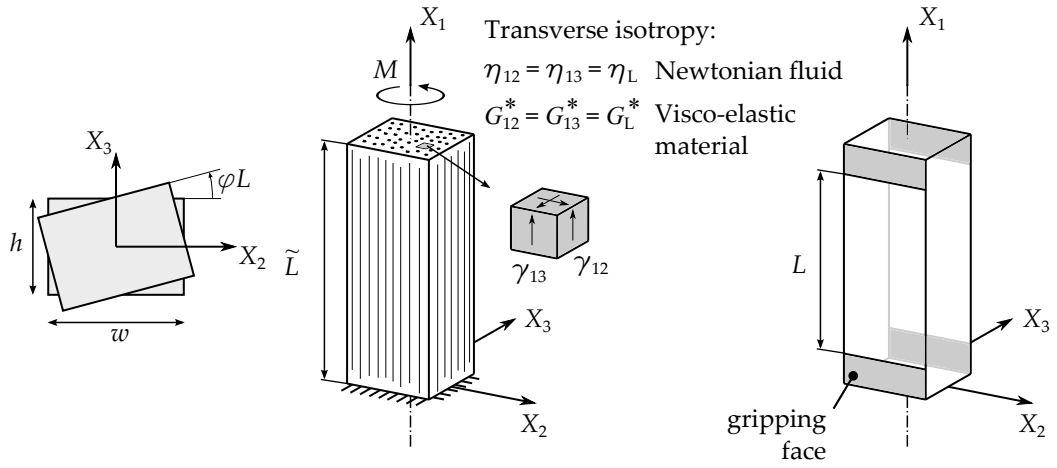

Figure 3.3 *Conceptual design of the torsion bar specimen. Left: cross-sectional geometry. Centre: fibre reinforced rectangular bar. Torsional loading invokes longitudinal shear mechanisms as indicated by the elementary cube. Right: grey areas represent the aimed gripping faces to conduct torsional loads in practice.*

3.2.1 Ideal Fibre Reinforced Newtonian fluid Model

The first approach assumes continuously collimated fibres, which is most representative for the material used in this research. An anisotropic elastic model that accounts for large deformations and the dominating presence of a single family of inextensible fibres was initially developed by Spencer [9]. The incompressibility assumption led to the addition of an arbitrary hydrostatic pressure term p. This model was adopted by Rogers [10] to account for visco-elastic fluids. The special case of a linear viscous fluid was obtained, which was referred to as the Ideal Fibre Reinforced Newtonian fluid Model (IFRM). The Cauchy stress σ is expressed as:

$$\boldsymbol{\sigma} = -p\boldsymbol{I} + T\hat{\boldsymbol{a}}\hat{\boldsymbol{a}} + \boldsymbol{\tau} \tag{3.1}$$

where the extra stress tensor $\boldsymbol{\tau}$ reads:

$$\boldsymbol{\tau} = 2\eta_T\boldsymbol{D} + 2(\eta_L - \eta_T)(\hat{\boldsymbol{a}}\hat{\boldsymbol{a}}\cdot\boldsymbol{D} + \boldsymbol{D}\cdot\hat{\boldsymbol{a}}\hat{\boldsymbol{a}})$$

The variable T is the fibre stress, $\hat{\boldsymbol{a}}$ is a unit vector that represents the fibre direction in the deformed state, $\boldsymbol{D}$ is the rate of deformation tensor, and $\boldsymbol{I}$ is the second order unit tensor. The parameters η_T and η_L represent the transverse and axial or longitudinal viscosity of the uni-directional ply respectively. These are related to the shearing mechanisms of a fibre reinforced viscous fluid, as shown in figure 3.2. If the fibre direction coincides with the X_1-axis, the matrix representation of this constitutive

model can be written as:

$$\begin{bmatrix} \sigma_{11}+p-T \\ \sigma_{22}+p \\ \sigma_{33}+p \\ \sigma_{23} \\ \sigma_{31} \\ \sigma_{12} \end{bmatrix} = \begin{bmatrix} 4\eta_L-2\eta_T & & & & & \\ & 2\eta_T & & & & \\ & & 2\eta_T & & & \\ & & & \eta_T & & \\ & & & & \eta_L & \\ & & & & & \eta_L \end{bmatrix} \begin{bmatrix} \dot{\varepsilon}_{11} \\ \dot{\varepsilon}_{22} \\ \dot{\varepsilon}_{33} \\ \dot{\gamma}_{23} \\ \dot{\gamma}_{31} \\ \dot{\gamma}_{12} \end{bmatrix} \tag{3.2}$$

where the components of $\boldsymbol{D}$ are for convenience replaced by the extensional strain rate $\dot{\varepsilon}_{ii}$, and the shear rate components $\dot{\gamma}_{ij}(=2\dot{\varepsilon}_{ij})$ (with $i \neq j$). The indices i and j correspond to the axes defined in figure 3.2. Strictly speaking, the first row of equation (3.2) is arbitrary as the material is inextensible in the fibre direction: $\dot{\varepsilon}_{11} = 0$.

3.2.2 Linear viscous transversely isotropic fluid

The second approach assumes discontinuously collimated fibres with typical lengths of 100 mm. Starting with the linear description of a fully anisotropic fluid, Beaussart *et al.* [11] reduced the 21 independent material parameters to three by assuming incompressibility and transverse isotropy. If the fibre direction is parallel to the X_1-axis, the resulting matrix formulation in compliance form then reads:

$$\begin{bmatrix} \dot{\varepsilon}_{11} \\ \dot{\varepsilon}_{22} \\ \dot{\varepsilon}_{33} \\ \dot{\gamma}_{23} \\ \dot{\gamma}_{31} \\ \dot{\gamma}_{12} \end{bmatrix} = \begin{bmatrix} \beta_{11} & -\beta_{11}/2 & -\beta_{11}/2 & & & \\ -\beta_{11}/2 & \beta_{22} & \beta_{11}/2-\beta_{22} & & & \\ -\beta_{11}/2 & \beta_{11}/2-\beta_{22} & \beta_{22} & & & \\ & & & 4\beta_{22}-\beta_{11} & & \\ & & & & \beta_{66} & \\ & & & & & \beta_{66} \end{bmatrix} \begin{bmatrix} \sigma_{11}+p \\ \sigma_{22}+p \\ \sigma_{33}+p \\ \sigma_{23} \\ \sigma_{31} \\ \sigma_{12} \end{bmatrix} \tag{3.3}$$

The parameters β_{11}, β_{22}, and β_{66} are the reciprocals of viscosities. Three independent viscosity parameters η_{ij} were defined [11]:

$$\eta_{11} = \beta_{11}^{-1} \qquad \eta_{22} = \eta_{33} = \beta_{22}^{-1} \qquad \eta_{23} = (4\beta_{22}-\beta_{11})^{-1} \qquad \eta_{12} = \eta_{13} = \beta_{66}^{-1} \tag{3.4}$$

and represent the axial elongational, transverse elongational, transverse shearing, and in-plane shearing viscosity, respectively. Analytical derivations for these viscosities were given by, for example, Pipes *et al.* [8] and Christensen [12].

The difference between the relations (3.3) and (3.2) is the result of the different material form assumption, namely the extensibility condition in the fibre direction. It can be shown that equation (3.3) simplifies to the IFRM formulation in equation

(3.2) when the inextensibility constraint is imposed. When the deviatoric stresses and strain rates are considered, the singular system in (3.3) can be inverted by using the constraints of incompressibility. The condition of inextensibility:

$$\dot{\varepsilon}_{11} = 0 \tag{3.5}$$

$$\dot{\varepsilon}_{33} = -\dot{\varepsilon}_{22} \tag{3.6}$$

can then be used to eliminate the off-diagonal terms, leading to:

$$\begin{bmatrix} \sigma_{11}+p \\ \sigma_{22}+p \\ \sigma_{33}+p \\ \sigma_{23} \\ \sigma_{31} \\ \sigma_{12} \end{bmatrix} = \begin{bmatrix} \frac{2}{3\beta_{11}} & \frac{2}{4\beta_{22}-\beta_{11}} & \frac{2}{4\beta_{22}-\beta_{11}} & & & \\ & & & \frac{1}{4\beta_{22}-\beta_{11}} & & \\ & & & & \frac{1}{\beta_{66}} & \\ & & & & & \frac{1}{\beta_{66}} \end{bmatrix} \begin{bmatrix} \dot{\varepsilon}_{11} \\ \dot{\varepsilon}_{22} \\ \dot{\varepsilon}_{33} \\ \dot{\gamma}_{23} \\ \dot{\gamma}_{31} \\ \dot{\gamma}_{12} \end{bmatrix} \tag{3.7}$$

where we again note that the first row is an arbitrary statement. Comparison of equation (3.7) with the IFRM relation in (3.2) confirms that:

$$\eta_{\mathrm{L}} = \frac{1}{\beta_{66}} = \eta_{12} = \eta_{13} \tag{3.8}$$

$$\eta_{\mathrm{T}} = \frac{1}{4\beta_{22}-\beta_{11}} = \eta_{23} \tag{3.9}$$

3.2.3 Rheometry

Deformation of a polymer melt is usually associated with mechanisms such as viscous dissipation and storage of elastic energy. Its constitutive behaviour can be described with the well-known Linear Visco-Elasticity (LVE) theory [7] for small strains. To measure the response of a material, it is favourable to apply a simple deformation such that it can be regarded as a 1D situation. Simple shearing invokes only one off-diagonal pair of the strain tensor components:

$$\gamma_{ij} = \begin{bmatrix} 0 & \gamma_{12} & 0 \\ \gamma_{21} & 0 & 0 \\ 0 & 0 & 0 \end{bmatrix} \tag{3.10}$$

Dynamic mechanical testing is often applied to measure material responses on short timescales. A sinusoidal deformation with angular frequency ω and strain amplitude γ_{12}^0 can be applied:

$$\gamma_{12}(t) = \gamma_{12}^0 \sin(\omega t) \tag{3.11}$$

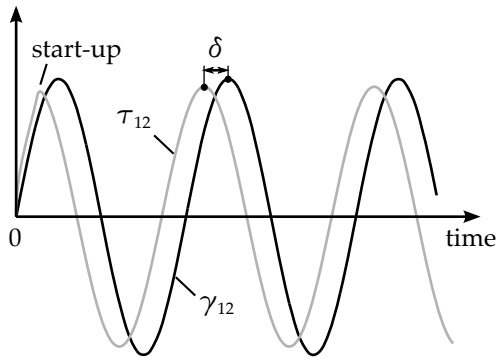

Figure 3.4 *The stress response of a visco-elastic material that is subjected to a sinusoidally applied strain.*

For linear material behaviour, the stress response is also sinusoidal:

$$\tau_{12}(t) = \tau_{12}^0 \sin(\omega t + \delta) \tag{3.12}$$

which runs out-of-phase with phase angle δ when the material behaves visco-elastically, as shown in figure 3.4. The linear visco-elastic material properties are represented by the storage and loss moduli, respectively [7]:

$$G' = \frac{\tau_{12}^0}{\gamma_{12}^0}\cos\delta \quad G'' = \frac{\tau_{12}^0}{\gamma_{12}^0}\sin\delta \tag{3.13}$$

The complex shear modulus is defined as:

$$G^* = G' + iG'' \tag{3.14}$$

where i denotes the imaginary number. The damping of the material is defined as:

$$\tan\delta = \frac{G''}{G'} \tag{3.15}$$

The dynamic and out-of-phase viscosities are respectively related to the loss and storage modulus through the angular frequency:

$$\eta' = \frac{G''}{\omega} \qquad \eta'' = \frac{G'}{\omega} \tag{3.16}$$

The complex viscosity is defined as:

$$\eta^* = \eta' - i\eta'' \tag{3.17}$$

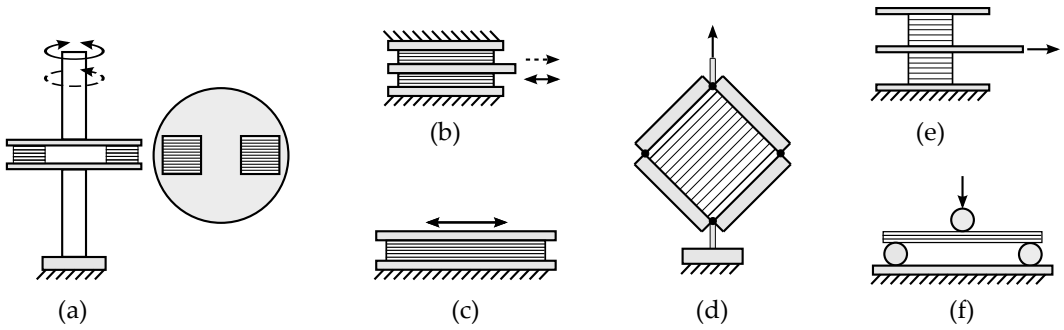

Figure 3.5 *Illustration of previously developed shear characterisation tests for UD reinforced melts. Tables 3.1 and 3.2 refer to the numbering (#).*

3.3 Review of shear characterisation methods

The development of intra-ply shear characterisation tests originates from the need to quantify the strength and stiffness of structural components. Different tests were developed to test composite laminates in their solidified state, which were summarised in several review papers [13, 14]. One can think of two and three rail shear tests, off-axis tests and picture-frame tests which are all standardised by, for example, the ASTM organisation, not necessarily intended for composite material testing. Shear characterisation methods by means of torsional loadings have also been developed. These comprise prismatic rods with a rectangular cross section and thin-walled tubes.

Other methods, some of them probably inspired by above-mentioned methods for solidified materials, have been developed to characterise composite materials in their flexible state as they are used in forming processes. An overview of methods was given by Harrison and Clifford [15]. A comparison between the measured material parameters showed deviations up to two orders of magnitude. Earlier work [16] showed that forming predictions are sensitive to the observed deviations. Accurate characterisation data is therefore required.

Tables 3.1 and 3.2 summarise previously developed methods to characterise the longitudinal shearing mechanism of fibre reinforced polymer melts. The methods differ in many aspects, for example the specimen size, geometry, and the type of load introduction, which can be done in a transient or dynamic manner. For the transient experiments, different strain rates were reported and shear strain magnitudes vary from small and linear up to large and non-linear. Dynamic experiments were carried out at different strain amplitudes and frequency ranges, where their translation to shear rates in the transient domain is not straightforward.

Groves *et al.* [17, 21, 28] introduced a characterisation test where laminates are positioned between two parallel plate fixtures (figure 3.5(a)). The first publication [17]

Table 3.1 *Longitudinal shear characterisation methods. (?) means that information was not explicitly given*

Ref.	Figure 3.5	Built-in device	Fixture type	Fixture movement	Movement type	Specimen dimension [mm] (in-plane dim. x thickness)
Groves [17]	(a)	rheometer	plate-plate	rotation	oscillating & transient	≈ Ø25x?
Scobbo [18, 19]	(b)	modified Mechanical Energy Resolver (MER)	plate-plate-plate	translation	oscillating	14x14x3
Wheeler [20]	(c)	custom-built linear oscillator	plate-plate	translation	oscillating	10x10x0.5
Groves [21]	(a)	rheometer	plate-plate	rotation	oscillating & transient	15x15x?
Jones [22]	(c)	custom-built linear oscillator	plate-plate	translation	oscillating	39x39x1
Roberts [23]	(c)	custom-built linear oscillator	plate-plate	translation	oscillating	39x39x3
Goshawk [24]	(b)	pull-out apparatus with weights	plate-plate-plate	translation	transient	39x39x1.7
McGuinness [25]	(d)	tensile tester	picture-frame	translation, pure shear	transient	200x200x(6.7..9)
Dykes [26]	(f)	tensile tester	V-bending	translation, bending	transient	120x40x?
Stanley [27]	(e)	Shearing apparatus	plate-plate-plate	translation,	transient	(5..10)x10x11

Table 3.2 *Longitudinal shear characterisation methods. (?) means that information was not explicitly given*

Ref.	Figure 3.5	Maximum shear magnitude γ, γ_0	Rates $\dot{\gamma}$ [s^{-1}] ω [$rad \cdot s^{-1}$]	Constitutive model used	Material tested	Number of plies
Groves [17]	(a)	0.01-0.5	0.1-100 [$rad \cdot s^{-1}$]	LVE (Voigt & Maxwell)	UD-Carbon/PEEK UD-Glass/PP	5-19
Scobbo [18, 19]	(b)	0.0150-0.025	64-376 [$rad \cdot s^{-1}$]	LVE (Voigt)	UD-Carbon/PEEK UD-Carbon/PAS	24 24
Wheeler [20]	(c)	0.4	0.1-100 [$rad \cdot s^{-1}$]	LVE (Voigt)	UD-Carbon/ Golden Syrup	4
Groves [21]	(a)	0.01-0.5	0.1..100 [$rad \cdot s^{-1}$]	LVE (Voigt & Maxwell)	UD-Carbon/PEEK UD-Glass/PP	?
Jones [22]	(c)	0.18-0.72	5-100 [$rad \cdot s^{-1}$]	LVE (Voigt)	UD-Nylon/Golden Syrup (model composite)	n/a
Roberts [23]	(c)	0.06-0.24	0.02-80 [$rad \cdot s^{-1}$]	LVE (Voigt)	UD-Nylon/Golden Syrup (model composite)	n/a
Goshawk [24]	(b)	0..11	0.01-0.7 [s^{-1}]	Newtonian fluid	UD-Nylon/Golden Syrup (model composite)	n/a
McGuinness [25]	(d)	0-0.2	0.0016-0.1 [s^{-1}]	IFRM + shear thinning	UD-Carbon/PEEK	48-64
Dykes [26]	(f)	0-0.8	0.014-0.14 [s^{-1}]	IFRM	UD-Glass/PP	8
Stanley [27]	(e)	0-0.5	0.002-0.02 [s^{-1}]	Power-law fluid (shear thinning)	UD-Carbon/PEEK	80

dealt with cross plied and UD laminates covering the whole platen surface. In this way, longitudinal and transverse shearing deformations are applied simultaneously. A shear deformation is applied by rotating one of the plates. Both oscillating shear and steady shear deformations were applied. Results for both types of laminates were similar and the response was said to be isotropic. A later publication [21] showed the results that were obtained by positioning two square laminates in an off-centred manner, such that both shearing modes could be characterised separately. The measured parameters were represented by using the LVE theory and the use of the well-known dynamic Voigt parameters G' and η'. Easier interpretation of the results was obtained by using the dynamic Maxwell parameters [29].

Instead of a rotating fixture, Scobbo and Nakajima [18, 19] induced an oscillating shear deformation by means of a translational motion of a plate-type fixture (figure 3.5(b)). The testing material is in contact with both sides of this dynamic plate, while fixed platens are in contact with the other sides of the specimens. Also here, results were presented in terms of the dynamic Voigt parameters by assuming the LVE theory.

An alternative set-up was developed by Wheeler and Jones [20]. A specimen is positioned between an upper fixed plate and a lower plate that is connected to an oscillatory drive mechanism, inducing a dynamic translational motion (figure 3.5(c)). The testing material comprised carbon fibres that were embedded within a Newtonian Golden Syrup resin, such that measurements could conveniently be performed at room temperature. The measured dynamic Voigt parameters were reported to be strain magnitude independent. Nevertheless, the sinusoidal load introduction led to responses with distorted sinusoidal shapes but which were further independent of strain amplitude. They also reported that a large scatter was observed between identical experiments, and the difficulty of producing identical samples with the carbon fibres was also a point of consideration. These reasons gave rise to conducting a research programme by Jones and Roberts [22, 23] with a better controllable model composite, utilising the same experimental set-up.

McGuinness and Ó Brádaigh [25] developed a picture-frame experiment to conduct tests with fibre reinforced thermoplastics at high temperatures (figure 3.5(d)). The picture-frame can be mounted in a tensile tester, after which a rhombus-type of shear deformation is induced by the upward displacement of the cross-head. UD carbon/PEEK (UD-C/PEEK, APC-2) laminates were enclosed by a polymeric diaphragm material. The specimen edges were tightly pressed against the legs of the frame to conduct the shearing deformation properly. Clamping the laminate on both faces would lead to complications, such as fibre tensioning. Such a mechanism is shown in figure 3.6 as an example with a single ply experiment, where it is observed that small fibre misalignments easily result in ply splitting. For cross-plied laminates, shearing deformation was introduced by clamping an over-sized specimen to the faces of the legs via pins. By correcting for the diaphragm foil,

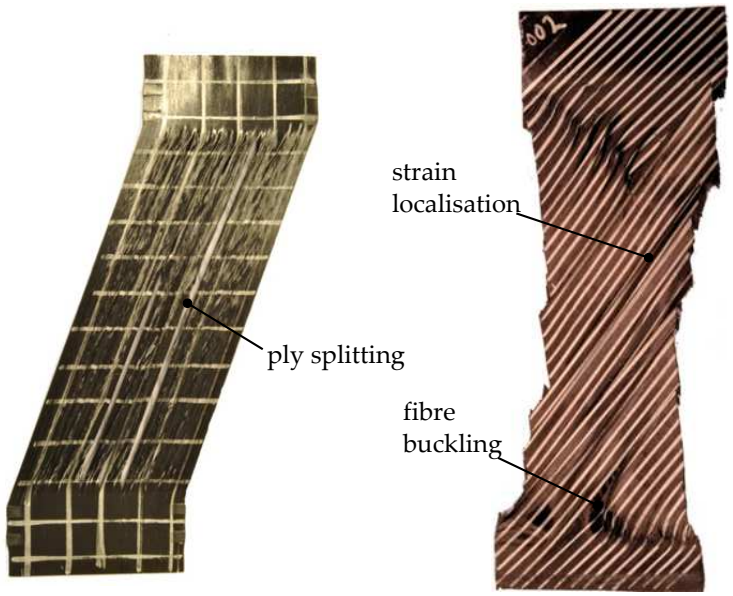

Figure 3.6 *Own attempts to characterise the shear behaviour of UD-C/PEEK with the picture-frame and the bias-extension method.*

longitudinal viscosities were determined as a function of shear rate. By utilising the IFRM model and expressing the viscosities as a function of shear rate, the viscosity could conveniently be described with a power-law relationship.

Stanley and Mallon [27] developed a test set-up (figure 3.5(e)) that shows some similarities with the device that was developed by Goshawk and Jones [24] (figure 5(b)). In both cases, specimens are positioned on either side of a centre plate. The other opposite sides of the specimens are pressed against fixed platens. Pulling out the centre plate introduces a steady transient shear deformation and large strain amplitudes can be obtained. Utilising the IFRM constitutive model just as McGuinness and Ó Brádaigh [25], a power-law relationship was again observed for the tested UD-C/PEEK (APC-2) material.

The bias-extension method is also a well-known test to characterise shear and has successfully been applied to molten thermoplastics with a woven fibre/bundle architecture [30]. This method cannot straightforwardly be applied to UD architectures due to the weak integrity of the laminate at high temperatures. Figure 3.6 shows the results of personal attempts to characterise UD-C/PEEK with this method. Specimen deformations were uncontrolled, yielding strain localisation and buckling. The method was, however, successfully applied to thermoset pre-preg materials [31–33] at relatively low temperatures. Integrity is believed to be enhanced by the tackiness of this material.

Many of the methods discussed introduce the longitudinal shear mechanism via tractions at the interfaces between fixture and specimen. These interfaces are parallel to the successively stacked ply-ply interfaces for the set-ups (a), (b), (c), and (e) in figure 3.5. In other words, load introduction is parallel to the fibre direction and parallel to the X_1-X_2 plane in figures 3.2 and 3.3. Resin-rich interfaces between successively stacked plies can be present [34], which could lead to concentrated shearing deformations at these interfaces. Inter-ply shearing or friction will then be more pronounced, rather than uniform longitudinal intra-ply shear through the thickness of the specimen. Dykes *et al.* [26] induce shear deformations with the V-bending set-up in figure 3.5(f), which next to the presence of fibre bending, could also lead to concentrated inter-ply shearing.

The method proposed in this chapter aims to characterise longitudinal shear with the aid of prismatic bars with a rectangular cross section. Torsional loads will be transferred via the gripping faces indicated in figure 3.3. Fibres are then pushed perpendicular to their alignment direction, namely perpendicular to the X_1-X_2 plane. This type of shear introduction has not been investigated yet for UD reinforced melts. Moreover, industry calls for an easily accessible standard test for shear characterisation of UD reinforced melts. The majority of the methods discussed utilise custom-built set-ups. Here, it is aimed to use a commercially available rheometer device with standard torsion fixtures. This may ultimately contribute to a successful adoption of this test.

3.4 Torsion of bars with a rectangular cross section

The method presented here deals with a prismatic bar that is subjected to torsion. The bar has a constant rectangular cross section, as shown in figure 3.3. Torque M and rotation angle ϕ for linear elastic prismatic bars are related as [35]:

$$M = G_{\mathrm{L}} J \frac{\phi}{L} \qquad \varphi = \frac{\phi}{L} \tag{3.18}$$

in which J is the torsional constant and depends on the cross-sectional geometry, L is the free specimen length, and G_{L} is the elastic shear modulus. The specific rotation angle φ can be used for convenience. It is assumed that the bar consists of UD fibres that run parallel to the rotation axis, although one could account for more complex situations with off-axis fibre alignments [36].

Applying a torsional deformation requires the application of fixtures that introduce these loads. These fixtures restrict the free warping of the cross sections, which results in a stiffening effect [35]. Clamping effects for such rectangular bars were experimentally investigated by Nederveen *et al.* [37, 38]. They developed a torsional pendulum device and a set of fixtures to perform shear property

characterisation of homogeneous and isotropic materials. Specimens were clamped and the free specimen length L was varied. The experiments showed deviations in the proportionality between the rotation angle ϕ and the specimen length L, which resulted in a length correction to be used in equation (3.18). A constant length correction was found for sufficiently long bars, as stated by Saint-Venant's principle [39]. Nevertheless, a few remarks were made. Experimental results were compared with theoretical predictions from Timoshenko [35] and Szabó [40], which assumed restricted warping of the cross sections at the end faces of the bar. Deviations between experimental results and model predictions were found. The experimental results were expected to be sensitive to fixture geometry, gripping forces, and material behaviour.

The restriction of warping due to clamping introduces stresses in the axial direction of the bar. These stresses vanish at sufficient distance from the clamping area. It was shown by Timoshenko [35] that the axial stress decays exponentially for isotropic bars for which one bar-end remains plane. Finite element analyses were conducted to investigate such clamping effects for anisotropic bars. The length over which the axial stress decays is dependent on the ratio between the shear and the axial rigidity of the bar. For the high anisotropy considered here (stiff fibres and a more compliant shear property), this length would be very large. For this reason, we assume that the axial stresses are present over the entire specimen length when it is fully clamped at both ends and subjected to torsion. In that case, the torsional constant J for free torsion in equation (3.18) does not hold. Therefore, a lower and an upper bound for the torsional constant will be determined for the case of small rotation angles. For larger rotation angles, the axial fibre stresses contribute rapidly to the torque. This situation is also considered afterwards.

3.4.1 Lower and upper bounds for the torsional constant

A lower bound for the torsional constant in equation (3.18) is obtained by assuming free warping (free torsion) of the cross section, which reads [35]:

$$J = \tfrac{1}{3}h^3 w \left(1 - \frac{192}{\pi^5}\frac{h}{w}\sum_{k=1}^{\infty}\frac{1}{(2k-1)^5}\tanh\left(\frac{(2k-1)\pi w}{2h}\right)\right) \tag{3.19}$$

It assumes transversely isotropic material properties (equal shear properties in the X_1-X_2 and X_1-X_3 planes). The cross-sectional dimensions w and h are shown in

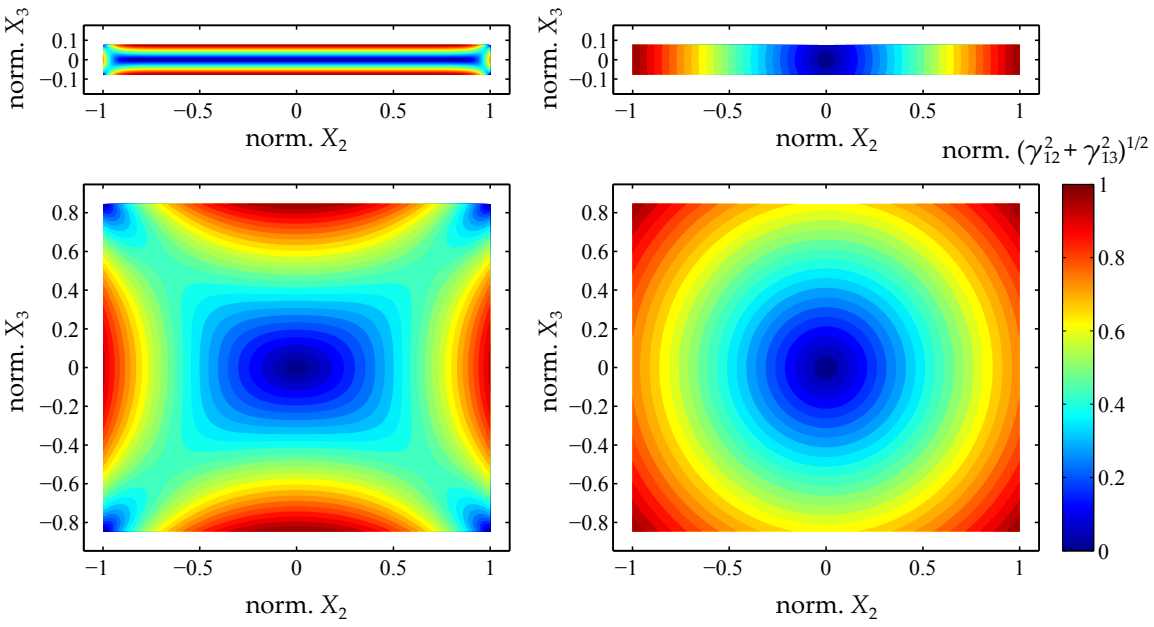

Figure 3.7 *Normalised equivalent strain distributions within the rectangular cross section. Cross-sectional dimensions are normalised as well. Left: assuming warping of the cross section. Right: assuming each cross-sectional slice to remain plane (simple torsion).*

figure 3.3. The shear strain components read [35]:

$$\gamma_{12}(X_2,X_3) = -\frac{\phi}{L}\frac{8h}{\pi^2}\sum_{k=1}^{\infty}\frac{(-1)^{k+1}}{(2k-1)^2}\left(1-\frac{\cosh\left(\frac{(2k-1)\pi X_2}{h}\right)}{\cosh\left(\frac{(2k-1)\pi w}{2h}\right)}\right)\sin\left(\frac{(2k-1)\pi X_3}{h}\right) \tag{3.20}$$

$$\gamma_{13}(X_2,X_3) = \frac{\phi}{L}\frac{8h}{\pi^2}\sum_{k=1}^{\infty}\frac{(-1)^{k+1}}{(2k-1)^2}\left(\frac{\sinh\left(\frac{(2k-1)\pi X_2}{h}\right)\cos\left(\frac{(2k-1)\pi X_3}{h}\right)}{\cosh\left(\frac{(2k-1)\pi w}{2h}\right)}\right) \tag{3.21}$$

Figure 3.7 shows the normalised equivalent shear strain distribution for a narrow and a thicker cross section.

An upper bound of the torsional constant in equation (3.18) is obtained by assuming that each cross section remains plane during loading. The polar moment of inertia for a rectangular cross section can be used for this special case:

$$J_p = \tfrac{1}{12}wh(w^2+h^2) \tag{3.22}$$

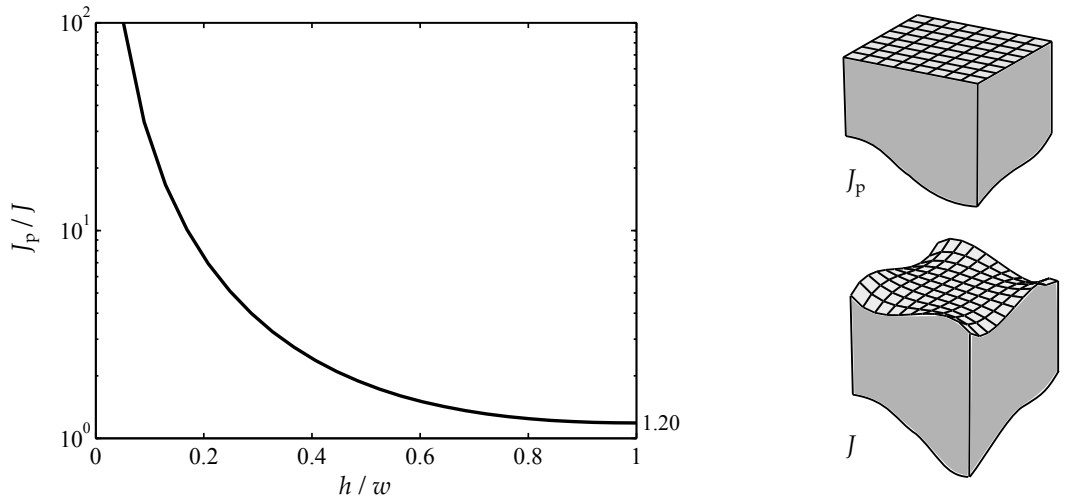

Figure 3.8 *Left: difference between the torsional constant for the situation where the cross sections are assumed to remain plane (J_p) and the situation where cross sections are free to warp (J). Right: illustration of cross-sectional warping for the two extreme cases considered.*

Shear strain components then read:

$$\gamma_{12} = -\frac{\phi}{L} X_3 \qquad \gamma_{13} = \frac{\phi}{L} X_2 \tag{3.23}$$

The equivalent shear strain distribution is very different from the free torsion situation, as shown in figure 3.7. The ratio between the polar moment of inertia J_p and the free torsion constant J is shown in figure 3.8. It can be seen that the difference between the lower and upper bound for the torsional rigidity reduces to 20% for square cross sections.

3.4.2 Small strain dynamic loadings applied to visco-elastic bars

The aim is to characterise prismatic bars comprising a visco-elastic material. Small strain dynamic testing allows for measuring the storage and loss moduli. The rotation angle and torque can be expressed analogously to equations (3.11) and (3.12). By applying the complex notation, we may express these as:

$$\phi^* = \phi_0 \cos(\omega t) + i\phi_0 \sin(\omega t) \tag{3.24}$$

$$M^* = M_0 \cos(\omega t + \delta) + iM_0 \sin(\omega t + \delta) \tag{3.25}$$

By replacing the variables in (3.18) with these complex variants and the introduction of a complex longitudinal shear modulus, one arrives at:

$$M^* = G_{\mathrm{L}}^* J \frac{\phi^*}{L} \tag{3.26}$$

Since J is a lower bound torsional constant, an upper bound for the separate storage and loss moduli can be determined from dynamic oscillatory experiments:

$$G'_{\mathrm{L}} = \frac{L}{J}\frac{M_0}{\phi_0}\cos(\delta) \qquad G''_{\mathrm{L}} = \frac{L}{J}\frac{M_0}{\phi_0}\sin(\delta) \tag{3.27}$$

in which the zero subscripts indicate torque and rotation amplitudes, and δ is the phase angle. For square cross sections, lower bounds for these dynamic moduli using J_{p} will be 16.67% lower than the upper bounds using J, as was concluded from the differences between the torsional constants in figure 3.8.

3.4.3 Adverse fibre tensions and larger dynamic deformations

The previous situation of restricted warping is elaborated here by including the effect of fibre tensions, which develop when the end faces of the bar remain at equal distance during torsion. The fibre tensions consequently contribute to the torque, which affects the measured shear property G^*. An analytical model of the fibre reinforced bar with restricted warping is presented, after which the sensitivity of the measured shear property to adverse fibre tensions is investigated.

Kinematics

When the fibre reinforced bar is subjected to torsion and fully clamped at both ends (no warping), each cross-sectional slice in the bar rotates rigidly. For this situation, the new coordinates x_i of each point in the rectangular bar are expressed as a function of the initial point coordinates X_i:

$$\begin{aligned} x_1 &= X_1 \\ x_2 &= X_2\cos\left(\varphi(t)X_1\right) - X_3\sin\left(\varphi(t)X_1\right) \qquad \text{with} \qquad \varphi(t) = \frac{\phi(t)}{L} \\ x_3 &= X_2\sin\left(\varphi(t)X_1\right) + X_3\cos\left(\varphi(t)X_1\right) \end{aligned} \tag{3.28}$$

in which the specific rotation angle φ is a function of time t for dynamic testing. We refer to this situation as simple torsion, since it is analogous to the well-known simple shear situation with an extension to the third dimension. The deformation gradient

$\boldsymbol{F}$ maps the old situation X_i to the new situation x_i:

$$\boldsymbol{F}(\boldsymbol{X},t) = \frac{\partial \boldsymbol{x}}{\partial \boldsymbol{X}}|_t = \begin{bmatrix} 1 & 0 & 0 \\ -\varphi(t)X_2\sin(\varphi(t)X_1) - \varphi(t)X_3\cos(\varphi(t)X_1) & \cos(\varphi(t)X_1) & -\sin(\varphi(t)X_1) \\ \varphi(t)X_2\cos(\varphi(t)X_1) - \varphi(t)X_3\sin(\varphi(t)X_1) & \sin(\varphi(t)X_1) & \cos(\varphi(t)X_1) \end{bmatrix} \tag{3.29}$$

The Green-Lagrange strain tensor components then read:

$$\boldsymbol{E} = \tfrac{1}{2}\left(\boldsymbol{F}^T\cdot\boldsymbol{F} - \boldsymbol{I}\right) = \tfrac{1}{2}\begin{bmatrix} \left(X_2^2\varphi^2(t) + X_3^2\varphi^2(t)\right) & -X_3\varphi(t) & X_2\varphi(t) \\ -X_3\varphi(t) & 0 & 0 \\ X_2\varphi(t) & 0 & 0 \end{bmatrix} \tag{3.30}$$

The E_{11} term represents the strain in the axial direction, which is related to the square of the specific rotation angle. The E_{12} and E_{13} terms represent the longitudinal shearing, similar to the shear terms in equation (3.23). Transverse shearing does not occur for the assumed kinematics.

The velocity of each point can be determined with (3.28), which can be used to determine the velocity gradient:

$$\boldsymbol{L} = \frac{\partial \boldsymbol{v}}{\partial \boldsymbol{X}}\cdot\boldsymbol{F}^{-1} = \boldsymbol{D} + \boldsymbol{W} \tag{3.31}$$

Each second order tensor can be decomposed into a symmetric and a skew-symmetric part, in this case the rate of deformation tensor $\boldsymbol{D}$ and the spin tensor $\boldsymbol{W}$, respectively. The components D_{ij} of the rate of deformation tensor read:

$$\begin{aligned} D_{11} &= D_{22} = D_{33} = D_{23} = D_{32} = 0 \\ D_{12} &= D_{21} = \tfrac{1}{2}\left\{-X_3\dot{\varphi}(t)\cos(X_1\varphi(t)) - X_2\dot{\varphi}(t)\sin(X_1\varphi(t))\right\} \\ D_{13} &= D_{31} = \tfrac{1}{2}\left\{X_2\dot{\varphi}(t)\cos(X_1\varphi(t)) - X_3\dot{\varphi}(t)\sin(X_1\varphi(t))\right\} \end{aligned} \tag{3.32}$$

where the dots denote the time derivatives of the particular variable.

Constitutive modelling

The torque that would be measured in this situation can be derived from the stress situation in an arbitrary cross section of the rectangular bar. The stresses are determined by the constitutive models considered. A constitutive formulation can be obtained successfully by using a free energy function per unit mass [41]. This function must be an invariant function of the right Cauchy-Green strain tensor $\boldsymbol{C}$ or

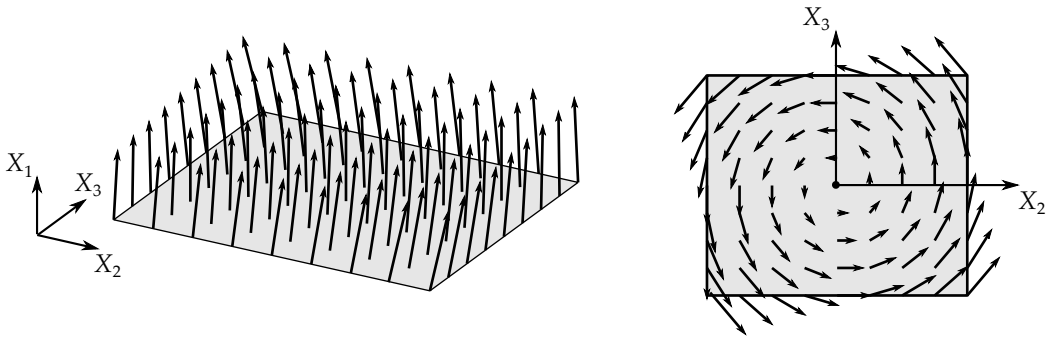

Figure 3.9 *Impression of the fibre directions* $\boldsymbol{a}$ *in the new situation at the* $X_1 = 0$ *plane, for a rotation angle* φ*. Left: 3D view. Right: top view.*

the Green-Lagrange strain tensor $\boldsymbol{E} = \boldsymbol{E}(\boldsymbol{C})$ in order to deal properly with anisotropy, as was shown by Huétink [42].

The Cauchy stress in the case of elastic fibres can be described with the following relation:

$$\boldsymbol{\sigma}_{\mathrm{E}} = \frac{\rho v_{\mathrm{f}} E_{\mathrm{f}}}{\rho_0 l_0^4} \boldsymbol{a}\boldsymbol{a}\boldsymbol{a}_0\boldsymbol{a}_0 : \boldsymbol{E} \tag{3.33}$$

which was given by Huétink [42] and Ten Thije [43]. The densities ρ and ρ_0 cancel out since the assumed kinematics in (3.28) yield incompressibility and thus $\det\boldsymbol{F} = 1$. A particle of the fibre in the initial state is described with vector $\boldsymbol{a_0}$ and length l_0. The fibre particle in the deformed state is given by vector $\boldsymbol{a}$:

$$\boldsymbol{a} = \boldsymbol{F} \cdot \boldsymbol{a}_0 \tag{3.34}$$

An impression of the distribution of the new fibre directions for a torsionally loaded bar is shown in figure 3.9. Elastic fibre tensions contribute to the torque with their in-plane decomposed components.

Let the viscous shear behaviour of the assumed fibre reinforced continuum be described with the Newtonian fluid model. The Cauchy stress then reads:

$$\boldsymbol{\sigma}_{\mathrm{V}} = 2\eta_{\mathrm{L}}\boldsymbol{D} \tag{3.35}$$

where η_{L} is the longitudinal shearing viscosity.

The total stress in each point in the bar can be determined by adding the elastic fibre stresses to the viscous shearing stresses:

$$\boldsymbol{\sigma} = \boldsymbol{\sigma}_{\mathrm{E}} + \boldsymbol{\sigma}_{\mathrm{V}} \tag{3.36}$$

After substitution of equations (3.29) until (3.32) into (3.36), the in-plane components σ_{ij} that contribute to the torque read:

$$\sigma_{12} = \sigma_{21} = -\tfrac{1}{2}\left\{X_3\cos(X_1\varphi(t)) + X_2\sin(X_1\varphi(t))\right\}\cdot \left\{v_\mathrm{f}E_\mathrm{f}\varphi^3(t)(X_2^2+X_3^2) + 2\eta_\mathrm{L}\dot{\varphi}(t)\right\} \tag{3.37}$$

$$\sigma_{13} = \sigma_{31} = \tfrac{1}{2}\left\{X_2\cos(X_1\varphi(t)) - X_3\sin(X_1\varphi(t))\right\}\cdot \left\{v_\mathrm{f}E_\mathrm{f}\varphi^3(t)(X_2^2+X_3^2) + 2\eta_\mathrm{L}\dot{\varphi}(t)\right\} \tag{3.38}$$

The torque at an arbitrary plane cross section is determined by considering the contribution of the in-plane stresses at each point times their arms, which are measured from the centre of rotation. Adding the contributions of all points yields the following integral formulation:

$$M(\varphi(t)) = \int_{-\frac{h}{2}}^{\frac{h}{2}}\int_{-w/2}^{\frac{w}{2}}\left\{x_2\sigma_{13} - x_3\sigma_{12}\right\}\mathrm{d}x_2\mathrm{d}x_3 \tag{3.39}$$

Solving this integral by evaluating the torque at the $X_1 = 0$ plane yields:

$$\begin{aligned} M(\varphi(t)) &= M_\mathrm{E} + M_\mathrm{V} \\ &= \varphi^3(t)\frac{v_\mathrm{f}E_\mathrm{f}}{160}\left(w^5h + h^5w + \tfrac{10}{9}w^3h^3\right) + \dot{\varphi}(t)\frac{\eta_\mathrm{L}}{12}\left(w^3h + wh^3\right) \end{aligned} \tag{3.40}$$

where the total torque is divided into an elastic and a viscous part.

Sensitivity analysis

The effect of fibre tensions on the measured response was investigated for the case in which one assumes the free torsion situation, whereas the specimen is actually clamped in such a way that warping is restricted. The aspect ratio of the cross section, material parameters, rotation amplitude and rotation frequency is varied. The analysis procedure is schematically shown in figure 3.10.

It is convenient to introduce a dimensionless number that represents the combination of the material parameters used:

$$\mathrm{Fd} = \frac{v_\mathrm{f}E_\mathrm{f}}{\omega\eta_\mathrm{L}} \tag{3.41}$$

This number is referred to as the fibre dominance number. The term ω is the already introduced angular frequency. As an example, a fibre dominance number of $1.33\cdot10^6$ represents the situation of a bar with longitudinal shear viscosity η_L = 1000 Pa·s, fibre volume fraction v_f = 0.6, and fibre elasticity modulus E_f = 221 GPa, which is

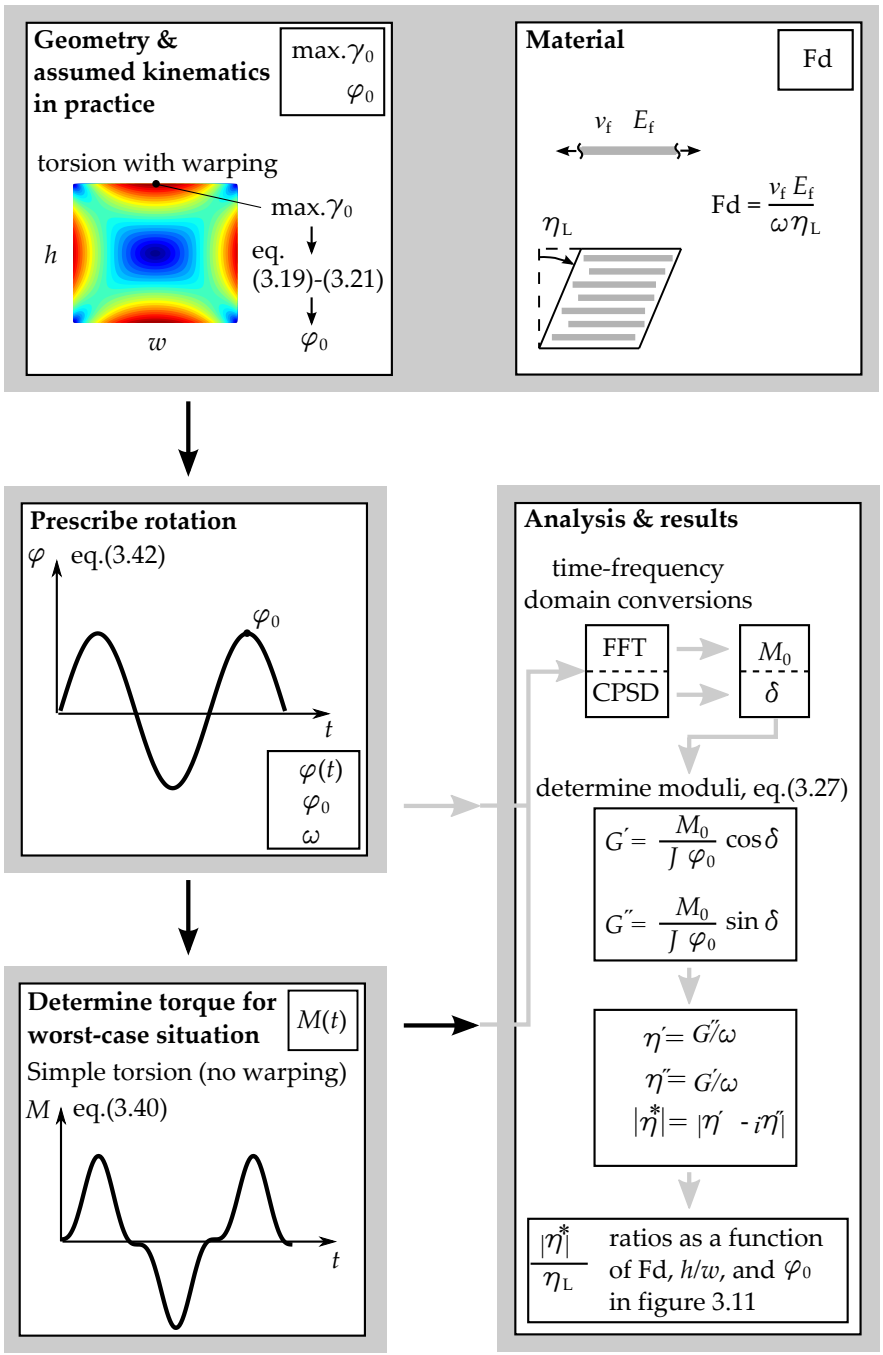

Figure 3.10 *Flow chart of the analysis procedure.*

tested at $\omega = 10$ rad/s.

In the case of dynamic testing, the rectangular bar is subjected to an oscillating

rotation angle with amplitude φ_0:

$$\varphi(t) = \varphi_0 \sin(\omega t) \qquad \dot{\varphi}(t) = \varphi_0 \omega \cos(\omega t) \tag{3.42}$$

The torque was evaluated by substituting equation (3.42) into (3.40) for a given Fd number. The torque amplitude M_0 and the phase angle δ were subsequently determined by means of spectral analyses. This was achieved by applying a Fast Fourier Transform (FFT) and a Cross Power Spectral Density (CPSD) algorithm, which is available in MATLAB.

Results

Without the presence of adverse fibre tensioning effects, one would ideally measure the desired material shearing parameter G_{L}^*. It would only have an imaginary part $G_{\mathrm{L}}'' = \eta_{\mathrm{L}}'$, since a purely Newtonian shearing viscosity η_{L} was assumed in (3.35). The deviation between the actual viscosity η_{L} and the measured dynamic viscosity is expressed as:

$$\frac{|\eta^*|}{\eta_{\mathrm{L}}} \tag{3.43}$$

which equals to unity when no fibre tensioning is present. The results of the sensitivity study are presented for a narrow and a square cross-sectional geometry in figure 3.11. Whereas the results can be represented as a function of cross-sectional aspect ratio, the rotation angle amplitude φ_0 necessary to achieve a certain strain amplitude γ_0 is dependent on the actual cross-sectional dimensions (see equations (3.20), (3.21) and (3.23)). Realistic dimensions ($h = 1..10$, $w = 10$ mm) were used to generate the rotation angle axis on top of the figures. This rotation angle was further determined from the maximum strain amplitude γ_0 that appears in the case of free torsion (no clamping effects), which is shown by the second x-axis. The evaluated model assumes no warping, which results in a different maximum strain γ_0 as shown by the third x-axis in grey.

Figure 3.11(a) shows the deviations for the narrow cross section as a function of strain amplitude and fibre dominance number. The measured material property is increasingly overestimated for increasing rotation angles. As expected, a larger fibre dominance number results in larger overestimations of the shearing property. For the rotation angle φ_0 considered, the maximum shear strain γ_0 for free torsion and for restricted warping deviates highly as well. This implies that the actual shear strain amplitude that appears in practice is quite uncertain, as the actual clamping effects in practice are unknown.

Figure 3.11(b) shows the deviations for the square cross section. Also here, an increasing rotation angle and fibre dominance number result in an increasing

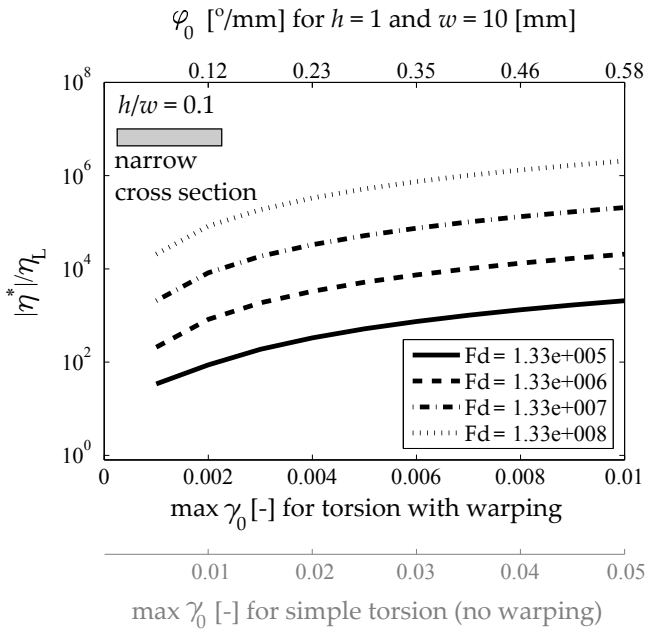

(a)

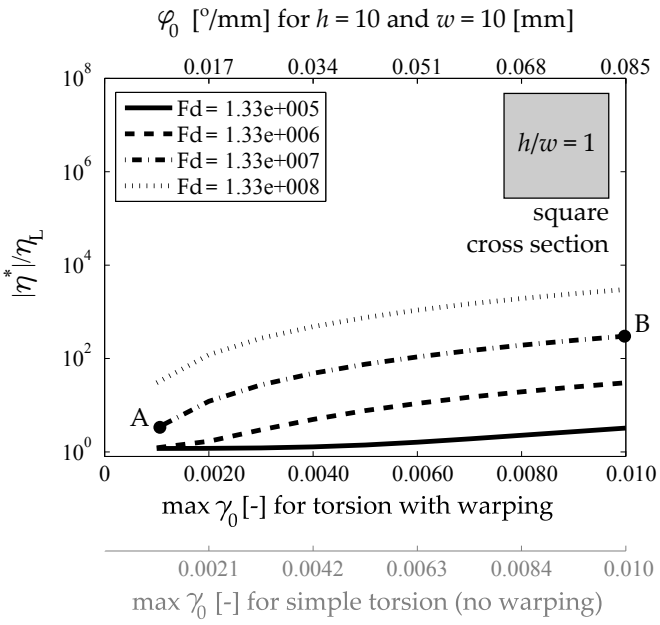

(b)

Figure 3.11 *Deviations of the measured complex viscosity $|\eta^*|$ with respect to the actual shearing viscosity η_L when fibres are tensioned according to the simple torsion model. (a) Narrow cross section. (b) Square cross section.*

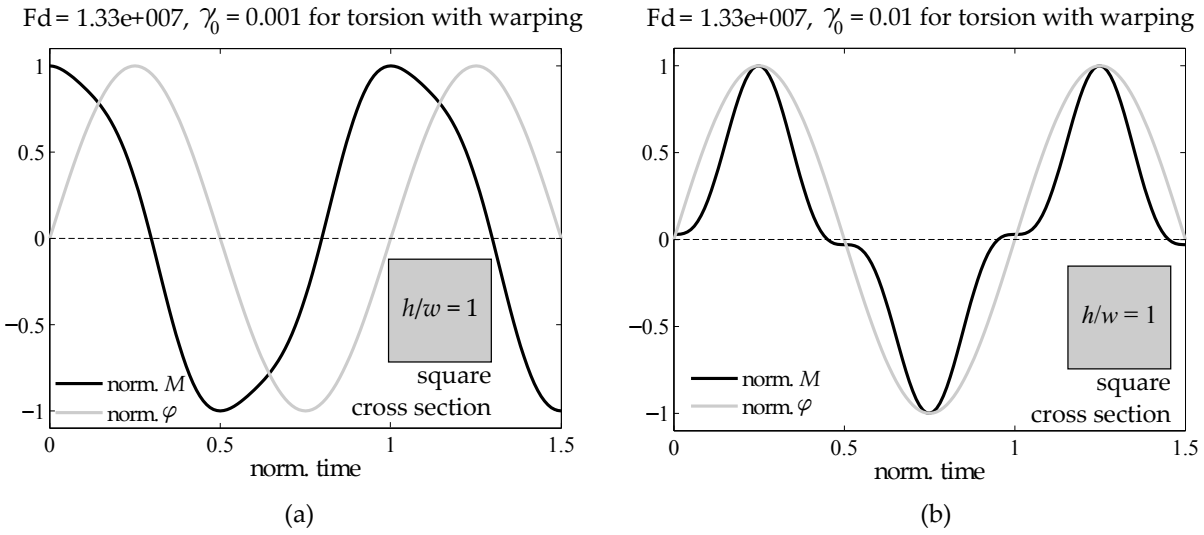

Figure 3.12 *Torsional responses as invoked by a sinusoidally applied rotation. (a) Parameter input as represented by point A in figure 3.11(b). (b) Parameter input as represented by point B in figure 3.11(b).*

overestimation of the measured shear property. The overestimations are smaller than those for the narrow cross section, for a certain fibre dominance number. Compared to the narrow cross section, smaller rotation angles are necessary to achieve a certain strain amplitude. Contrary to the narrow cross section results, the difference between the shear strain amplitudes for the free torsion and the restricted warping situation is negligible (lower two x-axes). In order to get an impression of the distorted responses, figure 3.12 shows the model predictions for points A and B indicated in figure 3.11(b). Clearly, the elastic fibres distort the purely sinusoidal torsional response (figure 3.4), as assumed by the LVE theory. These responses were validated with the aid of finite element analyses [44].

3.5 Torsion bar guidelines

Guidelines have been established for the torsion bar geometry. These are based on the previous analyses and the practical experience of the authors. Close to square cross sections of h/w = 0.85-1 are advised, because:

- Distorted torsional responses and therefore the deviation between the measured and actual shear property are then minimised.
- The difference between the maximum strain amplitude for free torsion and bars with restricted warping is minimal for square cross sections.

- The thicker the specimen, the better the integrity of the specimen is at high temperatures in practice.

Apart from the cross-sectional aspect ratio, the specimen width and thickness can be determined according to the available space in the rheometer device and fixtures as well as the load range of the instrument. A larger torque is required for larger cross-sectional dimensions. These can be determined such that the envisioned torque amplitude is within the accurate measurement range of the load cell. Large specimen lengths are advised. A larger length results in a larger volume to shear, which results in a better averaged response of the specimen. However, clamping effects are not weakened for larger lengths due to the high anisotropy. Moreover, the length is limited by the available space in the testing device and the acceptable temperature deviation within the specimen.

It is hard to give a maximum rotation angle that should be applied, since the actual clamping effects are unknown in practice. In order to determine the significance of adverse fibre tensioning effects that were induced by the fixtures, it is advised to test and compare specimens of different thicknesses. Alternatively, the measurements can be compared with those obtained by using another type of fixture, which loads the specimen differently.

As a final example, deviations from the actual viscosity η_L are given in table 3.3 for the situation of a bar with dimensions t = 11 mm, w = 13 mm, which is subjected to a testing frequency of 1 Hz. The calculations involved are shown by the flow chart in figure 3.10. Carbon fibres with an axial modulus of E_f = 221 GPa are considered with a fibre volume fraction v_f of 0.6. The longitudinal viscosity is unknown as this is the property to be measured. Nevertheless, we assume a typical neat thermoplastic polymer viscosity of 300 Pa·s. Harrison and Clifford [15] showed that these viscosities differ for several orders of magnitude, depending on the experimental set-up used. Therefore, the analysis is repeated for $3 \cdot 10^3$ and $3 \cdot 10^4$ Pa·s. The deviations in table 3.3 are fairly reasonable for strains up to 0.1%, as the kinematics assumed in equation (3.40) imply simple torsion (upper bound torsional constant J_p) and tensioning of all the fibres in the bar. A less severe condition is expected in practice.

Table 3.3 *Deviation of the measured viscosity from the actual longitudinal viscosity η_L, as determined according to the flow chart in figure 3.10. A bar with dimensions t = 11 mm, w = 13 mm is assumed. Other properties: E_f = 221 GPa, $v_f = 0.6$, $\omega = 2\pi$ rad/s.*

	γ_0 [%]				
η_L [Pa·s]	0.10	0.33	0.55	0.78	1.0
$3 \cdot 10^2$	$16.1\eta_L$	$170\eta_L$	$486\eta_L$	$966\eta_L$	$1610\eta_L$
$3 \cdot 10^3$	$2.02\eta_L$	$17.0\eta_L$	$48.7\eta_L$	$96.6\eta_L$	$161\eta_L$
$3 \cdot 10^4$	$1.22\eta_L$	$2.09\eta_L$	$5.01\eta_L$	$9.73\eta_L$	$16.1\eta_L$

3.6 Conclusions

A torsion bar test was proposed for the characterisation of the longitudinal shearing mechanism of UD fibre reinforced thermoplastic melts. It can be easily conducted with the aid of standard rheometers. Small strain dynamic testing can be utilised to perform a thorough rheological characterisation of the material. The kinematics of the torsionally loaded bar and the relations to determine its shear property were outlined.

Torsional loads must be introduced via fixtures in practice. The presence of axially aligned stiff fibres potentially influences the measured responses. As a result, the measured shear property deviates from the actual shear property. The sensitivity to these effects was investigated by means of a model, in order to develop guidelines for the specimen geometry. A worst-case situation was considered by assuming that all cross sections of the bar remain plane during torsion. The situation was investigated for small and larger rotations. The latter includes the elastic contribution of the fibres to the measured torque. All analyses showed that most reliable shear property measurements can be obtained by using specimens with a close to square cross section. The specimen dimensions must further be tailored to the available space in the aimed fixtures and the measurement device to be used.

References

[1] T.G. Gutowski. Resin flow/fiber deformation model for composites. *SAMPE quarterly*, **16**(4):58–64, 1985.

[2] J. Schlimbach and P. Mitschang. Process-based cycle time estimation for the thermoplastic tape placement. *Journal of Thermoplastic Composite Materials*, **19**(5):507–529, 2006.

[3] F.N. Cogswell. The experience of thermoplastic structural composites during processing. *Composites Manufacturing*, **2**(3-4):208–216, 1991.

[4] F.N. Cogswell. Flow and rheology in polymer composites manufacturing, chapter Continuous-Fibre Systems, 127–202. Elsevier Science B.V., 1994.

[5] A.M. Murtagh and P.J. Mallon. Composite Sheet Forming, volume 11 of *Composite Materials Series*, chapter Characterisation of Shearing and Frictional Behaviour during Sheet Forming, 163–216. Elsevier Science B.V., 1997.

[6] C.M. Ó Brádaigh. Flow and rheology in polymer composites manufacturing, chapter Sheet Forming of Composite Materials, 517–569. Elsevier Science B.V., 1994.

[7] J.D. Ferry. Viscoelastic properties of polymers. John Wiley & Sons, 3rd edition, 1980.

[8] R.B. Pipes, D.W. Coffin, P. Simacek, S.F. Shuler, and R.K. Okine. Flow and rheology in polymer composites manufacturing, chapter Rheological Behavior of Collimated Fiber Thermoplastic Composite Materials, 85–202. Elsevier Science B.V., 1994.

[9] A.J.M. Spencer. Continuum Theory Of the Mechanics Of Fibre - Reinforced Composites, chapter Constitutive theory for strongly anisotropic solids. Springer Verlag, 1984.

[10] T.G. Rogers. Rheological characterization of anisotropic materials. *Composites*, **20**(1):21–27, 1989.
[11] A.J. Beaussart, J.W.S. Hearle, and R.B. Pipes. Constitutive relationships for anisotropic viscous materials. *Composites Science and Technology*, **49**(4):335–339, 1993.
[12] R.M. Christensen. Effective viscous flow properties for fiber suspensions under concentrated conditions. *Journal of Rheology*, **37**(1):103–120, 1993.
[13] Y.M. Tarnopol'skii and T.Y. Kintsis. Methods for testing composites in shear (review). *Mechanics of Composite Materials*, **17**(3):364–376, 1981.
[14] S. Lee and M. Munro. Evaluation of in-plane shear test methods for advanced composite materials by the decision analysis technique. *Composites*, **17**(1):13–22, 1986.
[15] P. Harrison and M.J. Clifford. Design and manufacture of textile composites, chapter Rheological Behaviour of Pre-impregnated Textile Composites. Woodhead Publishing Ltd., Cambridge, UK, 2005.
[16] S.P. Haanappel, R. ten Thije, and R. Akkerman. Forming predictions of UD reinforced thermoplastic laminates. In 14th European Conference on Composite Materials, ECCM 2010, 2010.
[17] D.J. Groves. A characterization of shear flow in continuous fibre thermoplastic laminates. *Composites*, **20**(1):28–32, 1989.
[18] J.J. Scobbo Jr. and N. Nakajima. Dynamic mechanical analysis of molten thermoplastic/continuous graphite fiber composites in simple shear deformation. In National SAMPE Technical Conference, volume 21, 730–743, 1989.
[19] J.J. Scobbo Jr. and N. Nakajima. Modification of the mechanical energy resolver for high temperature and rigid material applications. *Polymer Testing*, **9**(4):245–255, 1990.
[20] A.B. Wheeler and R.S. Jones. A characterization of anisotropic shear flow in continuous fibre composite materials. *Composites Manufacturing*, **2**(3-4):192–196, 1991.
[21] D.J. Groves, A.M. Bellamy, and D.M. Stocks. Anisotropic rheology of continuous fibre thermoplastic composites. *Composites*, **23**(2):75–80, 1992.
[22] R.S. Jones and R.W. Roberts. Anisotropic shear flow in continuous fibre composites. *Composites*, **25**(3):171–176, 1994.
[23] R.W. Roberts and R.S. Jones. Rheological characterization of continuous fibre composites in oscillatory shear flow. *Composites Manufacturing*, **6**(3-4):161–167, 1995.
[24] J.A. Goshawk and R.S. Jones. Structure reorganization during the rheological characterization of continuous fibre-reinforced composites in plane shear. *Composites Part A: Applied Science and Manufacturing*, **27**:279–286, 1996.
[25] G.B. McGuinness and C.M. Ó Brádaigh. Characterisation of thermoplastic composite melts in rhombus-shear: The picture-frame experiment. *Composites Part A: Applied Science and Manufacturing*, **29**(1-2):115–132, 1998.
[26] R.J. Dykes, T.A. Martin, and D. Bhattacharyya. Determination of longitudinal and transverse shear behaviour of continuous fibre-reinforced composites from vee-bending. *Composites Part A: Applied Science and Manufacturing*, **29**(1-2):39–49, 1998.
[27] W.F. Stanley and P.J. Mallon. Intraply shear characterisation of a fibre reinforced thermoplastic composite. *Composites Part A: Applied Science and Manufacturing*, **37**:939–948, 2006.
[28] D.J. Groves and D.M. Stocks. Rheology of thermoplastic-carbon fibre composite in the

elastic and viscoelastic states. *Composites Manufacturing*, **2**(3-4):179–184, 1991.
[29] J.J. Benbow, F.N. Cogswell, and M.M. Cross. On the dynamic response of viscoelastic fluids. *Rheologica Acta*, **15**(5):231–237, 1976.
[30] J. Cao, R. Akkerman, P. Boisse, J. Chen, H.S. Cheng, E.F. de Graaf, J.L. Gorczyca, P. Harrison, G. Hivet, J. Launay, W. Lee, L. Liu, S.V. Lomov, A. Long, E. de Luycker, F. Morestin, J. Padvoiskis, X.Q. Peng, J. Sherwood, Tz Stoilova, X.M. Tao, I. Verpoest, A. Willems, J. Wiggers, T.X. Yu, and B. Zhu. Characterization of mechanical behavior of woven fabrics: Experimental methods and benchmark results. *Composites Part A: Applied Science and Manufacturing*, **39**(6):1037–1053, 2008.
[31] K. Potter. Bias extension measurements on cross-plied unidirectional prepreg. *Composites Part A: Applied Science and Manufacturing*, **33**(1):63–73, 2002.
[32] K. Potter. In-plane and out-of-plane deformation properties of unidirectional preimpregnated reinforcement. *Composites Part A: Applied Science and Manufacturing*, **33**(11):1469–1477, 2002.
[33] Y.R. Larberg and M. Åkermo. In-plane properties of cross-plied unidirectional prepreg. In ICCM International Conferences on Composite Materials, 2007.
[34] S.G. Advani, T.S. Creasy, and S.F. Shuler. Composite Sheet Forming, volume 11 of *Composite Materials Series*. Elsevier Science B.V., 1997.
[35] S.P. Timoshenko and J.N. Goodier. Theory of Elasticity. McGraw-Hill, 3rd edition, 1970.
[36] C.B. Demakos. Stress fields induced in fibre-reinforced composite laminate beams by torsion. *Composites Science and Technology*, **62**(2):213–222, 2002.
[37] C.J. Nederveen and C.W. van der Wal. A torsion pendulum for the determination of shear modulus and damping around 1 Hz. *Rheologica Acta*, **6**(4):316–323, 1967.
[38] C.J. Nederveen and J.F. Tilstra. Clamping corrections for torsional stiffness of prismatic bars. *Journal of Physics D: Applied Physics*, **4**(11):1661–1667, 1971.
[39] B. Saint-Venant. Memoires des Savants Etrangers 14, chapter Memoire sur la torsion des prismes, 233–560, 1855.
[40] I. Szabó. Höhere Technische Mechanik. Berlin: Springer Verlag, 1960.
[41] R. Akkerman. Euler-Lagrange simulations of nonisothermal viscoelastic flows. Ph.D. thesis, University of Twente, 1993.
[42] J. Huétink. On anisotropy, objectivity and invariancy in finite thermo-mechanical deformations. In 9th ESAFORM conference on Material Forming, 355–358, 2006.
[43] R.H.W. ten Thije. Finite element simulations of laminated composite forming processes. Ph.D. thesis, University of Twente, 2007.
[44] S.P. Haanappel, R.H.W. ten Thije, U. Sachs, A.D. Rietman, and R. Akkerman. In-plane shear characterisation of uni-directionally reinforced thermoplastic melts. In G. Menary, editor, the 14th International ESAFORM Conference on Material Forming, volume 1353 of *AIP Conference Proceedings*, 930–935. American Institute of Physics, 2011.

Chapter 4

Shear characterisation of uni-directional fibre reinforced thermoplastic melts by means of torsion*

Abstract

Hot forming of fibre reinforced thermoplastic laminates invokes several deformation mechanisms such as intra-ply shearing. The longitudinal intra-ply shearing mechanism can be characterised by applying torsional loads to prismatic bars with a close to square cross section. In this chapter, this characterisation method was implemented in practice and critically evaluated. Torsion bars of UD carbon/PEEK were tested at high temperatures with the aid of a commercially available rheometer. Storage and loss moduli were obtained by subjecting the specimens to oscillatory loading. Non-linear material behaviour was found for relatively small shear strains. In the linear regime, the characteristics were found to be similar to that of a visco-elastic solid or weak gel, confirmed by a dominant storage modulus and a weak frequency dependency. The small strain results are explained by the presence of an elastic fibrous network, which explains the temperature independency of the moduli as well. The method shows good potential to become a standard test, considering the relative ease in performing experiments, the obtained repeatability, and the nowadays widely available standard rheometers.

*Reproduced from: S.P. Haanappel, R. Akkerman. Shear characterisation of uni-directional fibre reinforced thermoplastic melts by means of torsion. Submitted to: *Composites Part A: Applied Science and Manufacturing*, **2013**.

4.1 Introduction

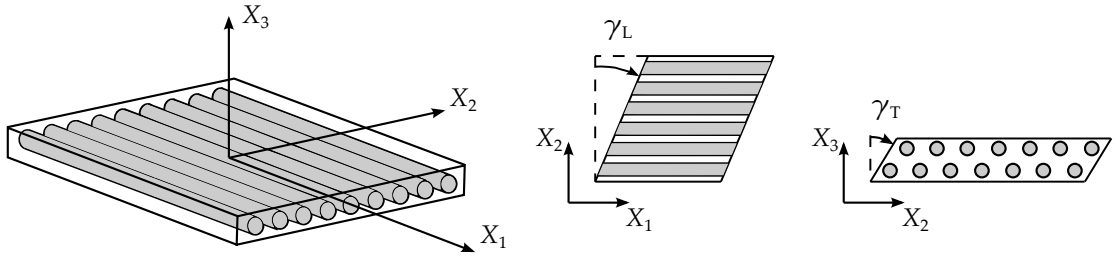

Figure 4.1 *Left: definition of the coordinate system with respect to the fibre direction. Centre: axial or longitudinal intra-ply shearing. Right: transverse intra-ply shearing.*

The re-melting capability of fibre reinforced thermoplastic laminates enables the application of hot stamp forming technologies for the production of thin-walled complex-shaped parts. A laminate consists of multiple stacked uni-directional plies, which can be rotated with respect to each other. After the tailored laminate is heated above the melting temperature of the thermoplastic resin, it is formed into the final product geometry. Ply deformations occur during the forming operation. Laminate deformation mechanisms have been categorised by Cogswell [1, 2]. Intra-ply and inter-ply deformation mechanisms occur within the ply and at the ply interfaces, respectively. Such mechanisms require proper characterisation to facilitate stamp forming prediction tools. Two intra-ply shearing mechanisms of uni-directional (UD) reinforced melts are generally considered [3]. As shown in figure 4.1, axial or longitudinal shearing refers to the parallel sliding of individual fibre filaments. The transverse movement of fibres as shown in figure 4.1 is referred to as transverse intra-ply shearing.

Several shear characterisation methods have been developed in the past as summarised by Harrison [4]. The methods differ in type of load introduction and therefore also in specimen geometry. An alternative shear characterisation technique was presented by Haanappel *et al.* [5]. It considers a rectangular prismatic bar comprising the UD fibre reinforced polymer melt, which is subjected to torsional loading as shown in figure 4.2. The considered material is assumed to be transversely isotropic. Axial or longitudinal intra-ply shearing is invoked when the fibres are aligned with the specimen's axis of rotation. The method utilises a commercially available rheometer and its accessories for specimen clamping and climate control. Limitations of the method were investigated in chapter 3, which resulted in a recommendation for specimen geometry and a maximum applicable torsion rotation angle.

In this chapter, the proposed torsion bar method is implemented in practice and critically evaluated. Prior to the description of the test, some essential parts of the

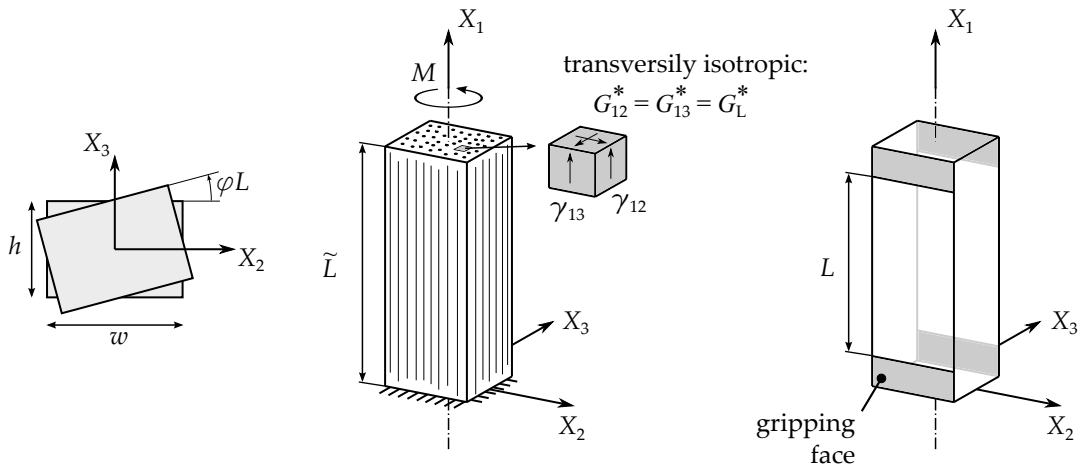

Figure 4.2 *Conceptual design of the torsion specimen. Left: cross-sectional geometry. Centre: fibre reinforced rectangular bar. Torsional loading invokes two longitudinal shear mechanisms as indicated by the elementary cube. Right: grey areas represent the gripping faces to conduct torsional loads in practice.*

Linear Visco-Elasticity (LVE) theory [6] and the kinematics of a torsionally loaded rectangular bar are revisited. Experiments are conducted with specimens that consist of AS4 carbon fibres with a polyetheretherketone (PEEK) matrix. This UD-C/PEEK pre-preg material is shown in figure 4.3. The micrograph gives an impression of the fibrous structure. Specimen responses are analysed in detail in order to explore the conditions that lead to linear and non-linear material behaviour. Small strain oscillatory tests are performed, after which the LVE theory is applied to interpret the results. Transient responses are of interest for stamp forming applications and thus a translation from the dynamic moduli to the relaxation modulus needs to be obtained. Finally, a stress-strain relationship is derived, which can be implemented in stamp forming simulation software.

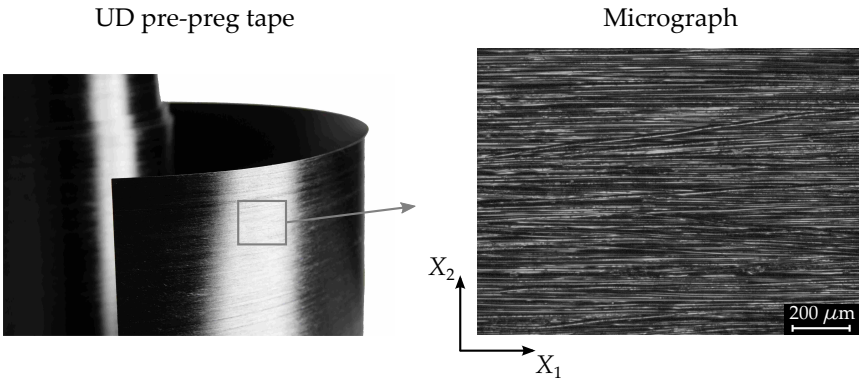

Figure 4.3 *UD-C/PEEK pre-preg tape and a micrograph giving an impression of its micro structure.*

4.2 Rheometry

The torsion bar specimen will be characterised by applying generic rheological procedures. Linear material responses are usually observed at relatively small strains. However, inertia effects of the set-up need to be overcome within this small strain region in order to obtain a steady transient response. This problem is circumvented by applying oscillatory loading with a certain shear strain amplitude γ_{12}^0 at angular frequency ω [6]:

$$\gamma_{12}(t) = \gamma_{12}^0 \sin(\omega t) \tag{4.1}$$

For linear material behaviour, the stress response is also sinusoidal [6]:

$$\tau_{12}(t) = \tau_{12}^0 \sin(\omega t + \delta) \tag{4.2}$$

which runs out-of-phase with phase angle δ when the material behaves visco-elastically, as schematically shown in figure 4.4. The linear visco-elastic material properties are represented by the storage and loss moduli, respectively [6]:

$$G' = \frac{\tau_{12}^0}{\gamma_{12}^0} \cos\delta \quad G'' = \frac{\tau_{12}^0}{\gamma_{12}^0} \sin\delta \tag{4.3}$$

The complex shear modulus is defined as:

$$G^* = G' + iG'' \tag{4.4}$$

where i denotes the imaginary number. The damping of the material is defined as:

$$\tan\delta = \frac{G''}{G'} \tag{4.5}$$

The dynamic and out-of-phase viscosities are respectively related to the loss and storage modulus through the angular frequency:

$$\eta' = \frac{G''}{\omega} \qquad \eta'' = \frac{G'}{\omega} \tag{4.6}$$

The complex viscosity is defined as:

$$\eta^* = \eta' - i\eta'' \tag{4.7}$$

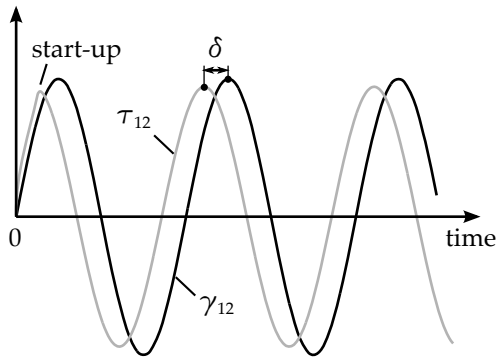

Figure 4.4 *The stress response as a result of a sinusoidally applied strain.*

4.3 Torsion of a prismatic bar with a rectangular cross section

The kinematics of a torsionally loaded prismatic bar with a rectangular cross section were first described by Saint-Venant [7]. Linear elastic and isotropic material properties were assumed. For small deformations, the torque M and rotation angle ϕ are related through:

$$M = GJ\frac{\phi}{L} \qquad \varphi = \frac{\phi}{L} \tag{4.8}$$

in which L is the free length of the bar (see figure 4.2) and φ is the specific rotation angle. A constant elastic shear modulus G describes the linear material behaviour for small strains. Free torsion was assumed and implies that all cross sections are free to warp, which appears for bars with a non-circular cross section. Then, the torsional constant J for a rectangular cross section with dimensions w and h reads [8]:

$$J = \tfrac{1}{3}h^3 w\left(1 - \frac{192}{\pi^5}\frac{h}{w}\sum_{k=1}^{\infty}\frac{1}{(2k-1)^5}\tanh\left(\frac{(2k-1)\pi w}{2h}\right)\right) \tag{4.9}$$

The shear strain components are distributed over the rectangular cross section according to [8]:

$$\begin{aligned}
\gamma_{12}(X_2, X_3) &= -\frac{\phi}{L}\frac{8h}{\pi^2}\sum_{k=1}^{\infty}\frac{(-1)^{k+1}}{(2k-1)^2}\left(1 - \frac{\cosh\left(\frac{(2k-1)\pi X_2}{h}\right)}{\cosh\left(\frac{(2k-1)\pi w}{2h}\right)}\right)\sin\left(\frac{(2k-1)\pi X_3}{h}\right) \\
\gamma_{13}(X_2, X_3) &= \frac{\phi}{L}\frac{8h}{\pi^2}\sum_{k=1}^{\infty}\frac{(-1)^{k+1}}{(2k-1)^2}\left(\frac{\sinh\left(\frac{(2k-1)\pi X_2}{h}\right)\cos\left(\frac{(2k-1)\pi X_3}{h}\right)}{\cosh\left(\frac{(2k-1)\pi w}{2h}\right)}\right)
\end{aligned} \tag{4.10}$$

Oscillatory loading is considered in this research, which implies the presence of a harmonic rotation angle and torque. In complex notation, these read:

$$\phi^* = \phi_0 \cos(\omega t) + i\phi_0 \sin(\omega t) \tag{4.11}$$
$$M^* = M_0 \cos(\omega t + \delta) + iM_0 \sin(\omega t + \delta) \tag{4.12}$$

in which the zero subscripts indicate the amplitude of any variable. The elastic shear modulus G can be replaced with its complex form G^* as it is used in the LVE theory (equation (4.4)). By assuming transverse isotropy for the UD reinforced material considered here, the longitudinal intra-ply shear moduli are determined as:

$$G'_{\mathrm{L}} = \frac{L}{J}\frac{M_0}{\phi_0}\cos\delta \qquad G''_{\mathrm{L}} = \frac{L}{J}\frac{M_0}{\phi_0}\sin\delta \tag{4.13}$$

The phase angle δ, the torque amplitude M_0, and rotation amplitude ϕ_0 are determined during an experiment.

4.4 Experimental work

An experimental programme was carried out to investigate the specimen responses obtained with this method. Firstly, a description of the used equipment, specimens, and testing procedure is given. Subsequently, measurement results are presented and evaluated.

4.4.1 Equipment

A standard Anton Paar® MCR501 rheometer was used, as shown in figure 4.5. It is able to perform rheological tests by conducting steady and oscillatory rotations. Torsional loads are generated by a synchronous electrical motor and can either be rotation or torque controlled. The rotation controlled mode was used as it yields the most stable responses for the type of experiments considered here.

The modular design allows for the use of different fixture types. For this study, the standard SRF-12 solid torsion bar fixtures were selected, which are generally used to perform measurements on solid bars in torsion. Storage and loss moduli are conventionally measured as a function of temperature, for example to determine glass transition temperatures of plastics [9]. Rectangular bar specimens with thicknesses up to 12 mm can be gripped at the end faces of the specimen, as shown in figure 4.5. One gripping face is part of a rigid modular block, whereas the opposite gripping face consists of a moveable plate and is loosely guided by two little pins. In order to achieve stable gripping for soft materials, the standard fixture was modified. The gripping is now introduced by two bolts instead of one.

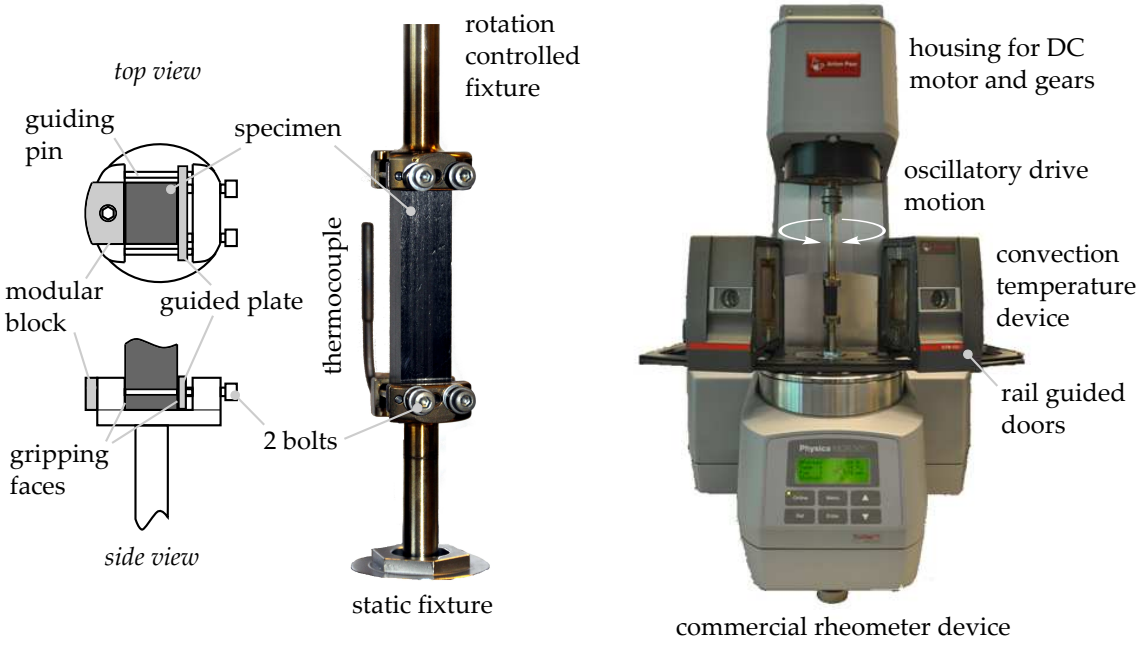

Figure 4.5 *Left: actual torsion specimen and fixtures. Right: commercially available rheometer.*

4.4.2 Specimen geometry

The specimen dimensions are based on the sensitivity analysis in chapter 3 and the allowable specimen size to fit in the rheometer device. The appearance of warping of the cross section was considered, which appears for free torsion of linear elastic bars [7] with a non-axisymmetric cross section. The warping can be restricted (partially) due to specimen clamping, which results in an increasing torsional rigidity. The difference between the situation of free warping and restricted warping was minimal for close to square cross sections. Taking into account these differences, the moduli in equation (4.13) can then be seen as upper bounds, whereas for aspect ratios of $0.85 \leq h/w \leq 1$, the lower bounds read:

$$\tilde{G}'_{\mathrm{L}} \approx \frac{G'_{\mathrm{L}}}{1.2} \qquad \tilde{G}''_{\mathrm{L}} \approx \frac{G''_{\mathrm{L}}}{1.2} \tag{4.14}$$

Another sensitivity analysis [5, 10] was conducted to investigate the effect of adverse fibre tensions on the measured specimen response. The situation of restricted cross sections was considered, such that all fibres in the specimen are stretched during torsional loading. Also here, the distortion of the responses was found to be smaller for more square cross sections.

A maximum specimen width of 13 mm fits in the rheometer clamps. A specimen thickness of 11 mm can be obtained by consolidating a stack of 80 pre-preg plies.

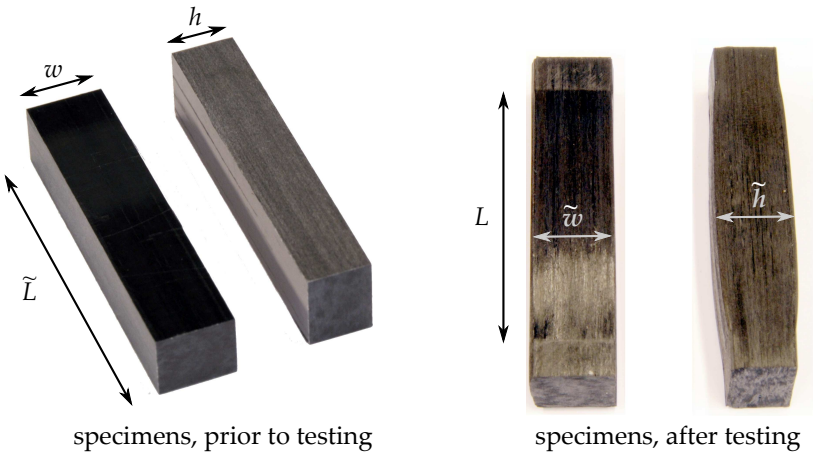

Figure 4.6 *Left: UD-C/PEEK specimens as cut from the laminate. Right: specimens after re-heating to processing/testing temperature. Frozen in consolidation stresses are released and distort the ideal testing geometry.*

Larger stacks become impractical to handle. The resulting cross-sectional dimensions were therefore set to 11×13 mm. For this geometry, the fibre sensitivity analysis showed that minimal distortions of the response were found for rotation angles up to $0.007°/\text{mm}$, which corresponds to a maximum shear strain of 0.1%. It is not expected that all fibres are stretched during the actual test, implying that somewhat larger rotation angles and shear strains are allowed.

4.4.3 Specimen production

Specimens were produced with the CETEX® TC1200 PEEK/AS4 pre-preg material from Ten Cate. The pre-preg material consists of a uni-directional AS4 carbon fibre reinforcement and a PEEK thermoplastic matrix (UD-C/PEEK). Glass transition and melt temperature of the PEEK polymer [11] are 143°C and 343°C, respectively. One pre-preg ply measures a thickness of 0.14 mm. Thick UD laminates were manufactured by stacking 80 equally oriented plies of the pre-preg material. The stack was positioned in a framed mould, which was utilised in order to minimise transverse flow. The framed mould was transferred to a flat platen press for consolidation. The temperature and pressure cycle were applied according to the material's datasheet. The resulting laminate measured a thickness of 11 mm and a nominal fibre volume fraction of 59.3%. Specimens were subsequently cut from the laminate with a diamond wheel saw to yield dimensions of $w = 13$, $h = 11$, and $\tilde{L} = 60$ mm, as indicated in figure 4.6. The specimens were dried in a vacuum oven at 80°C prior to testing.

4.4.4 Testing procedure

The specimen is carefully positioned in the fixtures, such that it is well aligned with the rotation axis. The specimen ends are gripped between the modular blocks and the guided plates, as shown in figure 4.5. The bottom surface of the specimen rests on the surface of the lower static fixture. A little gap of 0.5 to 1.0 mm between the top surface of the specimen and the top fixture is ensured to allow for thermal expansion.

A low flow of nitrogen gas is applied within the cavity in order to avoid polymer degradation effects that are driven by the presence of oxygen [12]. The testing temperature is controlled with a thermocouple. Tests with a specimen equipped with 3 embedded thermocouples indicated that a steady state temperature distribution in the specimen was achieved in approximately 10-15 minutes. Once the cavity temperature reaches the set temperature, these levelling times are ensured prior to testing. The temperature in the specimen deviates less than 10°C from this set temperature.

Torsional responses are measured by applying oscillating rotations to the upper fixture. Storage and loss shear moduli are determined with equation (4.13). Only these upper bound moduli are shown for a clear presentation of the results, however, it must be kept in mind that the lower bound moduli could be $\approx$ 16% lower (see equation (4.14)). The maximum shear strain that appears in the rectangular cross section is used as a reference throughout all the analyses. By assuming free torsion, equation (4.10) shows a maximum shear strain at the centre of the longest edge of the cross section.

4.4.5 Explorative measurements

Separate frequency sweeps with different strain amplitudes γ_0 were applied to explore the linear and non-linear behaviour of the material. Figure 4.7 shows the dynamic moduli to be dependent on the strain amplitude, indicating non-linear material behaviour. The moduli are large for the small strain amplitude, but rapidly decrease when the larger strain amplitude γ_0 is applied.

This behaviour was described by Nguyen and Boger [13]. Media with suspended particles show a critical strain amplitude between 0.01% and 5% in general. It was reported that the dynamic moduli decrease rapidly beyond this critical strain amplitude as also observed in figure 4.7. Instead of particle interactions, fibre interactions are expected in the present results. Jones and Roberts [14] tested a model composite comprising a Golden Syrup with embedded nylon fibres. They used a custom-built linear oscillator. Also here, a decreasing storage and loss modulus was measured for increasing strain amplitudes.

According to the LVE theory, the material behaves linearly when a sinusoidally applied deformation (rotation angle) results in a purely sinusoidal stress (torque

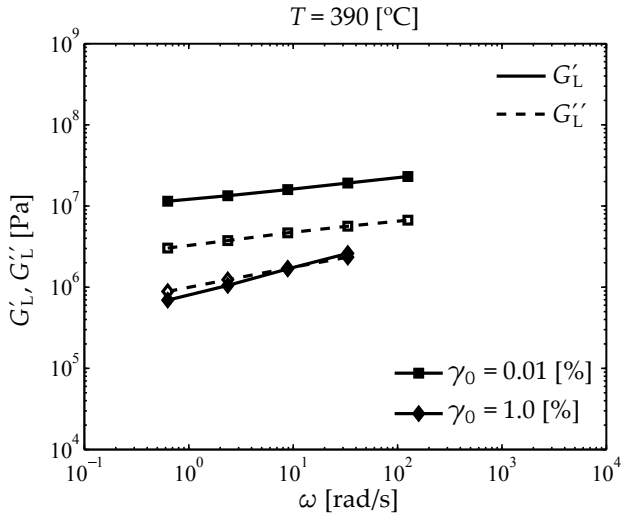

Figure 4.7 *Frequency sweeps with different strain amplitudes applied to UD-C/PEEK specimens. Only upper bounds for longitudinal shear moduli G'_L and G''_L are shown. Lower bounds can be determined according to equation* (4.14).

M) response. Non-linear material behaviour is indicated by deviations from the primary sine wave. Figure 4.8 shows the waveform data for several measurement points in figure 4.7. Pure sine wave responses are observed for the small strain amplitude of 0.01% at all frequencies. Sine wave distortions can be observed at the larger shear amplitude of 1.0%. Such distortions are defined in the field of large amplitude oscillatory shear (LAOS) testing [15]. The observed shapes are referred to as backward tilted shoulder waves. As shown for the data with $\gamma_0 = 1.0\%$, increasing the frequency decreases the backward tilted distortion.

Groves *et al.* [16] also performed high temperature shear tests on a UD-C/PEEK composite by means of an oscillatory plate-plate set-up. It was reported that deviations from the primary sine wave were observed for low frequencies and small strains, and at high frequencies and large strains. Another publication by Roberts and Jones [17] showed the waveform data obtained from experiments with the aforementioned model composite (nylon fibres embedded in Golden Syrup, tested with their custom-built linear oscillator) with a fibre volume fraction of 60%. Pure sine waves were found for relatively large shear strains of 6% at frequencies between 1 and 80 rad/s. Larger strain amplitudes resulted in backward tilted shoulder waves, as was observed here as well. The distortion was also smaller for higher frequencies. Flat topped sine waves were shown at frequencies lower than 0.1 rad/s, which was explained as being caused by yielding of the material [13].

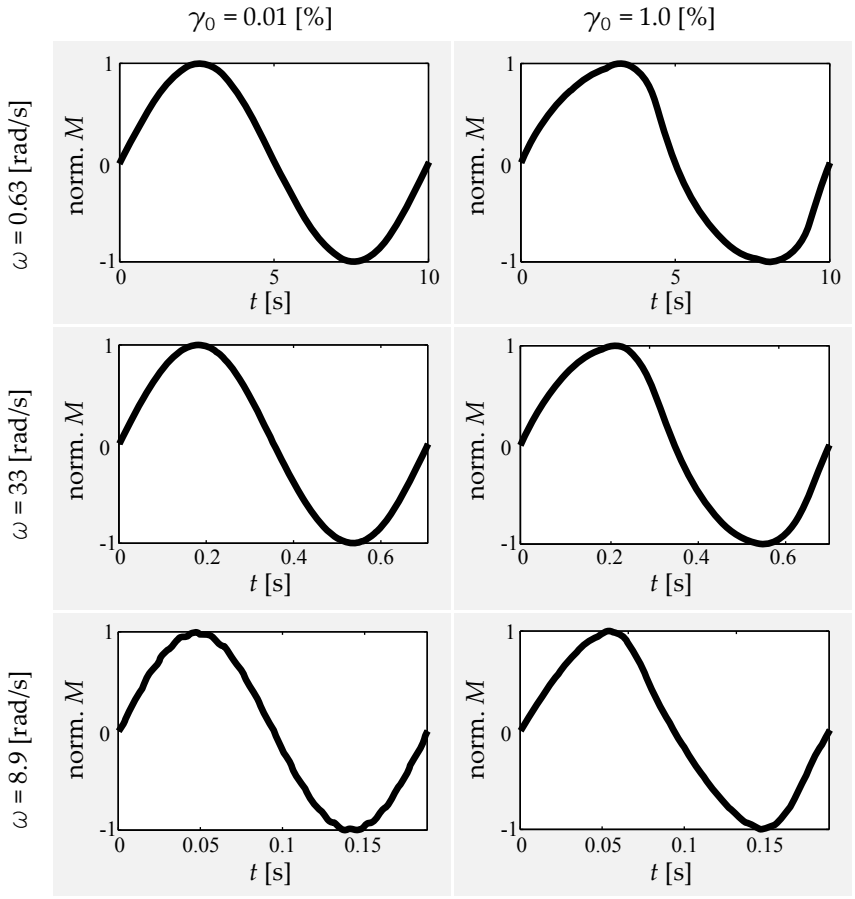

Figure 4.8 *Waveforms as a function of strain amplitude and angular frequency for the UD-C/PEEK specimens.*

4.4.6 Small strain measurements

Strain and frequency sweeps were conducted at 390°C for five UD-C/PEEK specimens. To assess the repeatability of the experiment, two subsequent runs with identical sweep settings were performed. For the small strain experiments to be discussed next, all subsequent runs reproduced well.

Figure 4.9 shows the results of both the amplitude and frequency sweeps for the five specimens. Averaged moduli and their standard deviations are shown. The solid lines represent the storage moduli, whereas the dashed lines represent the loss moduli. As mentioned previously, the specimens will expand when their temperature is above the material's melting point. Figure 4.6 shows that the specimens will expand non-uniformly due to the presence of the fixtures. This leads to a non-uniform torsional rigidity. The dynamic moduli in equation (4.13) were for this reason calculated for two geometries. The black lines show the results by assuming the initial geometry as shown in the left of figure 4.6. The grey lines were obtained by

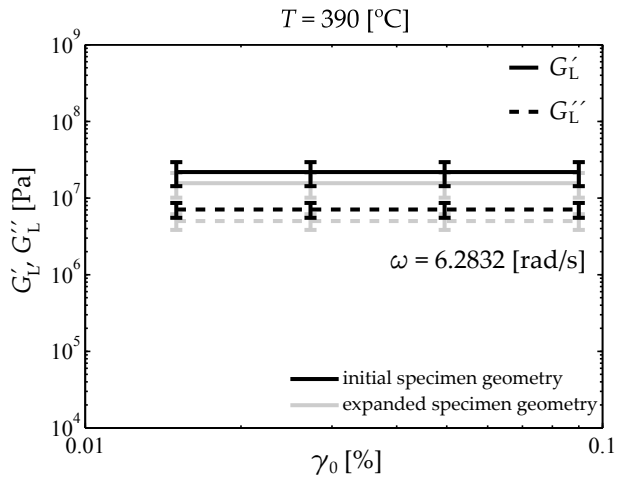

(a)

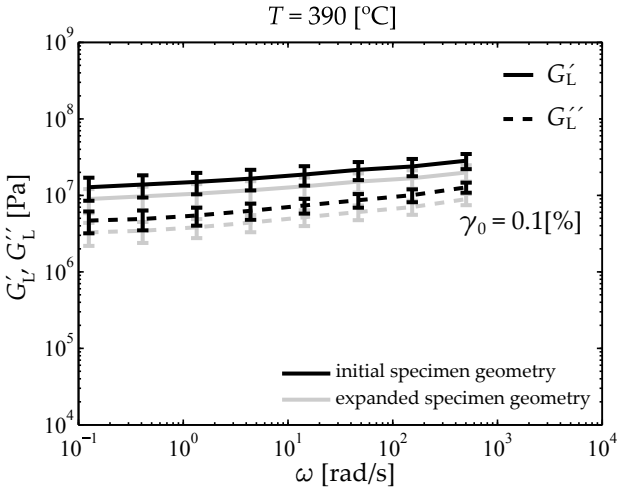

(b)

Figure 4.9 *Averaged dynamic moduli for the UD-C/PEEK material as a function of strain amplitude γ_0 (a) and angular frequency ω (b).*

assuming a uniform cross section over the specimen's length as well, but now using the maximum width and thickness as they appear in the expanded specimen after testing.

Amplitude sweeps were conducted within a strain range that covered approximately one decade only with a maximum strain amplitude of $\approx 0.1\%$. Figure 4.9 shows the results for the sweeps at a fixed frequency of 6.28 rad/s. The measured shear moduli were constant for the investigated shear strain range, which implies linear material

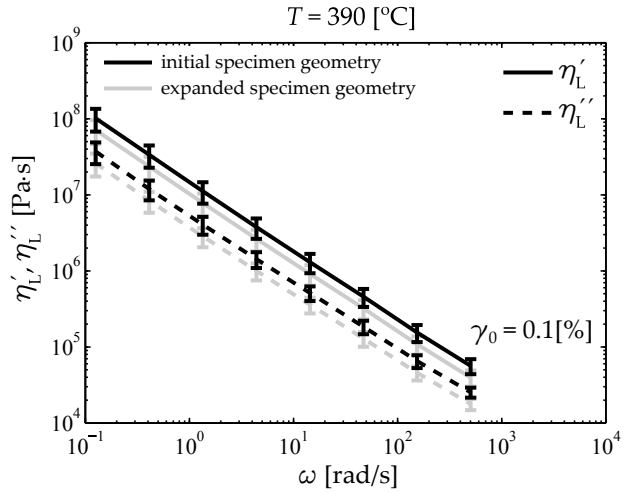

(a)

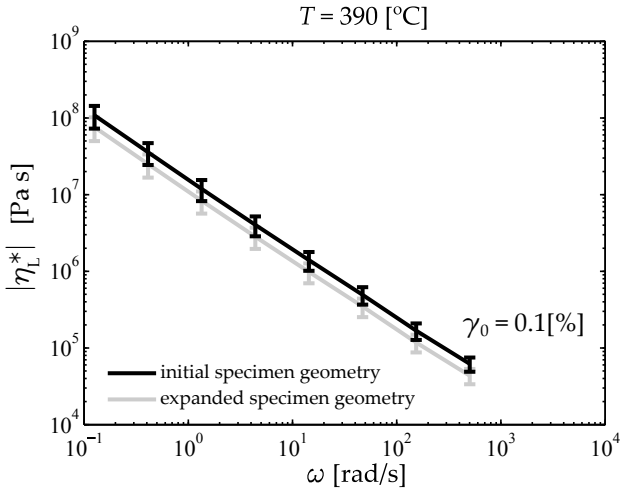

(b)

Figure 4.10 *Averaged dynamic (a) and absolute complex (b) viscosities for the UD-C/PEEK material, as a function of angular frequency ω.*

behaviour. As concluded from the exploratory measurements in the previous section, larger strain amplitudes result in non-linear material behaviour. It is possible that a permanent change of the specimen's structure, such as fibre migration, develops beyond this point. This could lead to a different specimen response. Larger strain amplitudes were therefore not applied.

Frequency sweeps were applied subsequently with shear strain amplitudes of $\gamma_0 =$ 0.1%. The measured dynamic moduli are shown in figure 4.9. The dynamic and

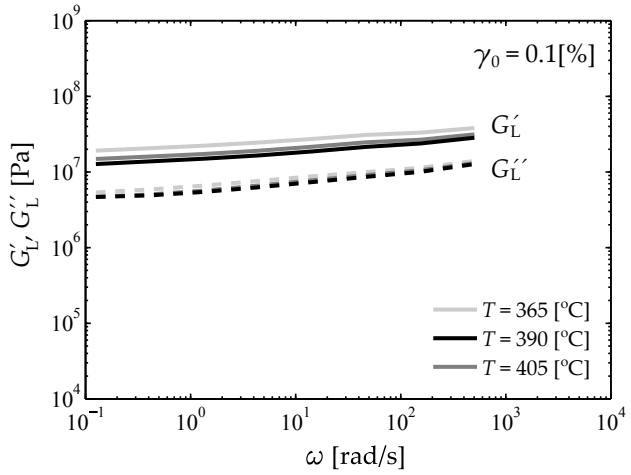

Figure 4.11 *Dynamic moduli for the UD-C/PEEK material at three temperatures.*

complex viscosities are shown in figure 4.10. Approximately four decades of angular frequency were covered, varying between 0.126 and 503 rad/s (0.02 to 80 Hz). Good reproducibility was obtained for all measurements, as indicated by the standard deviations for the sample of five specimens.

Tests at different temperatures were carried out as well, for which the results are shown in figure 4.11. Clearly, the temperature does not influence the moduli within the small strain regime.

4.4.7 Neat polymer characteristics

The measured moduli of the composite system weakly depend on frequency. A constantly increasing slope of moduli versus frequency can be observed for the range of frequencies considered (figure 4.9(b)). The storage terms are consistently larger than the loss terms within the range of investigated parameters. This behaviour is substantially different from the polymer characteristics without the presence of fibres.

Measurements were performed on the neat PEEK polymer with a rotating plate-plate set-up. Amplitude sweeps indicated linear material behaviour up to strain amplitudes of 10%. Frequency sweeps were conducted with a strain amplitude of $\gamma_0 = 1.0\%$ for which the results are shown in figure 4.12. As compared to the composite system, a larger frequency dependency of the moduli is observed. Moreover, a dominating loss modulus is present, which is representative for many molten polymers. The dynamic viscosities are constant at low frequencies. Steady shear measurements were conducted as well, resulting in the steady shear viscosity. A translation between the dynamic absolute complex viscosity and the transient steady

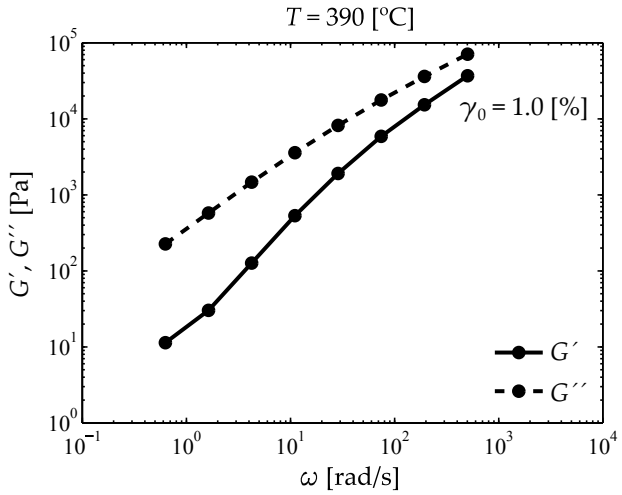

(a) Dynamic moduli.

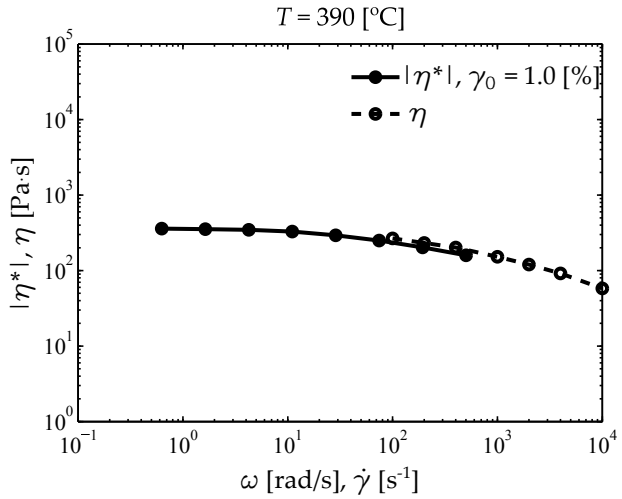

(b) Absolute complex viscosity and transient steady shear viscosity.

Figure 4.12 *Frequency response of the neat PEEK polymer at 390°C and $\gamma_0 = 1\%$, obtained with a parallel plate set-up.*

shear viscosity is given by the empirical Cox-Merz rule [18]:

$$\eta(\dot{\gamma} = \omega) \simeq |\eta^*(\omega)| \tag{4.15}$$

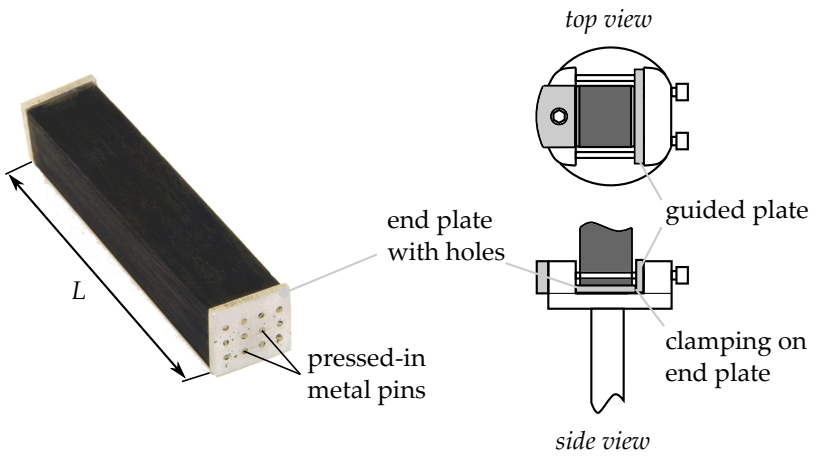

Figure 4.13 *Alternative fixture with short metal pins to conduct the torsional loads. The standard SRF-12 fixtures are used to clamp the aluminium end plates.*

4.4.8 Alternative load introduction

Although realistic responses were found so far for the composite system, experiments with an alternative clamping method were conducted for completeness. As shown in figure 4.13, two aluminium plates of 13×12×2 mm were glued on both ends of the specimen. A grid of 3×4 holes was drilled through the plate and 3 mm through the specimen itself. Little pins were cut from a weld wire with a diameter of 1 mm. These were pressed into the drilled holes. Torsional loading is now introduced via these pins. The assembly was positioned in the rheometer, where the fixtures grip at the aluminium plates. In this way, the specimen side planes were not in contact with the standard fixtures. Frequency sweeps were conducted at 390°C. The measured dynamic moduli are shown in figure 4.14. Similar material behaviour was found, as compared to the averaged responses that were found for the tests with the preferred simple gripping mechanism in figure 4.5.

4.5 Discussion

Figures 4.7 and 4.9 showed a predominantly elastic response of the composite system for small linear strains. It is interesting to note that as part of the non-linear response, the elastic dominance is weakened when larger strains are applied. Focusing on the linear material behaviour, the elastic dominance is most likely caused by the presence of the fibres. For the sake of argument, imagine a system containing fibres that are well aligned and uniformly distributed such that no fibre-fibre contacts are present. Then one should measure responses that are similar to the neat polymer characteristics. Next to the global or apparent shear rate, small spaces between the

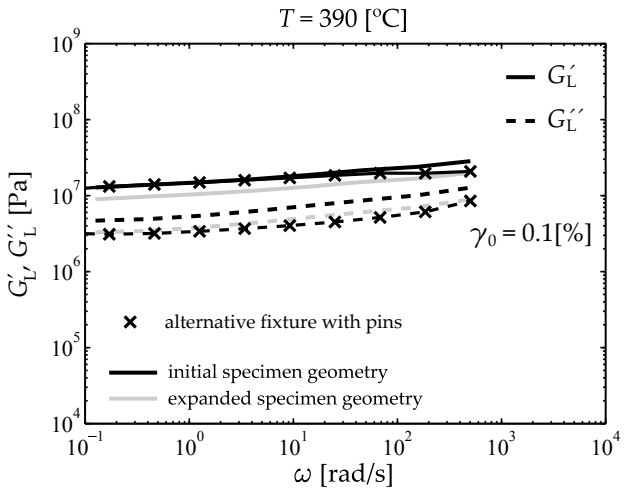

Figure 4.14 *Frequency sweeps and their resulting dynamic moduli for the UD-C/PEEK material. A comparison between the preferred simple gripping with existing fixtures (solid and dotted lines from figure 4.9(b)) and the alternative fixture with pins (crosses).*

rigid fibres lead to higher shear rates locally. This ideal situation was considered by Pipes *et al.* [19], where solely the fibre volume fraction and the packing geometry determine this shear rate magnification. Consequently, the neat polymer viscosity characteristic in figure 4.12 shifts horizontally towards smaller shear rates. The ideal alignment in question is unrealistic for the fibre volume fractions considered here, which is approximately 60%. As supported by the micrograph in figure 4.3, multiple fibre interactions are present. These invoke the measured elastic effects during deformation. This also explains the temperature-independent moduli (figure 4.11), as temperature influences the polymer melt only and not the fibrous structure itself. Similar assumptions have been argued and considered by Gutowski [20] in order to model the elastic response during laminate consolidation cycles. The elastic behaviour was also observed in the results of Stanley and Mallon [21], who measured the longitudinal response of APC2-PEEK with a translating plate-plate set-up.

The plateau-like characteristics of the dynamic moduli in figure 4.9(b) have also been observed by Roberts and Jones [17] for Golden Syrup with nylon fibres. Manual deposition of the nylon fibres allowed for a controlled fibre volume fraction. Increasing the fibre volume fraction from 0.1 to 0.7 resulted in a plateau developing for both the storage and loss moduli at lower frequencies. As discussed by Nguyen and Boger [13], more particle-particle and particle-polymer interactions develop for an increasing particle volume fraction. As argued by Onogi *et al.* [22], this leads to the formation of a network structure such that much longer relaxation times develop, compared to the longest relaxation time of the neat polymer. The relaxation time can be seen as the time needed by the material to adjust to the applied stress or

deformation, which is ≈ 0.05 s for PEEK [23]. The relaxation time of the composite is relatively large compared to the lowest testing frequency considered (high Deborah number [24]), and therefore a solid-like response is observed. Moreover, the low frequency plateaus in the dynamic moduli suggest the presence of yield stress behaviour in large strain steady shear tests [13]. A yield stress value was indeed found in the analysis of Groves [25] for the plate-plate shear characterisation test. It must be noted, however, that this was implicitly determined with the dynamic data and the use of dynamic Maxwell parameters [26], instead of the conventionally used dynamic Kelvin-Voigt moduli.

In the more general sense, the behaviour observed is a characteristic of a visco-elastic solid or weak gel [27]. Similar dynamic responses have been observed in other fields of research. Examples of media that show the same weak frequency dependency are biomass slurry [28], chestnut flour doughs [29], peanut butter [27], and brains [30].

The obtained characteristics are compared in figure 4.15 with frequency data from other characterisation tests applied to the UD-C/PEEK material. However, these reference data were obtained twenty years ago approximately. This comparison must therefore be interpreted with care, since polymer blends and fibre architectures are usually modified over the years. Groves *et al.* [16] utilised the previously mentioned rotating plate-plate set-up and Scobbo and Nakajima [31] used a translating plate-plate configuration. They used shear strain amplitudes of 1.0% and 2.0%, respectively. The moduli show much lower values, but it was shown by Groves *et al.* [16] that the material behaves non-linearly for relatively small strain amplitudes. This agrees with our observations that the dynamic moduli decrease rapidly beyond the transition from linear to non-linear strain responses. Such effects may partially explain the differences in this figure.

Next to a dominating loss modulus, both Groves *et al.* and, Scobbo and Nakajima found a larger frequency dependency of the moduli. As argued by Stanley and Mallon [21], the formation of resin-rich layers influences the load introduction into the reinforced part of the melt. As a result, inter-ply slip is likely to dominate the specimen deformation, instead of the intended intra-ply shearing itself. They confirmed such behaviour with their own measurements, where the specimens were loaded parallel and perpendicular to the inter-ply interfaces. Both the methods of Groves *et al.* and, Scobbo and Nakajima only introduce shear forces parallel to the inter-ply interfaces and thus parallel to the fibre direction. This is substantially different from the load introduction here. Torsional loads are introduced perpendicular to the fibre direction, which might also explain the differences observed.

As a final note to all shear characterisation methods, it is questionable whether the assumption of transverse isotropy (equal longitudinal shear moduli in the 12 and 13 planes) holds (see figure 4.2). In combination with the type of load introduction, parallel or perpendicular to the fibres, a difference between these moduli possibly

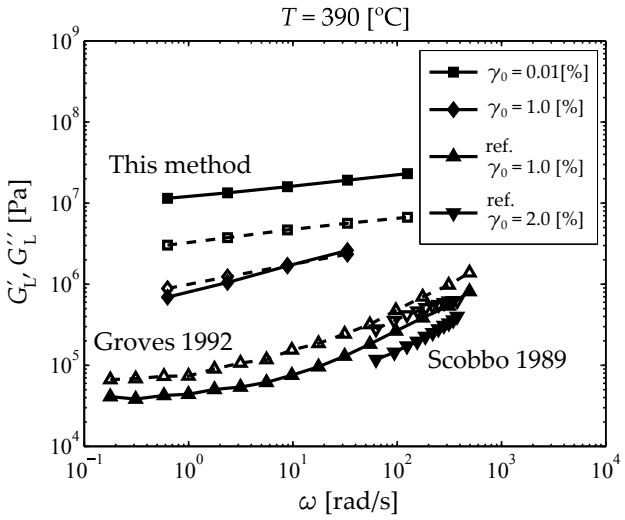

Figure 4.15 *Comparison of dynamic moduli at 390°C, with respect to those obtained from other shear characterisation techniques. Groves et al. [16] utilised a rotating plate-plate set-up. Scobbo and Nakajima [31] utilised a translating plate-plate set-up.*

affects the ratio between γ_{12} and γ_{13} at a certain point in the specimen, thereby deviating from the theoretical shear strain distributions that were assumed in equation (4.10).

The introduced torsion bar method was shown to yield plausible shear characterisation data. The small strain behaviour is important to describe the intra-ply shear mechanisms in laminate forming prediction software. The method shows good potential to become a standard test in the future, considering the relatively small effort to perform the experiments and the repeatability of the data obtained.

4.6 Conversion to the transient domain

The shear behaviour for small strains is now known in the frequency domain. Since the forming process of hot laminates takes place in the transient time domain, the measured characteristics (figure 4.9(b)) have to be translated. The aforementioned empirical Cox-Merz rule [18] in equation (4.15) is often used for neat polymer melts with a dominating loss modulus, as well as showing shear thinning behaviour at larger shear rates. Generally, this rule cannot be applied for media with suspended particles that interact during deformations. This was, for example, shown by Kitano *et al.* [32] for short glass fibre filled polyethylene.

Transient deformations of linear visco-elastic materials are described via the follow-

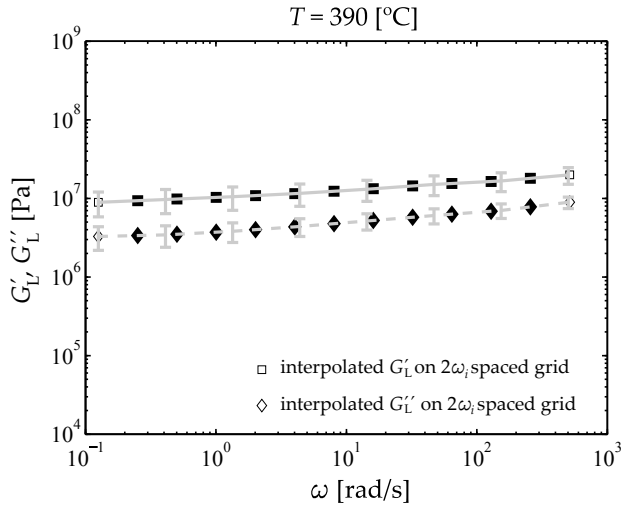

Figure 4.16 *Averaged frequency sweep data for the expanded UD-C/PEEK specimens. The experimental data is interpolated to a grid, as indicated by the square and rhombus type markers.*

ing constitutive relationship [6]:

$$\tau_{12}(t) = \int_{s=-\infty}^{t} G_{\mathrm{r}}(t-s)\dot{\gamma}_{12}(s)\mathrm{d}s \tag{4.16}$$

also known as the Boltzmann integral. Here, τ_{12} is the shear stress, $\dot{\gamma}_{12}$ the shear rate, and $G_{\mathrm{r}}(t)$ is the shear relaxation modulus. The integration is carried out over all past times s up to the current time t. The shear relaxation modulus G_{r} needs to be determined to describe the transient interaction between shear stress and shear strain at various loading rates.

The relaxation modulus can be determined in several ways. Fourier sine and cosine transformations relate this relaxation modulus to the storage and loss moduli [6], respectively. Such conversions can be performed if the dynamic moduli can be described with relatively simple functions of frequency, which consequently allows for analytical evaluation of the inverse sine or cosine transforms. Such an example has been shown by Campanella and Peleg [33] for visco-elastic liquids. The material considered here showed a response that corresponds more to a visco-elastic solid and therefore the presence of an equilibrium modulus G_∞ must be accounted for. Moreover, such conversions assume that the dynamic moduli are known through the entire frequency domain, whereas only three to four orders of frequency are generally available from experiments. It is hard to estimate the errors introduced due to this assumption.

Another way to apply a conversion was thoroughly described by Schwarzl and

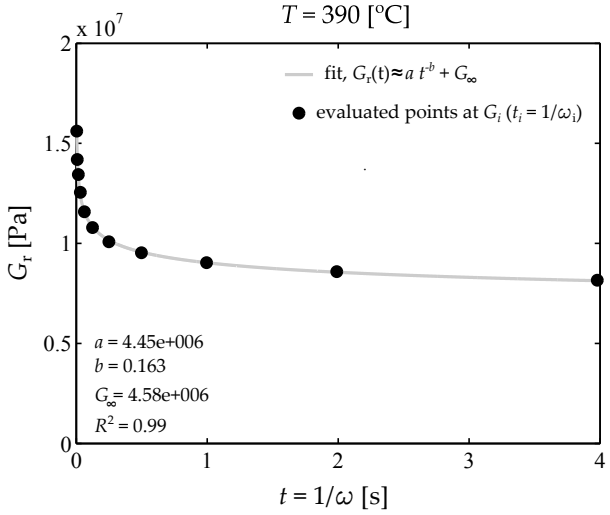

Figure 4.17 *Relaxation function G_r evaluated at several points $t_i = 1/\omega_i$ according to the finite difference scheme in* (4.18).

Struik [34, 35]. Applying a finite difference scheme for several points ω_i results in an approximation of the relaxation function G_r at the corresponding times $t_i = 1/\omega_i$. It was assumed that the measured dynamic moduli are available at a uniformly spaced grid of logarithmic frequencies. The ratio between successive frequencies is assumed to be a factor of two. The proposed approximation for the relaxation modulus reads:

$$G_\mathrm{r}(t) \simeq G'_\mathrm{L}(\omega) - \sum_k c_k G''_\mathrm{L}(2^k\omega) - \sum_k d_k \{G'_\mathrm{L}(2^{k+1}\omega) - G'_\mathrm{L}(2^k\omega)\} \tag{4.17}$$

The equilibrium modulus G_∞ is implicitly accounted for in the $G'(\omega)$ terms. Several sets of constants c_k and d_k were supplied [35] to yield an approximation for G_r, together with an estimation of the maximum error introduced. All schemes were evaluated, but minor differences were observed in the determined relaxation functions. Moreover, the estimated errors are much smaller than the standard deviations of G'_L and G''_L for the sample of five specimens tested here. The following scheme was selected:

$$G_\mathrm{r}(t) \simeq G'_\mathrm{L}(\omega) - 0.528 G''_\mathrm{L}(\omega/2) + 0.112 G''_\mathrm{L}(\omega) + 0.0383 G''_\mathrm{L}(2\omega) \qquad \text{with} \quad t = 1/\omega \tag{4.18}$$

The scheme (4.18) was applied to the data represented with the filled markers in figure 4.16 and resulted in the $G_\mathrm{r}(t_i)$ points as shown in figure 4.17. A continuous function is favourable to evaluate transient responses with equation (4.16). The grey line in figure 4.17 shows the exponential fit with coefficients a and b, and a constant representing the equilibrium modulus G_∞.

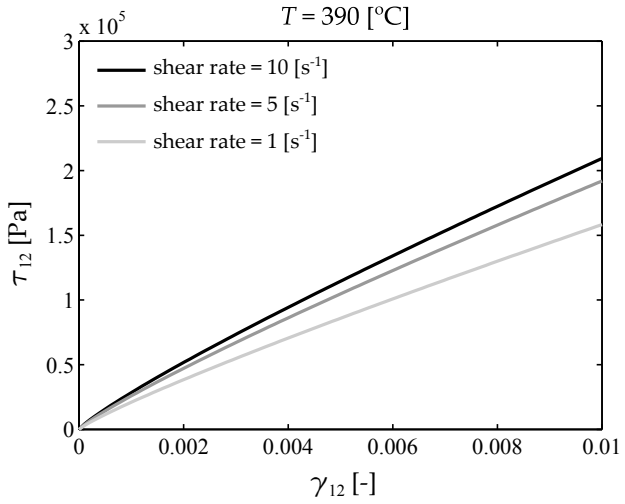

Figure 4.18 *Shear stress-strain response according to equation* (4.19) *for several constant shear rates.*

Consider a piece of material that behaves according to the approximated relaxation function G_r, and which is free of stresses initially at $s = 0$. By applying an instantaneous constant shear rate $\dot{\gamma}_{12}$, equation (4.16) can be further developed as:

$$\begin{aligned}\tau_{12}(t) &= \dot{\gamma}_{12} \int_{s=0}^{t} G_r(t-s)\mathrm{d}s \\ &\approx \dot{\gamma}_{12} \int_{s=0}^{t} a(t-s)^{-b}\mathrm{d}s + \dot{\gamma}_{12} G_\infty t \\ &= \dot{\gamma}_{12}\left(G_\infty t - \frac{a}{b-1}t^{1-b}\right) \qquad \text{for} \qquad \begin{matrix} b > 1 \\ b < 1 \end{matrix}\end{aligned} \tag{4.19}$$

Figure 4.18 shows these stress responses for three different shear strain rates $\dot{\gamma}_{12}$, which are typically in the order as they appear during the stamp forming process. The material shows a close to elastic response which is, however, slightly dependent on shear rate.

4.7 Conclusions

Chapter 3 introduced an alternative method for shear characterisation of UD fibre reinforced melts. The desired longitudinal shear mechanism, namely where fibres slide parallel to each other, is invoked when a fibre reinforced bar with a rectangular cross section is subjected to torsional loading. This characterisation method was

implemented in practice and critically evaluated in this chapter.

Exploratory experiments were performed on UD-C/PEEK specimens with a 60% fibre volume fraction at a temperature of 390°C. Dynamic moduli from linear visco-elasticity theory were determined. Non-linear material responses were observed for relatively small shear strain amplitudes. This was concluded from the distorted waveform data recorded during frequency sweeps carried out at various strain amplitudes.

Further analyses considered linear small strain frequency sweeps. The dynamic moduli were obtained with reasonably small standard deviations. A consistently larger storage modulus indicates predominantly elastic behaviour at small strains. The moduli were independent of temperature as well. The behaviour is attributed to the presence of multiple fibre-fibre interactions. Both storage and loss moduli weakly depend on frequency. These characteristics are representative for a visco-elastic solid or a weak gel.

The method shows good potential to become a standard test in the future, considering the relatively small effort to perform the experiments, the nowadays easily accessible standard rheometers, and the repeatability of the data obtained.

References

[1] F.N. Cogswell. The experience of thermoplastic structural composites during processing. *Composites Manufacturing*, **2**(3-4):208–216, 1991.

[2] F.N. Cogswell. Flow and rheology in polymer composites manufacturing, chapter Continuous-Fibre Systems, 127–202. Elsevier Science B.V., 1994.

[3] C.M. Ó Brádaigh. Flow and rheology in polymer composites manufacturing, chapter Sheet Forming of Composite Materials, 517–569. Elsevier Science B.V., 1994.

[4] P. Harrison and M.J. Clifford. Design and manufacture of textile composites, chapter Rheological Behaviour of Pre-impregnated Textile Composites. Woodhead Publishing Ltd., Cambridge, UK, 2005.

[5] S.P. Haanappel, R.H.W. ten Thije, U. Sachs, A.D. Rietman, and R. Akkerman. In-plane shear characterisation of uni-directionally reinforced thermoplastic melts. In G. Menary, editor, the 14th International ESAFORM Conference on Material Forming, volume 1353 of *AIP Conference Proceedings*, 930–935. American Institute of Physics, 2011.

[6] J.D. Ferry. Viscoelastic properties of polymers. John Wiley & Sons, 3rd edition, 1980.

[7] B. Saint-Venant. Memoires des Savants Etrangers 14, chapter Memoire sur la torsion des prismes, 233–560, 1855.

[8] S.P. Timoshenko and J.N. Goodier. Theory of Elasticity. McGraw-Hill, 3rd edition, 1970.

[9] ASTM. Standard test method for plastics: Dynamic mechanical properties: In torsion. *Annual Book of ASTM Standards*, **08.03: D 5279 Ű 01**.

[10] S.P. Haanappel and R. Akkerman. A method for shear characterisation of fibre reinforced thermoplastics by means of torsion. Submitted to *Composites Part A: applied science and manufacturing*, 2013.

[11] J.E. Mark, editor. Polymer Data Handbook. Oxford University Press, Inc., 1999.
[12] M. Day, D. Sally, and D.M. Wiles. Thermal degradation of poly(aryl-ether-ether-ketone). Experimental evaluation of crosslinking reactions. *Journal of Applied Polymer Science*, **40**(9-10):1615–1625, 1990.
[13] Q.D. Nguyen and D.V. Boger. Measuring the flow properties of yield stress fluids. *Annual Review of Fluid Mechanics*, **24**(1):47–88, 1992.
[14] R.S. Jones and R.W. Roberts. Anisotropic shear flow in continuous fibre composites. *Composites*, **25**(3):171–176, 1994.
[15] K. Hyun, M. Wilhelm, C.O. Klein, K.S. Cho, J.G. Nam, K.H. Ahn, S.J. Lee, R.H. Ewoldt, and G.H. McKinley. A review of nonlinear oscillatory shear tests: Analysis and application of large amplitude oscillatory shear (LAOS). *Progress in Polymer Science (Oxford)*, **36**(12):1697–1753, 2011.
[16] D.J. Groves, A.M. Bellamy, and D.M. Stocks. Anisotropic rheology of continuous fibre thermoplastic composites. *Composites*, **23**(2):75–80, 1992.
[17] R.W. Roberts and R.S. Jones. Rheological characterization of continuous fibre composites in oscillatory shear flow. *Composites Manufacturing*, **6**(3-4):161–167, 1995.
[18] W.P. Cox and E.H. Merz. Correlation of dynamic and steady flow viscosities. *Journal of Polymer Science*, **28**:619, 1958.
[19] R.B. Pipes, D.W. Coffin, P. Simacek, S.F. Shuler, and R.K. Okine. Flow and rheology in polymer composites manufacturing, chapter Rheological Behavior of Collimated Fiber Thermoplastic Composite Materials, 85–202. Elsevier Science B.V., 1994.
[20] T.G. Gutowski. Resin flow/fiber deformation model for composites. *SAMPE quarterly*, **16**(4):58–64, 1985.
[21] W.F. Stanley and P.J. Mallon. Intraply shear characterisation of a fibre reinforced thermoplastic composite. *Composites Part A: Applied Science and Manufacturing*, **37**:939–948, 2006.
[22] S. Onogi, T. Matsumoto, and Y. Warashina. Rheological properties of dispersions of spherical particles in polymer solutions. *Trans Soc Rheol*, **17**(1):175–190, 1973.
[23] M.A. Khan, P. Mitschang, and R. Schledjewski. Identification of some optimal parameters to achieve higher laminate quality through tape placement process. *Advances in Polymer Technology*, **29**(2):98–111, 2010.
[24] M. Reiner. The Deborah number. *Physics Today*, **17**(1):62, 1964.
[25] D.J. Groves. A characterization of shear flow in continuous fibre thermoplastic laminates. *Composites*, **20**(1):28–32, 1989.
[26] J.J. Benbow, F.N. Cogswell, and M.M. Cross. On the dynamic response of viscoelastic fluids. *Rheologica Acta*, **15**(5):231–237, 1976.
[27] G.P. Citerne, P.J. Carreau, and M. Moan. Rheological properties of peanut butter. *Rheologica Acta*, **40**(1):86–96, 2001.
[28] J.J. Stickel, J.S. Knutsen, M.W. Liberatore, W. Luu, D.W. Bousfield, D.J. Klingenberg, C.T. Scott, T.W. Root, M.R. Ehrhardt, and T.O. Monz. Rheology measurements of a biomass slurry: An inter-laboratory study. *Rheologica Acta*, **48**(9):1005–1015, 2009.
[29] R. Moreira, F. Chenlo, and M.D. Torres. Effect of sodium chloride, sucrose and chestnut starch on rheological properties of chestnut flour doughs. *Food Hydrocolloids*, **25**(5):1041–1050, 2011.

[30] F. Shen, T.E. Tay, J.Z. Li, S. Nigen, P.V.S. Lee, and H.K. Chan. Modified Bilston nonlinear viscoelastic model for finite element head injury studies. *Journal of Biomechanical Engineering*, **128**(5):797–801, 2006.

[31] J.J. Scobbo Jr. and N. Nakajima. Dynamic mechanical analysis of molten thermoplastic/continuous graphite fiber composites in simple shear deformation. In National SAMPE Technical Conference, volume 21, 730–743, 1989.

[32] T. Kitano, T. Kataoka, and Y. Nagatsuka. Dynamic flow properties of vinylon fibre and glass fiber reinforced polyethylene melts. *Rheologica Acta*, **23**(4):408–416, 1984.

[33] O.H. Campanella and M. Peleg. On the relationship between the dynamic viscosity and the relaxation modulus of viscoelastic liquids. *Journal of Rheology*, **31**(6):511–513, 1987.

[34] F.R. Schwarzl and L.C.E. Struik. Analysis of relaxation measurements. *Advances in Molecular Relaxation Processes*, **1**(3):201–255, 1968.

[35] F.R. Schwarzl. Numerical calculation of stress relaxation modulus from dynamic data for linear viscoelastic materials. *Rheologica Acta*, **14**(7):581–590, 1975.

Chapter 5

Formability analyses of uni-directional and textile reinforced thermoplastics*

Abstract

The formability of two different composite materials used in the aerospace industry has been investigated. UD carbon/PEEK and 8HS glass/PPS blanks with a quasi-isotropic lay-up were considered. A representative product geometry was selected. The deformation process of the blanks was monitored during the forming experiments. The materials showed different forming behaviour in terms of wrinkling and intra-ply shearing. The UD-C/PEEK product showed severe wrinkling in doubly curved areas, whereas the 8HS-G/PPS product showed better formability in those areas. This can be explained by the relatively high resistance to intra-ply shear for the UD-C/PEEK material. Moreover, the predictive capability of a finite element based simulation tool was shown. For both materials, the prediction of intra-ply shear and large wrinkles showed good agreement with the deformations observed in the product. The smaller wrinkles in the products cannot be accurately represented with the element size used. However, predicted waviness at the corresponding locations could indicate critical areas in the product. With the modelling approach presented, design modifications that aim to minimise or avoid the process-induced defects can be evaluated in the early product design phases, ultimately resulting in lead time reductions.

*Reproduced from: S.P. Haanappel, R.H.W. ten Thije, U. Sachs, B. Rietman, R. Akkerman. Formability analyses of uni-directional and textile reinforced thermoplastics. Submitted to: *Composites Part A: Applied Science and Manufacturing*, **2013**.

5.1 Introduction

The re-melting capability of fibre reinforced thermoplastic laminates allows for high volume production of thin-walled complex-shaped parts for the automotive and aerospace industry. This chapter considers the process of stamp forming a pre-heated laminate into the desired geometry. The potential of this process was already shown in the 1980s by Krone and Walker [1], and Okine [2] for high-performance composites. Such composites are currently used in the aerospace industry, where this process is applied to the production of stiffeners that appear in the wing and fuselage assemblies. The process also shows high potential for use in the automotive industry due to the high production rates that can be achieved. Product examples are car doors, hoods, and car construction pillars.

Two composite materials used in the aerospace industry are considered in this study. One material is the CETEX® TC1200 PEEK/AS4, which consists of a polyetheretherketone (PEEK) thermoplastic matrix and uni-directional AS4 carbon fibres. The other material is the CETEX® PPS glass fabric US style 7781. These are respectively referred to as UD-C/PEEK and 8HS-G/PPS throughout this chapter. The reinforcement architecture of these materials is shown in figure 5.1 at the meso and micro level. The industry encounters large formability differences between these materials. Defects such as wrinkling occur frequently. Such defects lead to a knock-down of the product's in-service performance. The local thickness increments caused by the wrinkle also results in poorly consolidated spots elsewhere in the product and possibly damage to the matched-metal tooling.

Comparative studies of materials with different reinforcement architectures are few and far between in the literature. De Luca *et al.* [3] investigated the forming behaviour of uni-directional (APC2-AS4) and textile (PEI-CETEX) reinforced thermoplastic laminates. A product was selected with a bead that consists of single and double curvature areas. Experiments with these materials were shown to have very different drapability characteristics, especially in terms of wrinkling. Formability analyses of solely textile reinforced laminates have been conducted by more researchers. Hou [4] studied the stamp forming of glass 8HS/PEI laminates into hemispherical moulds. The effects of blank size, blank holder pressure, and mould geometry on the formability was investigated experimentally. Product development times can be reduced when the effects of material parameters and process variables on the forming behaviour can be predicted. Forming prediction codes and constitutive models are becoming increasingly available. Validation of these is mainly performed with relatively simple products, such as domes [5–7]. A more complex geometry referred to as the "double dome" has been and is currently being benchmarked by several research groups [8–10].

In this chapter, the differences in forming behaviour between UD-C/PEEK and 8HS-G/PPS are investigated in detail for a representative product geometry used in

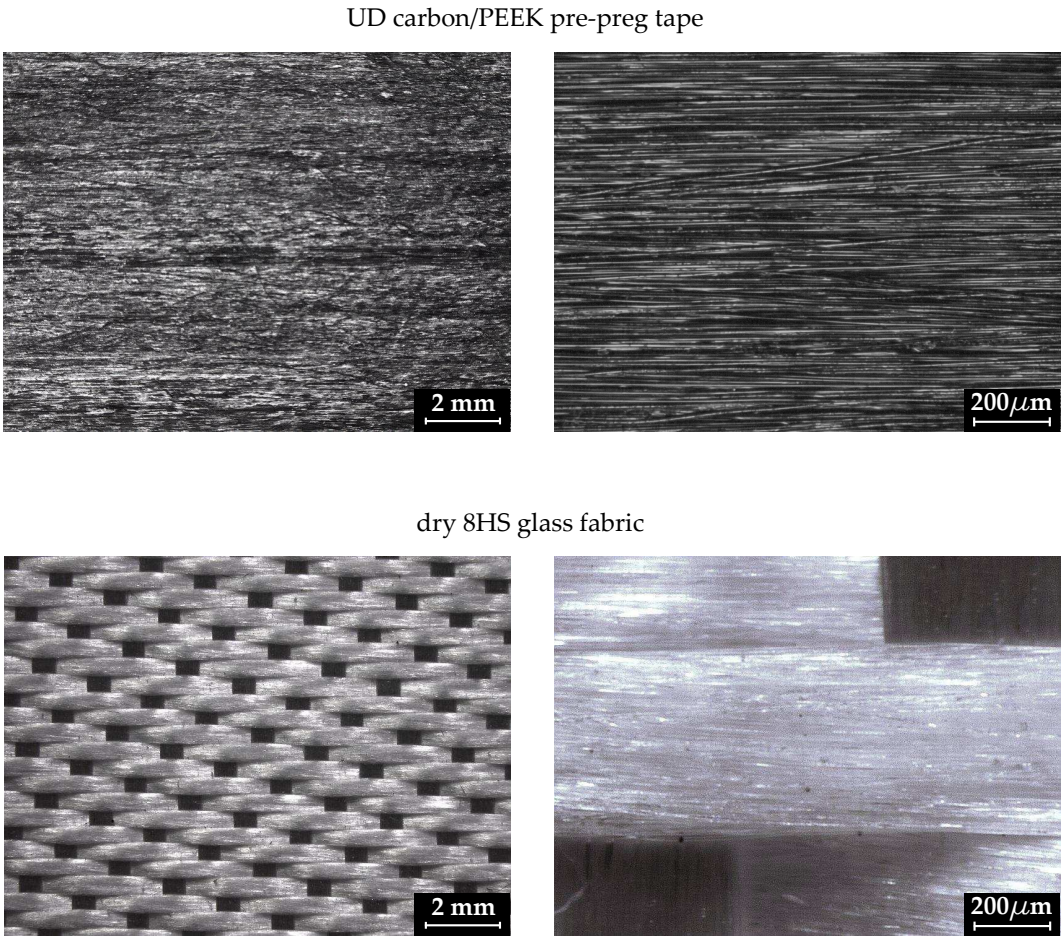

Figure 5.1 *Micrographs of the materials considered.*

the aerospace industry. Forming experiments are conducted and analysed firstly. Several deformation mechanisms are characterised for both materials. The results are subsequently processed in the forming simulation software AniForm [11]. Finally, forming predictions for the considered geometry are shown and compared with the results of the forming experiments.

5.2 Forming experiments

Forming experiments were carried out in order to investigate the formability differences between two different composite materials: UD-C/PEEK and 8HS-G/PPS. A representative product geometry for aerospace applications was selected as shown in figure 5.2. This stiffening part appears in a wing-fixed leading edge, designed and built by Fokker Aerostructures. The product contains a couple of

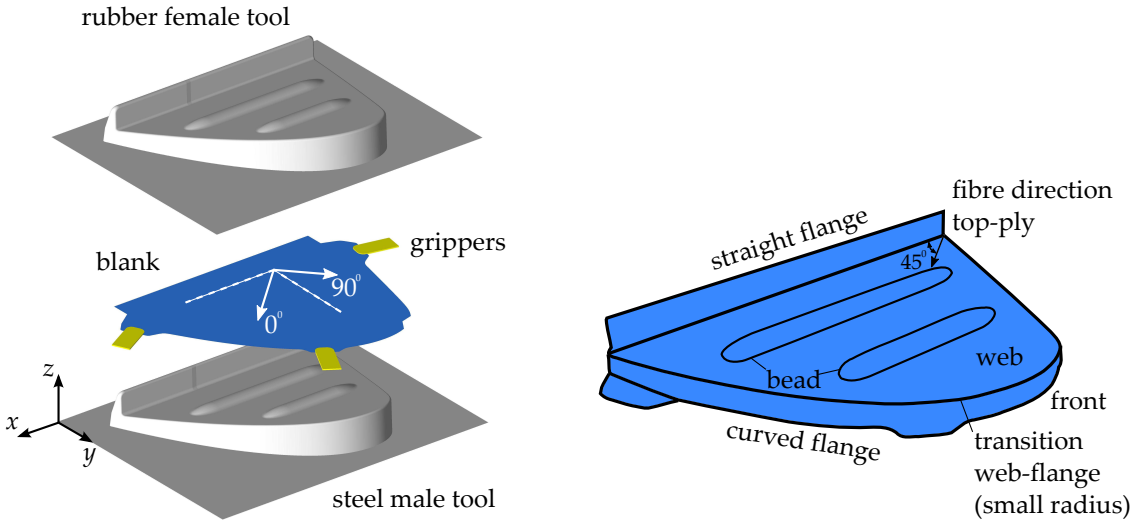

Figure 5.2 *Forming set-up and product geometry.*

features, such as the flat web and the long straight flange. Two beads and the curved flange are features with double curvature.

Blanks were manufactured from both materials. These were cut from quasi-isotropic laminates with $[0,45,90,-45]_S$ and $[(90/0),(-45/45)]_S$ lay-ups, for the UD-C/PEEK and 8HS-G/PPS materials, respectively. Such lay-ups are considered for the majority of the stamp-formed products in the aerospace industry. The laminates were consolidated in a hot press at Ten Cate Advanced Composites. The top-ply fibre direction is indicated in figure 5.2, which encloses a 45 degree angle with the long straight edge of the blank. The top plies of the blanks were accommodated with a regular grid of dots, which were applied with paint brush tooling. The grids were used to monitor the deformations of the blank after forming.

Forming experiments were performed with a stamp forming press at Fokker Aerostructures. It was equipped with a pre-heated steel male tool and a rubber female tool. A blank was positioned with the grippers as shown in figure 5.2. A shuttle frame transported the blank to an infra-red oven, which heated the blank sufficiently above the melting point of the thermoplastic resins. After the hot blank was rapidly transported towards the tooling, the forming action was initiated by the downwards movement of the female tool with a speed of 20 mm/s. Average blank temperatures were 390°C and 310°C for the UD-C/PEEK and 8HS-G/PPS materials, respectively.

5.2.1 Qualitative analyses

The forming process was stopped at several stages in order to monitor the intermediate blank deformations. Figure 5.3 shows four forming stages for the considered materials. Stage 1 shows the blanks after heating in the oven, prior to the forming process itself. The UD-C/PEEK blank shows less sag than the 8HS-G/PPS blank. Contact development between the blank and the tooling in the next stages is therefore different.

Stage 2 shows the initial tool-blank contact, which appears mainly in the area of the flanges. The 8HS-G/PPS blank shows smooth deformations, whereas the UD-C/PEEK blank shows irregular behaviour. The UD-C/PEEK material shows locally buckled areas as indicated in the figure, resulting in a bumpy appearance of the web. The straight flange of the UD-C/PEEK blank is curved downwards, whereas it is pointed upwards for the 8HS-G/PPS blank. This can be explained by the initial curvature due to sagging in stage 1, which was more pronounced for the 8HS-G/PPS.

In stage 3, in-plane tensions in the web decrease the bumpy appearance for the UD-C/PEEK blank. The contours of the beads start to develop, which is most pronounced for the 8HS-G/PPS material. Additionally, the curved flange is formed entirely, which is accompanied by the formation of small and large wrinkles.

Stage 4 shows the final products after the complete forming cycle. Close-up photographs are shown in figure 5.4. Small and large wrinkles are observed in and near regions with double curvature. Conforming a flat sheet to a doubly curved area always results in material deformations. Intra-ply shear and/or out-of-plane buckling are the mechanisms which are generally observed when forming fibre reinforced laminates. Focusing on the web and its bead-ends, a buckling mechanism is invoked for the UD-C/PEEK product, which results in the small wrinkles that are indicated by the dashed arrows in the figures. These wrinkles develop locally in a few plies but also globally through the laminate thickness as a whole. This will be discussed later in more detail.

Larger wrinkles are found in the curved flanges, as indicated by the solid arrows in figure 5.4 as well. These appear on both sides of the gripper area for both materials. The UD-C/PEEK product shows a large wrinkle on the front side, whereas the 8HS-G/PPS product does not. Other regions of the curved flange that are not shown in the figure show irregular shearing and waviness for the UD-C/PEEK product, whereas the 8HS-G/PPS product shows a smoothly deformed surface.

5.2.2 Quantitative analyses

A regular grid was applied to the blanks. The initial and deformed configuration of the grid were recorded with photogrammetry software. A 2D mapping between

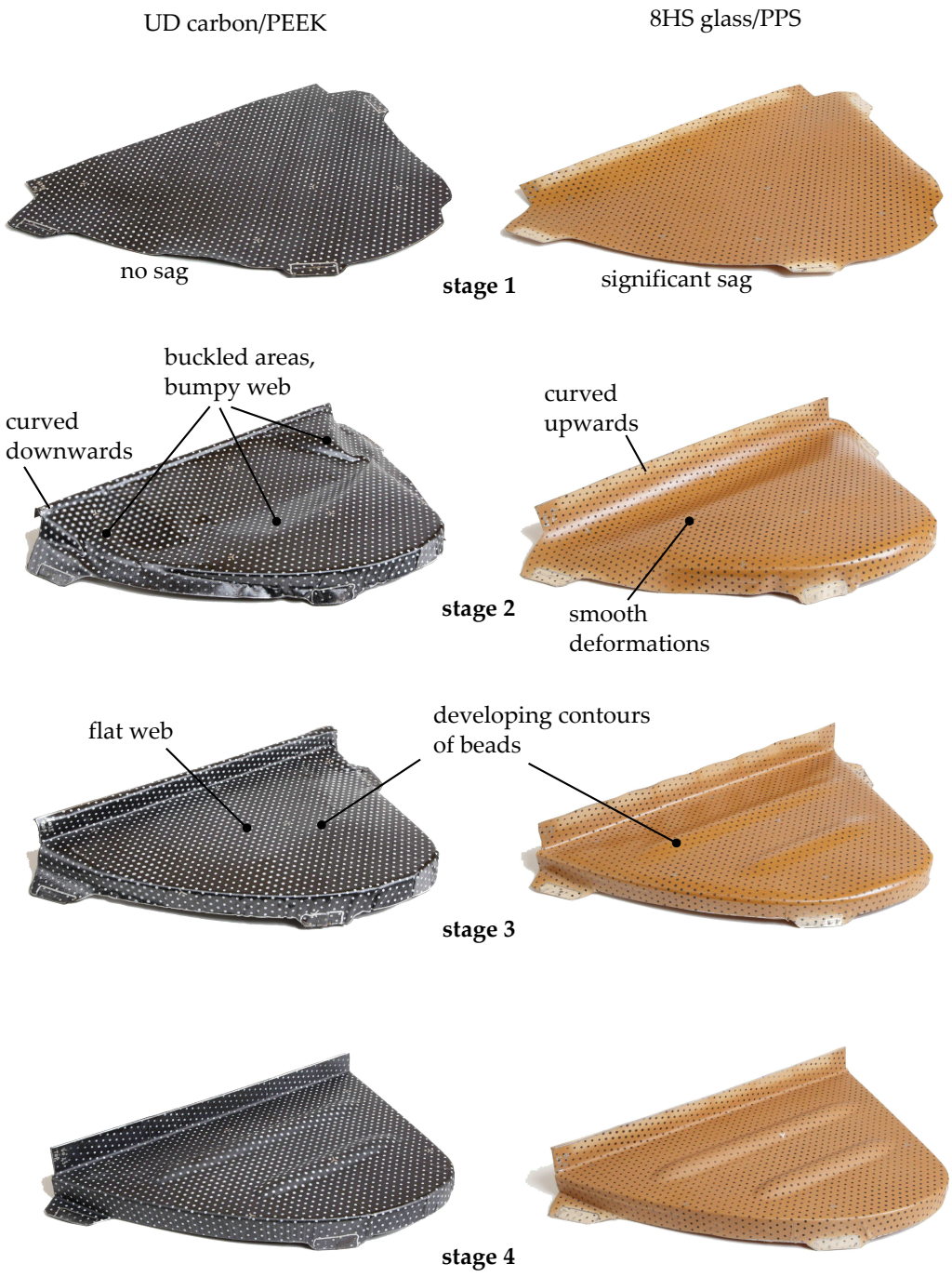

Figure 5.3 *Forming stages as observed during forming experiments.*

the configurations was determined, which resulted in the deformation gradient $\boldsymbol{F}$ in each grid point. The in-plane Green-Lagrange strain tensor components can then be

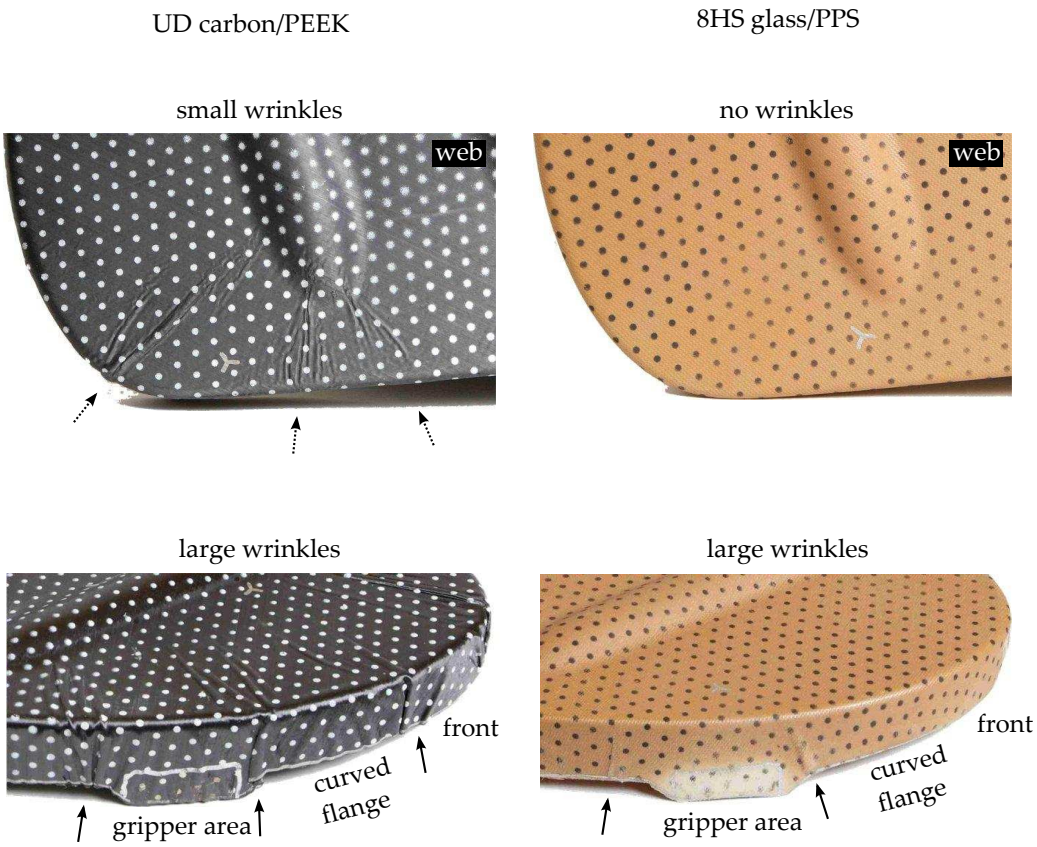

Figure 5.4 *Appearance of wrinkling in the final products (stage 4). Solid and dashed arrows correspond to relatively large and small wrinkles, respectively.*

calculated as:

$$\boldsymbol{E} = \tfrac{1}{2}(\boldsymbol{F}^{\mathrm{T}} \cdot \boldsymbol{F} - \boldsymbol{I}) \tag{5.1}$$

in which $\boldsymbol{I}$ is the identity tensor. The in-plane shear component of $\boldsymbol{E}$ is denoted as $\varepsilon_{12}^{\mathrm{GL}}$, which is plotted in figure 5.5 for both materials. The accuracy of this method was shown to yield an uncertainty bound of ± 0.003 for the shear strains in the case of flat surfaces and most unfavourable situations.

The UD-C/PEEK product in figure 5.5 shows concentrated shear strains. Small wrinkles were actually present at those locations, which locally distort the grid. Hence, these shear concentrations do not correspond with the physical shearing. However, true intra-ply shearing can be extracted from the wrinkle-free areas in the web. Here, small shear strains vary between -0.01 and 0.02. These regions (in yellow) appear mainly next to the beads, however, it must be concluded that intra-ply shearing is very limited for this material.

The results of the 8HS-G/PPS blank are shown in figure 5.5 as well. The blue shear

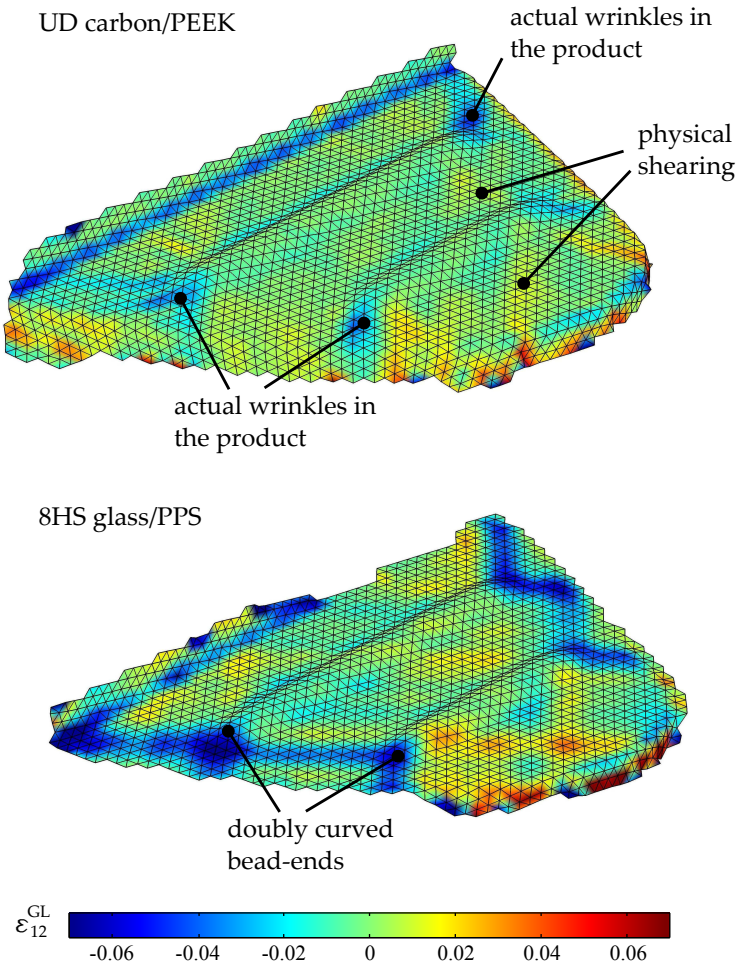

Figure 5.5 *Intra-ply shear strains of the top plies for stage 4, which are determined with photogrammetry.*

concentrations with a magnitude of -0.06 originate from the doubly curved ends of the beads. Regions with smaller strains with a magnitude of 0.02 are observed in the interior part of the web (yellow).

A clear formability difference between the two materials was concluded from the previous qualitative analyses of the deformed blanks. This was achieved by visual inspection of the wrinkling. The results from this photogrammetry analysis quantify the difference in formability in terms of shear magnitudes. Wrinkling is the most pronounced mechanism during the forming of the UD-C/PEEK product, leading to very limited intra-ply shearing. Significant intra-ply shear developed for the 8HS-G/PPS product, which resulted in a web without wrinkles.

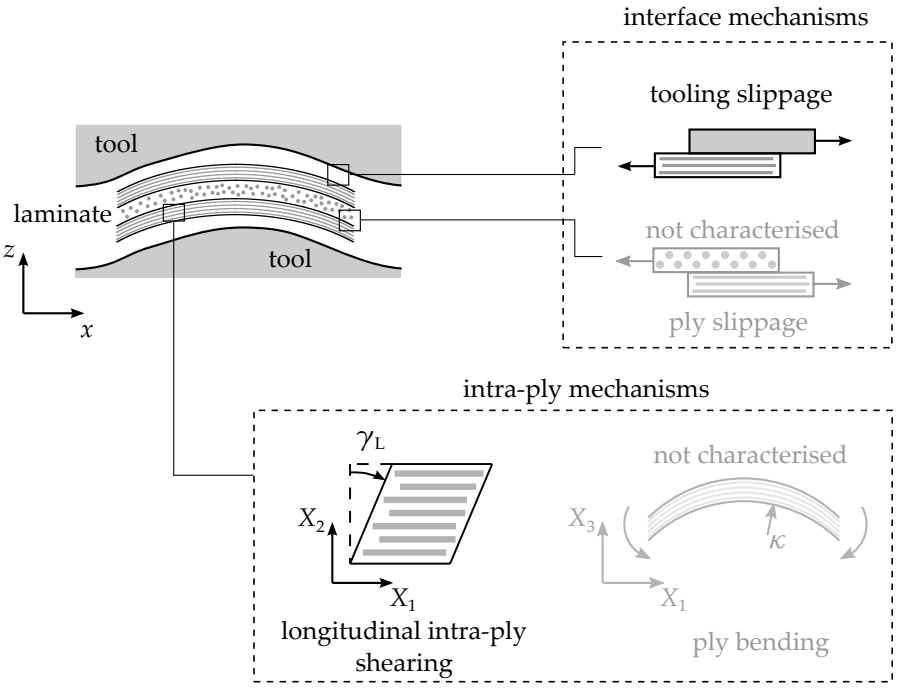

Figure 5.6 *Most relevant deformation mechanisms considered.*

5.3 Material characterisation

Intra-ply shear and tool-ply friction (figure 5.6) of the considered materials were characterised for simulation purposes, which is shown in this section. The data will be used as an input for the forming simulations, to be addressed in a later section. Moreover, the obtained material property data contribute to a better understanding of the formability differences observed in the previous section. Bending properties have not been characterised due to the absence of a mature bending test for fibre reinforced thermoplastics at elevated temperatures.

5.3.1 Intra-ply shear

UD-C/PEEK

Small strain intra-ply shear behaviour of the UD-C/PEEK material was characterised with the torsion bar test [12–14]. Specimens were tested in a rheometer, as shown in figure 5.7. Dynamic shear moduli from the linear visco-elasticity theory (LVE) [15] were determined and converted to the shear relaxation modulus [16].

The transient response at constant shear rate was derived using the LVE theory. Figure 5.7 shows the stress responses for three different shear strain rates, which

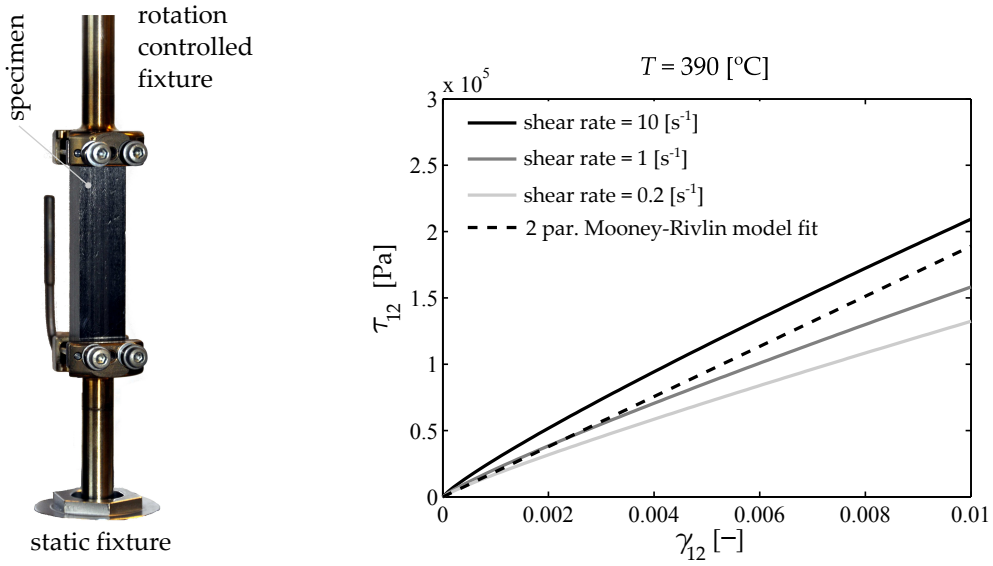

Figure 5.7 *Intra-ply shear characterisation results of UD-C/PEEK.*

are typically the magnitudes as they appear in the blanks during stamp forming processes. A predominantly elastic response is observed, which is caused by the presence of the fibres. Multiple fibre-fibre interactions invoke elastic effects during material loading [17]. Such behaviour was also concluded by Scobbo and Nakajima [18], who state that the material indeed acts as an elastic solid within the considered range of shear rates. For later use in the forming simulations, the transient responses are fitted with the two parameter Mooney-Rivlin model [19]:

$$\boldsymbol{\tau} = 2C_{10}(\boldsymbol{B} - \boldsymbol{I}) - 2C_{01}(\boldsymbol{B}^{-1} - \boldsymbol{I}) \tag{5.2}$$

where $\boldsymbol{B}$ is the left Cauchy-Green strain tensor. The fitted material parameters C_{10} and C_{01} are listed in table 5.1.

8HS-G/PPS

Trellis frame and bias-extension experiments are often applied to characterise the intra-ply shear behaviour of fabrics [20–22]. The bias-extension test is the most convenient test to carry out, due to the simple specimens and gripping system required. A rectangular specimen with dimensions satisfying $H > 2W$ is gripped in the clamps, as indicated in figure 5.8. The specimen is extended by moving the top clamp upwards, as indicated by the displacement u. The cross-over points in the fabric act as hinges. As a result of the 45°/-45° orientation of the fibres, three regions of uniform shear develop as indicated in the figure.

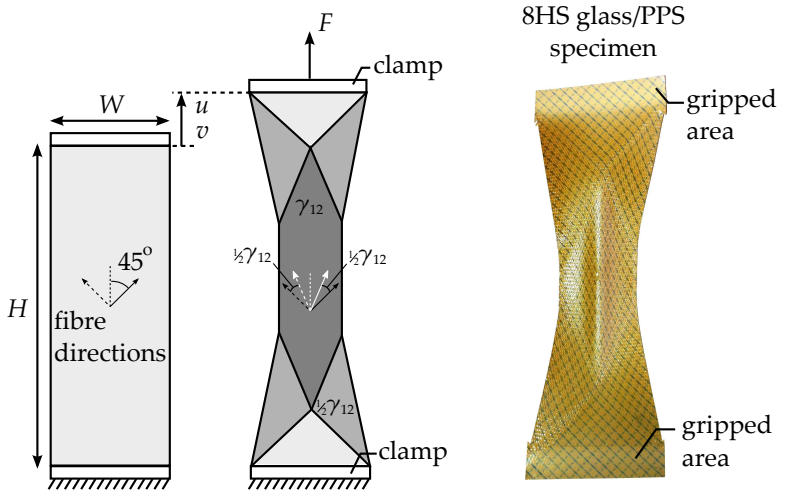

Figure 5.8 *Bias-extension specimens with indicated regions of uniform shear.*

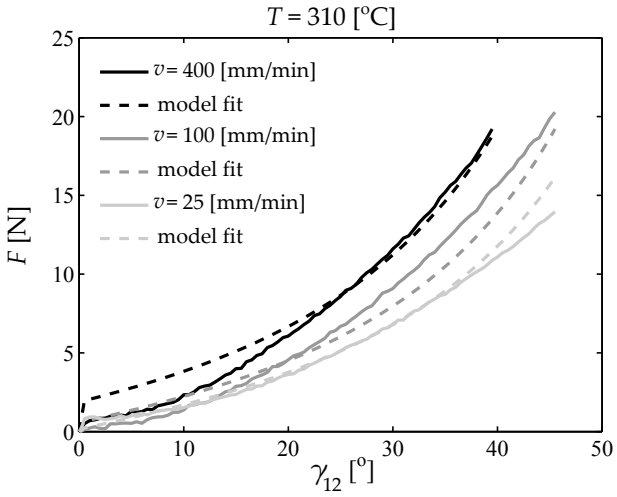

Figure 5.9 *Bias-extension responses and model fits.*

The characterisation of the 8HS-G/PPS material was performed at the University of Twente [23]. Specimens of 130x60 mm were cut from one layer of consolidated 8HS-G/PPS material. Specimens were gripped with two clamps, which were mounted in a tensile tester. The experiments were performed at elevated temperatures. The tests were conducted at three different displacement velocities v of 25, 100, and 400 mm/min, after a specimen temperature of 310°C was reached. This corresponds to initial shear rates $\dot{\gamma}_{12}$ of 0.012, 0.048, and 0.20 s^{-1}, which is equivalent to 0.68, 2.76, and 11.5°/s, respectively. When the initial fibre angle between the two fibre directions

is 90°, the shear angle is related to the displacement u of the upper gripper as [20]:

$$\gamma_{12} = \frac{\pi}{2} - 2\cos^{-1}\left(\frac{u + (H - W)}{\sqrt{2}(H - W)}\right) \tag{5.3}$$

Three specimens were tested per displacement speed, for which the average results are plotted in figure 5.9. The relative standard deviations of the obtained graphs were ±15%. An increasing shear stiffness is observed for an increasing shear angle. Higher displacement velocities (i.e. higher shear rates) result in a small offset of the tensile force F. Moreover, higher shear rates result in a higher stiffness for a certain shear angle. For later use in the forming simulations, the material behaviour is fitted with two material models connected in parallel, namely the two parameter elastic Mooney-Rivlin and a shear rate dependent viscous model:

$$\boldsymbol{\tau} = \Big(2C_{10}(\boldsymbol{B} - \boldsymbol{I}) - 2C_{01}(\boldsymbol{B}^{-1} - \boldsymbol{I})\Big) + 2\eta(\dot{\gamma}_{\text{eq}})\boldsymbol{D} \tag{5.4}$$

in which $\boldsymbol{D}$ is the rate of deformation tensor. The shear rate dependent viscosity is described with the Cross model [24]:

$$\eta = \frac{\eta_0 - \eta_\infty}{1 + m\dot{\gamma}_{\text{eq}}^{(1-n)}} + \eta_\infty \tag{5.5}$$

where the equivalent shear rate $\dot{\gamma}_{\text{eq}}$ is defined as:

$$\dot{\gamma}_{\text{eq}} = \sqrt{2\boldsymbol{D} : \boldsymbol{D}} \tag{5.6}$$

Newtonian plateaus at low and high shear rates are represented by η_0 and η_∞, respectively. The parameter n is the power-law viscosity exponent, which describes the viscosity at intermediate shear rates. The constant m determines the transition points between the plateaus and the shear rate dependent region. The stress situation in the specimen is related to the tensile force, for which more information is given by Cao *et al.* [25] and McGuinness and Ó Brádaigh [26]. The fitted material parameters are listed in table 5.2.

5.3.2 Friction

Different set-ups for the characterisation of tool-ply and ply-ply friction have been developed by several research groups. An overview was given by Gorczyca-Cole *et al.* [27] and Sachs *et al.* [28]. Both the friction of UD-C/PEEK and the 8HS-G/PPS material were characterised with the experimental set-up as shown in figure 5.10. A detailed description of the set-up was given by Akkerman *et al.* [29].

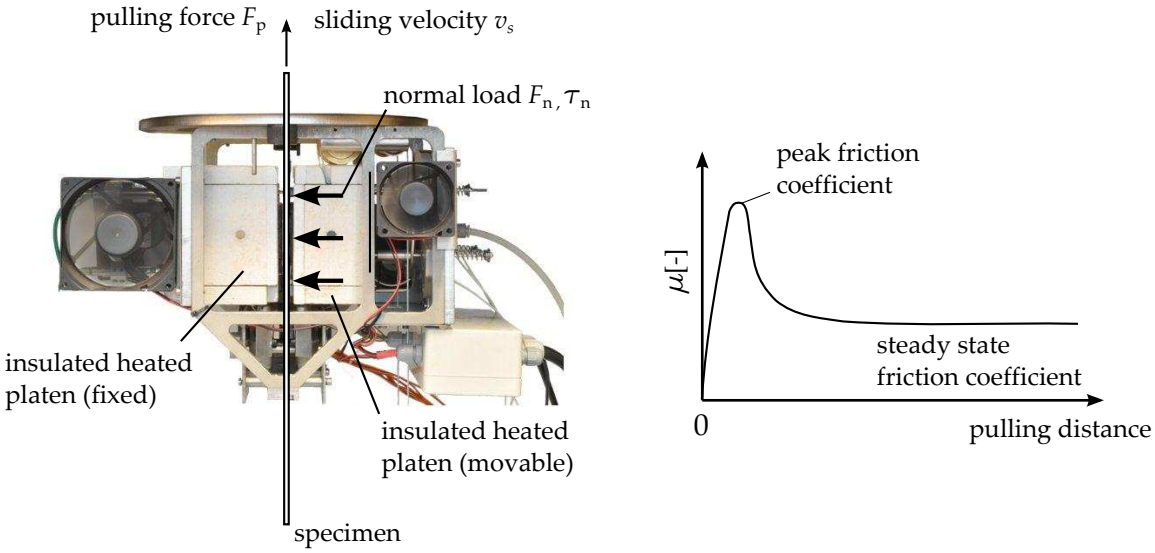

Figure 5.10 *Tool-ply friction characterisation set-up (left) and a schematic response that was typically observed (right).*

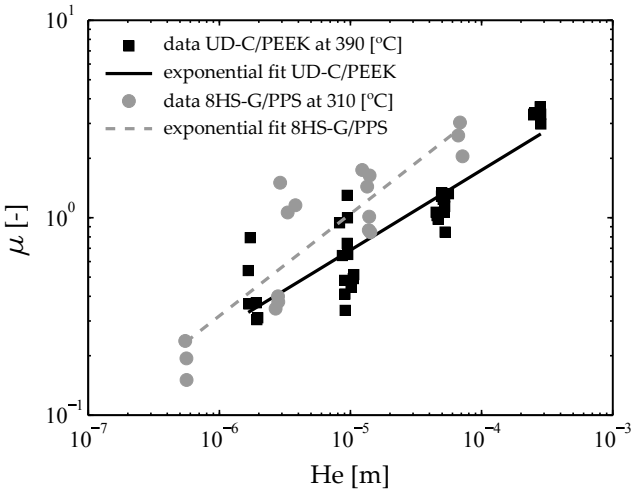

Figure 5.11 *Tool-ply friction characterisation results and model fits. The peak friction coefficients (see figure 5.10 (right)) were used.*

The set-up consists of two insulated heated platens. The specimen with typical dimensions of 50x200 mm is positioned between the platens. A flexible pneumatic actuator supplies the normal load, which is measured by three load cells. The specimen is pulled through the platens after the testing temperature is reached. The required pulling force F_p as a function of pulling distance is monitored. The friction

coefficient is determined as:

$$\mu = \frac{F_{\mathrm{p}}}{2F_{\mathrm{n}}} \tag{5.7}$$

Typical responses as schematically shown in the right of figure 5.10 are obtained. A peak of the friction coefficient is generally seen when fibre reinforced thermoplastics in their molten configuration are tested. After this peak, the pulling force and thus the derived friction coefficient reaches a steady state situation.

Experiments were conducted at the University of Twente [23] and the TPRC [30]. Only tool-ply measurements were available, for which the tooling surfaces used in stamp forming were represented by metal sheets. The results are shown in figure 5.11, where the friction coefficient is plotted against the Hersey number (He), defined as:

$$\mathrm{He} = \frac{\eta v_{\mathrm{s}}}{\tau_{\mathrm{n}}} \tag{5.8}$$

The measured friction coefficient is increasing with increasing sliding velocity v_{s} and bulk viscosity η of the thermoplastic resin. It decreases for increasing normal pressure τ_{n}. This behaviour is typical for fully hydrodynamic lubrication. The measurement data were fitted with the following exponential relation:

$$\mu = g\mathrm{He}^{q} \tag{5.9}$$

The results are shown in figure 5.11 and summarised in tables 5.1 and 5.2.

5.3.3 Discussion on forming experiments

The results of the forming experiments with the UD-C/PEEK and 8HS-G/PPS materials show different forming behaviour in terms of shear strain distributions and wrinkling, for which an explanation is presented here. Consider the situation of a flat laminate that is formed to a doubly curved surface. As a result, the laminate or plies must deform in-plane or out-of-plane. The resulting mechanism is determined by the balance between the apparent frictional (FR), intra-ply (IR) and bending rigidities (BR) of the laminate.

If more than two fibre orientations are present (which is the case in the considered quasi-isotropic lay-ups) and no out-of-plane deformations develop, the in-plane deformations of the plies are always accompanied by inter-ply slippage due to the inextensibility constraints of the fibres. This situation is illustrated in figure 5.12. During forming, the resulting in-plane or out-of-plane mechanism is determined by the balance between the apparent frictional and intra-ply rigidity, versus the bending rigidity.

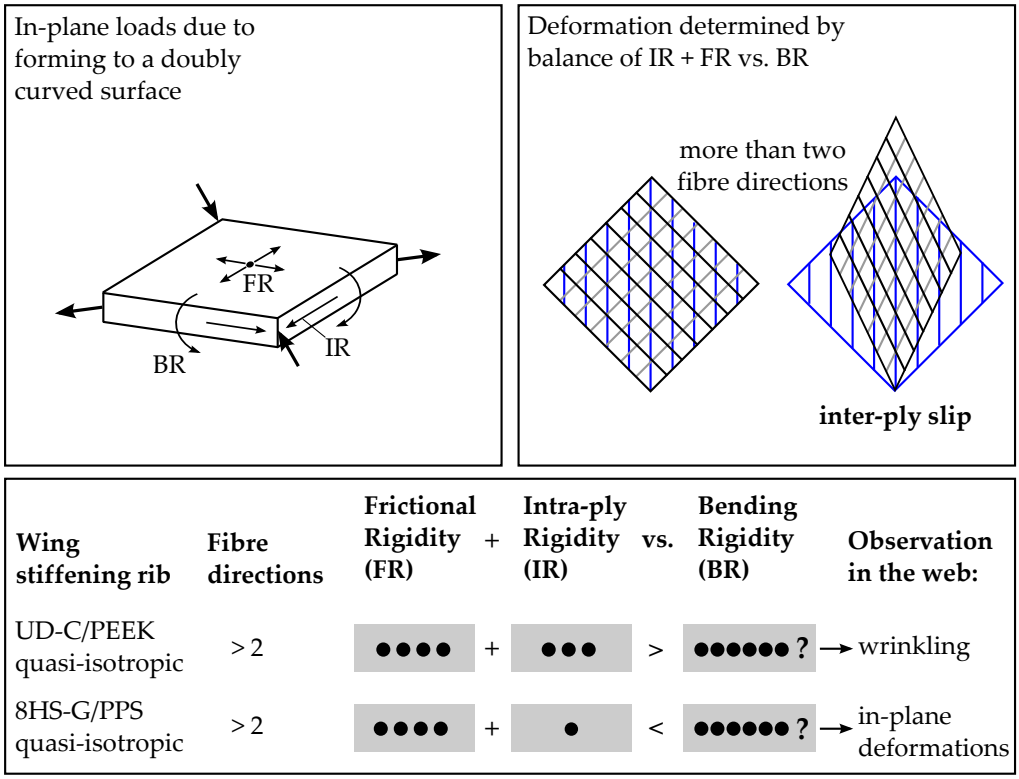

Figure 5.12 *Schematic explanation of the balance between the apparent intra-ply (IR), frictional (FR), and bending (BR) rigidity of the plies.*

The balance of the apparent rigidities is illustrated below in figure 5.12. The frictional behaviour was comparable for UD-C/PEEK and 8HS-G/PPS, as shown in figure 5.11. The intra-ply shear behaviour of the considered materials is compared in figure 5.13 for small strains when a constant shear rate is imposed instantaneously. For a shear rate with a magnitude as it typically appears in the forming process, a relatively high resistance to intra-ply shear is observed for the UD-C/PEEK, as compared to the 8HS-G/PPS material. This can be explained by the friction at the many fibre-fibre contact interfaces within the UD-C/PEEK material (figure 5.1). The woven reinforcement of the 8HS-G/PPS material consists of glass fibre bundles with resin in between. The space without fibres is filled with the PPS resin, which behaves as a visco-elastic fluid at forming temperatures. As the bundles act like rigid rods, shear deformation concentrates in the resin pockets. This explains the more compliant behaviour of the 8HS-G/PPS material.

Many wrinkles do develop for the quasi-isotropic UD-C/PEEK laminates, suggesting that the summation of the apparent frictional and intra-ply rigidity is high compared to the apparent bending rigidity. Only a few large wrinkles are found in the curved flange of the 8HS-G/PPS product and significant shearing was present in its winkle-free web. This suggests that the ratio between the bending rigidity and the

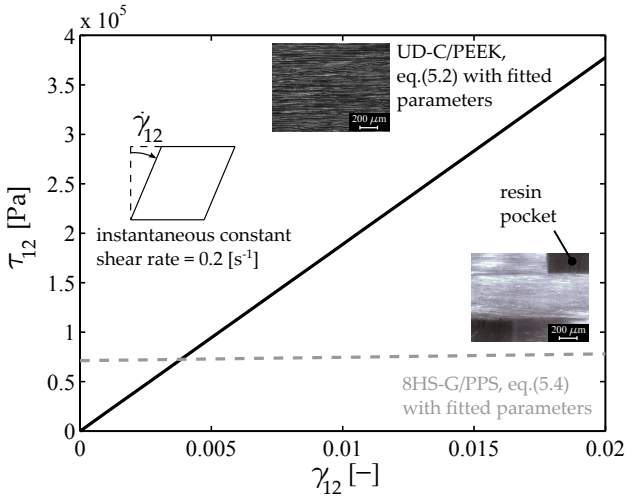

Figure 5.13 *Intra-ply shear response for an instantaneously applied constant shear rate. Comparison between UD-C/PEEK and 8HS-G/PPS*

summation of the frictional and intra-ply rigidity is relatively large, compared to the UD-C/PEEK material.

5.4 Forming simulations

A forming prediction tool can be used to obtain a better understanding of the deformations that appear during the forming of a particular blank design into the aimed product geometry. As a result, predicted critical spots can be anticipated by modifying the product and process design. Modifications of product geometry, material, lay-up, and process settings may eventually lead to the production of products without any defects. This section shows the set-up of a forming simulation for the geometry and the materials that were analysed in the previous sections. The simulations were conducted with the AniForm finite element forming simulation software developed by Ten Thije *et al.* [7, 31]. This 3D code makes use of an implicit solution scheme. Together with an appropriate decomposition of the deformation gradient and a proper material update scheme, this software is most suitable for modelling large deformations of highly anisotropic materials.

The forming process was modelled according to the set-up in figure 5.14. A similar modelling strategy was described in chapter 2. The male and female tools were modelled as rigid surfaces, each containing 37.000 elements. The male tool was fixed, while the female tool was moved downwards with 20 mm/s. Eight individual plies were modelled to represent the UD-C/PEEK blank and four plies were modelled for the 8HS-G/PPS blank, for which the lay-up is given in figure 5.14. Each ply was discretized with 17.000 elements. Three-node triangular shell elements were

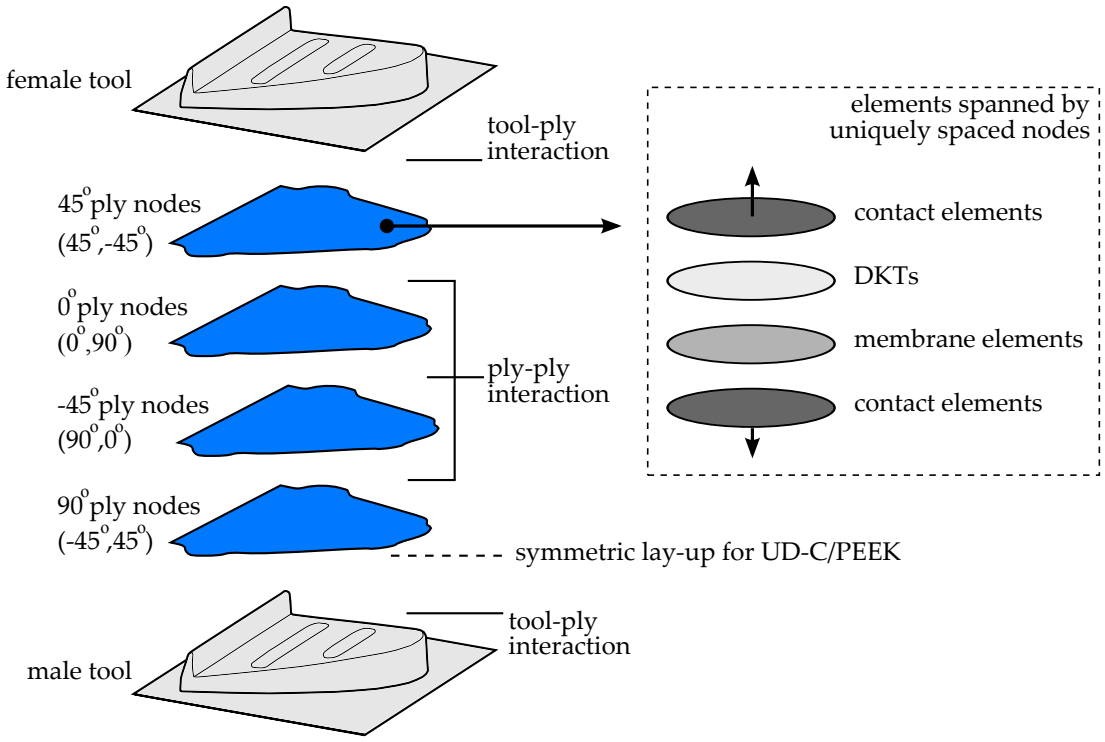

Figure 5.14 *Forming simulation set-up for both the UD-C/PEEK and 8HS-G/PPS laminates.*

used, which consist of a membrane element and a Discrete Kirchhoff Triangle (DKT). The membrane element was used to model the in-plane constitutive behaviour. The DKT was used to model the out-of-plane behaviour. This decoupled approach was employed to avoid over-prediction of the bending stiffness [32]. Contact logic at both sides of each ply was modelled with two groups of contact elements. The membranes, DKTs, and contact elements were supplied with constitutive models.

The total number of elements to model the laminate sums up to 272.000 and 544.000 for a simulation with four and eight plies, respectively. The simulations run typically for 40 to 160 hours on a computer with two quad-core Intel Xeon E5620 2.4 GHz processors.

5.4.1 Constitutive modelling

For the modelled UD-C/PEEK plies, the stresses in the membrane elements were described as [33]:

$$\boldsymbol{\sigma} = -p\boldsymbol{I} + T_{\mathrm{a}}\hat{\boldsymbol{a}}\hat{\boldsymbol{a}} + \boldsymbol{\tau} \tag{5.10}$$

in which $\hat{\boldsymbol{a}}$ is a unit vector indicating the fibre direction. Another fibre direction $\hat{\boldsymbol{b}}$ was added to model the 8HS-G/PPS plies:

$$\boldsymbol{\sigma} = -p\boldsymbol{I} + T_{\mathrm{a}}\hat{\boldsymbol{a}}\hat{\boldsymbol{a}} + T_{\mathrm{b}}\hat{\boldsymbol{b}}\hat{\boldsymbol{b}} + \boldsymbol{\tau} \tag{5.11}$$

where T_{a} and T_{b} are the fibre tensions and $-p\boldsymbol{I}$ is the hydrostatic pressure term. Constitutive relations for the extra stress tensor $\boldsymbol{\tau}$ were determined from the material characterisation experiments in the previous section. The material models used and their fitted parameters are listed in tables 5.1 and 5.2.

No bending characterisation results were available. At this stage, the bending parameters selected are an educated guess, which is based on free deflection experiments. The orthotropic formulation of Hooke's law [34] is used to model the bending behaviour of the UD-C/PEEK plies, whereas the isotropic formulation is used for the 8HS-G/PPS plies. The material parameters are listed in tables 5.1 and 5.2. The effect of these parameters is investigated in a later stage. The individual plies of the blank have the tendency to stick together. This tackiness of the plies is unknown. For now, it is set to 0.1 MPa, which means that a minimal tension of 10 N is required to separate a contact surface of 100 mm^2 between two adjacent plies. Isothermal conditions were assumed, however, measurements during the experiments indicated a significant drop in temperature at the gripper locations. The elements covering these areas were modelled by assigning one order of magnitude higher moduli at the corresponding locations in the ply.

5.4.2 Results

The forming stages

The forming predictions are shown in figure 5.15 for both materials. The stages can be compared with the stages from the experiments in figure 5.3. As expected, the flanges are formed firstly in stage 2, after which the web is spanned around the edges in stage 3. Subsequently, the beads are formed after stage 3, yielding the final product in stage 4.

The prediction for the UD-C/PEEK blank in stage 2 shows buckled areas, which results in a bumpy appearance of the web. This was also observed in the experiments in figure 5.3. However, the prediction of the 8HS-G/PPS blank shows a bumpy appearance as well, whereas the experiments showed smooth deformations in those areas. This can be explained by the absence of sag (gravity) in the model. In the experiments, significant sagging was present in stage 1 due to gravity, resulting in some initial curvature. This is likely to facilitate the smooth deformations in the web area, which is obviously not observed in the simulation. Additionally, the prediction shows the flange to be curved downwards, whereas it is curved upwards in the experimental result.

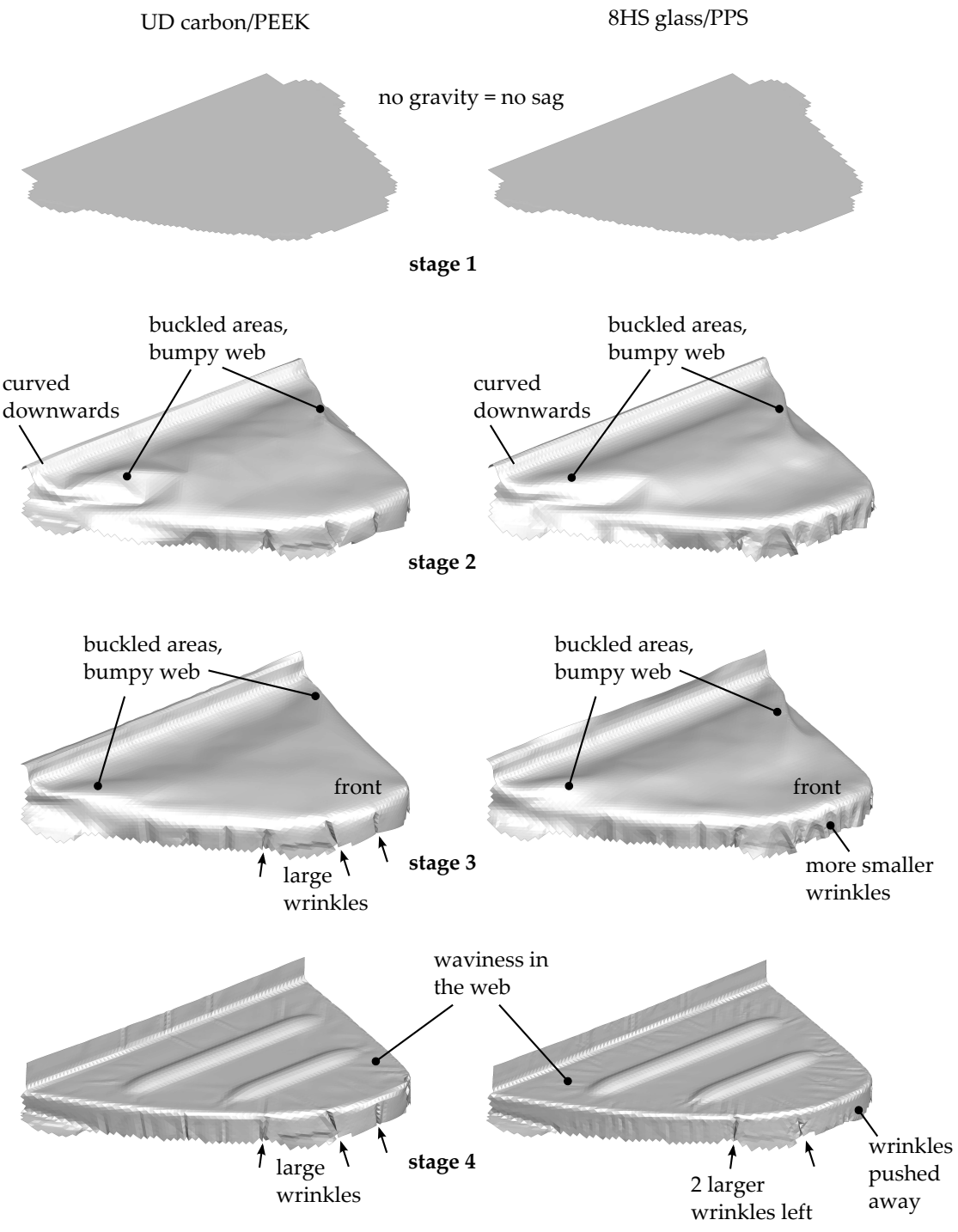

Figure 5.15 *Simulated forming evolution for the material parameter input as listed in tables 5.1 and 5.2.*

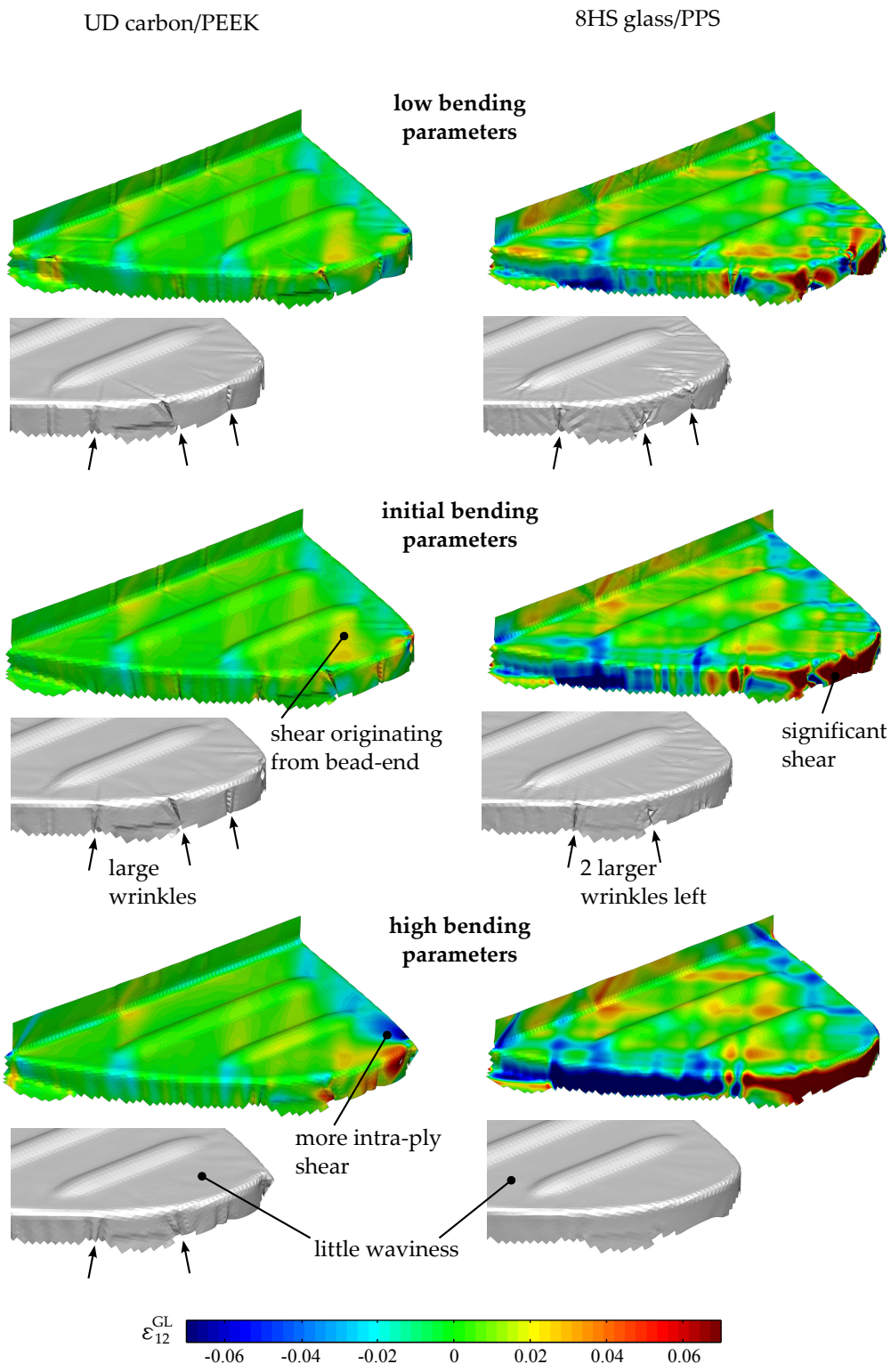

Figure 5.16 *Predictions for the final forming stage 4, as a function of the bending parameter input listed in table 5.3.*

In the experiments, stage 3 showed in-plane tensioned webs with developing contours of the beads. The predictions still show a bumpy appearance of the web for this stage. The contours of the beads are therefore not visible yet. Compared to stage 2, the curved flanges are further developed. Focusing on the front part, large wrinkles are observed for the UD-C/PEEK blank in this flange, which corresponds well with those observed in the product in figure 5.4. The curved flange of the 8HS-G/PPS blank shows more and smaller wrinkles compared to the UD-C/PEEK blank. These wrinkles were not observed in the experiments.

The final stage 4 still shows the large wrinkles in the curved flange of the UD-C/PEEK blank. However, the majority of the wrinkles of the 8HS-G/PPS blank from stage 3 are pushed away in stage 4. This is accompanied by significant intra-ply shear, as shown in the centre of figure 5.16 for the initial bending parameters. As a result, two larger wrinkles next to the gripper area are left. These two wrinkles were also observed in the product in figure 5.4. Moreover, stage 4 shows waviness in the web for both materials. This waviness is caused by a very little upwards displacement of the associated nodes. The position and orientation of the waves corresponds well with the position of small wrinkles in the UD-C/PEEK product in figure 5.4. It must be noted that the small wrinkles in the product are much smaller than the element size used (see figure 5.17), which implies that these defects cannot be predicted. Nevertheless, the waviness can be interpreted as an indicator of critical spots. This applies to the UD-C/PEEK product, however, the predicted waviness for the 8HS-G/PPS blank does not correspond with a critical area.

Intra-ply shear

The predicted intra-ply shear patterns in the web are here compared with the photogrammetry results in figure 5.5. The UD-C/PEEK prediction in figure 5.16 (see initial bending parameters setting) shows regions with shear originating from the bead-ends. Some of these areas are recognised in the product in figure 5.5. The prediction indicates limited intra-ply shear, which corresponds with the experimental findings. More intra-ply shear is predicted for the 8HS-G/PPS blank. The cross-like pattern as observed in the product in figure 5.5 is recognised. The predicted pattern is somewhat distorted, compared to the more continuous appearance in the actual product.

Effect of the bending parameters

No bending characterisation results were available. To investigate the effect of the bending parameters on the forming prediction, these were set to 0.1 and 10 times the initial moduli. Table 5.3 lists the considered settings. The predictions are shown in figure 5.16 (top and bottom results).

The low bending parameters lead to minor differences for the UD-C/PEEK blank. However, a large wrinkle is now predicted at the front part of the 8HS-G/PPS blank. This affects the shear behaviour within this area as well.

The high bending parameters result in fewer and smaller wrinkles for the UD-C/PEEK blank, which is accompanied by more intra-ply shear in the web. The curved flange of the 8HS-G/PPS blank is free of wrinkles for this setting, which also leads to more intra-ply shearing. Moreover, the waviness in the web has almost disappeared for both materials.

5.4.3 Discussion on forming simulations

The forming simulations resulted in the prediction of waviness in the web for both materials. The waves cover only a few elements and their heights were limited. Interpreting those effects must therefore be done with care. These could give an indication of potential problematic areas, which is indeed the case for the UD-C/PEEK blanks, but not for the 8HS-G/PPS blanks.

The wrinkles observed in the UD-C/PEEK products were smaller than the element size used, as schematically shown in figure 5.17. The figure shows the development of the small wrinkles near one of the bead-ends, which appear just before stage 4. These wrinkles develop both through the whole thickness and through a limited number of plies only. A more accurate prediction of such wrinkles can be obtained by refining the meshes of the plies. For example, local adaptive refinement of the mesh can be controlled by a wrinkling indicator, such as introduced for metal forming applications by Meinders *et al.* [35]. However, the criteria of the meshes for highly anisotropic materials restrict the flexibility in mesh refinement. Element edges must have a certain orientation with respect to the fibre directions in order to avoid intra-ply shear locking. Adaptive mesh refinement is therefore not straightforward. Unfortunately, an overall refinement of the meshes yields impractical calculation times.

A wrinkling indicator addresses critical areas in the blank, which can be used to avoid mesh-refining. For example, the approach of Hutchinson [36] compares the current stress state to a critical stress state for buckling. In the area of metal forming, this was, amongst others, applied by Selman *et al.* [37]. Another option to indicate critical spots could be the use of an experimentally determined forming limit diagram, as for example used by Dessenberger and Tucker [38] for single layer composite simulations. A critical region in the blank is indicated when the current state of strain is outside the forming limit envelope defined in the principle stretch ratio space. However, extending such indicators to multiple stacked plies with inter-ply contact is not straightforward either, which requires further research.

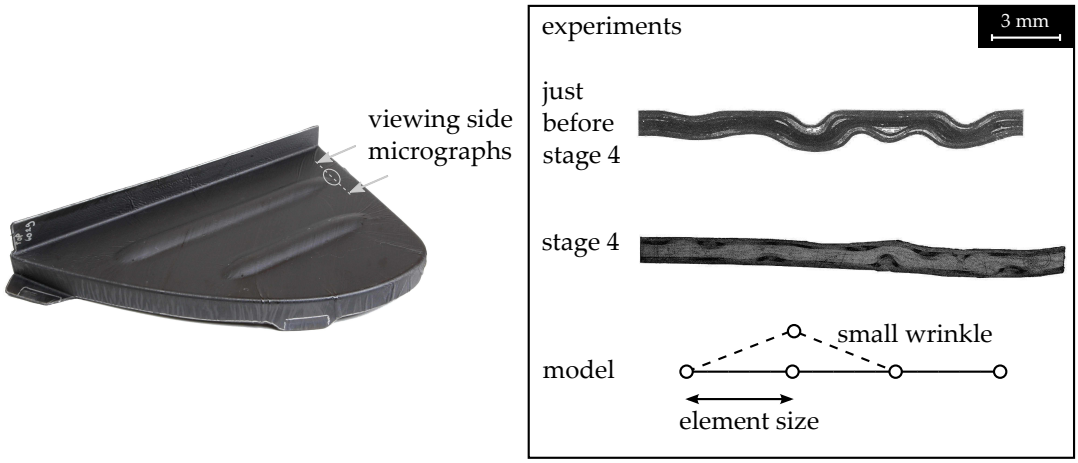

Figure 5.17 *Micrographs of a region in the product where the small wrinkles develop typically. Several stages were considered. The size of the small wrinkles are compared to the element size used.*

5.5 Conclusions

The formability of two different composite materials used in the aerospace industry was investigated. Quasi-isotropic laminates of PEEK with a uni-directional carbon fibre reinforcement (UD-C/PEEK), and PPS with a woven glass fibre reinforcement (8HS-G/PPS) were considered.

The UD-C/PEEK blanks were very sensitive to wrinkling near doubly curved areas. Many small wrinkles were observed in the web of the product, whereas the 8HS-G/PPS blanks deformed smoothly without defects in those areas. Both materials showed wrinkling in the curved flanges, however, the number of wrinkles, the size, and their distribution depend on the material. Blank deformations were recorded with the aid of photogrammetry from which it was concluded that the two materials show a large difference in intra-ply shear behaviour.

The balance between the apparent intra-ply, frictional and bending rigidity determines whether in-plane or out-of-plane mechanisms dominate the laminate deformation process. The considered product involved doubly curved surfaces. In that case, wrinkle-free forming of a laminate having more than two unique fibre orientations must invoke inter-ply slippage and intra-ply deformations. Material characterisation results for UD-C/PEEK and 8HS-G/PPS showed similar frictional properties, whereas the resistance to intra-ply shear for the UD-C/PEEK material was higher. This can explain the smooth deformation behaviour of the 8HS-G/PPS and the many wrinkles in the UD-C/PEEK product.

Forming simulations were conducted in order to assess their predictive capabilities. The predicted intra-ply shearing patterns were shown to match well with the experimental results. The large wrinkles in the curved flange of the product were

correctly predicted. Small wrinkles observed in practice cannot be predicted with the element size used, however, predicted waviness at the corresponding locations could indicate critical spots. Reliable bending material properties were not available, but it was shown that these have a significant effect on the predicted forming behaviour. This addresses the need for a mature bending characterisation test.

Acknowledgements

The laminates used for the experiments were supplied by Ten Cate Advanced Composites. Their good support during the experimental programme is gratefully acknowledged. The stamp forming experiments were conducted at the Fokker Aerostructures company and were guided by Steven Teunissen, Richard Roerink and Michael Wielandt. Preparations were done by Gijs Gijsbertse. Their help is also highly appreciated. We also thank Dirk Soeteman for his support with the photogrammetry analyses.

References

[1] J.R. Krone and J.H. Walker. Processing thermoplastic advanced composites. *Plastics Technology*, **32**(12):61–65, 1986.

[2] R.K. Okine. Analysis of forming parts from advanced thermoplastic composite sheet materials. *SAMPE Journal*, **25**(3):9–19, 1989.

[3] P. De Luca, P. Lefébure, and A.K. Pickett. Numerical and experimental investigation of some press forming parameters of two fibre reinforced thermoplastics: APC2-AS4 and PEI-CETEX. *Composites Part A: Applied Science and Manufacturing*, **29**(1-2):101–110, 1998.

[4] M. Hou. Stamp forming of fabric-reinforced thermoplastic composites. *Polymer Composites*, **17**(4):596–603, 1996.

[5] B. Zouari, J. Daniel, and P. Boisse. A woven reinforcement forming simulation method. Influence of the shear stiffness. *Computers and Structures*, **84**(5-6):351–363, 2006.

[6] Q. Chen, P. Boisse, C.H. Park, A. Saouab, and J. Bréard. Intra/inter-ply shear behaviors of continuous fiber reinforced thermoplastic composites in thermoforming processes. *Composite Structures*, **93**(7):1692–1703, 2011.

[7] R.H.W. ten Thije. Finite element simulations of laminated composite forming processes. Ph.D. thesis, University of Twente, 2007.

[8] M.A. Khan, T. Mabrouki, E. Vidal-Sallé, and P. Boisse. Numerical and experimental analyses of woven composite reinforcement forming using a hypoelastic behaviour. Application to the double dome benchmark. *Journal of Materials Processing Technology*, **210**(2):378–388, 2010.

[9] J. Sargent, J. Chen, J. Sherwood, J. Cao, P. Boisse, A. Willem, K. Vanclooster, S.V. Lomov, M. Khan, T. Mabrouki, K. Fetfatsidis, and D. Jauffrés. Benchmark study of finite

element models for simulating the thermostamping of woven-fabric reinforced composites. *International Journal of Material Forming*, **3**:683–686, 2010.

[10] B. Rietman, S.P. Haanappel, R.H.W. ten Thije, , and R. Akkerman. Forming simulation sensitivity study of the double-dome benchmark geometry. In The 15th International ESAFORM Conference on Material Forming, 2012.

[11] AniForm Virtual Forming. *http://www.aniform.com*.

[12] S.P. Haanappel, R.H.W. ten Thije, U. Sachs, A.D. Rietman, and R. Akkerman. In-plane shear characterisation of uni-directionally reinforced thermoplastic melts. In G. Menary, editor, the 14th International ESAFORM Conference on Material Forming, volume 1353 of *AIP Conference Proceedings*, 930–935. American Institute of Physics, 2011.

[13] S.P. Haanappel and R. Akkerman. A method for shear characterisation of fibre reinforced thermoplastics by means of torsion. Submitted to *Composites Part A: applied science and manufacturing*, 2013.

[14] S.P. Haanappel and R. Akkerman. Shear characterisation of uni-directional fibre reinforced thermoplastic melts by means of torsion. Submitted to *Composites Part A: applied science and manufacturing*, 2013.

[15] J.D. Ferry. Viscoelastic properties of polymers. John Wiley & Sons, 3rd edition, 1980.

[16] F.R. Schwarzl. Numerical calculation of stress relaxation modulus from dynamic data for linear viscoelastic materials. *Rheologica Acta*, **14**(7):581–590, 1975.

[17] T.G. Gutowski. Resin flow/fiber deformation model for composites. *SAMPE quarterly*, **16**(4):58–64, 1985.

[18] J.J. Scobbo Jr. and N. Nakajima. Dynamic mechanical analysis of molten thermoplastic/continuous graphite fiber composites in simple shear deformation. In National SAMPE Technical Conference, volume 21, 730–743, 1989.

[19] M. Mooney. A theory of large elastic deformation. *Journal of Applied Physics*, **11**(9):582–592, 1940.

[20] G. Lebrun, M.N. Bureau, and J. Denault. Evaluation of bias-extension and picture-frame test methods for the measurement of intraply shear properties of PP/glass commingled fabrics. *Composite Structures*, **61**(4):341–352, 2003.

[21] J. Wang, J.R. Page, and R. Paton. Experimental investigation of the draping properties of reinforcement fabrics. *Composites Science and Technology*, **58**(2):229–237, 1998.

[22] K. Potter. Bias extension measurements on cross-plied unidirectional prepreg. *Composites Part A: Applied Science and Manufacturing*, **33**(1):63–73, 2002.

[23] P. Jannink. Karakteriseren van materiaalgedrag van vezelversterkte thermoplasten onder smelt. Master's thesis, Saxion Hogescholen, 2009.

[24] C.W. Macosko. Rheology principles, measurements, and applications. Wiley-VCH, 1994.

[25] J. Cao, R. Akkerman, P. Boisse, J. Chen, H.S. Cheng, E.F. de Graaf, J.L. Gorczyca, P. Harrison, G. Hivet, J. Launay, W. Lee, L. Liu, S.V. Lomov, A. Long, E. de Luycker, F. Morestin, J. Padvoiskis, X.Q. Peng, J. Sherwood, Tz Stoilova, X.M. Tao, I. Verpoest, A. Willems, J. Wiggers, T.X. Yu, and B. Zhu. Characterization of mechanical behavior of woven fabrics: Experimental methods and benchmark results. *Composites Part A: Applied Science and Manufacturing*, **39**(6):1037–1053, 2008.

[26] G.B. McGuinness and C.M. Ó Brádaigh. Characterisation of thermoplastic composite

melts in rhombus-shear: The picture-frame experiment. *Composites Part A: Applied Science and Manufacturing*, **29**(1-2):115–132, 1998.

[27] J.L. Gorczyca-Cole, J.A. Sherwood, and J. Chen. A friction model for thermostamping commingled glass-polypropylene woven fabrics. *Composites Part A: Applied Science and Manufacturing*, **38**(2):393–406, 2007.

[28] U. Sachs, S.P. Haanappel, A.D. Rietman, and R. Akkerman. Friction testing of thermoplastic composites. In SAMPE Europe 32nd International Technical Conference & Forum, 2011.

[29] R. Akkerman, R. Ten Thije, U. Sachs, and M. De Rooij. Friction in textile thermoplastic composites forming. In Proceedings of the 10th International Conference on Textile Composites - TEXCOMP 10: Recent Advances in Textile Composites, 271–279, 2010.

[30] U. Sachs, R. Akkerman, S.P. Haanappel, R.H.W ten Thije, and M.B. de Rooij. Friction in forming of UD composites. In G. Menary, editor, the 14th International ESAFORM Conference on Material Forming, volume 1353 of *AIP Conference Proceedings*, 984–989. American Institute of Physics, 2011.

[31] R.H.W. ten Thije, R. Akkerman, and J. Huétink. Large deformation simulation of anisotropic material using an updated Lagrangian finite element method. *Computer Methods in Applied Mechanics and Engineering*, **196**(33-34):3141–3150, 2007.

[32] D. Soulat, A. Cheruet, and P. Boisse. Simulation of continuous fibre reinforced thermoplastic forming using a shell finite element with transverse stress. *Computers and Structures*, **84**(13-14):888–903, 2006.

[33] P. Harrison and M.J. Clifford. Design and manufacture of textile composites, chapter Rheological Behaviour of Pre-impregnated Textile Composites. Woodhead Publishing Ltd., Cambridge, UK, 2005.

[34] R.M. Jones. Mechanics of composite materials. Taylor & Francis, 2nd edition, 1999.

[35] T. Meinders, A.H. van den Boogaard, and J. Huétink. Advanced sheet metal forming. In V. Brucato, editor, The 6th International Esaform Conference on Material Forming, 159–162. Salerno, 2003.

[36] J.W. Hutchinson. Plastic Buckling, volume 14 of *Advances in Applied Mechanics*, 1974.

[37] A. Selman, T. Meinders, and A.H. van den Boogaard. Adaptive numerical analysis of wrinkling in sheet metal forming. *IJFP*, **6**:87–103, 2003.

[38] R.B. Dessenberger and C.L. Tucker. Ideal forming analysis for random fiber preforms. *Journal of Manufacturing Science and Engineering, Transactions of the ASME*, **125**(1):146–153, 2003.

[39] J. Huétink. On anisotropy, objectivity and invariancy in finite thermo-mechanical deformations. In 9th ESAFORM conference on Material Forming, 355–358, 2006.

5.A Appendix: Material data for its use in the forming simulations

Table 5.1 *Constitutive models and parameter input for the UD-C/PEEK simulation.*

Element type and models assigned	Reference	Parameter(s)	Input data
DKTs (bending)			
Orthotropic Hooke		E_1 [MPa]	250
		E_2 [MPa]	125
		ν_{12} [-]	0.32
		G_{12} [MPa]	100
Membrane elements (in-plane)			
Mooney Rivlin	eq. (5.2)	$C_{10} = C_{01}$ [MPa]	4.72
Elastic fibre model	[7, 39]	E_f [GPa]	1.0
Contact elements			
Hersey model	eq. (5.9)	g [m^{-q}]	72.6
		q [-]	0.405
		η [Pa · s]	286
Adhesion		Tension [MPa]	0.1
Penalty model		Penalty stiffness [N/mm^3]	1.0

Table 5.2 *Constitutive models and parameter input for the 8HS-G/PPS simulation.*

Element type and models assigned	Reference	Parameter(s)	Input data
DKTs (bending)			
Isotropic Hooke		E [MPa]	125
		ν [-]	0.33
Membrane elements (in-plane)			
Mooney Rivlin	eq. (5.4)	C_{10} [MPa]	0.165
		C_{01} [MPa]	0.00524
Viscous cross model	eq. (5.4) [24]	η_0 [MPa $\cdot$ s]	0.682
		η_∞	0
		m [s$^{(1-n)}$]	3.45
		n	0.175
Elastic fibre model	[7, 39]	E_f [GPa]	1.0
Contact elements			
Hersey model	eq. (5.9)	g [m^{-q}]	402
		q [-]	0.517
		η [Pa $\cdot$ s]	85
Adhesion		Tension [MPa]	0.1
Penalty model		Penalty stiffness [N/mm^3]	1.0

Table 5.3 *Small, medium, and large parameter input for bending.*

Element type and models assigned	Parameter(s)	Input data low	initial	high
UD-C/PEEK				
DKTs (bending)				
Orthotropic Hooke	E_1 [MPa]	25	250	2500
	E_2 [MPa]	12.5	125	1250
	ν_{12} [-]	0.32	0.32	0.32
	G_{12} [MPa]	10	100	1000
8HS-G/PPS				
DKTs (bending)				
Isotropic Hooke	E [MPa]	12.5	125	1250
	ν [-]	0.33	0.33	0.33

Chapter 6

Discussion

This chapter broadens the discussions from the previous chapters with respect to the objectives of this research. The first part discusses the deformation mechanisms of the UD fibre reinforced laminate during forming. The second part discusses the predictive capabilities of the employed forming simulation strategy.

6.1 Deformations in UD fibre reinforced laminates

Combining the findings of the previous chapters allows us to further discuss and improve the understanding of the deformation behaviour of UD reinforced laminates during forming. This discussion is supported by experiments, which have not been addressed earlier in this thesis. The interaction of intra-ply shear, inter-ply slippage, and bending is considered first, followed by a discussion on the individual mechanisms.

6.1.1 The interaction of deformation mechanisms

Industry currently focuses on quasi-isotropic lay-ups since these combine reasonable bending and torsional properties in all loading directions. These lay-ups were therefore considered in chapters 2 and 5, however, some findings with cross-ply laminates help us to elaborate on the discussion from chapter 5 on the balance between the apparent in-plane and out-of-plane rigidity of the laminate.

Figure 6.1 shows the forming results of the doubly curved dome geometry that was considered in chapter 2. Contact of the laminate with the tooling was initiated in the centre of the dome, which is referred to as the drape front origin. The quasi-isotropic lay-up of $[0,90,45,-45]_S$ for the UD carbon/PEKK laminate (figure 6.1(a)) shows a wrinkle initiation front that is close to the centre of the product. For the cross-ply lay-up of $[0,90]_S$ in figure 6.1(c), the first wrinkle formed at a much larger distance

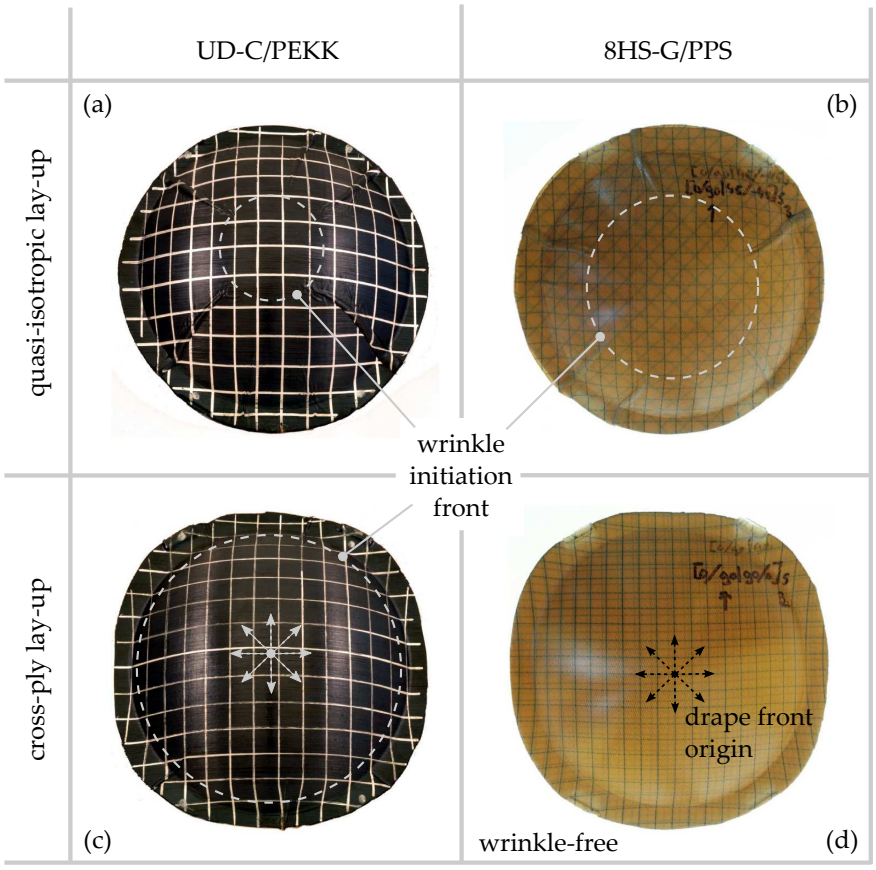

Figure 6.1 *Effects of lay-up and material on the wrinkling for a doubly curved dome geometry.*

from the centre. An almost wrinkle-free product was obtained. This demonstrates that a change in lay-up significantly affects the formability.

The formability of 8HS glass/PPS laminates with cross-ply $[(0/90),(90/0)]_S$ and quasi-isotropic $[(0/90),(45/-45)]_S$ laminates was investigated earlier by Ten Thije [1] for the doubly curved dome as well. The cross-ply lay-up in figure 6.1(d) shows no wrinkling at all. The quasi-isotropic 8HS-G/PPS laminate in figure 6.1(b) shows severe wrinkling, just as observed for the quasi-isotropic UD-C/PEKK laminate. However, when measured, the wrinkle initiation front is found to be at a larger distance from the centre compared to the UD-C/PEKK product, which results in higher shear angles in the wrinkle-free area. Also here, a change in lay-up significantly affects the formability of the 8HS-G/PPS material. Effects of lay-up were also demonstrated by Vanclooster *et al.* [2] for laminates comprising glass fibre reinforced polypropylene fabrics. Cross-ply laminates formed without wrinkles, while quasi-isotropic laminates showed severe wrinkling.

Figure 6.2 presents another overview of forming results for the wing stiffening rib from chapter 5. Compared to the forming results of the quasi-isotropic laminate in

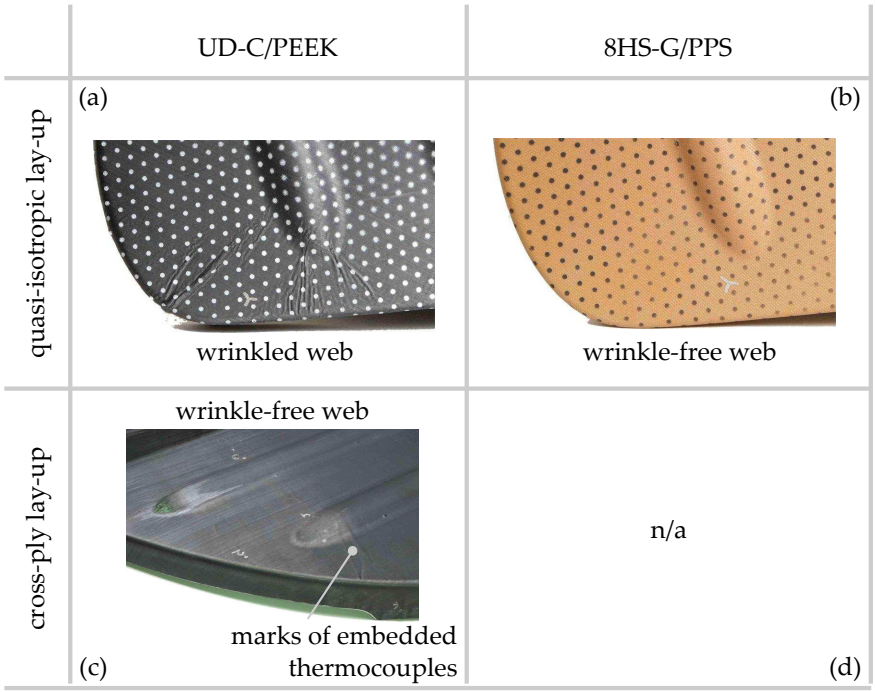

Figure 6.2 *Effects of lay-up and material on wrinkling for the wing stiffening rib.*

figure 6.2(a), the results of a UD-C/PEEK cross-ply lay-up in figure 6.2(c) showed no wrinkles in the web and far less wrinkles in the curved flange of the product. The 8HS-G/PPS quasi-isotropic laminate in figure 6.2(b) showed good formability for this product geometry.

When an initially flat laminate is formed to a doubly curved surface, its plies must deform in-plane and/or out-of-plane. Depending on the number of unique fibre orientations in the laminate, a balance between the apparent frictional (FR), intra-ply (IR), and bending rigidity (BR) of the plies determines the local deformation. This is illustrated in figure 6.3(a).

If only two unique fibre orientations are present in a laminate, solely inter-ply slip (in combination with strain perpendicular to the fibres) or intra-ply shearing is sufficient to achieve in-plane deformations. A trellis action without inter-ply slippage is likely to occur when the frictional rigidity is higher than the intra-ply rigidity. This situation is illustrated in figure 6.3(b). During forming, the resulting in-plane or out-of-plane deformation is then determined by the balance between the intra-ply (IR) and the bending (BR) rigidity.

If more than two fibre orientations are present (which is the case in quasi-isotropic lay-ups) and no out-of-plane deformations develop, the in-plane deformations of the plies are always accompanied by inter-ply slippage due to the inextensibility constraints in the fibre directions. This situation is illustrated in figure 6.3(c). During

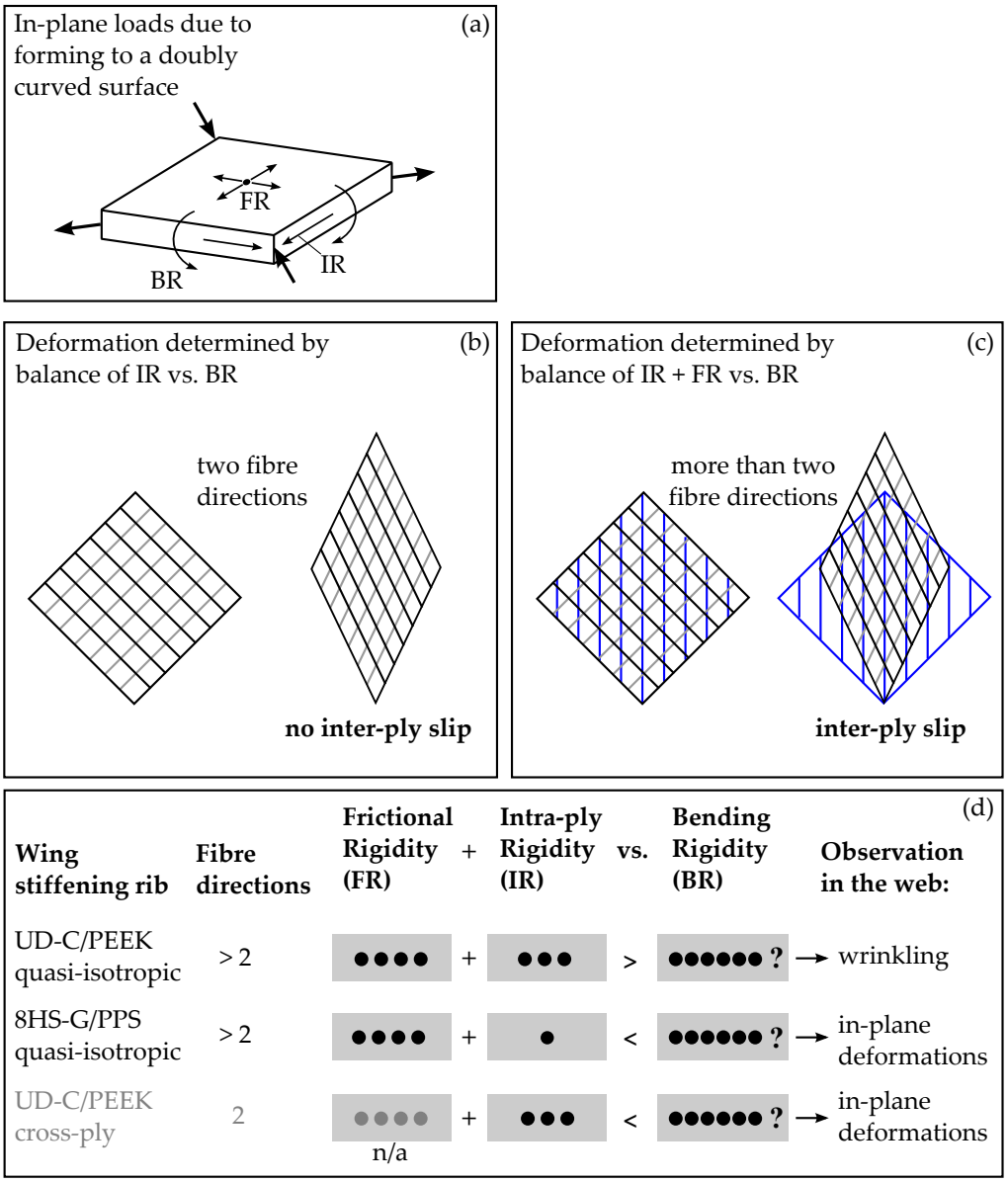

Figure 6.3 *Schematic explanation of the balance between the apparent intra-ply (IR), frictional (FR), and bending (BR) rigidity of the plies.*

forming, the resulting deformation is then determined by the balance between the apparent frictional (FR), intra-ply (IR), and the bending rigidity (BR).

An overview of the balances is given in figure 6.3(d), which was concluded from the forming results of the wing stiffening rib in figure 6.2. Figure 5.11 from chapter 5 showed similar friction characterisation data for the UD-C/PEEK and 8HS-G/PPS material, which is indicated in the FR column of figure 6.3(d). Figure 5.13 showed a relatively high intra-ply shear rigidity for the UD-C/PEEK material, compared to the 8HS-G/PPS material. This is indicated in the IR column of figure 6.3(d). Severe

wrinkling was observed for the quasi-isotropic UD-C/PEEK laminates in figure 6.2(a), which implies that local bending was favoured over in-plane deformations. This is explained by a relatively high apparent in-plane rigidity (FR+IR), compared to the apparent bending rigidity (BR). The quasi-isotropic 8HS-G/PPS laminates in figure 6.2(b) formed with no wrinkles in the web of the product, which implies that in-plane deformations are favoured over local bending. This in turn can be explained by a relatively low in-plane rigidity (FR+IR), compared to the apparent bending rigidity (BR) of the quasi-isotropic 8HS-G/PPS laminates.

The overview is extended with the forming results of the cross-ply UD-C/PEEK laminate from figure 6.2(c). The product shows no wrinkling and significant intra-ply shear in the web. These results can be explained by a low in-plane rigidity due to the absence of inter-ply slip when only two unique fibre orientations are present, as was schematically explained in figure 6.3(b).

Based on the considered products in this work (e.g. figures 1.5, 2.8 and 5.4), it is concluded that bending is favoured over in-plane deformations for UD carbon fibre reinforced laminates with a quasi-isotropic lay-up. This is further substantiated with the forming predictions in figure 6.4 of the wing stiffening rib from chapter 5. Local bending is favoured over intra-ply shear in the initial stages. Significant but small intra-ply shear in the web only develops in the final forming stage, when further bending and wrinkling are prohibited by the tooling. This situation was also illustrated earlier below in figure 2.9 from chapter 2.

6.1.2 Intra-ply shear

Small shear strains

The torsion bar method presented in chapter 3 was applied in chapter 4 to characterise the longitudinal intra-ply shear mechanism of the UD-C/PEEK material. Small strain characterisation data was obtained by applying oscillatory loads. The storage and loss moduli were weakly frequency dependent and a predominantly elastic response was measured as shown in figure 4.9(b). This behaviour corresponds to that of a visco-elastic solid or weak gel, which was shown to be completely different from the behaviour of the neat polymer characteristics in figure 4.12(a).

Steady shear responses in figure 4.18 were evaluated with the determined shear relaxation function. A close to elastic response was found for the considered range of shear rates. Nevertheless, the data shows a more pronounced visco-elastic response for decreasing shear rates. This can be explained with the Deborah number (De) [3], which is defined as the ratio between a characteristic relaxation time t_r of the material and the timescale of observation. Elastic effects dominate for high Deborah numbers (De $>>$ 1), whereas predominantly viscous responses show relatively low

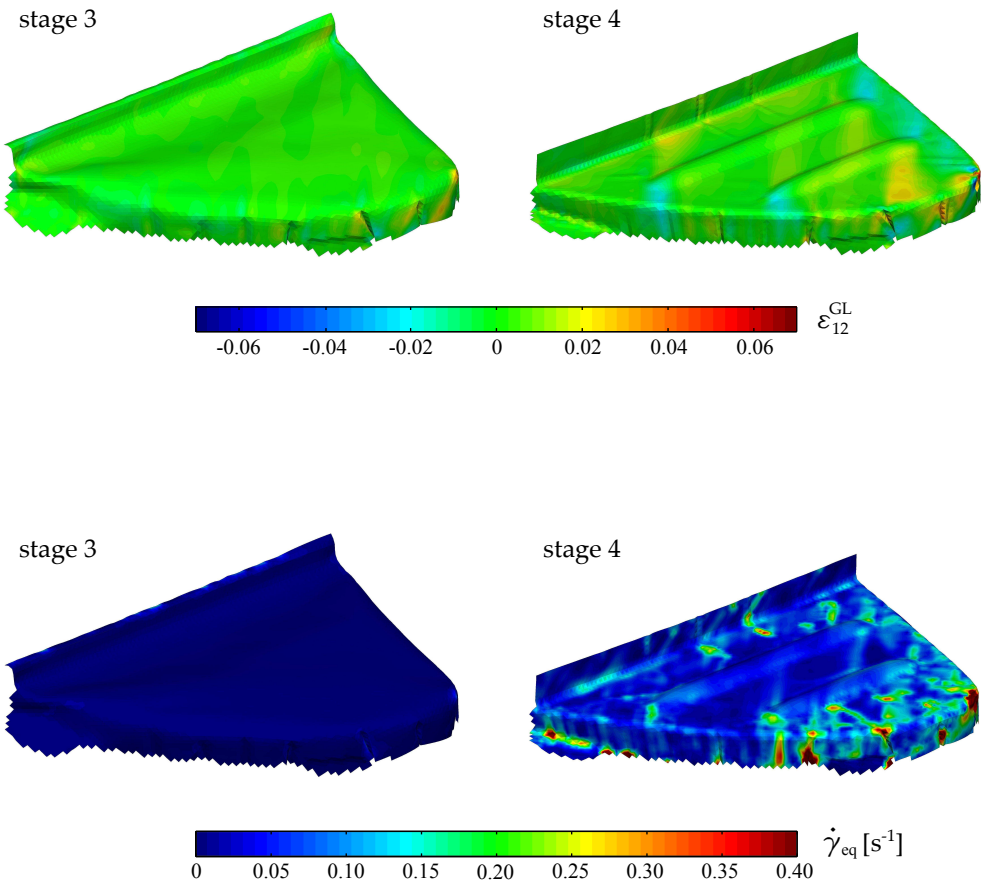

Figure 6.4 *Predicted intra-ply shear strains and rates (top ply) for the forming stages of the quasi-isotropic UD-C/PEEK laminate, which is formed into the wing stiffening rib geometry considered in chapter 5.*

De numbers (De $<<$ 1). The intermediate situation shows a pronounced visco-elastic response.

As was pointed out by Dealy [4], the determination of a characteristic relaxation time is not straightforward for visco-elastic materials exhibiting a spectrum of relaxation times, which is the case for the material characterised in chapter 4. Stress relaxation of a much simpler 1D Maxwell material after an instantaneously applied step of strain γ_{12}^0, is described with:

$$\tau_{12}(t) = \gamma_{12}^0 G e^{-t\frac{G}{\eta}} = \tau_{12}^0 e^{-\frac{t}{t_r}} \tag{6.1}$$

where G is the modulus of the elastic part, η the viscosity of the viscous part, and t_r the characteristic relaxation time. The initial stress τ_{12}^0 has decayed to τ_{12}^0/e when the time t during this relaxation equals the relaxation time t_r. A similar approach is

applied here to determine the characteristic relaxation time of UD-C/PEEK at small strains. With respect to the relaxation curve in figure 4.17, t_r is defined by:

$$\frac{G_r(t = t_r) - G_\infty}{G_r^0 - G_\infty} = 1/e \tag{6.2}$$

where G_∞ is the equilibrium modulus, and G_r^0 is here defined as the value of G_r corresponding to the measurement data at the smallest time available. This results a characteristic relaxation time of $t_r \approx 2$ s.

The timescale of observation is here considered as the inverse of the shear rate $\dot{\gamma}^{-1}$. To evaluate the De number by an example, the last step of the forming simulation with the wing stiffening rib geometry in figure 6.4 is considered. Regions with significant intra-ply shear are accompanied with equivalent shear rates $\dot{\gamma}_{eq}$ (as defined in equation 5.6) around 0.20 s^{-1}, which corresponds to a De($= \dot{\gamma} t_r$) number of 0.4. Although the experimental findings with this product matched well with the forming predictions, the relatively low De number indicates predominantly visco-elastic behaviour. Elastic shear behaviour was modelled with the two parameter Mooney-Rivlin model in chapter 5, however, Maxwell-type models would be more appropriate in this particular case to represent the visco-elastic behaviour. The assumed elastic behaviour, however, is more appropriate for geometries where larger shear strains (and thus higher shear rates and De numbers) are encountered in the laminates being formed.

The IFRM model

Conventionally, the IFRM model from equation (2.2) is used to model UD reinforced melts [5, 6]. It assumes the Newtonian viscosities η_L and η_T to describe the in-plane deformations. In the literature, intra-ply shear characterisation data is usually fitted to these viscosities in the large strain regime. This was, for example, performed by McGuinness and Ó Brádaigh [7], and Stanley and Mallon [8]. They used the picture-frame (figure 3.5(d)), and the translating plate-plate method (figure 3.5(e)), respectively. The linear viscous behaviour assumed by the IFRM model is generally not observed. Power-law viscosities are mostly used instead.

Nevertheless, the forming results in this thesis with quasi-isotropic UD-C/PEEK laminates show limited in-plane deformations. To predict the forming behaviour of such laminates therefore requires accurate characterisation data in the small strain regime. This was achieved for intra-ply shear in this work with the aid of the introduced torsion bar method. A predominantly elastic behaviour was measured, rather than the conventionally assumed viscous behaviour in the IFRM.

The selection of the appropriate model and characterisation data is currently based on the in-plane deformations expected: small or large intra-ply shear strains. Product

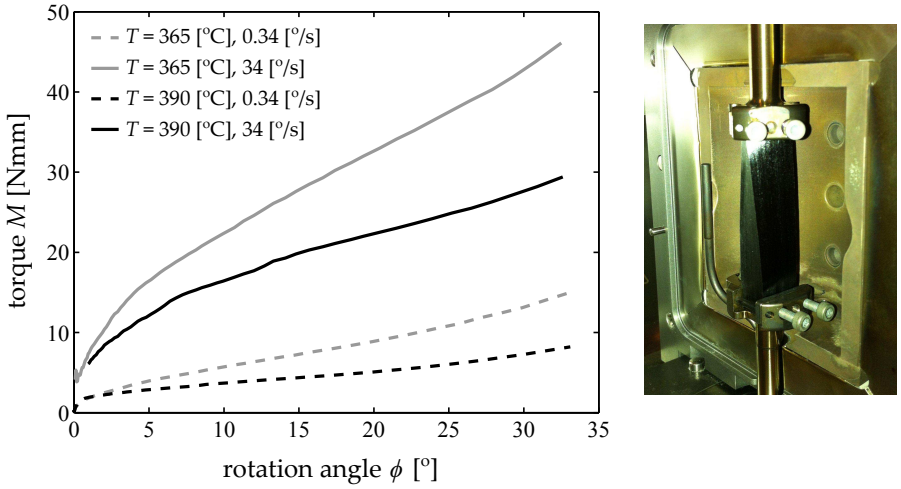

Figure 6.5 *Explorative large shear characterisation results: torsional responses as a function of rotation angle are shown for instantaneously applied constant rotation speeds.*

and process optimisation may ultimately lead to large intra-ply shear strains in wrinkle-free quasi-isotropic UD-C/PEEK products. Forming predictions that support the optimisation then require a model that describes the behaviour at both small and large deformations. Again, implementation of Maxwell-type models are expected to support this.

Large shear strains

Large intra-ply shear characterisation data is required to predict laminate deformation processes involving large intra-ply shear strains. Several methods from literature (tables 3.1 and 3.2) can be employed to obtain these data. The torsion bar method presented in this thesis shows potential to characterise the large strain regime as well, but requires further research. The torque can be measured while subjecting the specimen to an instantaneously applied constant rotation rate until a given maximum rotation angle has been reached. Figure 6.5 shows the measurements for two rotation rates and two temperatures, which were obtained for a torsion bar specimen of 11x13x61 mm. The shear strain and stress distribution within the cross section are yet unknown, because:

- The relations for shear strain in equations (3.20) and (3.21) were developed by assuming small displacements, which is not the case for the large rotations in figure 6.5.
- Fibre tensioning and bending effects are expected to affect the response in the large strain regime.

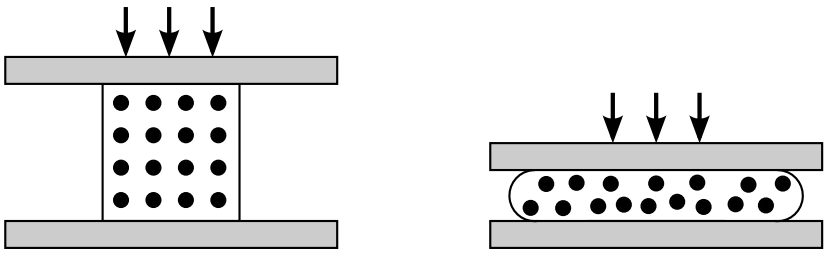

Figure 6.6 *Squeeze flow experiments to characterise transverse intra-ply shear.*

- A stress or strain distribution as illustrated in figure 3.7 for free torsion or torsion with restricted warping is different in the case of non-linear material properties. A correct stress-strain relationship can be established by applying parameter identification methods, by which the material property data are determined that lead to the best approximation of the measured torque/rotation response.

Nevertheless, an indication of the material behaviour can be deduced from the characteristics in figure 6.5. The responses are rate dependent and show yielding behaviour. The weak frequency dependency of small strain characterisation data is indeed known to indicate the presence of a yield stress when larger strains are applied [9], as was discussed earlier in chapter 4.

Transverse shear

The possibility to characterise the transverse shear mechanism with the torsion bar method was considered. This mechanism is invoked when the specimen contains fibres that are not aligned with the axis of rotation. A specimen with a fully $[90]_{80}$ lay-up is too fragile at high temperatures. This can be solved by adding axially aligned 0° plies. However, a complex combination of shear mechanisms will then develop, because the 0° plies invoke the longitudinal shearing mechanism, whereas the 90° plies invoke both the longitudinal and transverse shearing mechanisms. If the longitudinal material property is known, it should be possible to extract the transverse shearing mechanism. Several attempts were made to measure torsion bar responses with $[0_{20}, 90_{20}]_S$ and $[90_{20}, 0_{20}]_S$ lay-ups. However, deconsolidation effects in the thickness direction caused specimen splitting at the 0-90 interfaces, which make the results difficult to interpret.

Characterisation methods that invoke solely the transverse shear mechanism are favoured due to the more straightforward analyses of the deformations. Translating plate-plate set-ups [8, 10, 11] are able to do this (figure 3.5(b,c,e)). However, loads

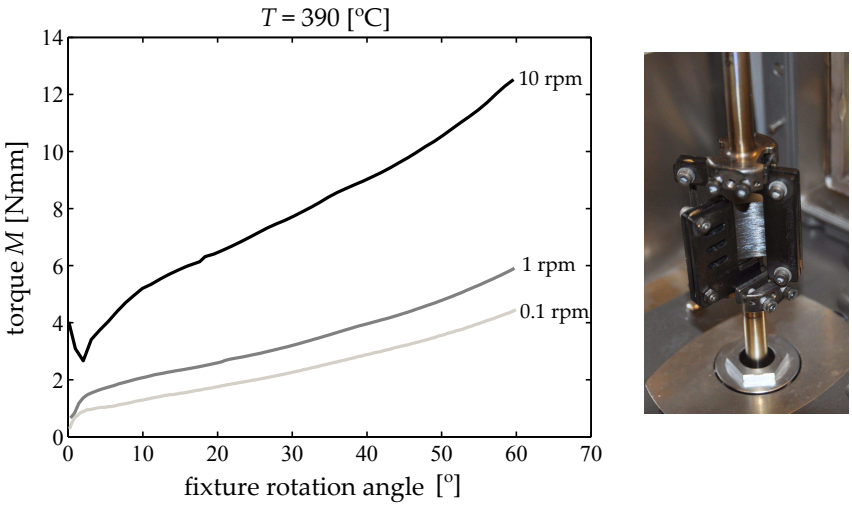

Figure 6.7 *Explorative bending fixtures positioned in a standard rheometer.*

are introduced parallel to the specimen surfaces via tractions, which make them vulnerable to concentrated deformation at the resin-rich interfaces. Another option is to conduct squeeze flow experiments as shown in figure 6.6 [12, 13], which introduce loads perpendicular to the fixture-specimen interfaces. The transverse shear characterisation data presented so far for carbon fibre reinforced PEEK [14, 15] are comparable to the longitudinal shear characterisation data in terms of trends and magnitudes.

6.1.3 Bending and friction

Chapters 2 and 5 showed the laminate/ply bending properties to have a significant effect on the forming predictions. For this reason, more research must be dedicated to the characterisation of this mechanism. Most bending characterisation data available is based on quasi-static free-deflection experiments, which is, for example, shown by Larberg [16] for UD reinforced epoxy pre-pregs. A larger variety of test conditions can be investigated with the novel set-up (figure 6.7) developed recently by Ten Hove [17], where a custom-made bending fixture is positioned in a standard rheometer. The test is based on the Kawabata Evaluation System for Fabric Bending (KES-FB) [18].

Explorative tests are currently conducted with this new set-up, for which some preliminary results [17] at one temperature are shown in figure 6.7. A specimen was cut from a pre-consolidated UD-C/PEEK laminate with a $[0]_8$ lay-up and positioned in the fixtures. The responses to an instantaneously applied rotation of the upper fixture are shown for three rotation speeds. A stiff response is observed initially, but decreases rapidly for larger deformations. Just as for the explorative large strain intra-ply shear tests in section 6.1.2, the curves indicate the presence of yielding.

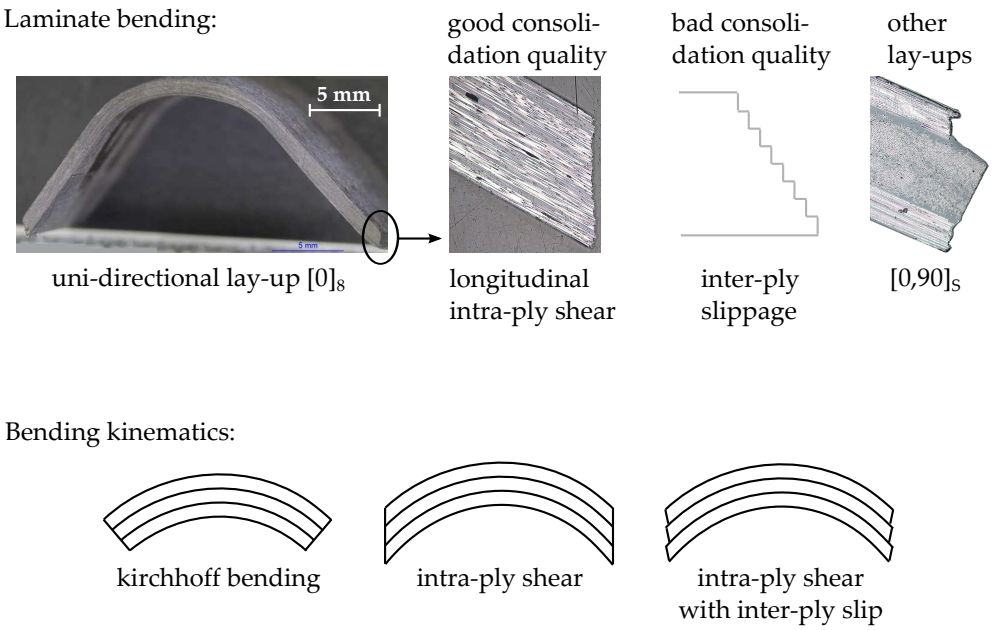

Figure 6.8 *Preliminary results of laminate bending tests.*

Figure 6.8 shows the typical shape of a bent specimen. A close-up of the edge shows the developed continuous intra-ply shear field. However, it was shown elsewhere [19] that these through-the-thickness shear deformations highly depend on the consolidation quality of the laminate. Moreover, the deformation will differ for other than uni-directional lay-ups as shown by Scherer and Friedrich [20]. This has also been observed in a bent cross-ply $[0,90]_S$ specimen, which was obtained by preliminary experiments with the bending test set-up from figure 6.7.

It can be concluded from this discussion that the deformation in a bent laminate with differently oriented plies and high modulus fibres, consists of a combination of intra-ply shear (through-the-thickness) with inter-ply slip. This implies that the characterisation results of these individual mechanisms can be combined to describe the bending behaviour (by neglecting the bending stiffness of the carbon fibres), or vice versa. The friction data in figure 5.11 is, however, obtained by applying a normal pressure to the interface to be characterised. In fact, the bending test can be employed to conduct a pressureless friction experiment.

6.1.4 Concluding remarks

Not only the forming prediction sensitivity study from chapter 2, but also the discussion on the forming of cross-ply and quasi-isotropic UD laminates in this chapter explains that the formability is determined by a delicate balance between

intra-ply shear, inter-ply slip, and bending. The balance is in favour of bending for the conventional forming process of quasi-isotropic UD laminates, based on the work presented in this thesis. Simulations with the wing stiffening rib have shown that intra-ply shearing develops when further bending and wrinkling are prohibited.

Large intra-ply shear strains are encountered when cross-ply laminates are formed, but may also develop in quasi-isotropic laminates when blank holder and/or tensioning systems are used (for product optimisation). The material behaviour at larger strains is different from the behaviour at small strains. The small strain intra-ply shear characterisation data indicates yielding behaviour at larger strains, which was further substantiated by indicative large strain experiments presented in this chapter. Other preliminary experiments show that bending of UD reinforced laminates involves a combination of intra-ply shear (though-the-thickness) and inter-ply slip.

6.2 Predictive capabilities with the current simulation strategy

Chapters 2 and 5 have shown the application and validation of the employed forming simulation strategy for two product geometries. A more general application of forming predictions for product optimisation is discussed here. Limited simulation times are desired to conduct efficient optimisation procedures. Simulation times are directly related to simulation quality, which is addressed firstly. Secondly, it is shown in what perspective simulation tools can be employed to seek the optimum product.

6.2.1 Simulation quality

The forming predictions presented in chapters 2 and 5 showed the development of the large wrinkles observed in practice for the dome and the wing stiffening rib. The smaller wrinkles observed near the beads of the wing stiffening rib in figure 5.4 cannot be accurately represented with the element size used. The waviness observed in the mesh could at least indicate critical spots within the product.

Mesh refinements need to be applied to give the possibility of predicting small wrinkles, which would supply the design engineer with more decisive information about wrinkle development. Mesh refinement strategies are hindered due to the restrictions that arise from the highly anisotropic nature of the material. Shear locking problems develop when the element edges within the meshed plies are not aligned with the stiff fibres [21]. The model is therefore limited to the use of a regularly structured grid of elements, which implies that local refinement is not feasible.

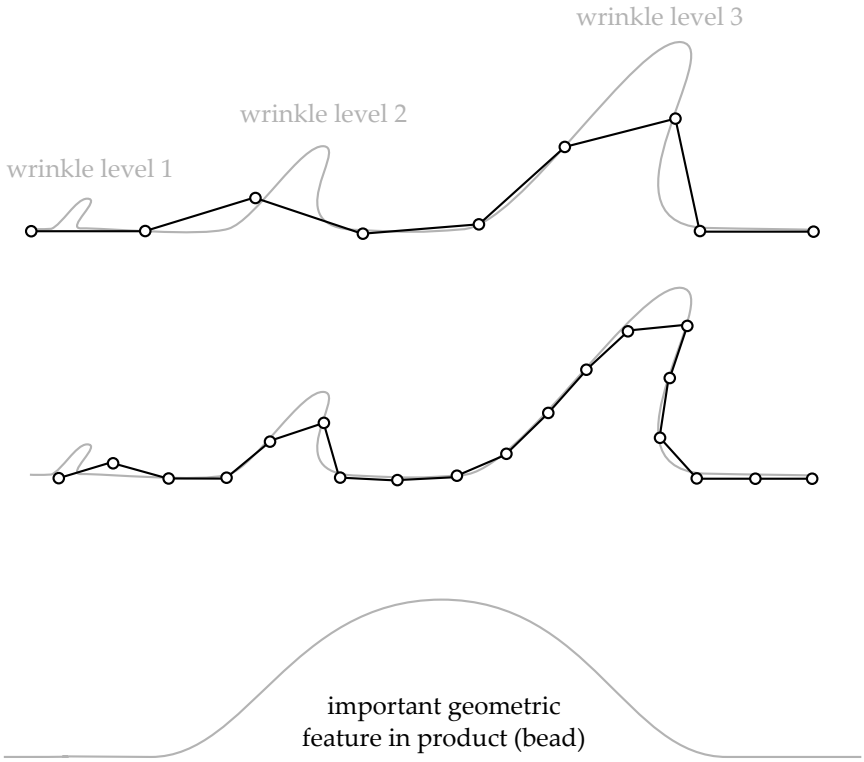

Figure 6.9 *Element size versus geometric feature size.*

Global mesh refinement leads to a rapid increase of the number of elements and the associated CPU time for a simulation.

The element size to be used is based on the important product features and the minimum wrinkle size to be involved in the analysis. This is schematically explained in figure 6.9. Wrinkles develop at different scales with respect to the size of the important product features, for example, one of the beads in figure 5.2. A relatively coarse mesh can be used to predict the wrinkle at level 3, whereas this element size could indicate the wrinkle at level 2. More elements are needed to predict the wrinkle at level 1. Then the size of the system to be solved increases rapidly, such that impractical calculation times develop, especially when all plies of a laminate are modelled. For example, one forming predictions in chapter 5 required a calculation time of 40 to 160 hours on a computer with two quad-core Intel Xeon E5620 2.4 GHz processors. Usually, an indication of the position and size of the wrinkles is sufficient, rather than predicting the wrinkle geometry in detail. Nevertheless, the product designer must be aware of the fact that defects at all scales can hardly be predicted with this forming prediction strategy.

The development of a critical stress state indicator [22] might help to circumvent the

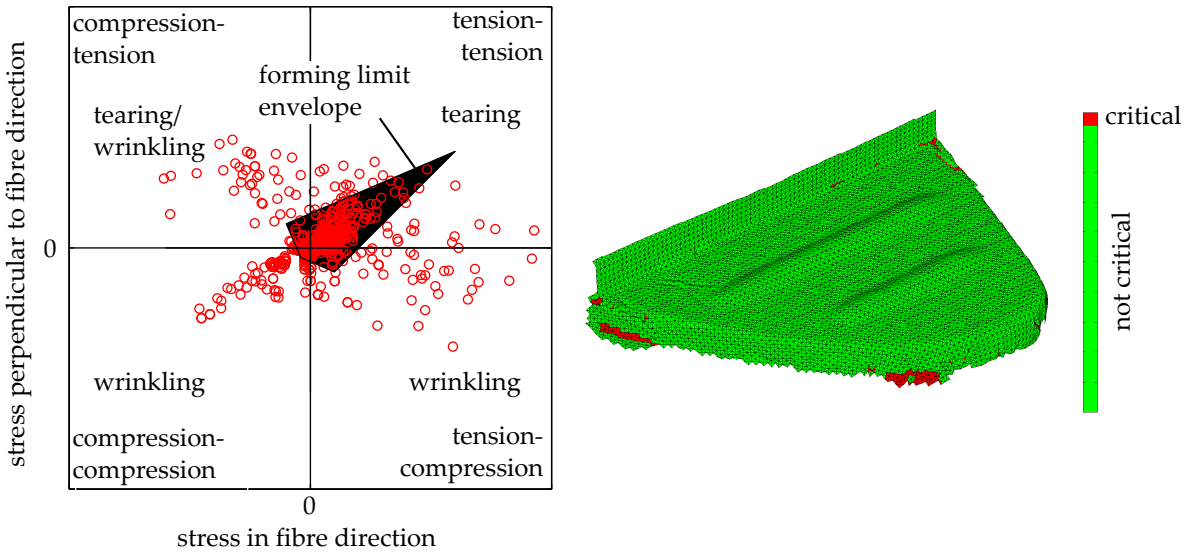

Figure 6.10 *Conceptual representation of a stress indicator.*

element size limitations. A critical region in the ply or blank is then indicated when its state of stress is outside a forming limit envelope, as illustrated in figure 6.10. For example, ply-splitting or tearing can be expected if a tensile stress perpendicular to the fibre direction exceeds a critical value. Wrinkling is expected when a critical compressive stress develops. Such an approach does not necessarily require the wrinkles themselves to be simulated.

The use of multi-layer elements is another possibility of increasing the detail in the model, while acceptable computational times can still be achieved. Instead of modelling a piece of the ply with a DKT, a membrane, and two contact elements, all plies in the thickness direction are described by one element. In that case, a single 2D mesh represents the laminate to be formed. A multi-layer element was developed by Ten Thije and Akkerman [23] for this purpose. Again, intra-ply shear locking problems arise when multiple fibre orientations are involved. The key in solving these issues is the development of an element for which this locking problem is circumvented. This is currently being investigated by Wolthuizen *et al.* [24].

6.2.2 Application of simulations

As explained in figure 1.6, forming simulation tools are intended to facilitate the detailed design phase in the product development process. Within this phase, the product design optimisation addresses the aspects of product geometry design, material configuration or selection, and the production process iteratively, as illustrated in figure 6.11. As an example, the forming speed is a production process

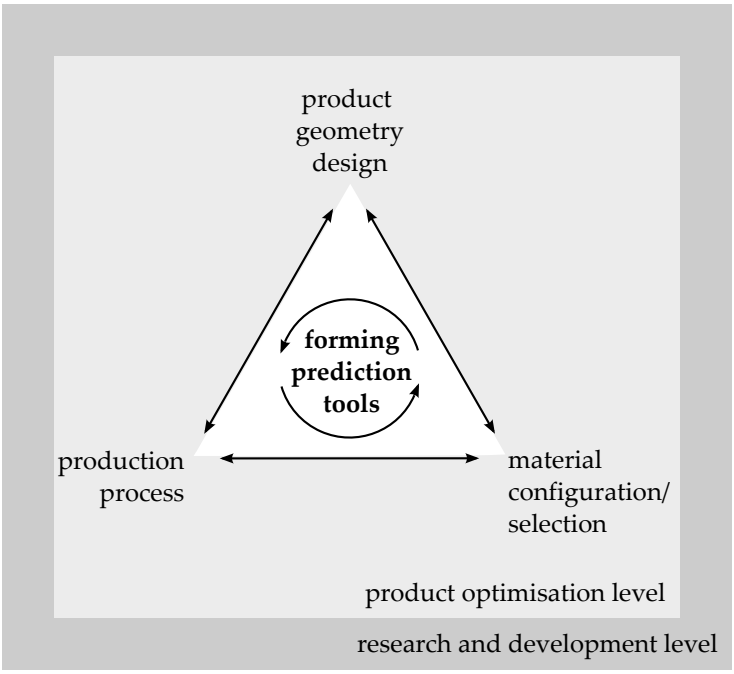

Figure 6.11 *Interrelations between the product design, material, and production process aspects: at the product engineering and the R&D level.*

setting, which may affect the material behaviour. The combination of the forming speed and the material response determines the formability of a laminate with respect to the product geometry. If formability issues are encountered, the process settings, the material, or the product geometry can be modified to obtain the optimised product. However, the modification may in turn lead to other issues as the aspects are usually interrelated. The forming simulation strategy as presented in chapters 2 and 5 can be employed to optimise the three aspects in figure 6.11 virtually, ultimately leading to cost reductions. Regarding these aspects, a distinction is made at the product design level and the research and development level.

Product optimisation

Wrinkle-free forming of UD-C/PEEK laminates with respect to products having double curvature is not straightforward. Several possibilities for optimisation are outlined in figure 6.12 with respect to the aspects in figure 6.11.

The simulation tool can be employed to study the effects of product geometry and blank design on the formability, thereby circumventing the costly tool and blank manufacturing. These are important variables as was, for example, shown by Hou [25] for circular blanks with various radii, which were formed into a dome geometry. The wrinkle development was shown to be highly dependent on the ratio between the initial blank area and the fraction of this area formed to the doubly curved surface.

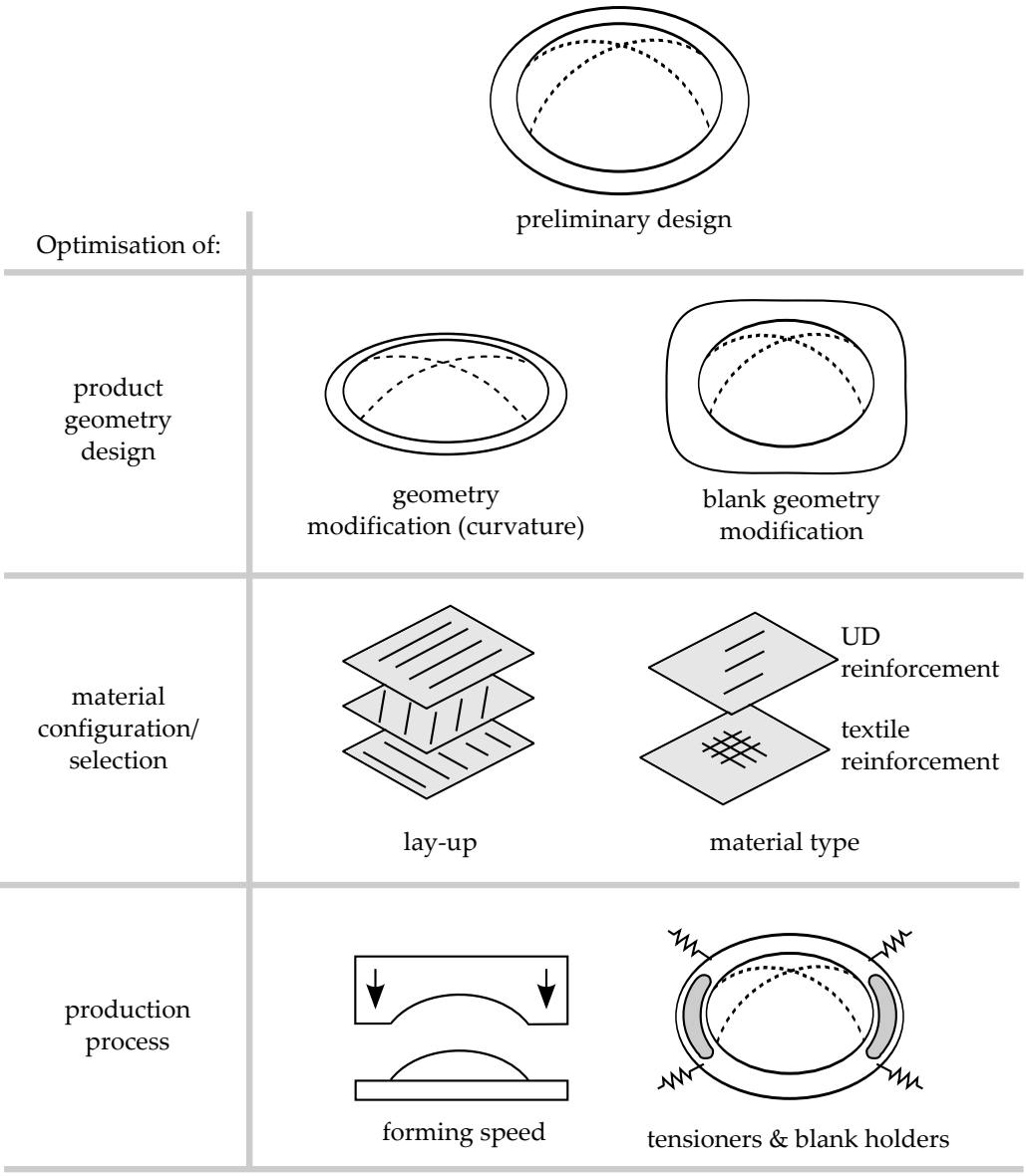

Figure 6.12 *Several ways to optimise the product design with respect to formability.*

Regarding the material aspects, effects of ply stacking can be studied as well. As shown in practice, cross-ply UD-C/PEEK laminates show significantly different forming behaviour than quasi-isotropic laminates. However, the mechanical properties of the formed part are determined by the lay-up, which means that an optimum with respect to formability and mechanical performance must be established. If the quality or the mechanical performance of the press-formed UD-C/PEEK product does not meet the requirements, the selection of another type of material (such as a textile reinforced thermoplastic) can be evaluated virtually.

Finally, the simulation tool can be utilised to study the effects of process variables and the use of external tooling such as blank holders and tensioners. Blank holders as in figure 6.12 are often applied in the sheet-metal forming industry, and are gradually being applied in the composite sheet forming area [26, 27].

Research and development

The forming simulation strategy can also be utilised at the research and development level. It is able to support the material design process, as explained by the following example. Both the intra-ply shear and frictional properties of the UD-C/PEEK material seem to behave rigidly. As concluded from previous sections, both mechanisms deal with a yield stress value, which must be exceeded before large deformations develop. It is generally known that yield stress values decrease with a decreasing concentration of particles [9]. One could, for example, lower the fibre volume fraction v_f within the UD-C/PEEK pre-preg to achieve a lower rigidity of the deformation mechanisms. The addition of resin-rich layers or films to the ply-ply interfaces is another interesting modification. It is expected to decrease the inter-ply friction, which contributes to better laminate formability as well. The effects of such material modifications can be studied virtually again.

The prediction tools are of great value to evaluate ideas for alternative process steps, prior to investing in expensive tailor-made equipment. As an example, the good formability of cross-ply laminates can be exploited in a multi-step forming process. As a first step, cross-ply parts having different orientations with respect to the final product can be manufactured initially, after which the separate parts can be fused together in a second consolidation step.

Tape-placement techniques can be utilised to manufacture tailored blanks, as for example shown in figure 1.4. Better formability characteristics can be achieved by virtually optimising the fibre paths. Tape-placing [28] near net-shaped products is another option to circumvent large deformations during forming, for which we again address the added value of forming prediction tools.

Design guideline development is the last example where virtual tools facilitate. Simulations allow for a relatively quick and low cost systematic evaluation of basic product features, such as beads and curved flanges. Characteristic dimensions of the geometric features can be altered to study their effect on the formability, from which design guidelines can be derived. Guidelines support the earlier design phases, which was schematically illustrated in figure 1.6.

6.2.3 Concluding remarks

The simulation strategy can be employed to optimise a product and to derive design guidelines by studying the virtual modifications of product geometry, material, and

production process. The product design engineer must determine a trade-off between simulation calculation time and simulation quality, which are both related to the number of elements used. The mesh must be tailored to the minimum wrinkle size to be represented, the important geometry features to be involved, and the aimed simulation times. An efficient optimisation procedure ideally involves short simulation times and sufficient simulation quality, which supports the development of multi-layer elements and stress or strain state indicators.

References

[1] R.H.W. ten Thije. Finite element simulations of laminated composite forming processes. Ph.D. thesis, University of Twente, 2007.

[2] K. Vanclooster, S. V. Lomov, and I. Verpoest. On the formability of multi-layered fabric composites. In ICCM International Conferences on Composite Materials, 2009.

[3] M. Reiner. The Deborah number. *Physics Today*, **17**(1):62, 1964.

[4] J.M. Dealy. Weissenberg and Deborah numbers - their definition and use. *Rheology Bulletin*, **79**(2):14–18, 2010.

[5] A.K. Pickett, T. Queckbörner, P. De Luca, and E. Haug. An explicit finite element solution for the forming prediction of continuous fibre-reinforced thermoplastic sheets. *Composites Manufacturing*, **6**(3-4):237–243, 1995.

[6] P. De Luca, P. Lefébure, and A.K. Pickett. Numerical and experimental investigation of some press forming parameters of two fibre reinforced thermoplastics: APC2-AS4 and PEI-CETEX. *Composites Part A: Applied Science and Manufacturing*, **29**(1-2):101–110, 1998.

[7] G.B. McGuinness and C.M. Ó Brádaigh. Characterisation of thermoplastic composite melts in rhombus-shear: The picture-frame experiment. *Composites Part A: Applied Science and Manufacturing*, **29**(1-2):115–132, 1998.

[8] W.F. Stanley and P.J. Mallon. Intraply shear characterisation of a fibre reinforced thermoplastic composite. *Composites Part A: Applied Science and Manufacturing*, **37**:939–948, 2006.

[9] Q.D. Nguyen and D.V. Boger. Measuring the flow properties of yield stress fluids. *Annual Review of Fluid Mechanics*, **24**(1):47–88, 1992.

[10] A.B. Wheeler and R.S. Jones. A characterization of anisotropic shear flow in continuous fibre composite materials. *Composites Manufacturing*, **2**(3-4):192–196, 1991.

[11] R.S. Jones and R.W. Roberts. Anisotropic shear flow in continuous fibre composites. *Composites*, **25**(3):171–176, 1994.

[12] S.F. Shuler and S.G. Advani. Transverse squeeze flow of concentrated aligned fibers in viscous fluids. *Journal of Non-Newtonian Fluid Mechanics*, **65**(1):47–74, 1996.

[13] P. Harrison, T. Haylock, and A.C. Long. Measurement of the transverse and longitudinal viscosities of continuous fibre reinforced composites. In The 8th International ESAFORM Conference on Material Forming, 2005.

[14] J.J. Scobbo Jr. and N. Nakajima. Dynamic mechanical analysis of molten thermoplastic/continuous graphite fiber composites in simple shear deformation. In National SAMPE Technical Conference, volume 21, 730–743, 1989.

[15] D.J. Groves, A.M. Bellamy, and D.M. Stocks. Anisotropic rheology of continuous fibre thermoplastic composites. *Composites*, **23**(2):75–80, 1992.

[16] Y.R. Larberg. Forming of Stacked Unidirectional Prepreg Materials. Ph.D. thesis, KTH Engineering Sciences, 2012.

[17] C.H. ten Hove. Bending of CF/PEEK prepregs. Master's thesis, University of Twente, 2012.

[18] S. Kawabata. The standardization and analysis of hand evaluation. The Textile Machinery Society of Japan, Osaka, 2nd edition, 1986.

[19] S.G. Advani, T.S. Creasy, and S.F. Shuler. Composite Sheet Forming, volume 11 of *Composite Materials Series*. Elsevier Science B.V., 1997.

[20] R. Scherer and K. Friedrich. Inter- and intraply-slip flow processes during thermoforming of cf/pp-laminates. *Composites Manufacturing*, **2**(2):92–96, 1991.

[21] R.H.W. ten Thije and R. Akkerman. Solutions to intra-ply shear locking in finite element analyses of fibre reinforced materials. *Composites Part A: Applied Science and Manufacturing*, **39**(7):1167–1176, 2008.

[22] R.B. Dessenberger and C.L. Tucker. Ideal forming analysis for random fiber preforms. *Journal of Manufacturing Science and Engineering, Transactions of the ASME*, **125**(1):146–153, 2003.

[23] R.H.W. ten Thije and R. Akkerman. A multi-layer triangular membrane finite element for the forming simulation of laminated composites. *Composites Part A: Applied Science and Manufacturing*, **40**(6-7):739–753, 2009.

[24] D.J. Wolthuizen, R.H.W. ten Thije, and R. Akkerman. Simple tests as critical indicator of intra-ply shear locking. In the 16th International ESAFORM Conference on Material Forming, 2013.

[25] M. Hou. Stamp forming of continuous glass fibre reinforced polypropylene. *Composites Part A: Applied Science and Manufacturing*, **28**(8):695–702, 1997.

[26] M. Hazeleger. Vezelversterkte kunststoffen: Onderzoek naar het gedrag van vezels bij het draperen in een mal. Master's thesis, Saxion Hogescholen, Opleiding Werktuigbouwkunde, 2006.

[27] J. Sargent, J. Chen, J. Sherwood, J. Cao, P. Boisse, A. Willem, K. Vanclooster, S.V. Lomov, M. Khan, T. Mabrouki, K. Fetfatsidis, and D. Jauffrés. Benchmark study of finite element models for simulating the thermostamping of woven-fabric reinforced composites. *International Journal of Material Forming*, **3**:683–686, 2010.

[28] J. Schlimbach and P. Mitschang. Process-based cycle time estimation for the thermoplastic tape placement. *Journal of Thermoplastic Composite Materials*, **19**(5):507–529, 2006.

Chapter 7

Conclusions and Recommendations

The forming behaviour of UD carbon fibre reinforced thermoplastic laminates in melt condition was investigated. The results of this research contribute to a better understanding of the deformation behaviour and the formability issues encountered in practice. The predictive capabilities of a forming simulation strategy have been assessed as well. The major conclusions and recommendations from these achievements are summarised in this chapter.

7.1 Conclusions

The major conclusions of this work with respect to the objectives of this thesis are presented below.

Deformation behaviour

1. The stamp forming process of an initially flat laminate to a geometry with double curvature involves both in-plane deformations (intra-ply shear and/or inter-ply slip) and bending. The formability of laminates with a UD carbon fibre reinforcement is determined by a delicate balance between intra-ply shear, inter-ply slippage and ply/laminate bending.

2. This balance is in favour of bending for quasi-isotropic laminates, assuming the absence of blank holder and tensioning systems. Simulations show that in-plane deformations only occur in the final stages of forming, where further bending and wrinkling are prohibited.

3. Small strain experiments with the developed torsion bar method showed the initial response of UD carbon fibre reinforced PEEK (UD-C/PEEK) to be predominantly elastic, instead of the usually assumed linear viscous

(Newtonian) behaviour. This is explained by multiple fibre-fibre interactions. The response in the small strain regime is hardly affected by the temperature.

4. The shear moduli of the UD-C/PEEK material show a weak frequency dependency and decrease rapidly for increasing strain amplitudes. Both characteristics indicate yielding behaviour at larger deformations, which was further substantiated by preliminary large strain experiments.

5. The high sensitivity to wrinkling of the UD-C/PEEK material is explained by the relatively high resistance to intra-ply shear and inter-ply slip.

Predictive capabilities

1. Finite element forming simulations have proven to be instrumental in obtaining a better understanding of the laminate deformations during the stamp forming process.

2. The laminate deformations and defects such as wrinkles can be predicted with the employed simulation strategy, of course provided the constitutive models and material property data are properly representing the material considered.

3. The size of the wrinkles that can be accurately predicted is limited by the size of the elements used.

4. The simulations can be used for product optimisation, as well as to derive design guidelines in a more general sense. In addition, simulations can be used to optimise process settings and to support material design for this specific forming process.

7.2 Recommendations

The presented work has led to recommendations for further research on the forming of UD fibre reinforced thermoplastics. These are listed below, again with respect to the objectives of this thesis.

Deformation behaviour

1. Extend the deformations during characterisation to the large strain regime.

2. Validate and where possible improve the developed torsion bar characterisation test by round-robin benchmarking.

3. Improve characterisation of other deformation mechanisms at forming temperatures, in particular of bending and delamination.

Predictive capabilities

1. Simulation calculation times need to be reduced. Simulation of thicker laminates with many plies require the development of a robust multi-layer element with a minimum number degrees of freedom.

2. The prediction of defects smaller than the element size requires the development of one or more indicators, based on the element stress or strain state.

Nomenclature

Abbreviations

ANOVA	analysis of variance
BR	bending rigidity
CFRP	continuous fibre reinforced polymer
CPSD algorithm	cross power spectral density algorithm
DKT	discrete Kirchhoff triangle
DoE	design of experiments
FFT	fast Fourier transform
FR	frictional rigidity
IFRM	ideal fibre reinforced Newtonian fluid model
IR	intra-ply rigidity
LVE theory	linear visco-elasticity theory
PA	polyamide
PEEK	polyetheretherketone
PEKK	polyetherketoneketone
PP	polypropylene
PPS	polyphenylenesulfide
TPRC	ThermoPlastic composite Research Center
UD	uni-directional
UD-C/PEEK	PEEK with a UD carbon fibre reinforcement
8HS-G/PPS	PPS with a woven 8HS glass fibre reinforcement

Scalars

A	area	[m^2]
A_B	total blank area	[m^2]
a, b, c, d	constants	
C_{01}, C_{10}	Mooney-Rivlin parameters	[Pa]
De	Deborah number	
e	e-number (irrational)	
E, E_i	elasticity modulus	[Pa]

E_f	fibre modulus	[Pa]
E_p	penalty stiffness	[N/mm^3]
F	force	[N]
F_n	normal load	[N]
F_p	pulling load	[N]
F_0	F-statistic	
Fd	fibre dominance number	
g	constant for fitting friction data	[m^{-q}]
G, G_{ij}	elastic shear modulus	[Pa]
G^*, G^*_{ij}	complex shear modulus	[Pa]
G'	storage shear modulus	[Pa]
G''	loss shear modulus	[Pa]
G_r	shear relaxation modulus	[Pa]
G_∞	equilibrium modulus	[Pa]
h	fluid film thickness	[m]
h	thickness of torsion bar specimen	[m]
$\tilde{h}$	expanded thickness of torsion bar specimen	[m]
H	specimen dimension	[m]
He	Hersey number	
i	indicates an imaginary number	
J	torsional constant	[m^4]
J_p	polar moment of inertia	[m^4]
K^E	element tool-blank mismatch	[1/m]
K_i	local tool-blank mismatch	[1/m]
l	fibre length	[m]
L	free specimen length	[m]
$\tilde{L}$	total specimen length	[m]
M	torque	[Nm]
M, N	a total number	
m	constant for Cross viscosity model	[s^{1-n}]
n	power-law viscosity exponent	
p	hydrostatic pressure	[Pa]
p	p-value	
q	constant for fitting friction data	[-]
R	radius	[m]
R^2	R^2-value	
R^2_adj	adjusted R^2-value	
s	time	[s]
t	time	[s]
t_r	relaxation time	[s]
T	fibre tension	[Pa]

T	temperature	[°C]
u, u_{ij}	displacement	[m]
v	velocity	[m/s]
v_f	fibre volume fraction	
v_s	slip/sliding velocity	[m/s]
w	width of torsion bar specimen	[m]
$\tilde{w}$	expanded width of torsion bar specimen	[m]
W	specimen dimension	[m]
x, y, z	Cartesian coordinates	[m]
α	significance level	
β_i, β_{ij}	regression coefficient	[1/m]
$\hat{\beta}_i$, $\hat{\beta}_{ij}$	approximated regression coefficient	[1/m]
β_{ij}	reciprocal viscosity	$[(\mathrm{Pa}\cdot\mathrm{s})^{-1}]$
γ, γ_{ij}	shear strain	
$\dot{\gamma}$, $\dot{\gamma}_{ij}$	shear rate	[1/s]
$\dot{\gamma}_\mathrm{eq}$	equivalent shear rate	[1/s]
δ	penetration depth	[m]
δ	phase angle	[rad]
ϵ	random error	
$\varepsilon_{ij}^\mathrm{GL}$	component of Green-Lagrange strain tensor $\boldsymbol{E}$	[1/s]
$\dot{\varepsilon}_{ii}$	extensional strain rate	[1/s]
η, η_{ij}	viscosity	$[\mathrm{Pa}\cdot\mathrm{s}]$
η'	dynamic viscosity	$[\mathrm{Pa}\cdot\mathrm{s}]$
η''	out-of-phase viscosity	$[\mathrm{Pa}\cdot\mathrm{s}]$
η_0, η_∞	viscosity values for Cross model	$[\mathrm{Pa}\cdot\mathrm{s}]$
θ_{ij}	rotation	[rad]
κ	curvature	[1/m]
κ_I, κ_II	first and second principle curvature	[1/m]
κ_MM	modified mean curvature	[1/m]
$\kappa_\mathrm{MM,B}$	modified mean curvature at the blank	[1/m]
$\kappa_\mathrm{MM,T}$	modified mean curvature at the tool	[1/m]
μ	friction coefficient	
ν_{ij}	Poisson's ratio	
ξ	global tool-blank mismatch	[1/m]
ρ	density	$[\mathrm{kg/m^3}]$
σ_{ij}	stress	[Pa]
τ_{ij}	stress	[Pa]
τ_n	normal pressure at contact surface	[Pa]
τ_tr	in-plane surface traction	[Pa]
ϕ	rotation angle	[rad]

φ	specific rotation angle	[rad/m]
$\dot{\varphi}$	specific rotation speed	[rad/(m · s)]
χ_i	DoE design variable	
ω	angular frequency	[rad/s]

Vectors

$\boldsymbol{a}$, $\boldsymbol{b}$	directions of fibre families a and b	[m]
$\hat{\boldsymbol{a}}$, $\hat{\boldsymbol{b}}$	unit vectors representing fibre family a and b	
$\boldsymbol{v}$	velocity	[m/s]
$\boldsymbol{x}$	spatial position	[m]
$\boldsymbol{X}$	reference position	[m]

Second order tensors

$\boldsymbol{B}$	left Cauchy-Green strain tensor	
$\boldsymbol{C}$	right Cauchy-Green strain tensor	
$\boldsymbol{D}$	rate of deformation tensor	
$\boldsymbol{E}$	Green-Lagrange strain tensor	
$\boldsymbol{F}$	deformation gradient	
$\boldsymbol{I}$	identity tensor	
$\boldsymbol{L}$	velocity gradient	[1/s]
$\boldsymbol{W}$	spin tensor	[1/s]
$\boldsymbol{\sigma}$	Cauchy stress	[Pa]
$\boldsymbol{\tau}$	extra stress tensor	[Pa]

Subscripts

0	initial value
0	amplitude value
i, ij with $i, j = 1, 2, 3$	indicating the component of a quantity
i, j, m	indicating the i^{th}, j^{th}, or m^{th} component from a collection of components
a	denoting fibre direction a
b	denoting fibre direction b
E	denoting elastic part
L	longitudinal/axial
S	symmetric
T	transverse
V	denoting viscous part

Superscripts

-1	inverse
0	amplitude value
i, j	indicating i^{th} and j^{th} component from a collection of components
T	transposed
$*$	denoting a complex variable

Mathematical

(default)	dyadic product
$\cdot$	single contraction
:	double contraction

Nawoord

Zondag, 3 maart 2013

Nu is daar het moment om achterover te leunen, waarvan ik had gehoopt dit buiten met een lekker zonnetje te kunnen doen. Maar zoals dat hoort in Nederland is het prachtig grijs buiten. De hangmat en de BBQ achter slot en grendel, de zomerkleding inmiddels bij de Kringloopwinkel. Geitenwollen sokken aan, een bak warme koffie, gebakken eitje, en een krantje. Een greep uit de ochtendbladen: het uurtarief van Hongaarse vrachtwagen chauffeurs bij Nederlandse Bv's is gelijk aan de prijs van een pak koekjes. Investeren in een huis loont even niet meer. Scheefhuurders worden gestimuleerd een huis te kopen door een verhoging van de huur. Maar lichtpuntjes zijn er ook. Aan de mysterieuze stilte van zo'n 10 jaar rondom David Bowie komt een einde, een nieuw album anno 2013 wordt vergeleken met zijn album uit 1983, geweldig, prachtig jaar overigens. Iets minder belangrijk: het boekje is af. Veel belangrijker, de steun, de inspiratie, de lol, en de samenwerking die ik de afgelopen jaren van al die geweldige mensen heb mogen genieten om tot dit resultaat te komen.

Beginnende bij mijn promotor Remko Akkerman, die mijn begeleider tijdens afstudeer- en promotiewerk is geweest. Ik heb de vrijheid gekregen om lichtelijk van koers te wijzigen na het eerste jaar van mijn promotie. De daarop volgende jaren ben ik ook altijd vrij geweest een eigen invulling aan het onderzoek te geven. Remko, jouw onuitputtelijke vertrouwen hierin heeft me flink geholpen mijzelf verder te ontwikkelen. Het geeft voldoening om op deze manier zelf invulling te hebben kunnen geven aan het resultaat wat er nu ligt. Ik kon op ieder moment met je aan tafel zitten voor een discussie met betrekking tot het onderzoek en andere zaken. Daar nam je altijd de tijd voor, ondanks de overvolle agenda. Je scherpe en nuchtere blik is hierbij van onschatbare waarde geweest. Remko, bedankt voor de waardevolle en prettige samenwerking!

My research has been conducted at the ThermoPlastic composite Research Center (TPRC). This opportunity was created by the Consortium and Technical Advisory Board (TAB) of TPRC, of which I am very grateful. My work-related activities have been moved from the University of Twente to the new TPRC location in October 2011. I enjoyed the fresh, inspirational, and comfortable atmosphere over there, for which I am especially thankful to Remko Akkerman and Harald Heerink. During the projects, I have been cooperating with companies that joined the TPRC. It is beautiful to experience the process where technicians from industry and researchers

combine their efforts in solving research questions. It was an honor to work with the technicians from the TAB, thank you all for the pleasant times! In particular, I would like to mention the cooperation with Alex Rubin and Gregg Bogucki from Boeing. Alex, Gregg, thanks for all the input and the pleasant talks. It was an honor to work with you. I also would like to mention the collaboration with Winand Kok from Ten Cate, and Michael Wielandt and Arnt Offringa from Fokker Aerostructures. I have learned a lot from your views and approaches regarding the challenges we have faced during the projects. I could always count on your support during the research, of which I am very thankful as well.

De vakgroep Productietechniek aan de Universiteit Twente is voor een groot deel mijn thuisbasis geweest. De humor die ik met menig collega kon delen was als energiedrank tijdens een mountainbiketrip. Directe collega's Wouter Grouve, Ulrich Sachs, René ten Thije, Bert Rietman, Roy Visser, Bo Cornelissen, Arnoud van der Stelt, Johan van Ravenhorst en Devi Wolthuizen stonden altijd klaar voor werk- en privé-gerelateerde discussies. Ik heb veel gehad aan jullie ingevingen en motiverende ideeën. Heren, bedankt! Laurent Warnet wil ik ook graag bedanken voor fiets- en werkgerelateerde discussies, de geniale ingaven tijdens het opzetten van experimenten, en het besmetten met het mountainbike virus. Ook bedank ik Ton Bor en Durk van Dijk voor de technisch-inhoudelijke discussies. Ton, je peptalks smeren als WD-40, waarvoor dank! Werken in de labs was ondenkbaar zonder de technici Bert Vos, Laura Vargas Llona, Gert-Jan Nevenzel, Patrick de Nooijer en Anton van Berkum. Dame en heren, dank voor jullie ondersteuning! In het bijzonder wil ik ook de mannen van de werkplaats en andere technici bedanken omdat ze altijd voor je klaar staan; Martin Sprenkeler, Norbert Spikker, Theo Pünt, Jeroen Beeloo, Herman van Corbach, Willie Kerver, Erik de Vries, Walter Lette, Henk-Jan Moed en Bert Wolbert, bedankt!

Tijdens dit onderzoeksproject heb ik direct samengewerkt met Ulrich Sachs. Uli, het was mij een genoegen om samen met jou dit project te trekken. Je scherpe en kritische blik tilde onze discussies naar een hoger niveau, waarvoor dank. Ook bij René ten Thije kon ik altijd terecht voor discussies en vragen, waarvan ik ongelofelijk veel heb geleerd. René, bedankt voor je onuitputtelijke bron van geduld! Onze samenwerking was erg prettig en ik kijk er naar uit om onze krachten te bundelen in een nieuwe fase.

Ook dank ik de collega's en oud-collega's Ashok Shridar, Dimitris Christoulis, Vitali Koysin, Andriejus Demcenko, Ted Ooijevaar, Emiel Drenth, Diane Liu, Sybren Jansma, Iqbal Abdul Rasheed, Jeroen Houwers, Alexandre Paternoster, Iris de Klerk, Luca Mainini, Kyrill Il'in, Vaidotas Cicenas, Mahmoud Ravanan, Lily Shaojie Liu en Yibo Su voor de prettige sfeer. In het bijzonder dank ik Christiaan ten Hove, Thijs Donderwinkel, Dirk Soeteman en Paul Jannink (allen destijds student) voor de fijne samenwerking en hun bijdrage aan mijn onderzoek. De secretaresses Belinda en Debbie dank ik voor de ondersteuning tijdens de soms stressvolle tijden. Jullie zijn engeltjes!

Ter inspiratie of gewoon ter ontspanning werd af en toe een Iskender besteld, of bezochten we "Café Het Bolwerk". De avonden met Bert Rietman, Wouter Grouve, Wouter Quak, Arjan Schutte en Martin Sprenkeler waren extreem gezellig. Dat moeten we blijven doen! Wouter Grouve en Wouter Quak zijn tevens mijn paranimfen. Door de jaren heen heb ik veel aan jullie gehad, de afleiding met mountainbiken, schaken en slap geouwehoer heeft me goed gedaan! Het is fijn dat jullie me tijdens de verdediging willen behoeden voor eventuele aanvallen met rottend fruit.

De steun van mijn familie: pa, ma, broers, oma, en schoonfamilie wil ik niet onvermeld laten. Ondanks dat het wellicht een wat "ver van jullie bed show" was, hebben jullie altijd vertrouwen gehad in een succesvolle afronding, waarvoor dank. Tenslotte noem ik mijn lief, Janine. Jouw onbeperkte vertrouwen was van onschatbare waarde en heeft me enorm geholpen. Relativeren moet je leren. Je bent de beste! Terug naar waar we waren begonnen, als de zon niet hier komt, dan zoeken we hem op. Een wijntje met lokale lekkernijen en een heerlijk klimaat, we gaan een mooi weekje genieten!

Sebastiaan

Publications

Journal articles

1. S.P. Haanappel, R.H.W. ten Thije, and R. Akkerman. Material parameter sensitivities in composite forming simulations. Submitted to: *Composites Part A: Applied Science and Manufacturing*, **2013**. (Chapter 2 of this thesis)
2. S.P. Haanappel and R. Akkerman. A method for shear characterisation of fibre reinforced thermoplastics by means of torsion. Submitted to: *Composites Part A: Applied Science and Manufacturing*, **2013**. (Chapter 3 of this thesis)
3. S.P. Haanappel and R. Akkerman. Shear characterisation of uni-directional fibre reinforced thermoplastic melts by means of torsion. Submitted to: *Composites Part A: Applied Science and Manufacturing*, **2013**. (Chapter 4 of this thesis)
4. S.P. Haanappel, R.H.W. ten Thije, U. Sachs, B. Rietman, and R. Akkerman. Formability analyses of uni-directional and textile reinforced thermoplastics. Submitted to: *Composites Part A: Applied Science and Manufacturing*, **2013**. (Chapter 5 of this thesis)

Conference proceedings

1. S.P. Haanappel, B. Rietman, and R. Akkerman. Shear characterisation of UD thermoplastic composites. *11th International Conference on Flow Processing in Composite Materials (FPCM-11)*, Auckland, New Zealand, **2012**.
2. S.P. Haanappel, U. Sachs, R.H.W. ten Thije, B. Rietman, and R. Akkerman. Forming of thermoplastic composites. *The 15th International ESAFORM Conference on Material Forming*, Erlangen, Germany. In Key Engineering Materials, volume 504-506, p237-242, **2012**.
3. S.P. Haanappel, R.H.W. ten Thije, U. Sachs, A.D. Rietman, and R. Akkerman. In-Plane Shear Characterisation of Uni-Directionally Reinforced Thermoplastic Melts. *The 14th International ESAFORM Conference on Material Forming*, Belfast, Northern Ireland, **2011**.
4. S.P. Haanappel, R. ten Thije, and R. Akkerman. Constitutive modelling of UD reinforced thermoplastic laminates. *10th International Conference on Flow Processes in Composite Materials (FPCM-10)*, Ascona, Switzerland, **2010**.
5. S.P. Haanappel, R. ten Thije, and R. Akkerman. Forming predictions of UD reinforced thermoplastic laminates. *14th European Conference on Composite Materials (ECCM-14)*, Budapest, Hungary, **2010**.
6. S.P. Haanappel and R. Akkerman. Non-crimp fabric permeability modelling. *9th International Conference on Flow Processes in Composite Materials (FPCM-9)*, Montreal, Canada, **2008**.

Co-author conference proceedings

1. U. Sachs, S.P. Haanappel, B. Rietman, R. ten Thije, and R. Akkerman. Formability of fiber-reinforced thermoplastics in hot press forming process based on friction properties. *The 16th International ESAFORM Conference on Material Forming*, Aveiro, Portugal, **2013**.

2. R. Akkerman, B. Rietman, S. Haanappel, and U. Sachs. Towards Design for Thermoplastic Composites Manufacturing Using Process Simulation. *International Conference & Exhibition on Thermoplastic Composites (ITHEC)*, Bremen, Germany. Book: p78-82, **2012**.

3. B. Rietman, S.P. Haanappel, R.H.W. ten Thije, and R. Akkerman. Forming simulation sensitivity study of the double-dome benchmark geometry. *The 15th International ESAFORM Conference on Material Forming*, Erlangen, Germany. In Key Engineering Materials, volume 504-506, p301-306, **2012**.

4. R. ten Thije and S.P. Haanappel. Multi-layer thermoplastic composites manufacturing processes: simulations and experiments. *SAMPE Europe International Conference & Forum (SEICO 2011)*, Paris, France, **2011**.

5. U. Sachs, S.P. Haanappel, B. Rietman, and R. Akkerman. Friction Testing of Thermoplastic Composites. *SAMPE Europe International Conference & Forum (SEICO 2011)*, Paris, France, **2011**.

6. U. Sachs, R. Akkerman, S.P. Haanappel, R.H.W. ten Thije, and M.B. de Rooij. Friction in Forming of UD Composites. *The 14th International ESAFORM Conference on Material Forming*, Belfast, Northern Ireland, **2011**.

7. B. Rietman, S.P. Haanappel, U. Sachs, and R. Akkerman. Process Simulations for Composites Forming of UD Tape Laminates. *CFK-Valley Stade Convention*, Stade, Germany. CD: p32-38, **2011**.

8. B. Rietman, U. Sachs, S.P. Haanappel, and R. Akkerman. Complex stamp forming of advanced thermoplastic composites. *ECCOMAS 3rd Thematic Conference on Mechanical Response of Composites*, Hannover, Germany. Book: p27-34, **2011**.

Posters or presentations

1. Engineering Mechanics Symposia, Lunteren, the Netherlands:
   (a) Forming Predictions of Thermoplastic Composites (poster), **2011**.
   (b) Constitutive Modelling of UD Reinforced Thermoplastic Laminates (poster), **2010**.
   (c) Joining of Thermoplastic Composites (poster), **2009**.
   (d) Non-Crimp Fabric Permeability Modelling (poster), **2008**.
   (e) Non-Crimp Fabric Permeability Modelling (presentation), **2007**.

2. S.P. Haanappel and R. Akkerman. Assessment of joining methods for thermoplastic composites (presentation). *15th International Conference on Composite Structures (ICCS 15)*, Porto, Portugal, **2009**.

3. S.P. Haanappel and R. Akkerman. Non-Crimp Fabric Permeability Modelling (presentation). *SAMPE Benelux Student Seminar 6*, Bergeyk, the Netherlands, **2008**.


UNIVERSITY OF TWENTE.

ISBN: 978-90-365-3501-4